MUSE-4 Experiment Measurements and Analysis

Gerardo Aliberti, George Imel, Giuseppe Palmiotti

Argonne National Laboratory
Nuclear Engineering Division

Argonne National Laboratory
9700 S. Cass Avenue
Argonne, IL 60439

September 2003

MUSE-4 Experiment Measurements and Analysis

Gerardo Aliberti, George Imel, Giuseppe Palmiotti
Argonne National Laboratory

Abstract

This report presents a review of the activities performed by the five teams involved in the MUSE-4 experimental program. More details are provided on the contribution by ANL during the year 9/02 to 9/03. The ANL activity consisted both in direct participation in the experimental measurements and in the physics analysis of the experimental data, mainly for the reactivity level, adjoint flux and fission rate distributions and the analysis of dynamic measurements for reactivity determination techniques in subcritical systems. The results provided to complete the Benchmark organized by the OECD and the CEA on the experiment MUSE-4 are also presented. Deterministic calculations have been performed via the ERANOS code system in connection with JEF2.2, ENDF/B-V and ENDF/B-VI data files.

Table of Contents

List of Figures

List of Tables

Glossary

APSD: Auto Power Spectral Density

ASM: Approached Source Method/Multiplication

CPSD: Cross Power Spectral Density

EW: East/West

MSM: Modified Source Method/Multiplication

NS: North/South

PNS: Pulse neutron source

PR: Pilot Rod

SC: SubCritical

SR: Safety Rods

Summary

This report presents a review of the activities performed by the five teams involved in the MUSE-4 experimental program. More details are provided on the contribution by ANL during the year 9/02 to 9/03. The ANL activity consists both in direct participation in the experimental measurements by G. Imel currently at CEA-CADARACHE and in the physics analysis of the experimental data.

After an introduction this report is divided in four main sections.

1. **Section II.** provides a description of the experimental program and the main measurement techniques employed for the acquisition of data.

   The main events characterizing the program are detailed in **Section II.A.**

   Section II.B. is devoted to the GENEPI accelerator performances and to the neutron source absolute calibration results performed by the ISN experimental team. A brief description of the various measurement acquisition systems used by the experimental teams is also presented.

   Section II.C. recaps the main characteristics of the monitors and detectors which were available during these measurement campaigns.

   Experimental techniques used for physical measurements are briefly described in **Section II.D.**

   All the core configurations which have been achieved from January 2001 to March 2003 are defined in **Section II.E**.
2. **Section III.** reports the analysis results which have been performed by ANL in support of the experimental program during the period 9/02 to 9/03 and in particular for:

   the reactivity level (**Section III.A.**);

   the adjoint flux distributions (**Section III.B.**);

   the reaction rate distributions (**Section III.C.**);

   the analysis of dynamic measurements especially for reactivity determination techniques in subcritical systems (**Section IIII.D.**).
3. The results provided to complete the Benchmark organized by the OECD and the CEA on the experiment MUSE-4 are presented in **Section IV**.
4. Conclusions and recommendations are given in **Section V**.

I. Introduction

The commissioning of a future industrial Accelerator Driven System (ADS) **[1]** qualified to transmute large amounts of minor actinides and long lived fission products **[2]** would require numerous technological demonstrations sustained by an extensive basic R&D program in the field of nuclear data, accelerators, spallations targets, fuels and subcritical systems. Regarding this last theme, the MUSE experiments performed at Cadarache Center (France) in the MASURCA reactor represents a fundamental step for the understanding of the neutronic behaviour of a subcritical multiplying medium driven by an external neutron source. Conducted in a low poutilize are based on the use of a well known external source, in terms of intensity and neutron energy, allowing separation of the experimental validation of the multiplying medium behaviour from the experimental validation of the source characteristics.

From 1995, the MUSE-1 **[3]** experiments then the MUSE-2 **[4]** experiments, performed with a ^{252}Cf source located at the centre of the MASURCA core, aimed to demonstrate that experimental measurement techniques used for critical cores could also be used for subcritical configurations. Later, the MUSE-3 **[5,6]** experiments represented the first important parametric study with the loading of several configurations characterized by an increasing subcriticality level. Based on the use of a commercial neutron generator, once more located at the core centre, these experiments helped to define the conditions to carry out a MUSE-4 program **[7,8]** and to specify the characteristics of a neutron source, more intense and more suitable to the envisaged measurements.

Funded by the 5th Euratom Framework Program and supported by the GEDEON French research organizations (newly GEDEPEON), the MUSE-4 experiments are now taking place within the framework of a large international collaboration including sixteen organizations from twelve countries. The three main objectives of this program are:

1- to improve the knowledge of the neutronic behaviour of multiplying media driven by an external neutron source, in order to characterize configurations of experimental interest;

2- to define experimental methods to measure sub-criticality levels (without the need to achieve the criticality) in support to the operation of an ADS;

3- to define recommended physics analysis methods for the neutronic predictions of an ADS (including nuclear data, calculation tools, biases and residual uncertainties).

Pivotal for MUSE-4 experiments, the GENEPI (Générateur de Neutrons Pulsés Intenses) **[9]** neutron generator was developed in a close collaboration between CEA and CNRS. Built specifically for these experiments, its main characteristic is to deliver very short pulses (<1μs) with a repetition rate going from some hertz to 5kHz.

The MUSE-4 measurement program is based on a parametric approach (1 critical + 3 subcritical sodium cooled configurations, 1 configuration with a small lead cooled zone, 2 kinds of target, variation of the GENEPI frequencies) and on the use of many diverse experimental techniques and analysis methods.

After a very long preparation phase due to the necessity to answer numerous French safety authority requirements, the first coupling between MASURCA and GENEPI with deuterium target happened on November 27, 2001. A series of preliminary measurements in slightly subcritical configurations ($\rho \approx -500$ pcm) was performed at the beginning of the year 2002 not only to get preliminary results but also to have a first feedback on the experimental conditions, to improve measurements in the next phases. The calibration of the (d,d) source was also realized. Then, the full characterization of the reference critical configuration was achieved from April to June 2002. This program included importance traverses using a ^{252}Cf source and numerous axial and radial traverses of fission reaction rates without external source. Fourteen different isotopes were used for these measurements. The study of subcritical states began at the beginning of October 2002 with the investigation of the clean core configuration SC0 using respectively the (t,d) then the (t,t) target. Since this measurement phase ended on March 2003, configurations with reactivity levels more representative of an industrial ADS are being studied: the SC2 configuration ($K_{eff} = 0.95$) was from April to July 2003, the SC3 configuration study should be from August to October 2003.

Regarding the definition of a recommended route for the prediction of the ADS features, two main actions have been launched.
First, a calculation benchmark under the auspices of the OECD/NEA **[10]** has been defined. Sixteen organizations (ANL included) from fourteen countries have taken part in this exercise. Then, the problems related to the propagation and the streaming of the spallation neutrons are investigated in the SAD experiments. This program aims to study different spallation neutron sources (Pb, Pb-Bi, W targets) produced by the 660 MeV protons of the Dubna synchrotron, with and without the presence of a multiplying medium. These experiments will allow validation of the transport calculation tools and the nuclear data treating the deep penetration and the activation of the materials far away from the source and the multiplying medium.

Among the neutronic parameters of main interest during the experimental phase, the determination of the reactivity level is of prime importance. In fact, among the safety demonstrations requested for the commissioning of an ADS, the proof of the reactivity level is decisive for the acceptability of such a machine. This objective characterizes all experiments involved in the MUSE program.

In a practical way, two families of analysis methods are used **[11]**. The first one aims to study the decreasing of the neutron population (prompts or delayed neutrons) after a modification of the source level (pulsed neutron source method (PNS) and frequency variation method). The second family investigates the neutronic fluctuations in the fission chains (noise measurements). The analysis methods which are employed, such as Rossi-α and Feynman-α methods, as well as the transfer function method (e.g. CPSD), when no external source is in place, need an acquisition time and/or detectors with adequate sensitivity as the subcriticality level is large. Of course, these durations are reduced when the core is driven by GENEPI.
However, all these techniques and analysis methods do not directly measure the reactivity levels but rather the alpha parameter: $\alpha = (\rho-\beta)/\Lambda$. Thus, the reactivity measurement needs to determine Λ and β, or β/Λ when the reactivity is expressed in dollars ($\rho_{\$} = 1 - \alpha \frac{\beta}{\Lambda}$). These parameters can be deduced partly from the Rossi-alpha method, the transfer function method and from the frequency variation method.

We first present a review of the activities performed by the five teams involved in the MUSE-4 experimental program. Then more details about the contribution provided by ANL during the year 9/02 to 9/03 are presented (see **Ref. 12** for an accurate description of previous work). The ANL activity consists both in direct participation in the experimental measurements by G. Imel currently at CEA-CADARACHE and in the physics analysis of the experimental data.

II. Experimental program and measurement techniques

II.A. MUSE-4 experiment main events

Up to now, the main events related to the MUSE-4 experiment are as follows:

- the first criticality state of the MUSE-4 reference configuration was achieved on January 9, 2001 (see **Figure 3**). The number of ZONA2 fuel cells was equal to 1112. The calculated value was 1072 **[13].**
- the first application of the GENEPI accelerator with the deuterium target and all the safety rods down, was obtained on February 15, 2001.
- the authorization to perform the experimental program with the reference critical configuration was delivered on May 25, 2001.
- the authorization to couple the MASURCA facility with the GENEPI neutron source was delivered by the French Safety Authority on September 19, 2001.

- the authorization to perform the experimental program in the three successive MUSE-4 subcritical configurations was delivered by the CEA directorate about two months later: on November 13, 2001.
- the first coupling of the accelerator and the reactor with all safety rods up occurred on November 27, 2001; at this date the experimental program commenced. The reactivity level with the pilot rod up was about –126 cents **[14]**. Two weeks of measurements in this configuration with GENEPI ON could be achieved with the techniques and methods proposed by partners. These experiments tested the acquisition systems, in particular the new CEA system **[14],** and the efficiency of several monitors operating in subcritical state.

The successive configurations which have been carried out are detailed in **Section II.E.**

II.B. The GENEPI accelerator

The realization of the MUSE-4 experiments needed the design and the development of a specific accelerator: GENEPI (GEnérateur de NEutrons Pulsés Intense). The main events were as follows :

- September 1996 : first studies and calculations;
- September to December 1998 : building of the track A at Joseph Fourier University Grenoble 1;
- 1999 : physical studies and measurements by the ISN team;
- February 2000 : Dismantling of GENEPI at ISN;
- June 2000 : End of the set-up in the MASURCA facility;
- August 2000 : first d^+ beams on an inert target;
- November 2000 : set up of the (t,d) target;
- March 2001 : first neutrons produced by (d,d) reactions with all the safety rods down;
- November 27, 2001 : first coupling with all rods up in a slight subcritical level;
- November 2002 : set up of the (t,t) target and first neutrons produced by the (d,t) reactions.

II.B.1. The GENEPI operation

In spite of changes of several components, the operation of GENEPI was satisfactory during the experimental phase. The real performances were very close to the initial specifications (see **Table 1**).

Table 1: GENEPI beam characteristics

Beam energy (keV)	140 to 240
Peak current (mA)	50
Repetition rate (Hz)	10 to 5 000
Minimum pulse duration (10^{-9} s)	700
Mean beam current (μA)	200 (for a duty cycle of 5 000 Hz)
Spot size (mm)	≈ 20 in the diameter
Pulses reproducibility	Fluctuations at 1% level

A second GENEPI accelerator is being built at ISN. The main improvement concerns the reduction of the pulse width. The objective is to reach less than 500 ns at mid height.

II.B.2. Neutron Source Absolute Calibration

To characterize the neutron source produced by the GENEPI accelerator, irradiation experiments were performed. Nickel foils were disposed on a target holder inserted vertically in the MASURCA core, as close as possible (~10 cm) to the target producing neutrons under deuteron impact. Several reactions on Ni were exploited. These irradiations were performed with all the control rods inserted and at a repetition rate of about 4 kHz in order to minimize the activation due to the intrinsic source. After irradiation the activity of each Ni target was measured in the Low Activity Lab of the ISN, using a low background germanium detector. These activities, compared to MCNP simulations of activation, allow the number of neutrons per pulse to be estimated. The results are as follows:

- the neutron production rate of the deuterium target was found equal to $3.0 \pm 0.3 \times 10^{4}$ neutrons per pulse on April 5, 2001 (for a 60 mA peak current);
- the neutron production with the tritium target was found equal to $3.3 \pm 0.3 \times 10^{6}$ neutrons per pulse (40 mA peak current) on January 22, 2003. By recording simultaneously the monitoring detectors, which consist of silicon detectors counting the charged particles associated to the neutron production, it was also possible to associate the number of these particle detected to the absolute neutron production, and then to have an online monitoring of the source;
- the detection rate was found equal to $1.92 \pm 0.20 \times 10^{-7}$ proton per source neutron ((d,d) source monitoring) and $2.44 \pm 0.24 \times 10^{-7}$ alpha-particle per source neutron ((d,t) source monitoring). More details about these measurements and results can be found in **Ref. 15**.

II.B.3. Description of measurement acquisition systems

II.B.3.a. CEA systems

The standard acquisition system at MASURCA (SAM) is composed of Multi-Channel Scalar and Pulse Height Analyser cards to investigate the dynamic or static counting rate for classical measurements (e.g. rod-drop, source multiplication, axial and radial distributions and spectral indices). This system was set up in 2002-2003 to perform simple and reproducible parallel measurements on all standard MASURCA monitors. At the same time, a new Neutronic tIme marKing acquisitiOn system (NIKO) was developed in order to replay neutronic experiments off-line using different analysis techniques. The aim of the NIKO project has been to provide means to perform several analytical techniques using one data set when possible. For that purpose, one needs an acquisition system for timing any event such as counts outgoing from detectors operated in pulse mode. No events are pre-selected by the use of any kind of triggering analog electronics.

The main part of the time marking acquisition system is the MEDaS PC-card designed by the CESIGMA Company. Unlike most similar devices, this acquisition card records the elapsed time between TTL pulses coming into any one of its 32 input channels. Using a clock of 40MHz, the time resolution is quite high: the dwell time can be fixed at 25 ns minimum. That quantization time is compatible not only with the fission chain characteristic time, which is about 200 μs at delayed critical in a fast neutronic system, but also with the dead time of the U235-fission chambers, which is about 50 ns. This small dead time is attributed to the fact that the fission chambers are operated in pulse mode with current-sensitive amplifiers. For any incoming TTL pulse, a pair of 32-bit words is first stored in the internal First-in-First-out (FIFO) memory associated with a 33-MHz PCI bus. The First binary word carries the elapsed time from the last event while each bit of the second word is set equal to 1 when the corresponding input channel has detected a TTL signal. With the 33-MHz and 32-bit PCI bus, the MEDaS card makes possible an acquisition rate up to 10 millions events/second. In order to sustain a satisfying acquisition rate, the capabilities of the host PC are highly important. For that reason, the acquisition PC is a 800-MHz bi-processor PC whose one processor is dedicated to the PCI bus of the time marking card. Through the dynamic memory access (DMA) of the host PC, data that are read out from the card FIFO memory are either stored into the random access memory (RAM) or into the hard disk memory when the counting rate is not too high.

II.B.3.b. ISN system

The ISN data acquisition system is based on the use of 12b-flash-ADC, 12b-ADC and scales installed on a VME system piloted by a SUN Station, which work all together synchronized on the source pulse. The GENEPI frequency signal opens a 300μs time window: during this time fission chambers and ^{3}He detector signals are recorded on the flash-ADC, with a 100ns per channel sampling, while neutron source monitoring signals are

recorded on the ADC. This allows one to obtain time and energy spectra without deadtime over the range of interest, i.e. close to the neutron pulse and during the neutron multiplication.

II.B.3.c. SCK•CEN system

The measurements were performed with the SCK•CEN home-made data-acquisition hardware instrument called TICS-analyzer or with a PC-based system with Labview and a data-acquisition board from National Instruments.

II.B.3.d The TICS-analyzer

The TICS-analyzer (Time Interval Correlation Spectroscopy) is an electronic device developed for measuring time interval correlation spectra. The TICS-analyzer is based on fast signal processing technology with Programmable Logic Devices (PLD). The TICS-analyzer allows handling count-rates up to 1 Mpulses/s without any loss of information during the measurement due to the hardware implementation of the construction algorithms for the different distributions.

In particular, the TICS-device is able to record directly and to construct the conventional one-dimensional Rossi-alpha distribution encountered in experimental reactor physics and safeguards. Moreover the original design of the TICS-analyzer allows recording the two-dimensional Rossi-alpha distribution used in safeguards for neutron multiplicity analysis. To more specifically apply the TICS-analyzer in experimental reactor physics for sub-critical measurements, the recording of the two-dimensional Rossi-alpha distribution was replaced by the recording of the time response resulting from Pulsed Source Analysis.

II.B.3.e. The PC-based data-acquisition system

Due to the increased computing speed of PC's and the availability of high performance acquisition boards, the development of a more flexible PC based system became possible. Compared with the hardware system, the specifications are somewhat inferior but still meet the requirements for the measurements to be performed in the MUSE project. The developed measurement programs allow recording of the Rossi-alpha spectrum and the time response to a pulsed neutron source. Acquisition, construction of the histogram and visualization are performed in real time. Count-rates from 50kHz up to 200kHz can be handled, depending on the setting of time resolution and window length. The minimum resolution time is 12.5ns.

The system uses the following components:

- PCI-6602: National Instruments counter/timer board. This board interfaces to the PC through the PCI bus. It contains 8 32-bit counter/timer functions. High speed continuous data transfer through DMA (Direct Memory Access) without using the DMA recourses from the PC is possible on three counters simultaneously;

- DELL Optiplex GX240 PC;
- Labview 6.1 programming language;
- "Time Interval Spectroscopy Analyser" and "Impulse Response Recorder" measuring programs in Labview: developed at the SCK-CEN.

II.B.3.f. IRI system

When the reactor is critical, the neutron detector signals are monitored in continuous (charge integrating) current mode. The measuring hardware solution consists of separate high voltage supplies and inline shunt resistors and high voltage current to voltage conversion electronics with built in DC blocking high pass filters.

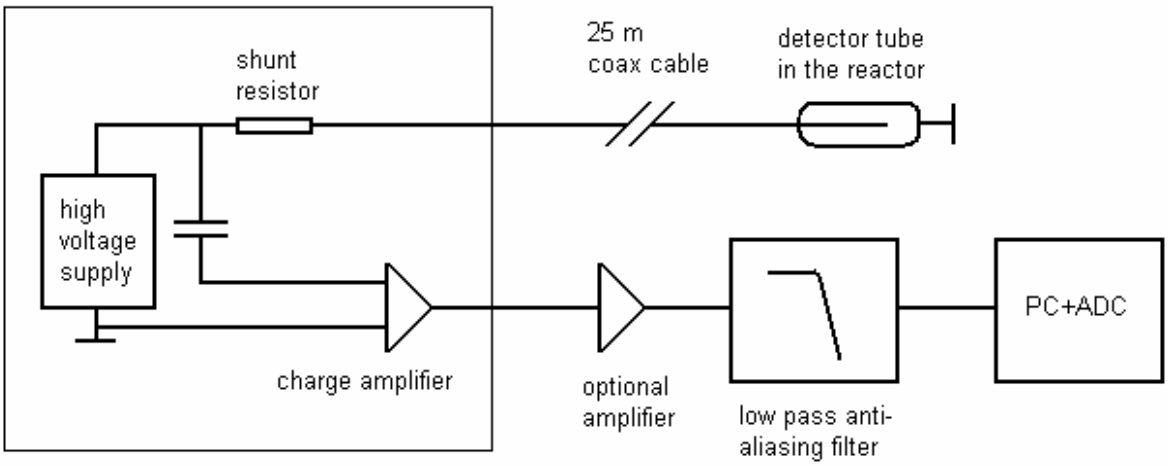

Figure 1: IRI system

The resulting ground-referenced voltage signals are amplified by a home made eight channels SCXI amplifier module and filtered by 8th order anti-aliasing National Instruments SCXI1141 filter module with additional amplification. A 16 bit NI PCI6035 ADC card connected to this module samples up to eight channels. Software applications were developed in Labview and allow full control of the measurement and online analysis in time- and frequency domain. All recorded raw data are stored on a removable hard disk for further off-line analysis.

Rossi-α and reactivity will be determined by the (cross correlation) analysis of the frequency content of the current signals. The data sampling system is able to record 200 kS/s continuously divided over the number of channels. Typically two continuous current mode signals are available, which can thus be sampled by 100 kS/s simultaneous. The upper frequency –3 dB bandwidth limit of the measurement system however is about 10kHz, which is determined by the RC pole, consisting of the shunt resistor and the cable capacitance. The minimum cable length was used to maximize the bandwidth.

With the reactor in sub-critical mode the continuous current signal is vanishingly small so that pulse counting is required. The small fast neutron MUSE core requires pulse countings with high temporal resolution. By the combined high voltage supply and pulse amplifying electronics (CEA), the neutron pulses from the detectors are discriminated from gamma pulses, amplified and shaped into square TTL-like voltage pulses of 50 ns width and 5 to 8 V amplitude into 50 ohm load. These pulses are to be counted by a relatively high-speed commercially available PCI bus based multi channel TTL level countercard (NI type PCI6602) with high nominal impedance (20kohm). Adding 50 ohm cable termination and variable attenuation at the counter-card input ensures TTL compatible input and minimizes distortion.

Labview software is used to perform the recording of neutron pulse arrival in two measurement modes:

- The buffered event counting mode for up to three channels simultaneous records the number of valid pulses arrived at the channel input during a maximum of about 100 million connected constant time intervals. This format is especially convenient for Feynman analysis. The minimum time interval size (or maximum time resolution) depends on the number of channels (Nchn) to be measured simultaneously, and it was about 1.5xNchn μs. At maximum time resolution and 3 simultaneous channels, each continuous run is limited by the amount of RAM in the host PC to about 100s.
- The buffered period measurement mode records periods between subsequent neutron pulses for up to three channels simultaneous. Accumulating all periods from the start results in a complete time-trace of incoming neutron pulses. The time resolution of this mode is 50 ns. The time resolution of the period measurement mode is much better than the event counting mode one, but in special cases, like rod drop experiments, the event counting mode was shown to be quite useful.

II.C. Generalities on standard CEA monitors and detectors used for the measurements at MASURCA

Two kinds of detector are mainly used inside the MASURCA facility: Monitors and Experimental Fission Chambers. The monitors are fixed counters while the detectors can be moved during the measurements using a special device named "TRANSLATEUR".

CFUK09 high efficiency detectors are also used for current mode measurements and in particular for delayed neutron fraction measurements. Due to their dimension, these detectors are part of special instrumental subassemblies. The introduction of such devices notably modifies the core critical mass.

II.C.1. The monitors

The characteristics of the fourteen monitors (A, B, C, …M, N) used for the measurements are detailed in **Table 2**. These monitors, produced by PHOTONIS firm, are themselves divided in 2 types: Fission Chambers with ^{235}U

deposit and proportional Boron Chambers which are most sensitive to thermal neutrons. All detectors are used in current pulse and therefore are not calibrated in terms of absolute deposit mass because the shape of the signal could not be used. They are always used to measure relative rates between 2 states of the core. Their location inside the core changed during the MUSE-4 program to optimize their use (decreasing the dead time or increasing the counting rate); except for the I and L monitors which did not change.

Table 2 : Characteristics of the monitors

Monitor	Chamber model	Isotope	Approximate mass of deposit	Efficiency (counts/n.s^{-1})
A	CFUM 21	^{235}U	0.013 g	0.06
B	CFUM 21	^{235}U	0.013 g	0.06
C	CFUM 21	^{235}U	0.013 g	0.06
D	CFUM 21	^{235}U	0.013 g	0.06
E	CFUM 21	^{235}U	0.013 g	0.06
F	CFUE 22	^{235}U	0.015 g	0.01
G	CFUL 01	^{235}U	1 g	1
H	CFUL 01	^{235}U	1 g	1
I	CFUE 24	^{235}U	0.015 g	0.01
J	BF_3	^{10}B	0.4 mg/cm2	3
K	BF_3	^{10}B	0.4 mg/cm2	3
L	CFUE 22	^{235}U	0.015 g	0.01
M	CFUL 01	^{235}U	1 g	1
N	CFUL 01	^{235}U	1 g	1

II.C.2. The experimental fission chambers

The experimental fission chambers are produced by the CEA/LPE with variable deposits in term of mass from 1µg to 10 mg and of nature (U, Pu and Am isotopes, ^{237}Np, ^{232}Th, ^{10}B, ^{244}Cm,…). The fission chamber dimensions have a 3 to 5 cm length (1 to 2 cm of deposit) and a 4 to 8 mm diameter. They are used in voltage pulse mode and can be calibrated in term of absolute mass of deposit. Absolute reaction rates and spectral indices can be derived from these chambers. Due to the nature of the deposit they have different sensitivity to a selected ranges of the neutron spectrum (isotopes with threshold cross section) but their efficiency is quite low. They are introduced inside the core in the experimental radial and axial channels (the external square section of this channels is 12.7mm x 12.7mm). Then, these fission chambers are used for the realization of the reaction rates traverses using a specific design, the “TRANSLATEUR”, which allows movement of the fission chamber inside the experimental channels with a precision of less than 1 mm. Moreover, thirteen axial channels have been

set up in the subassemblies located at the following positions: W15-17, E15-16, E16-15, E17-16, E18-17, E19-18, W20-18, W21-17, W22-17, W22-18, E22-17 and E22-16. Note that the location of the assemblies in the MASURCA loading is specified by a sequence of three data: the first data is a letter (E or W) which defines the region (East or West) with respect to the axis of symmetry Noth-South (NS). Then, two numbers give the exact position by its Y and X coordinates in the MASURCA lattice (see, as example, **Figure 2**).

II.C.3. The CFUK09 chambers

These high efficiency fission chambers contain a ^{235}U deposit of about 4.5 g. Their diameter is equal to 60 mm; their length, connectors included, is 385 mm. Due to these dimensions, they are included in special subassemblies **[16]**. Compared to a standard fuel subassembly, several fuel cells are withdrawn. The reactivity effect due to this modification depends on the neutronic characteristics of the material which surrounds the chamber. These chambers are mainly used to perform current mode measurements and especially for delayed neutron fraction measurements.

II.D. Measurement techniques

In this section the several kinds of measurements performed during the MUSE-4 experiments are described. Generally speaking, we can distinguish two series of measurements: safety measurements and physical measurements.

II.D.1. Safety measurements

At the beginning of each experimental program, some particular measurements have to be performed on the first critical configuration to ensure that the safety rules and some special requirements are fulfilled. These measurements consist in:

- the reactor power calibration;
- the reactivity worth of the safety rods;
- the reactivity worth of the pilot rod;
- the reactivity worth of some peripheral fuel cells.

II.D.2. Physical measurements

These are the measurements which are performed in the frame of the experimental program. For the MUSE-4 experiments, they consisted of:

- *Critical mass measurement*

  The criticality of the core is reached by adjusting the number of fuel cells on the following basis:

  - first, all the rods being down, less than a half core critical mass is loaded;
  - then, some successive subcritical approaches are achieved by pulling down in turn each safety rod. From a subcritical approach to the other, the reactivity effect due to the loading of fuel cells has always to be less than half a dollar;
  - when all the safety rods are up, the pilot rod is put in high position to get overcritical;
  - last, the pilot rod position is adjusted to stabilize the reactor. Depending on the power level, the position of this rod can be modified several times a day to compensate the effect caused by the increasing temperature in the subassemblies.

  One will note that, at MASURCA, a safety rule requires that the reactivity worth of the pilot rod is less than half a dollar. The position of the subassembly, where the pilot rod is located, has to be chosen taking into account this constraint.

- *Rod-drop experiment*

  This experiment generally aims to determine a reference reactivity level. There could be two manners to carry out this experiment:

  1st solution - The pilot rod position is adjusted so that the reactor is critical and stable. The power level is about some tens of watts. Then, one withdraws the pilot rod as quickly as possible. When it reaches the high position, this configuration is kept about a tenth of a second, then, the rod is dropped.

  2nd solution - The pilot rod position is adjusted so that the reactor is critical and stable. The power level is about some tens of watts. Then, the pilot rod is dropped.

  One can deduce the final reactivity level from the inverse kinetics equations in the point model.

- *Importance traverse*

  This measurement is performed in two phases :

  1st step – The reactor is subcritical and stable. One stores the counting rates due to the inherent source ($C_{ref.}$).

  2nd step – The reactor is subcritical. One introduces an external source in the core. When stability is reached (gamma flux), one stores the new counting rates ($C_{pert.}$).

  Then, one deduces the ratio (C_{pert}/C_{ref}). The intensity of the external source has to be known to allow calculation vs measurement comparisons.

- *Reaction rate traverses*

  This kind of measurement allows one to determine the relative distribution of a reaction rate for a given isotope. Using the TRANSLATEUR device, the experimental fission chamber is moved inside an experimental channel. For each position, the number of events per second due to the nuclear reactions inside the chamber is stored.

- *Spectral indices*

  These measurement aims to determine the ratio of two fission rates of two isotopes whose mass deposit is well known. These experimental values are then compared to the calculated ones. If the isotopes used are numerous and sensitive to different energetic domains, these spectral indices give an information which can allow to assess the neutron energy spectrum.

- *PNS measurements*

  This kind of measurement aims to study the neutron population decreasing after a neutron pulse. Several analysis methods can be applied. The main ones are:
  - the surface method, which allows to assess directly the reactivity in dollars;
  - the fitting method, which allows to determine the neutron prompt decay value, $\alpha=(\beta-\rho)/\Lambda$.

  These measurements were largely performed. More details are given in **Ref. 11**.

- *Noise measurements*

  This time, one studies the fluctuation of the fission chain. These experiments can be performed with or without neutron external source. Once again, several analysis methods can be applied. The main ones are:
  - the Rossi-alpha method;
  - the Feynman-alpha method;
  - the Power Spectral Density.

  These measurements were also largely performed. More details are given in **Ref. 11**.

- *Frequency modulation technique*

  This technique is quite similar to the Source Jerk Method. For a given sub-critical level, the external neutron source rate is suddenly changed from a high level R_0 to a low level R_1. This can be obtained here by changing suddenly the GENEPI source intensity. The response $n(t)$ of a neutron detector immediately before and after the source change, allows the determination of the ratio ρ/β between the reactivity and the fraction of delayed neutrons.

II.E. The MUSE-4 core configurations

II.E.1. Experimental phase planning

From January 2001 to March 2003, twelve configurations have been carried out (see **Table 3**).

Table 3: Core configurations from January 2001 to March 2003

Period	Number of equivalent fuel cells	Critical or Subcritical	Target	Special subassemblies
01/08/2001 ➔ 06/29/2001	1112	Critical	Deuterium	
06/29/2001 ➔ 08/06/2001	1114	Critical	Deuterium	
08/06/2001 ➔ 09/13/2001	1119	Critical	Deuterium	CFUK09 surrounded with CH_2
09/13/2001 ➔ 11/20/2001	1114	Critical	Deuterium	
11/23/2001 ➔ 01/25/2002	1086	Subcritical	Deuterium	Three fixed ISN tubes + ISN mobile tube at E23-17 position
02/06/2002 ➔ 03/18/2002	1115	Critical	Deuterium	
03/21/2002 ➔ 04/24/2002	1115	Critical	Deuterium	
04/25/2002 ➔ 09/08/2002	1115	Critical	Deuterium	
09/12/2002 ➔ 09/16/2002	1132	Critical	Deuterium	CFUK09 surrounded with CH_2
09/24/2002 ➔ 09/27/2002	1125	Critical	Deuterium	CFUK09 surrounded with Al
10/22/2002 ➔ 11/15/2002	1108	Subcritical	Tritium	CFUK09 surrounded with Al
01/21/2002 ➔ 03/14/2003	1108	Subcritical	Tritium	CFUK09 surrounded with Al

Because of some core heterogeneities (the GENEPI channel, the ISN tubes, the lead buffer) the official fuel cell numbers cannot be deduced safely from the layout of the configurations. The cells number is estimated by analysing in detail the composition of each tube. For example, the ISN mobile tube is estimated to weight 14 cells instead of 16 in a standard fuel sub-assembly. The detailed descriptions of all kinds of subassembly loaded in the MUSE-4 cores are provided in **Refs. 17** to **20**.

Most of the measurements have been achieved with all safety rods up. Some measurements have been performed with one or more safety rods in low position either to investigate deep subcriticality level, or to study asymmetrical configurations. In the present experiment, the safety rod n°1 (SR n°1) is the one located at W position; the safety rod n°2 (SR n°2) is the one located at E position (see **Figure 2**).

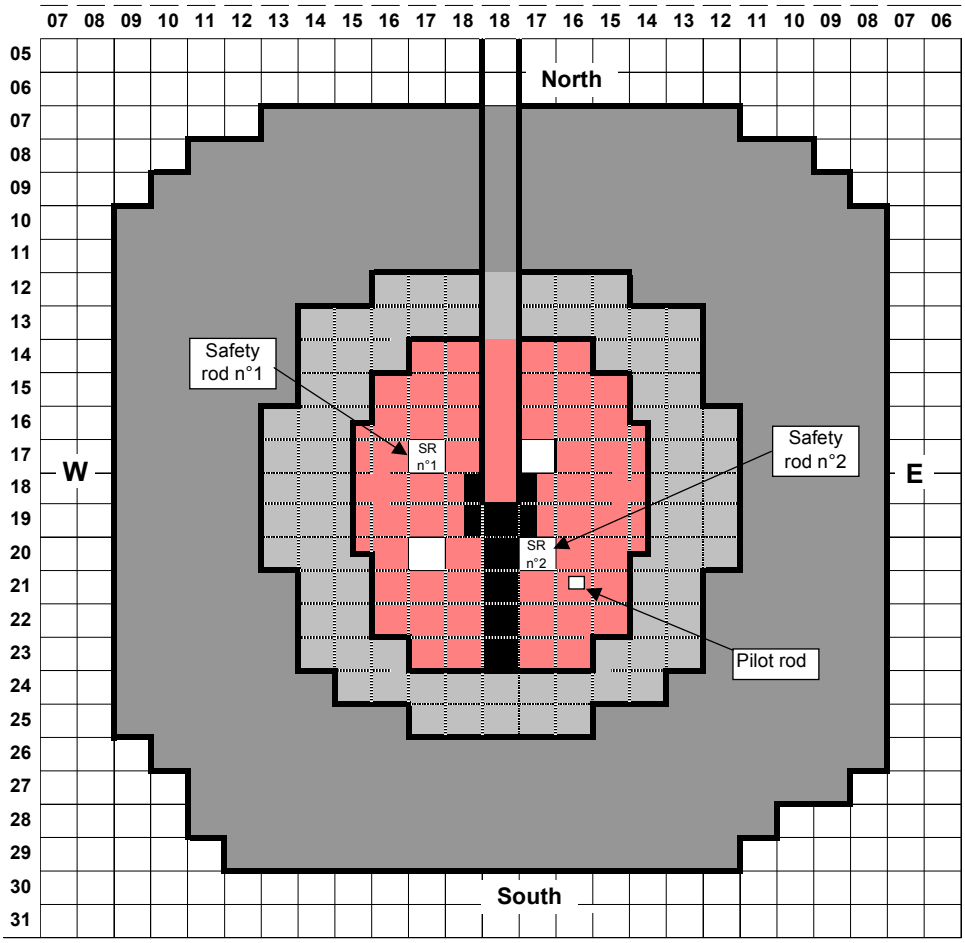

Figure 2: Position of the safety rods n°1 and 2 in the core.

II.E.2. Main measurements performed on the various configurations

From October 2000 to March 2003, twelve configurations have been investigated. Each of them is characterised by an equivalent fuel cells number. These configurations were as follows:

- 01/08/2001 ➔ 06/29/2001: **critical** configuration with 1112 fuel cells (see **Figure 3, 4, and 5**).

This is the first MUSE-4 critical configuration. It was mainly used for safety parameter measurements. This configuration has also been considered as the reference for the calculations, detailed in **Section III**, in support to the MUSE-4 program.

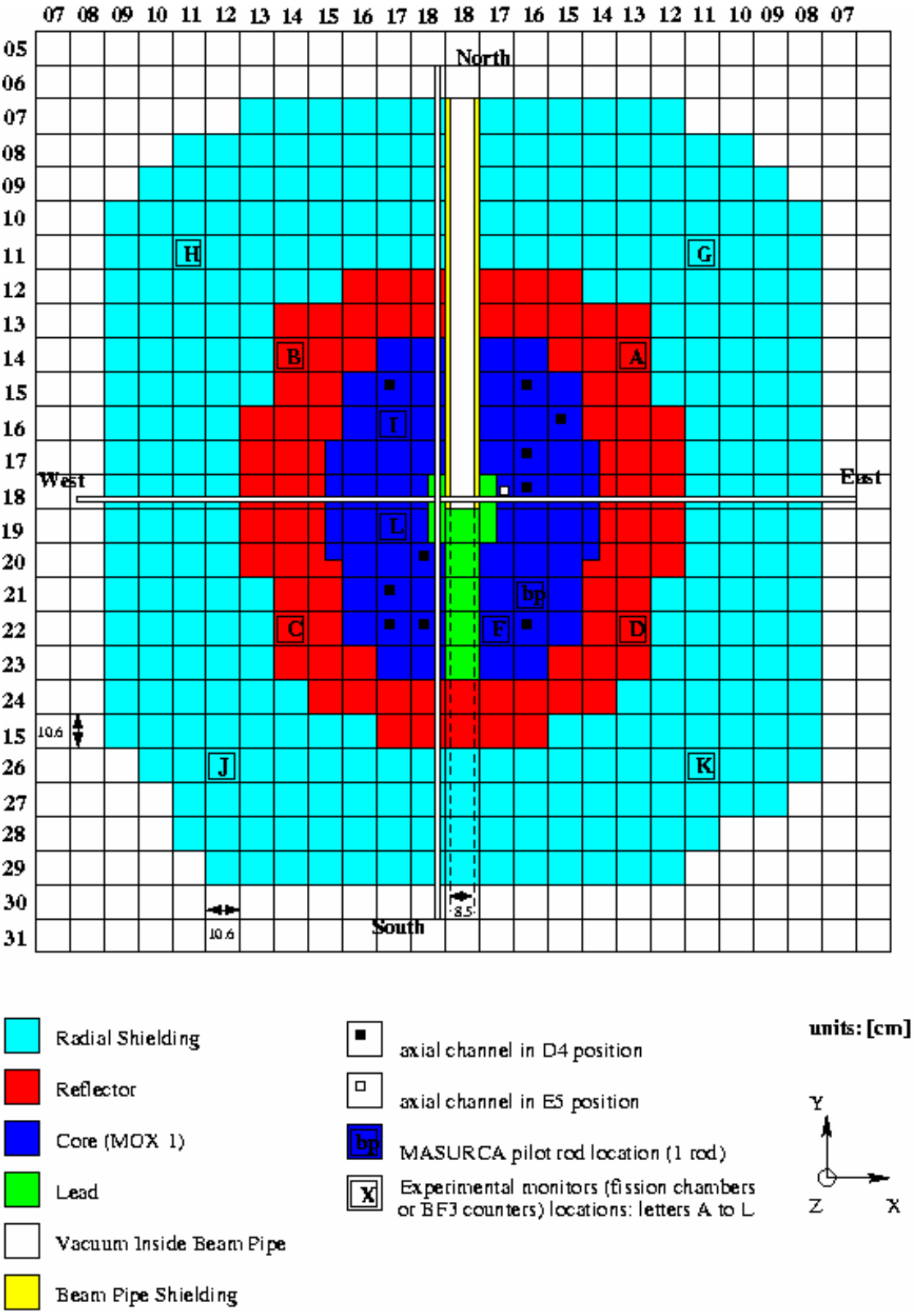

Figure 3: MUSE-4 Critical Reference Configuration – View XY

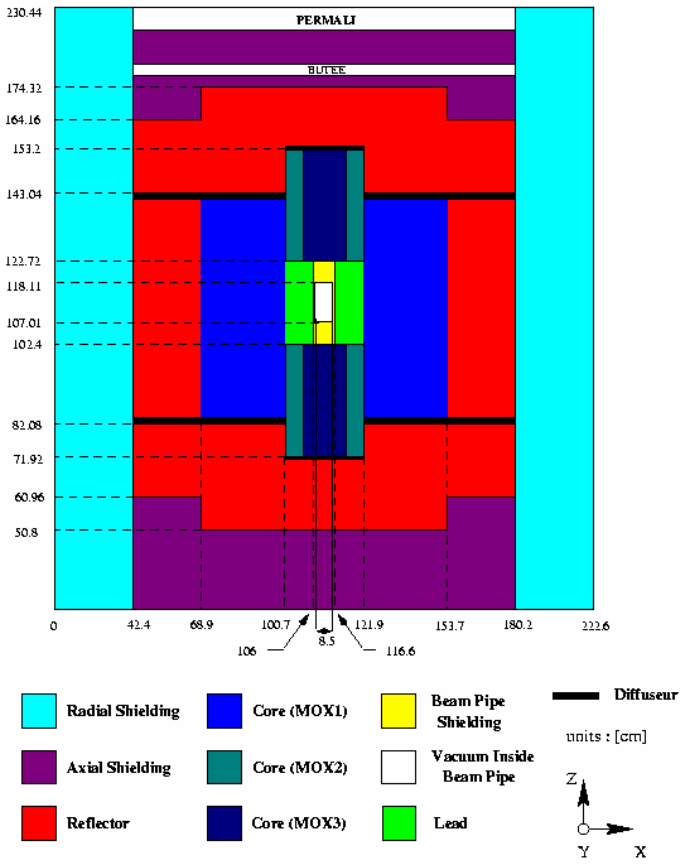

Figure 4: MUSE-4 Reference Configuration – View XZ

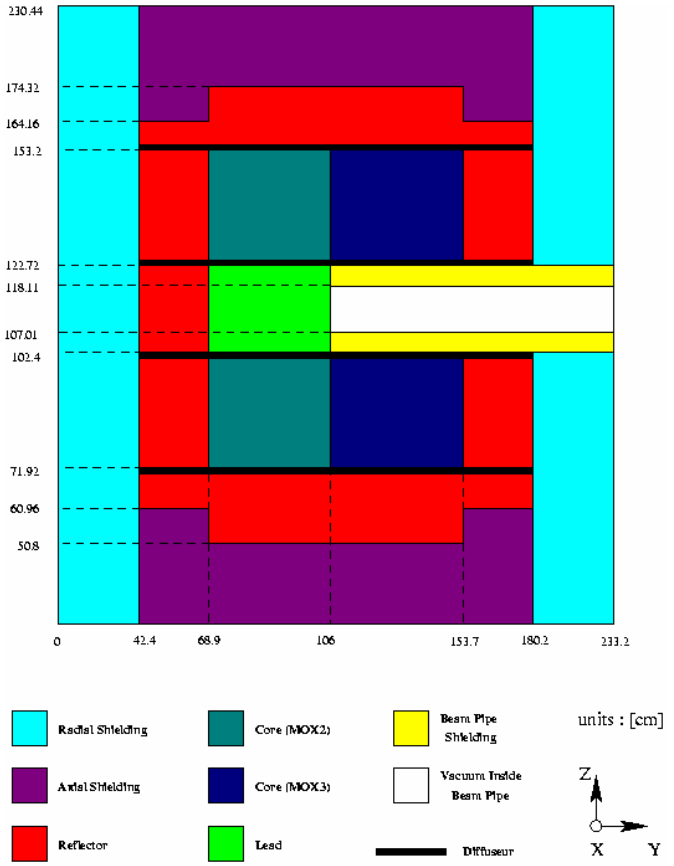

Figure 5: MUSE-4 Reference Configuration – View YZ

- 06/29/2001 ➔ 08/06/2001: **critical** configuration with 1114 fuel cells (see **Figure 6**).

Compared to the previous configuration, the only modification consisted of the addition of two fuel cells to compensate the ^{241}Pu decay. The monitor calibrations were performed during this period.

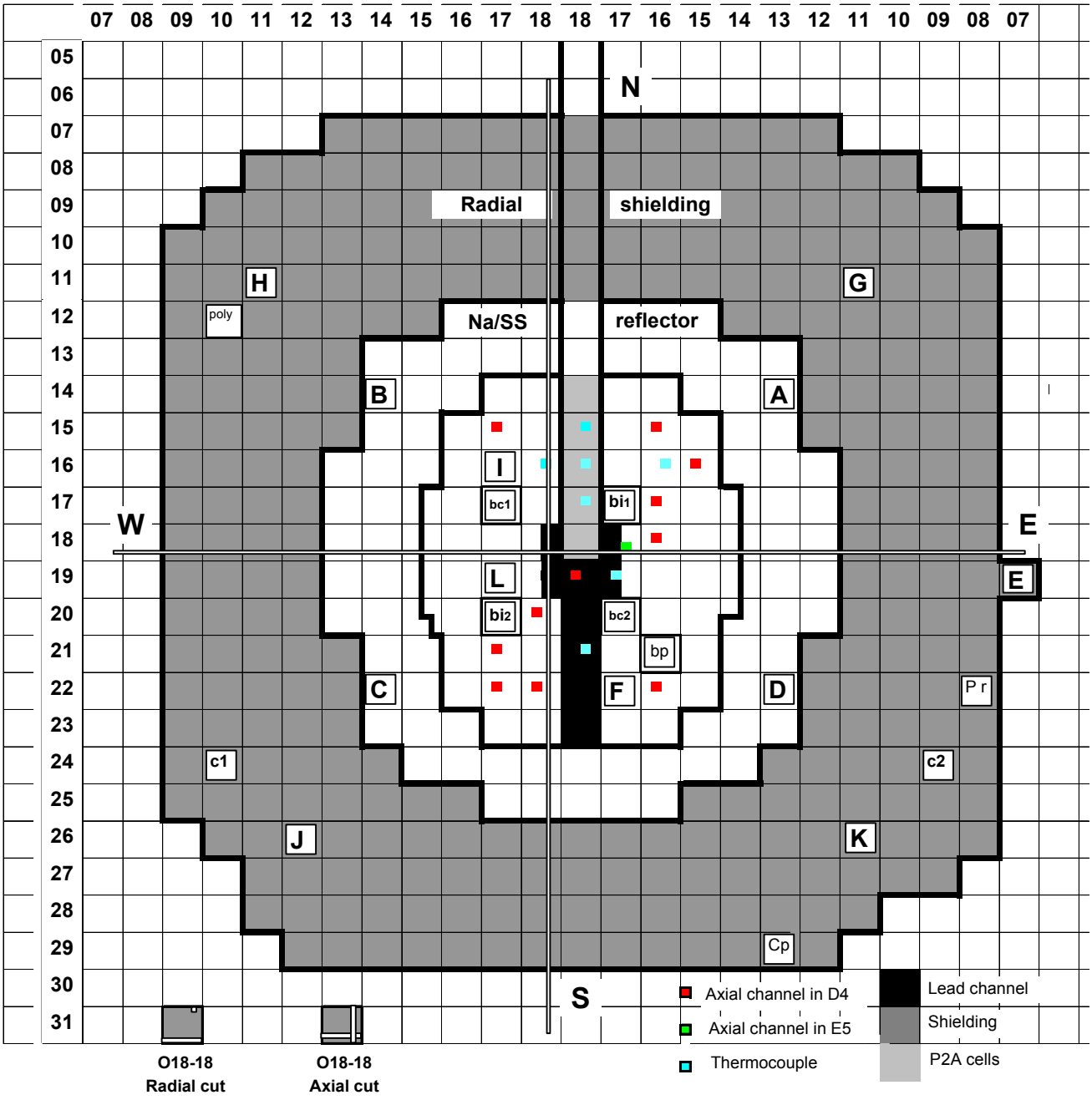

Figure 6: MUSE-4 Reference Configuration 1114 Cells

- 08/06/2001 ➔ 09/13/2001: **critical** configuration with 1119 fuel cells (see **Figure 7**).

Two tubes with high efficiency CFUK09 fission chambers and surrounded with polythene were loaded in the reflector zone to perform some delayed neutron fraction measurement tests. Five fuel cells were added to compensate the negative reactivity effect due to the loading of these subassemblies.

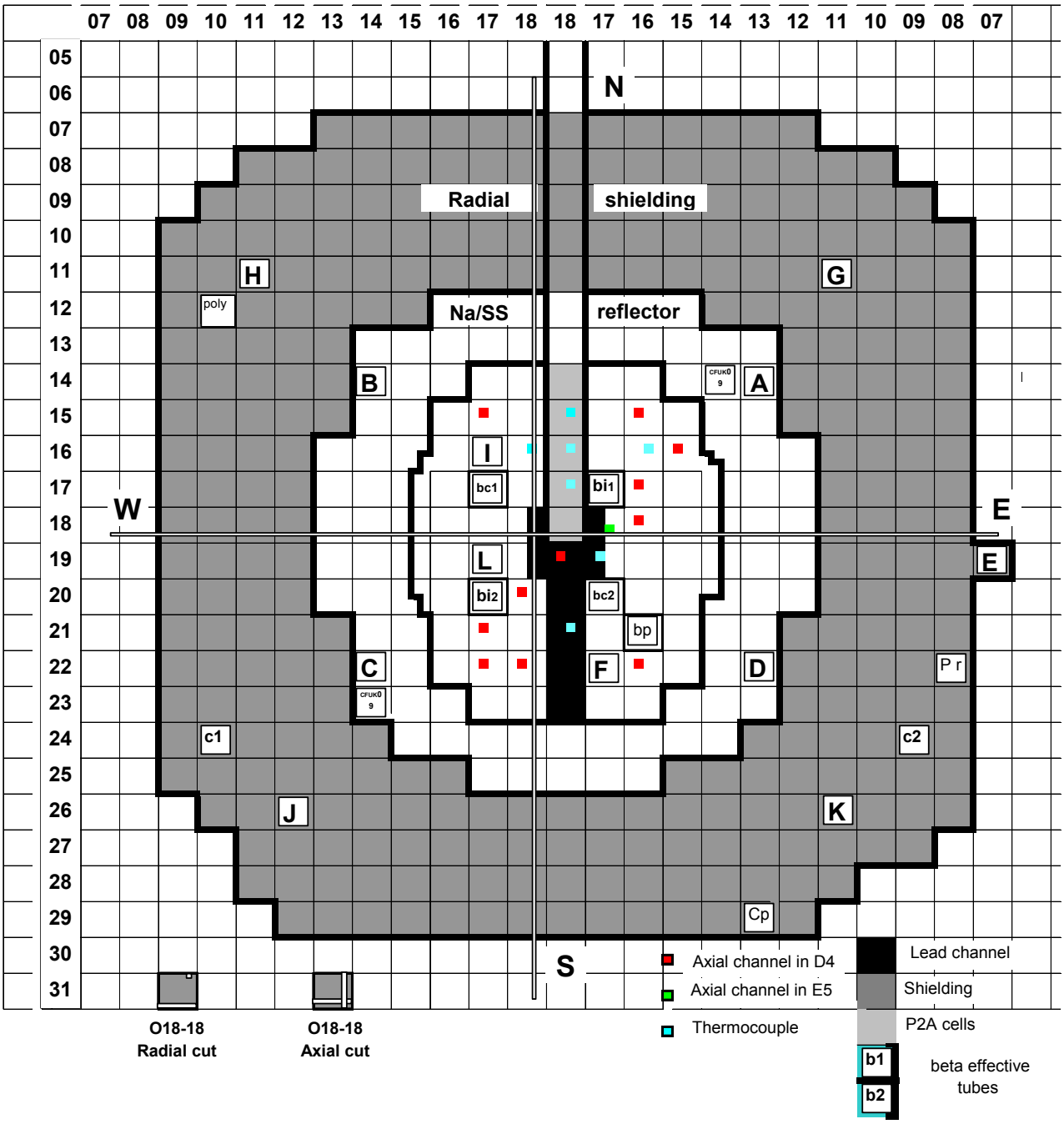

Figure 7: MUSE-4 Reference Configuration 1119 Cells

- 09/13/2001 ➔ 11/20/2001: **critical** configuration with 1114 fuel cells (see **Figure 8**).

The two special subassemblies used for delayed neutron fraction measurements were unloaded. Then, this period was mainly dedicated to:

- the power calibration;
- the importance distribution measurements with a ^{252}Cf source introduced in East/West and North/South radial channels and four axial channels (E19-18, W22-17, E16-15, W20-18);
- the irradiation of thick foils of various isotopes within the frame of the CEA/PSI collaboration **[14]**.

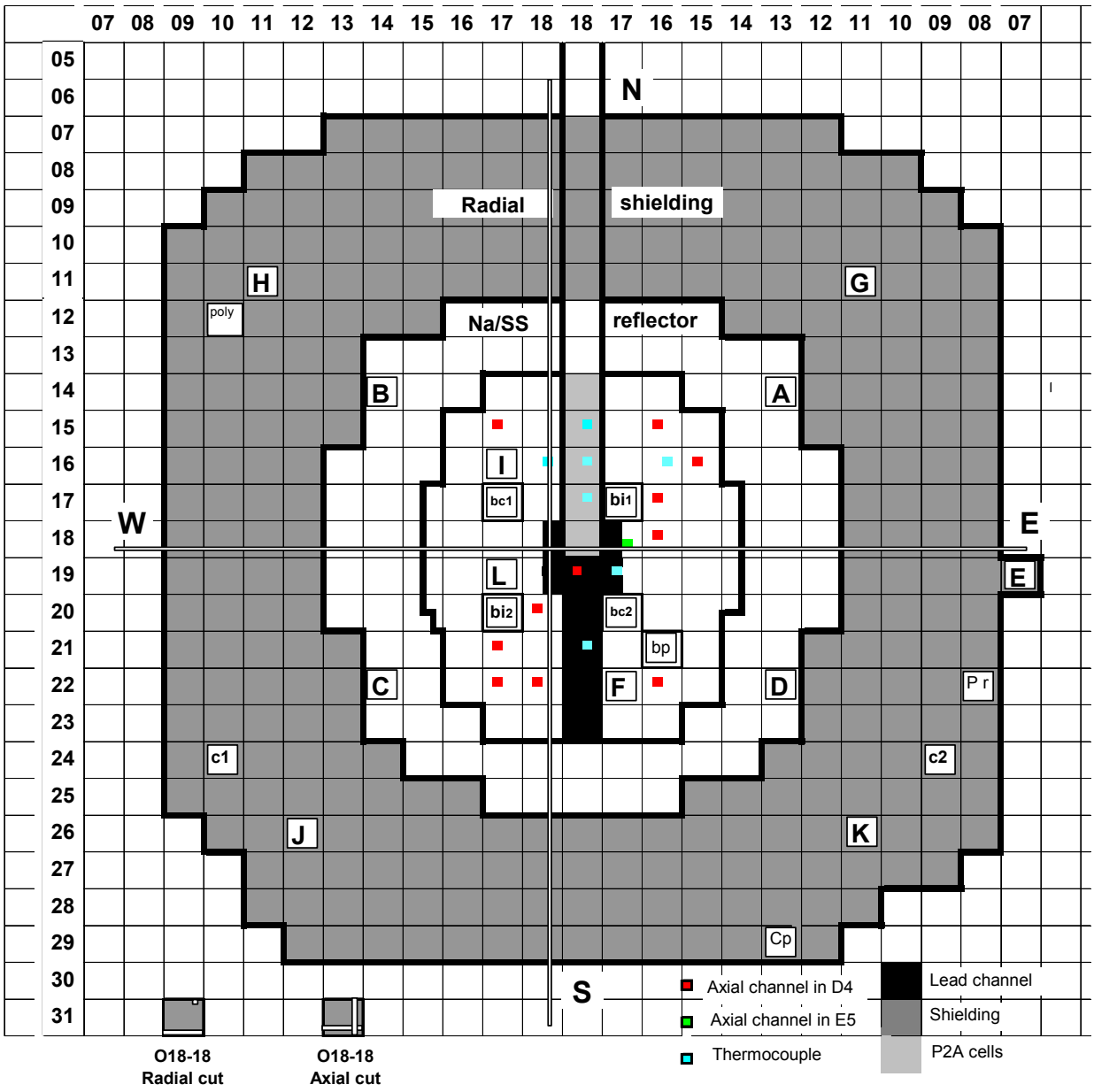

Figure 8: MUSE-4 Reference Configuration 1114 Cells

On November 13, 2001, the safety authorization to perform the experimental program with subcritical configurations was obtained. The subassemblies loading/unloading operations to move from the reference critical configuration to the SC0 subcritical configuration began on 11/20/2001 and ended on 11/23/2001 .

- 11/23/2001 ➔ 01/25/2002 : **subcritical** configuration with 1086 fuel cells (see **Figure 9**).

The first coupling of GENEPI and MASURCA with all rods up occurred on November 27, 2001. The reactivity level was about –167 cents. In December, the annual statutory tests were performed. Then, a short measurement program was performed in January 2002 to test and to improve the CEA acquisition system performances. This configuration included the three fixed ISN subassemblies as well as the ISN mobile tube at the E23-17 position.

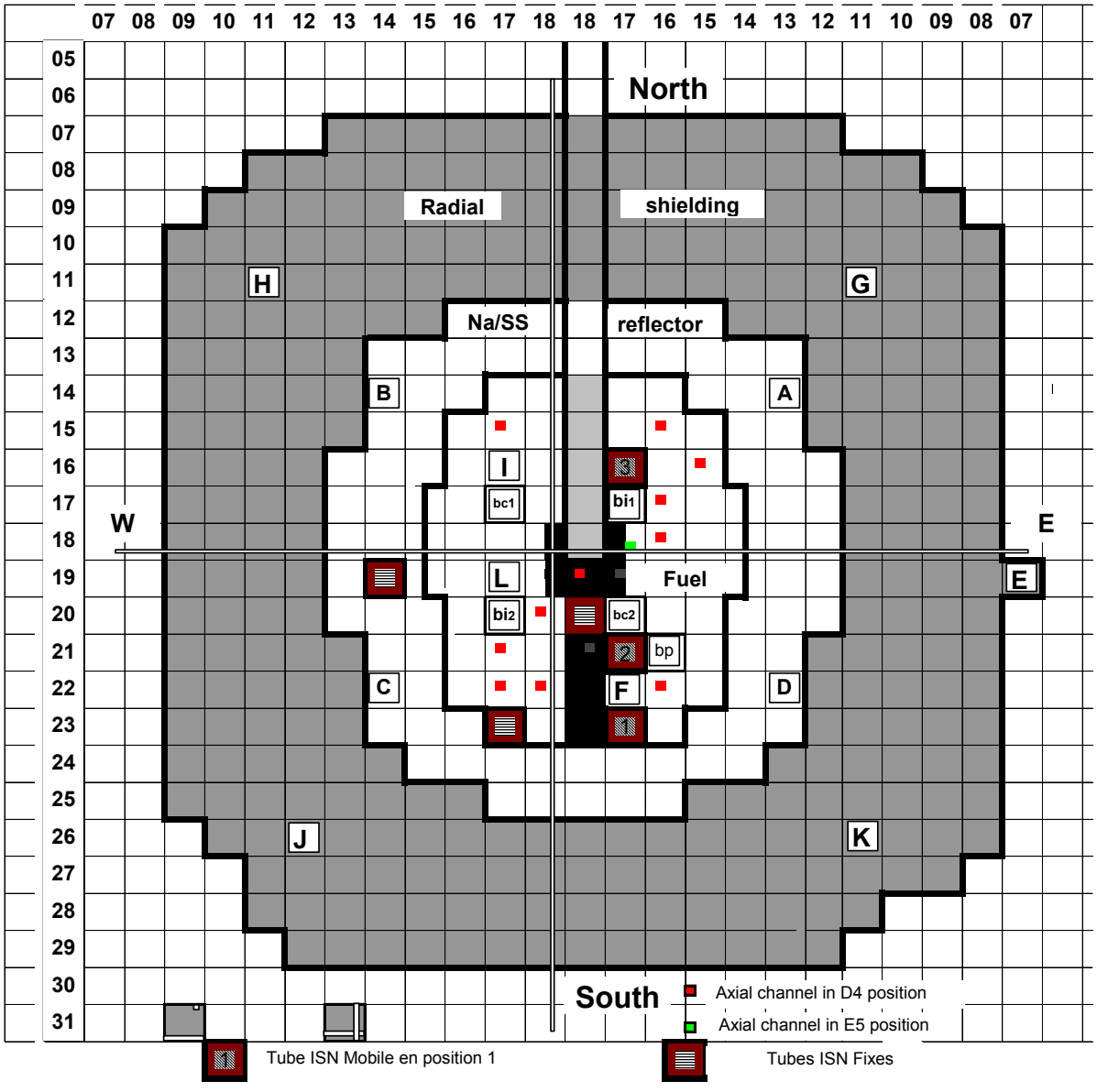

Figure 9: MUSE-4 SC0 Configuration 1086 Cells

- 02/06/2002 ➔ 03/18/2002: **critical** configuration with 1115 fuel cells (see **Figure 10**).

After a short measurement program in a clean sub critical state (clean means "with all control rods up"), the reference configuration was carried out again. One more fuel cell was loaded to compensate the ^{241}Pu decay. Noise techniques were performed with the pilot rod down. The corresponding reactivity level of this configuration was determined by the well known modified source method (MSM) using the twelve detectors located in the core and radial reflector: ρ = -0,352 ± 0,02 \$ (1\$=1β_{eff}). Nevertheless, the MSM factors used to infer this reference reactivity level were calculated considering a critical configuration with 1112 fuel cells **[21].**

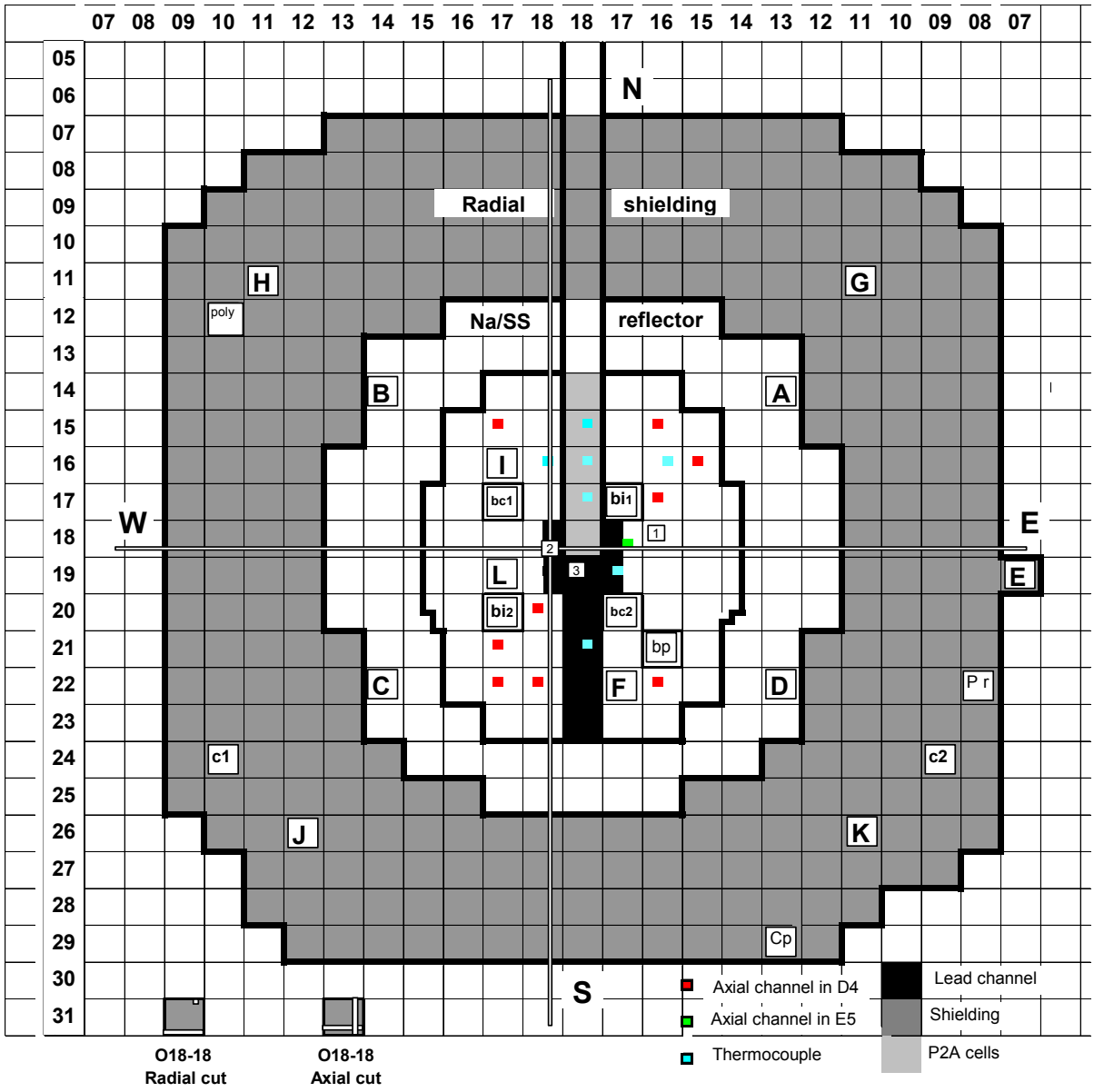

Figure 10: MUSE-4 Reference Configuration 1115 Cells

- 03/21/2002 ➔ 04/24/2002: **critical** configuration with 1115 fuel cells (see **Figure 11**).

Monitors A and B were respectively reversed with G and H. The first phase of time marking measurements continued in this configuration. Sub critical configurations were obtained by inserting the pilot rod or a safety rod.

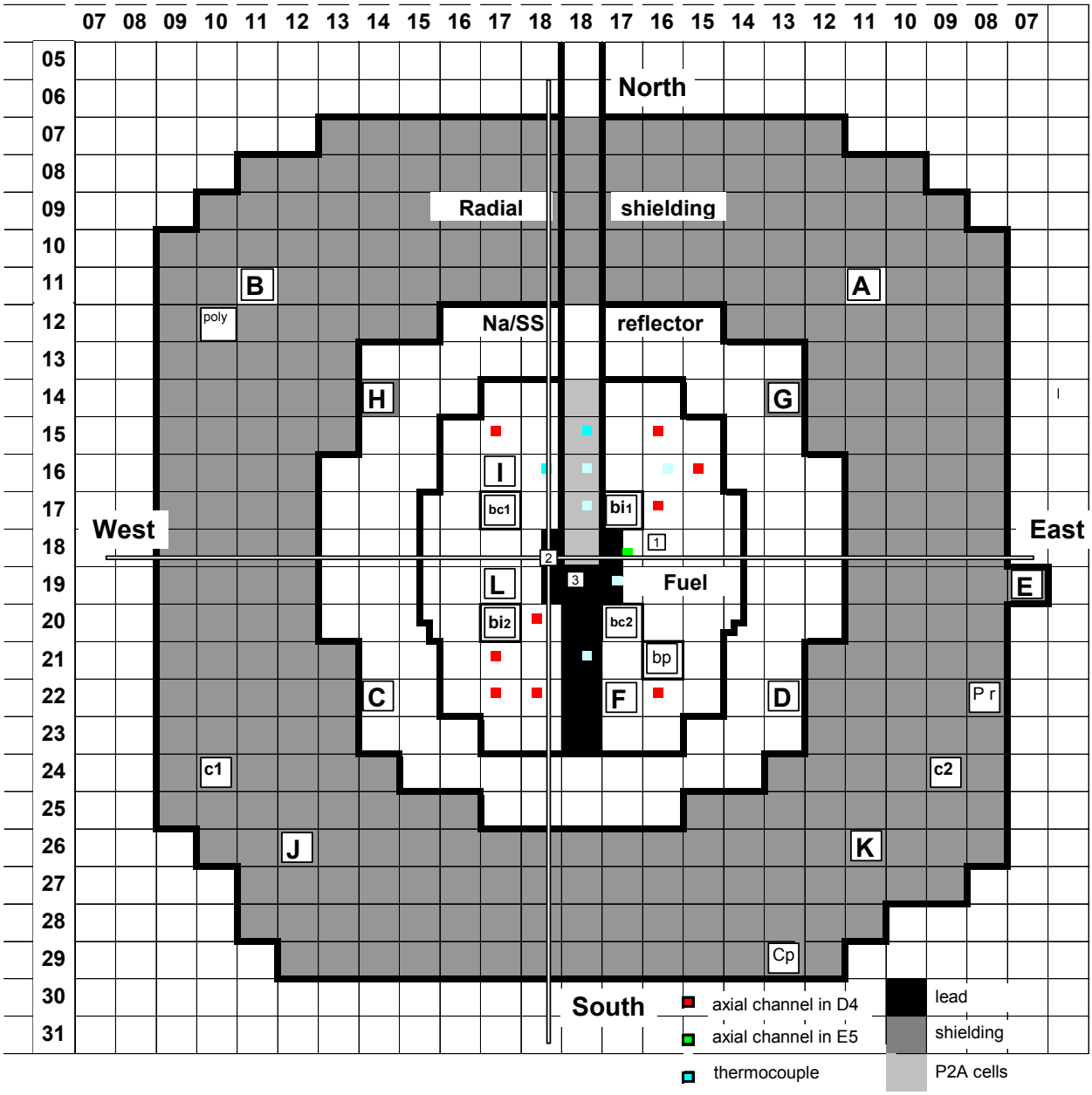

Figure 11: MUSE-4 Reference Configuration 1115 Cells

- 04/25/2002 ➔ 09/08/2002 : **critical** configuration with 1115 fuel cells (see **Figure 12**).

The monitors A and B were again reversed with G and H. At delayed critical (~-330 pcm), an extensive measurement program was carried out. Reaction rate traverses and spectral indices were performed for fourteen isotopes: ^{10}B, ^{237}Np, ^{233}U, ^{235}U, ^{238}U, ^{238}Pu, ^{239}Pu, ^{240}Pu, ^{241}Pu, ^{242}Pu, ^{241}Am, ^{243}Am, ^{244}Cm (only indices) and ^{232}Th. These acquisitions were carried out in six different channels (two radial and four axial). The entire list of all the reaction rates and spectral indices performed on this configuration is presented in **Ref. 14**. One will note that:

- some measurements with ^{10}B chamber are unusable. The operating conditions for this detector are too complicated. Moreover, this kind of detector is not really suitable for fast spectra.
- The ^{241}Pu fission chamber is rather old and it contains an important amount of Am241.

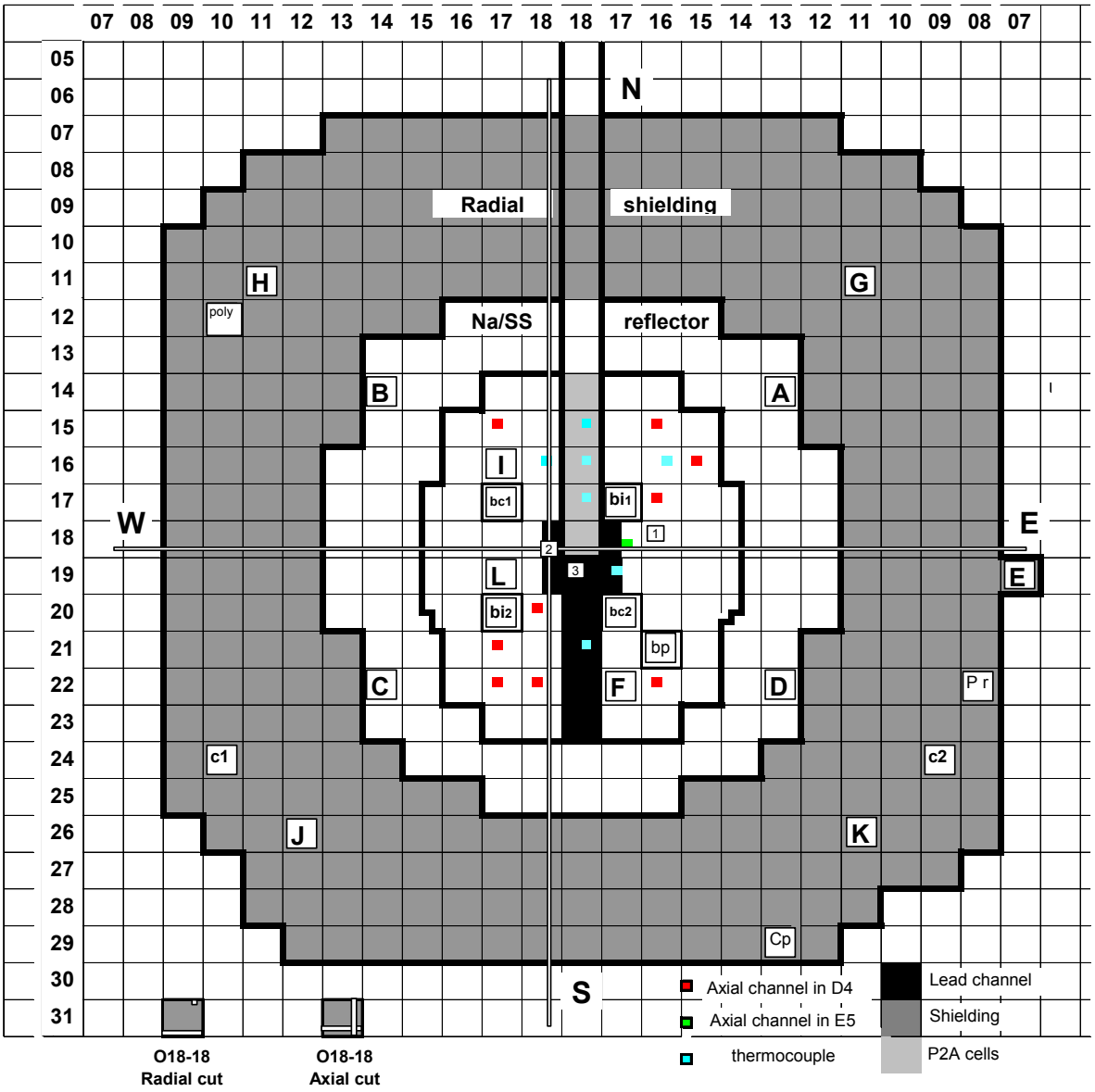

Figure 12: MUSE-4 Reference Configuration 1115 Cells

Several sub critical states were also carried out, with safety rod n°2 and/or the pilot rod inserted, to perform noise measurements.

Two foil irradiations were performed at the same time within the frame of the CEA/PSI collaboration.

- 09/12/2002 ➔ 09/16/2002: **critical** configuration with 1132 fuel cells (see **Figure 13**).

Two special subassemblies with a high efficiency ^{235}U fission chamber (CFUK09) inside, were loaded to perform β_{eff} measurements in current mode. The fission chamber was surrounded with CH_2 to increase the signal and the correlation level. During this period, the connection between CFUK09 and the acquisition system had to be set up under the core. The safety policy authorized this temporary solution until the end of March 2003. This modification needs no safety requirement.

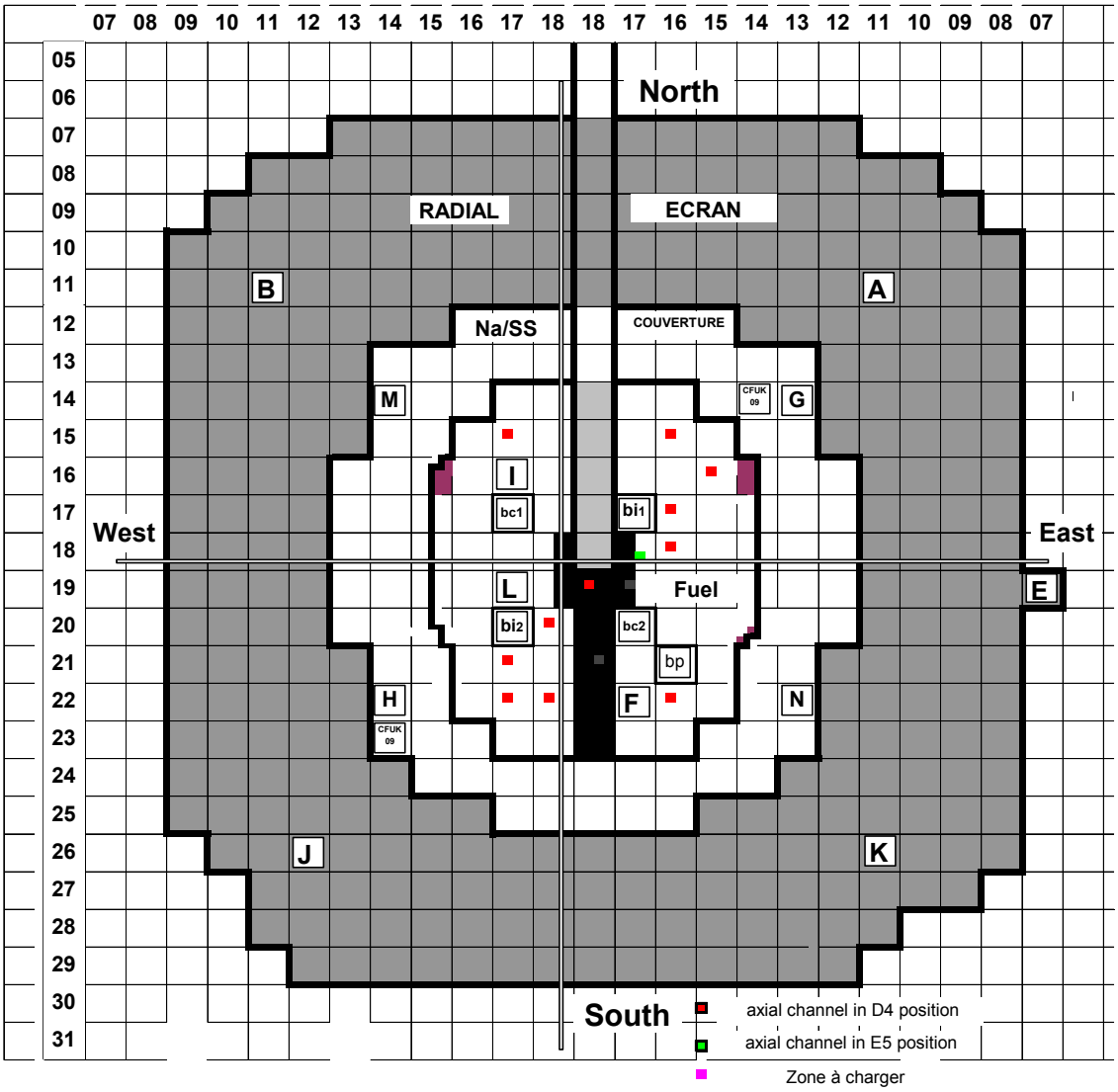

Figure 13: MUSE-4 Reference Configuration 1132 Cells

- 09/24/2002 ➔ 09/27/2002: **critical** configuration with 1125 fuel cells (see **Figure 14**).

The two previous special subassemblies used for β_{eff} measurements were unloaded to replace CH_2 by aluminum around the fission chamber. In such conditions, there is not enough correlation and it was shown that it was not possible to have satisfying β_{eff} values.

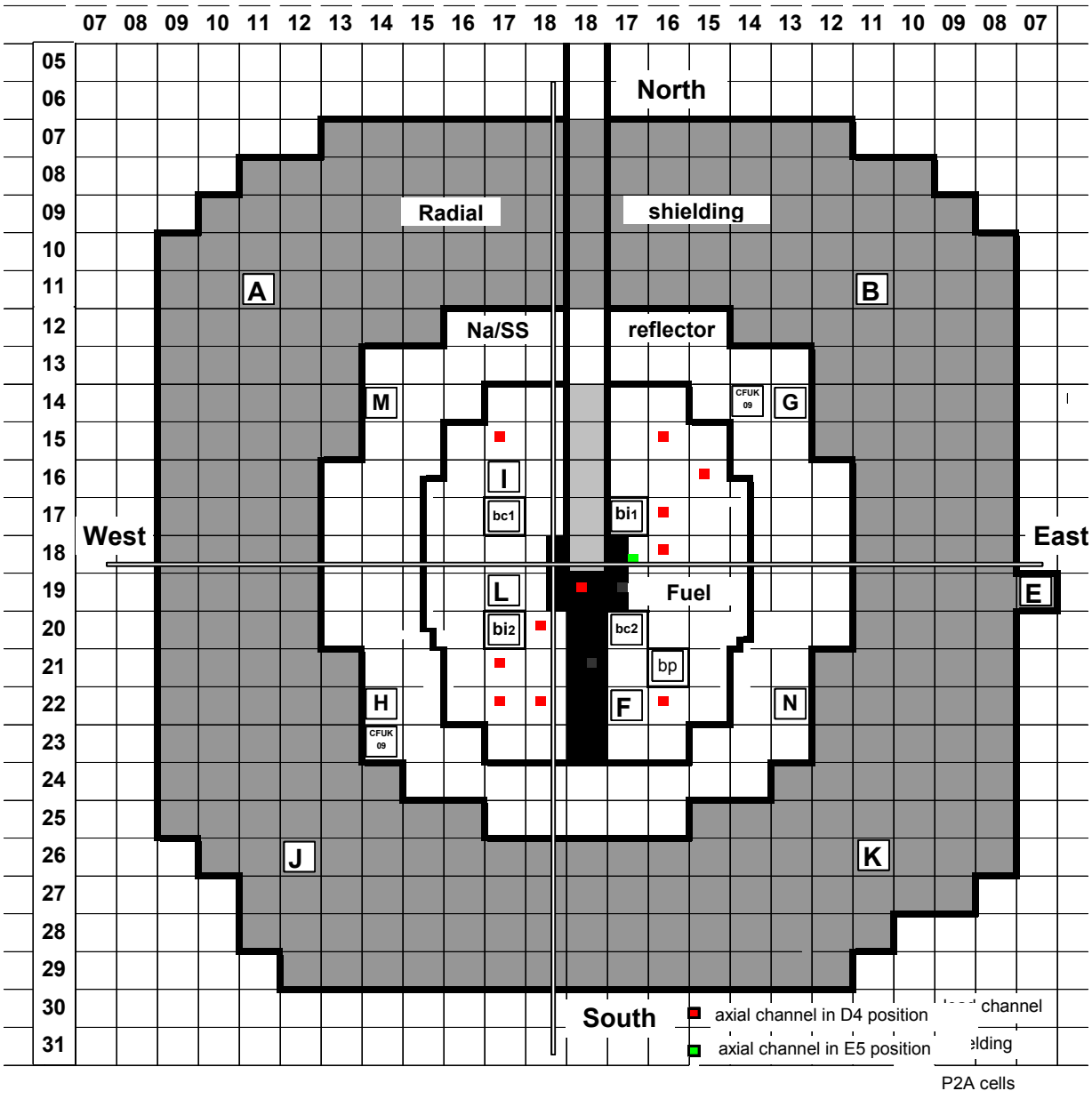

Figure 14: MUSE-4 Reference Configuration 1125 Cells

- 10/22/2002 ➔11/15/2002: SC0 **subcritical** configuration with the (t,d) target (see **Figure 15**).

This configuration showed the real beginning of measurement campaigns with clean sub critical configurations ("clean" means "with all rods up"). The number of fuel cells was reduced to 1108, which corresponds to a subcriticality level of –190 cents. The ISN mobile tube was not loaded.

^{235}U reaction rate traverses and spectral indices were performed in the 2 radial experimental channels with GENEPI ON.

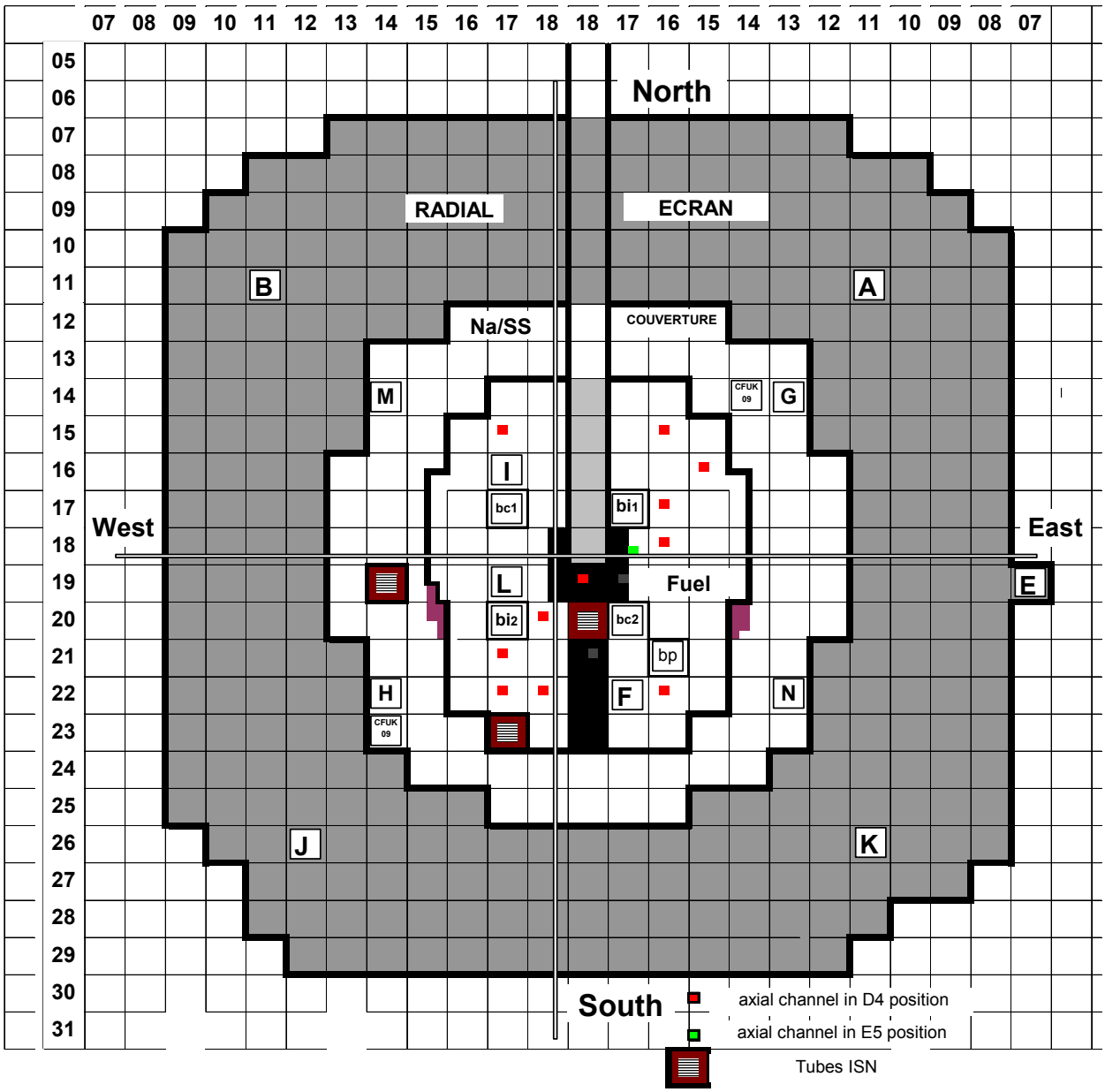

Figure 15: MUSE-4 SC0 Configuration 1108 Cells

- 11/15/2002 ➔01/20/2003: no measurement

The (t,d) target was replaced by the (t,t) target from November 18 th to November 22 th. Then, annual statutory tests have been carried out until the end of the year 2002. During this period, some work on GENEPI was achieved. In particular, the GENEPI filament was changed three times. Several electronic components were also replaced.

These modifications were not foreseen and generated a delay of two weeks.

- 01/21/2002 ➔ 03/14/2003: SC0 **subcritical** configuration with the (t,t) target (see **Figure 16**).

The source calibration was from January 21st to January 24th.

Then, ^{235}U and ^{238}U reaction rate traverses and spectral indices were performed in the 2 radial experimental channels with GENEPI ON. ^{235}U reaction rates traverse and spectrum indices were also performed in the NS radial experimental channel with GENEPI OFF.

Adjoint flux importance distributions and jerk measurements with a ^{252}Cf source introduced in the East/West radial channel were performed. This external source was about 2.05 10^9 n/s on November 11, 2002. In collaboration with PSI, irradiations of thick foils of various isotopes were performed.

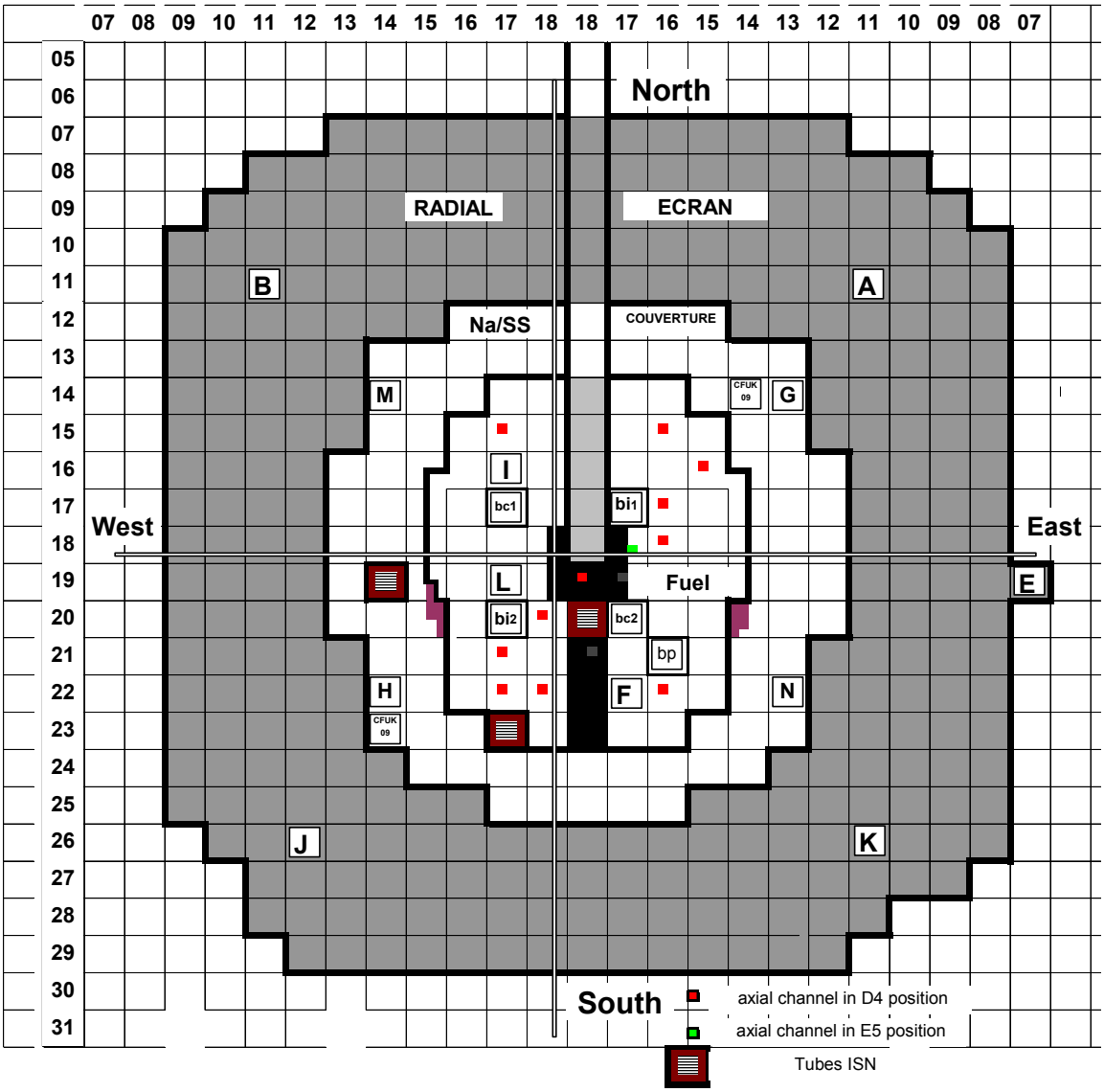

Figure 16: MUSE-4 SC0 Configuration 1108 Cells

- 03/17/2002 ➔ 03/21/2003: Going from the SC0 to the SC2 configuration.

Loading/unloading operations to move from the SC0 configuration to the SC2 configuration were from March 17th to March 20th because of some problems with the handling machine. The number of fuel cells became 1006.

III. Calculations in support of the MUSE-4 Project

III.A. Reactivity measurement and calculation.

For the reactivity calculation, the ERANOS (v. 1.2) code suite **[22]** was used, in conjunction with the JEF2.2 **[23]**, ENDF/B-V and ENDF/B-VI libraries. The multigroup cross sections have been condensed in different

number of energy groups, in order to investigate the effects on the reactivity results. The processing of the cross-sections has been performed via the ECCO code **[24]** in conjunction with the JEF2.2 library only, and via the MC^2-2 code **[25**] using any nuclear data. Nodal transport theory has been used in three dimensions with the VARIANT code **[26]**. A simplified configuration **[12]** has been investigated, with no PERMALI and BUTEE30 in the ECRAX region. The "DIFFUSEUR" has been omitted and opportunely replaced by the REFLECTOR. Finally an accurate homogenization has been performed for the beam duct region (void + AG3 + lead + diffuseur). The impact of each approximation has been fully investigated.

Both the experimental and the calculated results with the associated uncertainties have been summarized in **Tables 4** to **7** for each nuclear data set. The details are given in the **Sections III.A.1., III.A.2. and III.A.3**.

The JEF2.2-ECCO calculation results have been already presented in the **Ref. 12**. For comparison, the results are recalled in this section. The processing of the cross-sections with the MC^2-2 code performs the correction of the P_1 within-group scattering required by the balance of the terms in the P_1 transport equations, when the current is chosen as weighting function for the total cross section (see **Appendix A** for details)

Table 4: Experimental and JEF2.2-ECCO Calculated Reactivities

Reactivity [pcm]	**MUSE-4 Reference**	**MUSE-4 SC0**	**MUSE4-SC0 with BC1 down**
Experiment:	-80.1	-400	-3200 (PNS) -4200 (MSM)
Calculation			
Fine Energy Group Estimation	234.3	-26	-3729
Corrections:			
Angular expansion order 3	+71	+71	+71
Anisotropic scattering order 3	+80	+80	+80
Model simplification	-288	-222	-222
Best calculated estimation	+97.3	-97	-3800
Uncertanty			
Experiment: I_E	±150	±250	±400
Calculation			
Method	±77	±77	±77
Composition	±181	±181	±181
Modelisation	±66	±66	±66
Total: $I_C = \sqrt{\sum_x I_x}$	±208	±208	±208
Total uncertainty: $I_{tot} = \sqrt{I_C^2 + I_E^2}$	±257	±325	±451

Table 5: Experimental and ENDF/B-V-MC^2-2 Calculated Reactivities

Reactivity [pcm]:	**MUSE-4 Reference**	**MUSE-4 SC0**	**MUSE4-SC0 with BC1 down**
Experiment	-80.1	-400	-3200 (PNS) -4200 (MSM)
Calculation			
Fine Energy Group Estimation	177.7	-94.6	-3781
Corrections:			
Angular expansion order 3	+43	+43	+43
Anisotropic scattering order 3	+111	+111	+111
Model simplification	-288	-222	-222
Best calculated estimation	47.7	-158.6	-3845
Uncertanty			
Experiment: I_E	±150	±250	±400
Calculation			
Method	±77	±77	±77
Composition	±181	±181	±181
Modelisation	±66	±66	±66
Total: $I_C = \sqrt{\sum_x I_x}$	±208	±208	±208
Total uncertainty: $I_{tot} = \sqrt{I_C^2 + I_E^2}$	±257	±325	±451

Table 6: Experimental and ENDF/B-VI- MC^2-2 Calculated Reactivities

Reactivity [pcm]:	**MUSE-4 Reference**	**MUSE-4 SC0**	**MUSE4-SC0 with BC1 down**
Experiment	-80.1	-400	-3200 (PNS) -4200 (MSM)
Calculation			
Fine Energy Group Estimation	826.0	527.6	-3012
Corrections:			
Angular expansion order 3	+47	+47	+47
Anisotropic scattering order 3	+116	+116	+116
Model simplification	-288	-222	-222
Best calculated estimation	711	478.6	-3061
Uncertainty			
Experiment: I_E	±150	±250	±400
Calculation			
Method	±77	±77	±77
Composition	±181	±181	±181
Modelisation	±66	±66	±66
Total: $I_C = \sqrt{\sum_x I_x}$	±208	±208	±208
Total uncertainty: $I_{tot} = \sqrt{I_C^2 + I_E^2}$	±257	±325	±451

Table 7: Experimental and JEF2.2- MC^2-2 Calculated Reactivities

Reactivity [pcm]:	**MUSE-4 Reference**	**MUSE-4 SC0**	**MUSE4-SC0 with BC1 down**
Experiment	-80.1	-400	-3200 (PNS) -4200 (MSM)
Calculation			
Fine Energy Group Estimation	362.5	207.3	-3415
Corrections:			
Angular expansion order 3	+57	+57	+57
Anisotropic scattering order 3	+82	+82	+82
Model simplification	-288	-222	-222
Best calculated estimation	199.5	110.3	-3512
Uncertanty			
Experiment: I_E	±150	±250	±400
Calculation			
Method	±77	±77	±77
Composition	±181	±181	±181
Modelisation	±66	±66	±66
Total: $I_C = \sqrt{\sum_x I_x}$	±208	±208	±208
Total uncertainty: $I_{tot} = \sqrt{I_C^2 + I_E^2}$	±257	±325	±451

III.A.1. MUSE-4 reference configuration

For the MUSE-4 reference critical configuration (see **Figure 3**) the reactivity scale has been determined by the usual techniques employed on the MASURCA facility and consequently the measured reactivity level of the experimental loading, with the Pilot rod (PR rod) fully inserted **[17]** is:

$K_{eff} = 0.99920 \pm 0.00150$; ($\rho = -80.1 \pm 150$ pcm).

The determination of the reactivity level has been achieved through different steps as follows.

1. **Effect due to the energy group number.**

   The simplifications performed on the model allowed to use a double symmetry with respect to the axes X and Z. In this condition a deterministic calculation with an higher number of energy groups (NG) compared with the usual 33 groups simulations was possible (NG=838 in the JEF2-ECCO case, NG=887 when processing the cross-sections with the MC^2-2 code). The following table shows the reactivity change with NG and **Figures 17** to **20** show the results of an extrapolation up to the fine group structure (NG=1968 and NG=2032 in the ECCO and MC^2-2 case respectively).

Table 8: MUSE-4 Reference Configuration - K_{eff} ECCO - VARIANT

NG	JEF2.2 - ECCO	
	VARIANT(1) - ERANOS:	
	K_{eff}	ρ [pcm]
33 (2)	0.989920	-1018.3
299 (2)	0.999191	-81.0
471 (2)	1.000556	55.6
838 (2)	1.001788	178.5

Table 9: MUSE-4 Reference Configuration - K_{eff} MC^2-2 - VARIANT

NG	ENDF/B-V – MC^2-2		ENDF/B-VI – MC^2-2		JEF2.2 – MC^2-2	
	VARIANT(1) - ERANOS:		VARIANT(1) - ERANOS:		VARIANT(1) - ERANOS:	
	K_{eff}	ρ [pcm]	K_{eff}	ρ [pcm]	K_{eff}	ρ [pcm]
33 (2)	0.986766	-1341.2	0.993063	-698.5	0.990570	-952
231 (2)	0.994357	-567.5	0.999737	-26.3	0.996389	-362.4
460 (2)	0.998390	-161.3	1.004710	468.8	0.999894	-10.6
887 (2)	1.000866	86.5	1.007437	738.2	1.002668	266.1

(1) Flux and leakage expansion order 3 WITH SIMPLIFIED SPHERICAL HARMONIC (HS)
(2) With condensation from a fine step to NG

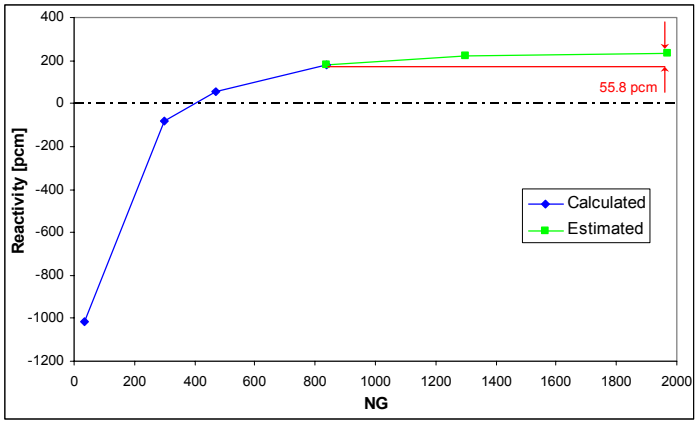

Figure 17: MUSE-4 Ref. - Reactivity JEF2.2 – ECCO

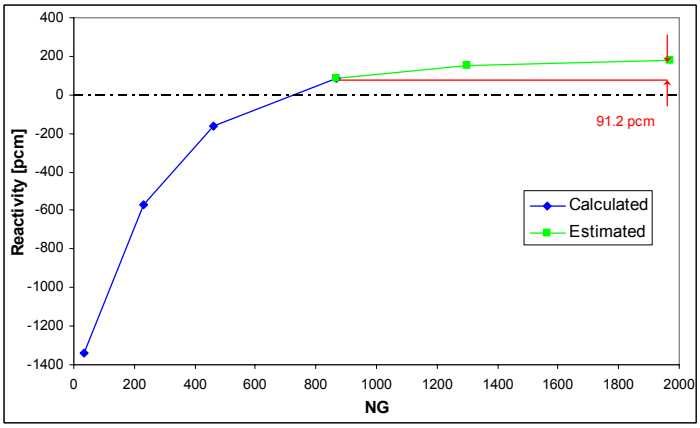

Figure 18: MUSE-4 Ref. - Reactivity ENDF/B-V – MC^2-2

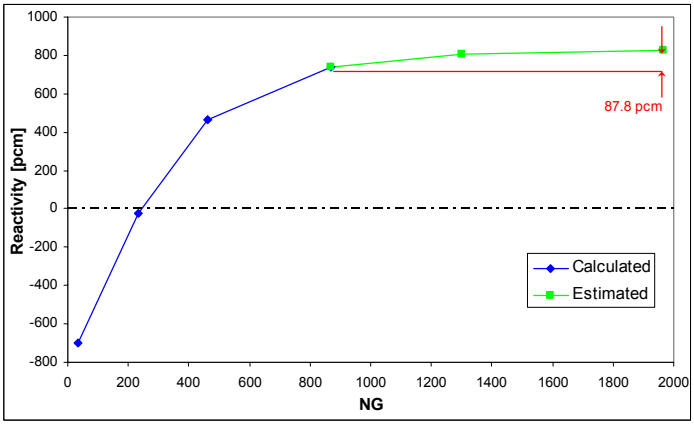

Figure 19: MUSE-4 Ref. - Reactivity ENDF/B-VI – MC^2-2

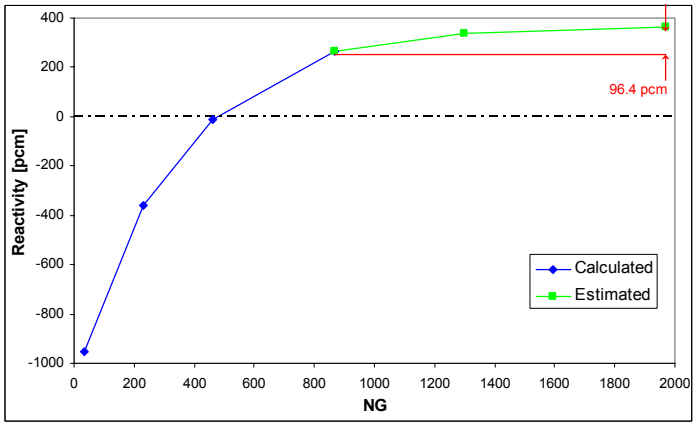

Figure 20: MUSE-4 Ref. - Reactivity JEF2.2 – MC^2-2

The multiplication factor (reactivity) at the end of the step 1 is:

JEF2.2-ECCO-VARIANT: K_{eff} = 1.002349 (ρ = 234.3 pcm)

ENDF/B-V – MC^2-2 – VARIANT: K_{eff} = 1.001780 (ρ = +177.7 pcm)

ENDF/B-VI – MC^2-2 – VARIANT: K_{eff} = 1.008329 (ρ = +826.0 pcm)

JEF2.2 – MC^2-2 – VARIANT: K_{eff} = 1.003638 (ρ = +362.5 pcm)

2. Effect due to the flux and leakage full angular expansion order 3 (P3) in the transport calculation.

The order of this correction has been taken from the Benchmark calculation, where it was calculated with NG=33 for the MUSE3 REF configuration **[12]**:

Table 10: MUSE4 Critical Config. - Transport P3 (Full Flux and Leakage Expansion Order 3) Correction

MUSE4 Critical – NG=33	HS – ρ [pcm]	P3 – ρ [pcm]	Δ ρ = P3 - HS
JEF2.2 – ECCO	-1354	-1283	+71
ENDF/B-V – MC^2-2	1530	1577	+47
ENDF/B-VI – MC^2-2	2292	2349	+57
JEF2.2 – MC^2-2	2304	2347	+43

The multiplication factor (reactivity) at the end of the step 2 is:

JEF2.2-ECCO-VARIANT: K_{eff} = 1.003062 (ρ = 305.3 pcm)

ENDF/B-V – MC^2-2 – VARIANT: K_{eff} = 1.002252 (ρ = 224.7 pcm)

ENDF/B-VI – MC^2-2 – VARIANT: K_{eff} = 1.008909 (ρ = 883.0 pcm)

JEF2.2 – MC^2-2 – VARIANT: K_{eff} = 1.004072 (ρ = 405.5 pcm)

3. Effect due to the anisotropic order 3 (P3) transport calculation.

The order of this correction has been taken from the Benchmark calculation, where it was calculated with NG=33 for the MUSE3 REF configuration **[12]**:

Table 11: MUSE4 Critical Configuration - Anisotropic Order 3 Transport Correction

MUSE4 Critical – NG=33	P1 – ρ [pcm]	P3 – ρ [pcm]	Δρ = P3 – P1
JEF2.2 – ECCO	-1354	-1274	+80
ENDF/B-V – MC^2-2	1530	1641	+111
ENDF/B-VI – MC^2-2	2292	2408	+116
JEF2.2 – MC^2-2	2304	2386	+82

The multiplication factor (reactivity) at the end of the step 3 is:

JEF2.2-ECCO-VARIANT: K_{eff} = 1.003868 (ρ = 385.3 pcm)

ENDF/B-V – MC^2-2 – VARIANT: K_{eff} = 1.003368 (ρ = 335.7 pcm)

ENDF/B-VI – MC^2-2 – VARIANT: K_{eff} = 1.010091 (ρ = 999.0 pcm)

JEF2.2 – MC^2-2 – VARIANT: K_{eff} = 1.004899 (ρ = 487.5 pcm)

4. Effect due to the geometrical simplification of the model.

The order of this impact is essentially due to the omission of the structures PERMALI, BUTEE and "DIFFUSEUR", of the measurement channels and to the homogenization of the beam duct. The effects have been separately investigated and even if they have been calculated via JEF2.2-ECCO they are supposed to be the same for each simulation.

- *Omission of PERMALI*. The correction has been evaluated with a 3D transport calculation and 33 energy groups, anisotropic scattering order 1 (P_1), simplified spherical harmonics (HS): Δρ (with – without PERMALI) = -1 pcm
- *Omission of BUTEE*. The correction has been evaluated with a 3D transport calculation and 33 energy groups, anisotropic scattering order 1 (P_1), simplified spherical harmonics (HS): Δρ (with – without BUTEE) = -11 pcm
- *Omission of the "DIFFUSEUR"*. The correction has been evaluated for a RZ model representing the MUSE3 configuration with a S_8P_1 transport calculation and 33 energy groups: Δρ (with – without "DIFFUSEUR") = -296 pcm.

  The result has been validated by a Monte-Carlo calculation.
- *Omission of the measurement channel*. The correction hasn't been provided yet by the experimentalists for the MUSE-4 configurations. It has been taken from the previous experiment MUSE3: Δρ (with – without measurement channels) = -66 pcm.
- *Homogenization of the beam duct*. The correction has been estimated comparing the results obtained with the homogenized composition and with a more accurate description of the beam duct (AG3 and void region separated). The calculations have been performed in transport 3D with 33 energy groups, anisotropic scattering order 1 (P_1), simplified spherical harmonics (HS): Δρ (homogenized – no homogenized beam duct) = +86 pcm.

The total effect from the geometrical simplifications of the model is -288 pcm.

The multiplication factor (reactivity) at the end of the step 3 is:

JEF2.2-ECCO-VARIANT: K_{eff} = 1.000974 (ρ = 97.3 pcm)

ENDF/B-V – MC^2-2 – VARIANT: K_{eff} = 1.000477 (ρ = 47.7 pcm)

ENDF/B-VI – MC^2-2 – VARIANT: K_{eff} = 1.007161 (ρ = 711.0 pcm)

JEF2.2 – MC^2-2 – VARIANT: K_{eff} = 1.001999 (ρ = 199.5 pcm)

5. Effect due to the Pu241 decay.

This effect is supposed null for the present analysis as the compositions have been updated to the date of the experiment: January 9, 2001.

Taking in account all the correction above mentioned, the best estimated result for the calculated multiplication factor consequently is:

JEF2.2-ECCO-VARIANT: K_{eff} = 1.000974 (ρ = 97.3 pcm)

ENDF/B-V – MC^2-2 – VARIANT: K_{eff} = 1.000477 (ρ = 47.7 pcm)

ENDF/B-VI – MC^2-2 – VARIANT: K_{eff} = 1.007161 (ρ = 711.0 pcm)

JEF2.2 – MC^2-2 – VARIANT: K_{eff} = 1.001999 (ρ = 199.5 pcm)

In order to compare the calculation with the experiment, one should take into account the uncertainty associated both with the simulation and the experiment. In this context, for the MUSE-4 reference configuration the uncertainty associated to the reactivity measurement has been estimated to be equal to I_E = 150 pcm. Concerning the calculation, the uncertainty has been determined as follows:

1. *Uncertainty associated to the calculation method.*

   The same value adopted for the MUSE3 analysis has been applied. It was determined with a comparison of the K_{eff} values obtained with TRIPOLI-4 (K_{T4}, with its associated dispersion I_{T4}) and an optimized deterministic JEF2.2-ECCO-ERANOS calculation (K_{ER} with its associated dispersion $I_{ER} = | K_{ER} - K_{T4}|$). The total uncertainty $I_{meth} = \sqrt{I_{ER}^2 + I_{T4}^2}$ of 77 pcm was estimated. The same uncertainty is assumed to apply to each simulation.

2. *Uncertainty associated to the compositions.*

   The value has been taken from previous studies, where it was deduced from the accuracy associated to the chemical analysis of the components of each medium: I_{compo} = 181 pcm (1σ). The same uncertainty is supposed to apply to each simulation.

3. *Uncertainty associated to the modelization.*

   As in the previous experiment MUSE3, a constant uncertainty of 20% (1σ) of each correction (omission of BUTEE, PERMALI, DIFFUSEUR, measurement channels and homogenization of the beam duct) has been applied. Finally, an uncertainty I_{temp} = 15 pcm is associated to the reproducibility of the experiment and another one, I_{load} = 13 pcm, refers to the loading of the core (indeed we don't take in account the exact loading, but an average lot of rodlets). The total uncertainty obtained by the square root of the sum of the square of each component is I_{mod} = 66 pcm. The same uncertainty is supposed to apply to each simulation.

With the assumption that the different sources of uncertainty are completely non-correlated, the total uncertainty associated to the calculated reactivity value is I_{calc} = 208 pcm.

Finally, the total absolute uncertainty: $I_{tot} = \sqrt{I_E^2 + I_{calc}^2}$ = 257 pcm.

The following observations can be made:

- This study shows a strong dependence of the calculated reactivity value on the number of energy groups used. Indeed, in order to accurately account for the spectral effects at the interface core/reflector a detailed multigroup energy treatment is needed **[27]**. By the way, significant difficulties occur when performing a deterministic calculation with a high number of energy groups: the computational resources, in term of time, disk space and memory, are very demanding. For this purpose, in **Appendix B** we propose different methods to process correctly the cross-sections over a broad group energy structure (e.g. with the usual NG=33), able to reproduce the same results (reactivity and reaction rate distributions) of the fine spatial calculation;
- The impact on the reactivity calculation due to the use of different nuclear data can be observed when the cross-sections are processed with the MC^2-2 code: moving from the ENDF/B-V to the ENDF/B-VI library causes a spread on the reactivity results of about 700 pcm. While the comparison between the JEF2.2-ECCO and JEF2.2- MC^2-2 results allows to estimate the effect due to the use of different codes (ECCO vs MC^2-2) when the nuclear data are the same: this effect is of about 150 pcm for the present configuration;
- The experiment-calculation discrepancy observed on the reactivity values fit well within the margin of the uncertainty in the cases JEF2.2-ECCO and ENDF/B-V - MC^2-2 ($\Delta \rho$ = 177 and 17 pcm respectively). Some difficulties appear when using the MC^2-2 code in conjunction with the JEF2.2 and ENDF/B-VI data. Note that among the sources of uncertainties there is of course also the uncertainty associated to the nuclear data that has not been considered in the present analysis.

III.A.2. MUSE-4 SC0 reference configuration

In this section the MUSE-4 SC0 configuration with pilot rod (PR) up has been investigated (see **Figure 9**).

The measured reactivity is -400 ± 250 pcm.

For reactivity calculations, the same procedure as for the reference configuration has been used.

The following table shows the reactivity change through NG and **Figures 21** to **24** show the results of an extrapolation up to the fine group structure (NG=1968 and NG=2032 in the ECCO and MC^2-2 case respectively). Note that the experimental channels are already included in the simulation.

Table 12: MUSE-4 SC0 Configuration with BP Out - K_{eff} ECCO - VARIANT

NG	JEF2.2 - ECCO	
	VARIANT(1) - ERANOS: K_{eff}	ρ [pcm]
33 (2)	0.987321	-1284.2
299 (2)	0.996572	-344
471 (2)	0.997990	-201.4
838 (2)	0.999234	-76.7

Table 13: MUSE-4 SC0 Configuration with BP Out - K_{eff} MC^2-2 - VARIANT

NG	ENDF/B-V – MC^2-2		ENDF/B-VI – MC^2-2		JEF2.2 – MC^2-2	
	VARIANT(1) - ERANOS: K_{eff}	ρ [pcm]	VARIANT(1) - ERANOS: K_{eff}	ρ [pcm]	VARIANT(1) - ERANOS: K_{eff}	ρ [pcm]
33 (2)	0.984211	-1604.2	0.990405	-968.8	0.989053	-1106.8
231 (2)	0.991704	-836.5	0.996994	-301.5	0.994924	-510.2
460 (2)	0.995727	-429.1	1.001821	181.8	0.998488	-151.4
887 (2)	0.998198	-180.5	1.004589	456.8	1.001204	120.3

(1) Flux and leakage expansion order 3 WITH SIMPLIFIED SPHERICAL HARMONIC (HS)
(2) With condensation from a fine step to NG

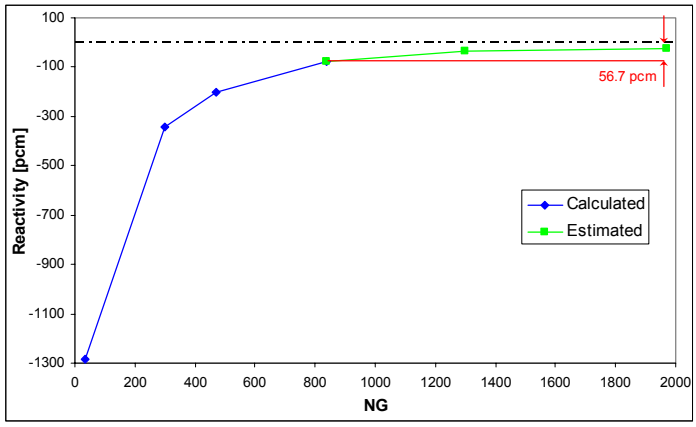

Figure 21: MUSE-4 SC0 - Reactivity JEF2.2 – ECCO

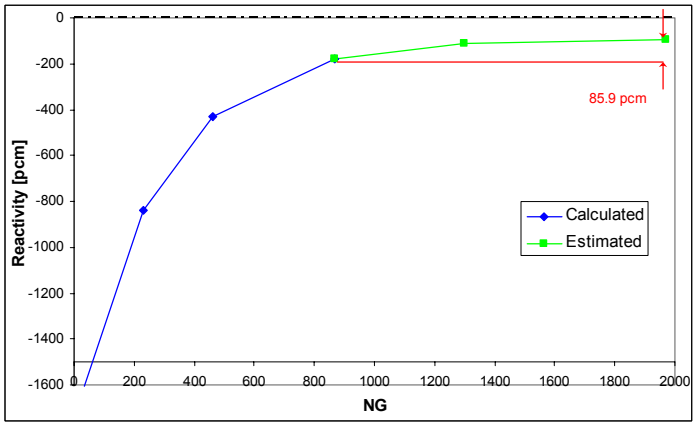

Figure 22: MUSE-4 SC0 - Reactivity ENDF/B-V – MC^2-2

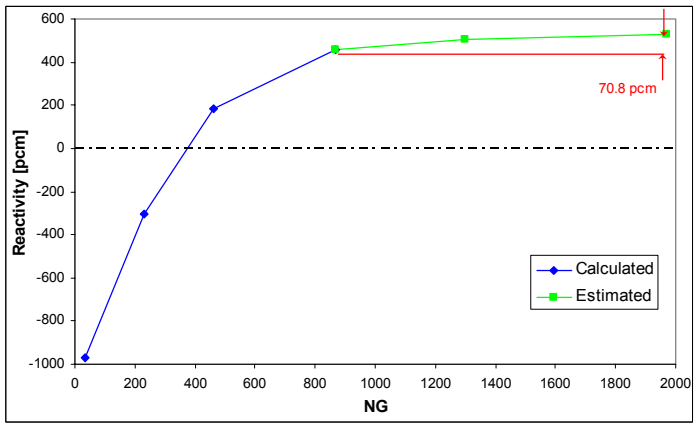

Figure 23: MUSE-4 SC0 - Reactivity ENDF/B-VI – MC^2-2

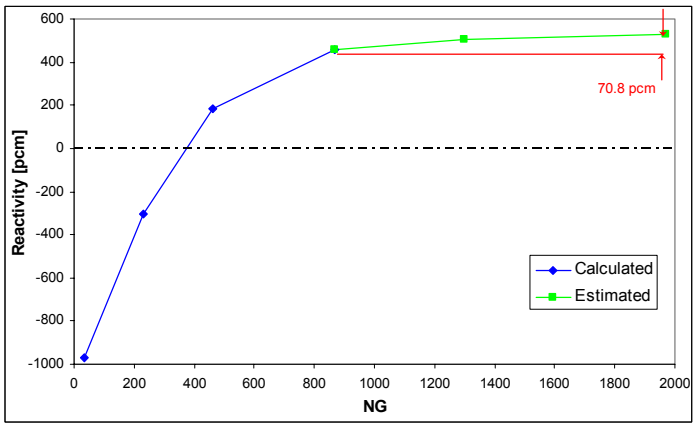

Figure 24: MUSE-4 SC0 - Reactivity JEF2.2 – MC^2-2

After extrapolation to the fine energy group structure, the multiplication factor (reactivity) is:

JEF2.2-ECCO-VARIANT: K_{eff} = 0.999740 (ρ = -26 pcm)

ENDF/B-V – MC^2-2 – VARIANT: K_{eff} = 0.999055 (ρ = -94.6 pcm)

ENDF/B-VI – MC^2-2 – VARIANT: K_{eff} = 1.005304 (ρ = 527.6 pcm)

JEF2.2 – MC^2-2 – VARIANT: K_{eff} = 1.002077 (ρ = 207.3 pcm)

Taking in account all the corrections (angular expansion order 3, anisotropic scattering order 3, geometrical simplifications of the model) as in the case of the reference configuration and reported in **Tables 4** to **7**, the best estimated result for the calculated multiplication factor is:

JEF2.2-ECCO-VARIANT: K_{eff} = 0.999031 (ρ = -97 pcm)

ENDF/B-V – MC^2-2 – VARIANT: K_{eff} = 0.998417 (ρ = -158.6 pcm)

ENDF/B-VI – MC^2-2 – VARIANT: K_{eff} = 1.004809 (ρ = 478.6 pcm)

JEF2.2 – MC^2-2 – VARIANT: K_{eff} = 1.001104 (ρ = 110.3 pcm)

The uncertainty associated to the calculation has been supposed to be the same of the reference configuration. The uncertainty associated to the experiment is 250 pcm. Consequently the total uncertainty becomes 325**.**

Investigating the reactivity calculated results and their comparison with the experimental ones, observations similar to the reference configuration can be made.

The results presented in this section also apply to the MUSE-4 SC0 configuration with pilot rod (PR) inserted if corrected by the reactivity worth of the pilot rod which has been estimated by the experimentalists equal to -140 pcm.

III.A.3. MUSE-4 SC0 reference configuration with bc1 inserted

In this section the MUSE-4 SC0 configuration with control rod BC1 and pilot rod (PR) inserted has been investigated (see **Figure 9**).

The measured reactivity is -3200 pcm (by PNS method), -4200 pcm (by MSM method). The MSM method determines subcritical reactivities by ratios of count rates corrected for changes in detector efficiencies and source importance between two subcritical states. In the PNS method, information on the subcritical level is deduced from the decay of the response P(t) arising from an external neutron pulse.

The wide discrepancy (-4200 vs. –3200 pcm) obtained using the two methods is being investigated by the experimentalists.

The experimental uncertainty is ± 400 pcm.

For reactivity calculations, the same procedure as for the reference configuration has been used.

The following table shows the reactivity change through NG and **Figures 25** to **28** show the results of an extrapolation up to the fine group structure (NG=1968 and NG=2032 in the ECCO and MC^2-2 case respectively). Note that the experimental channels are already included in the simulation.

Table 14: MUSE-4 SC0 Configuration with BC1 and PR Inserted - K_{eff} ECCO - VARIANT

NG	JEF2.2 - ECCO	
	VARIANT(1) - ERANOS:	
	K_{eff}	ρ [pcm]
33 (2)	0.952524	-4984.2
299 (2)	0.961091	-4048.4
471 (2)	0.962347	-3912.6
838 (2)	0.963489	-3789.5

Table 15: MUSE-4 SC0 Configuration with BC1 and BP Inserted - K_{eff} MC^2-2 - VARIANT

NG	ENDF/B-V – MC^2-2		ENDF/B-VI – MC^2-2		JEF2.2 – MC^2-2	
	VARIANT(1) - ERANOS:		VARIANT(1) - ERANOS:		VARIANT(1) - ERANOS:	
	K_{eff}	ρ [pcm]	K_{eff}	ρ [pcm]	K_{eff}	ρ [pcm]
33 (2)	0.949659	-5300.9	0.956657	-4530.7	0.954693	-4745.7
231 (2)	0.956634	-4533.2	0.962812	-3862.4	0.960162	-4149.1
460 (2)	0.960377	-4125.8	0.967314	-3379.1	0.963481	-3790.3
887 (2)	0.962675	-3877.2	0.969900	-3103.4	0.966010	-3518.6

(1) Flux and leakage expansion order 3 WITH SIMPLIFIED SPHERICAL HARMONIC (HS)
(2) With condensation from a fine step to NG

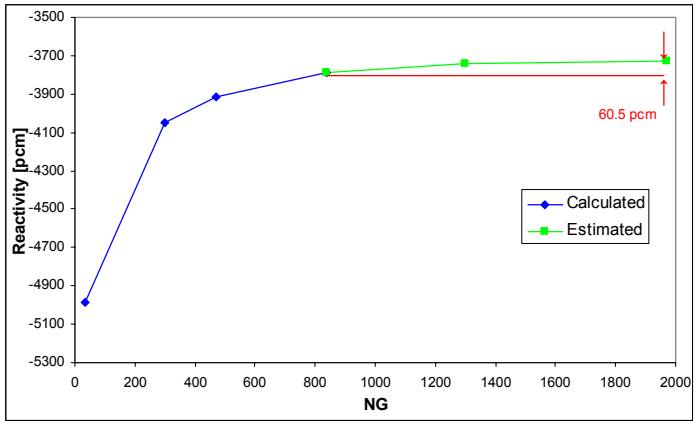

Figure 25: MUSE-4 SC0 (BC1 in) - Reactivity JEF2.2 – ECCO

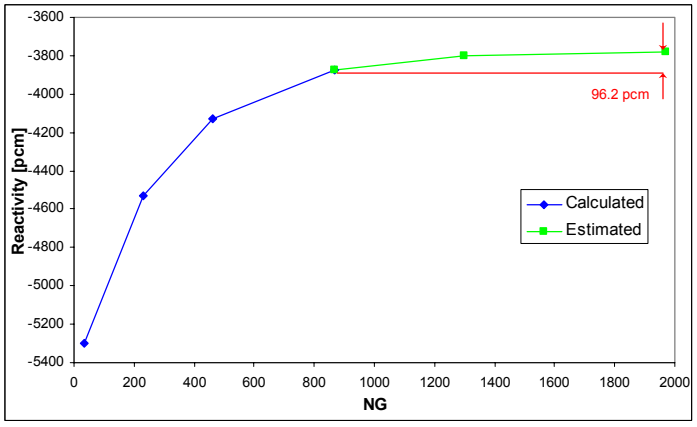

Figure 26: MUSE-4 SC0 (BC1 in) - Reactivity ENDF/B-V – MC^2-2

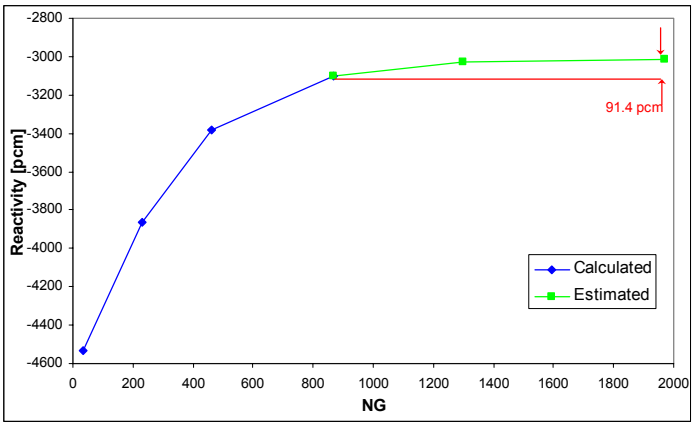

Figure 27: MUSE-4 SC0 (BC1 in) - Reactivity ENDF/B-VI – MC^2-2

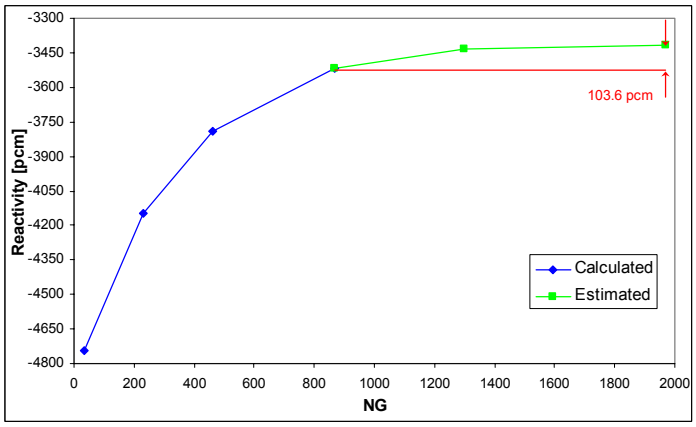

Figure 28: MUSE-4 SC0 (BC1 in) - Reactivity JEF2.2 – MC^2-2

After extrapolation to the fine energy group structure, the multiplication factor (reactivity) is:

JEF2.2-ECCO-VARIANT: K_{eff} = 0.964051 (ρ = -3729 pcm)

ENDF/B-V – MC^2-2 – VARIANT: K_{eff} = 0.963568 (ρ = -3781 pcm)

ENDF/B-VI – MC^2-2 – VARIANT: K_{eff} = 0.970761 (ρ = -3012 pcm)

JEF2.2 – MC^2-2 – VARIANT: K_{eff} = 0.966978 (ρ = -3415 pcm)

Taking in account all the corrections (angular expansion order 3, anisotropic scattering order 3, geometrical simplifications of the model) as in the case of the reference configuration and reported in **Tables 4** to **7**, the best estimated result for the calculated multiplication factor is:

JEF2.2-ECCO-VARIANT: K_{eff} = 0.963391 (ρ = -3800 pcm)

ENDF/B-V – MC^2-2 – VARIANT: K_{eff} = 0.962974 (ρ = -3845 pcm)

ENDF/B-VI – MC^2-2 – VARIANT: K_{eff} = 0.970299 (ρ = -3061 pcm)

JEF2.2 – MC^2-2 – VARIANT: K_{eff} = 0.966072 (ρ = -3512 pcm)

The uncertainty associated to the calculation has been supposed to be the same of the reference configuration. The uncertainty associated to the experiment is 400 pcm. Consequently the total uncertainty becomes 451.

Investigating the reactivity calculated results and their comparison with the experimental ones, observations similar to the reference configuration can be seen.

III.B. Adjoint flux measurement and calculation.

We perform in this section the analysis of the experimental traverses with californium source **[28]** for the MUSE-4 reference configuration (see **Figure 3**). These traverses represent the adjoint flux distribution **[28]**.

Axial and radial distributions are analyzed. The axial traverses have been performed at the positions E1615, E1818, W2018 and W2217. The positions E1615 and W2217 are relatively unperturbed, while the position E1918 is in the lead buffer zone and W2018 is near both to the lead buffer zone and to a control rod. The channel locations, shown in **Figure 3**, have also been represented in 3 dimensions in Fig.29 and 30 to provide an illustration of their configuration:

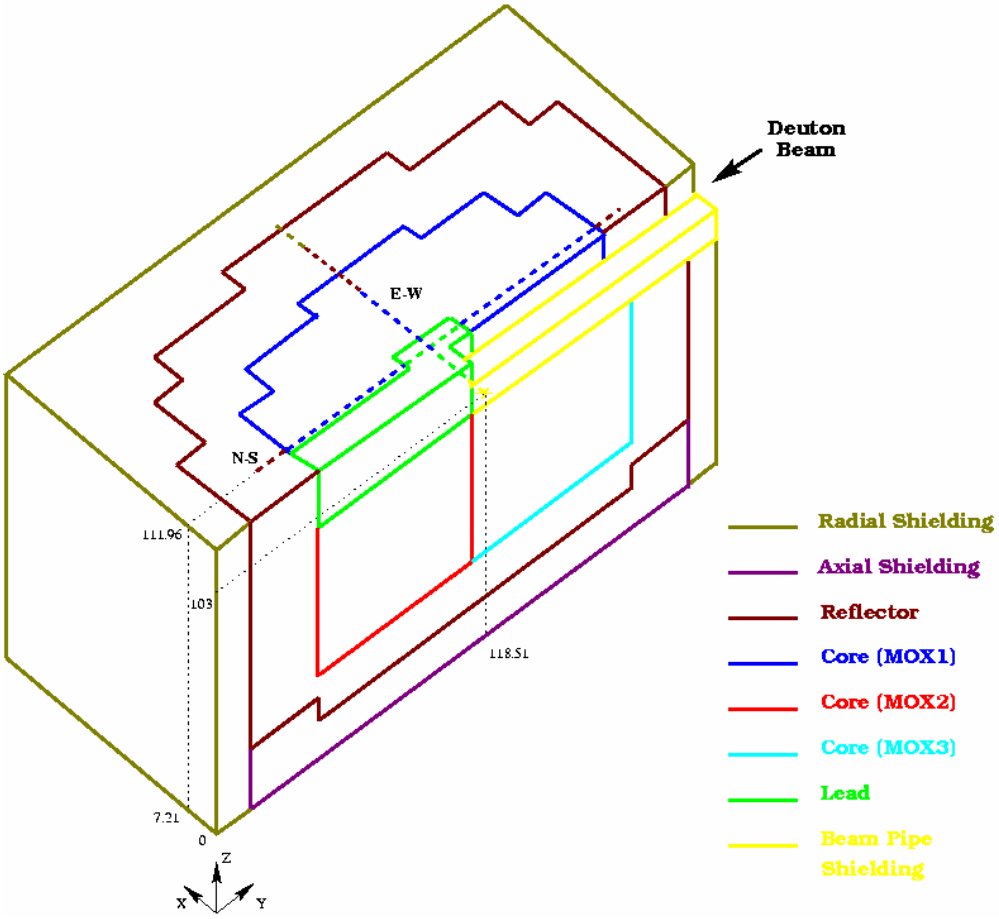

Figure 29: MUSE-4 Critical Configuration – Horizontal Channels Locations

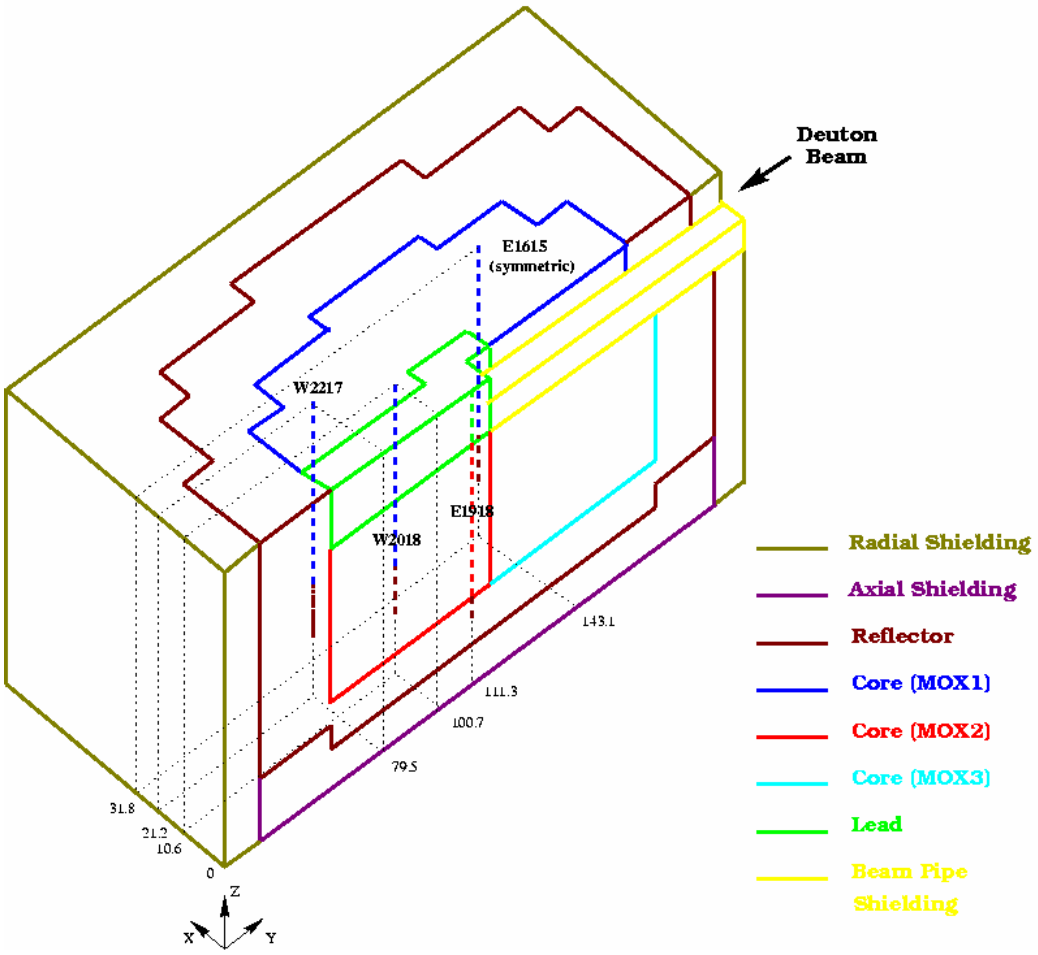

Figure 30: MUSE-4 Critical Configuration – Axial Channels Locations

The traverses were made at two reactivity levels: roughly –70 pcm with the pilot rod (PR) down and roughly –20 pcm with the PR at 600 mm. North-South (NS) and East-West (EW) radial traverses were also performed for the two reactivities.

The calculation results have been performed with the ERANOS code **[22]** suite in conjunction with the JEF2.2 **[23],** ENDF/B-V and ENDF/B-VI libraries. The multigroup cross sections have been condensed in different number of energy groups, in order to investigate the effects on the calculated adjoint flux traverses. The processing of the cross-sections has been performed via the ECCO code **[24]** in conjunction with the JEF2.2 library only, and via the MC^2-2 code **[25**] using any nuclear data. The VARIANT code **[26]** was used with a three dimension geometry. All geometrical and material compositions are as shown for the model used to calculate the reactivity value. Transport theory was used in P_1 approximation. The core models assume that the Reference MUSE-4 configuration contains 1112 fuel cells (as given in **Ref. 17**). This corresponds to a total fuel mass of 1550.1 kg (using a mass of 0.697 kg as given in the MASURCA catalogue for MOX in one fuel rod). Note, however, that due to the Pu241 decay the number of fuel cells to achieve the criticality has increased to

1114 in October 2001. It is assumed that the subsequent effect on the calculated traverses is negligible. Then, a brief discussion on the observed results is given.

The following notation is introduced in the following: "B" as in "E1615B" refers to the deeper subcritical state (PR down) and "H" as in "E1615H" refers to the case with PR at 600 mm. The normalized adjoint flux has been measured from the count data according to the following relation:

$$\frac{\Phi_i^*}{\Phi_o^*} = \frac{C_i - C_r}{C_o - C_r} \qquad \textbf{Eq.1}$$

In this relation, the adjoint flux at the point *i* relative to the point *o* is proportional to the counts at those positions. The value is offset with respect to the reference (point *r*) by the amount corresponding to the intrinsic source.

The uncertainties related to the experimental data have been also provided for each monitor channel **[28]**. It was assumed that the best estimate of the normalized adjoint flux would be simply the average of the 10 monitor channels, and the associated uncertainty would be calculated using the following relation:

$$\frac{1}{\sigma_x^2} = \sum_j^N \frac{1}{\sigma_j^2} \qquad \textbf{Eq.2}$$

The calculation results show that the model does not accurately fit the adjoint flux outside the core when only 33 energy groups are used. The model consistently underestimates the adjoint flux in all the traverses (see **Figures 31** to **55**). Indeed, a correct description of the slowing down of the neutrons and their reflection in the fuel at the interface core/reflector, requires the use of a higher number of energy groups NG **[27]** (see section **III.A**).
In fact, the discrepancies are sharply reduced when NG increases. In this case, the calculations performed for example via JEF2.2-ECCO with NG = 299, 471, 838 show approximately the same results (see e.g. **Figure 31**), consequently a 299 energy group structure seems to be enough for the analysis of the experimental data. The same remark applies when the MC^2-2 code is used, but in this case 231 energy groups are employed instead of 299. Using 299 (or 231) energy groups the model still underestimates the adjoint flux, but the observed discrepancies seem to be within the margins if an uncertainty associated to the calculation would be taken in account together with the experimental one.

All the measured traverses have been studied, but in the following just the adjoint flux distributions observed with PR at 600 mm are discussed. Indeed, with PR down the measured and calculated results are about the same; slight differences appear just in the case of the E1918 traverse which is at the same time close to a control rod and it is also the closest traverse to the PR.

The use of different nuclear data libraries doesn't seem to affect the calculated adjoint flux distributions if the same number of energy group is used. In particular, this can be observed in **Figures 58** to **61** that compare the experimental data with the results provided with the ECCO code using the JEF2.2 data and via the MC2-2 code in conjunction with any library.

However, an asymmetry is observed in some data that is not seen in the model. This is especially true for the W2018H traverses (see **Figures 34, 40, 46, 52** and **58**), but it also appears for the E1918H traverse (see **Figures 33, 39, 45, 51** and **57**). At the present time, it is not clear whether the asymmetries seen in the data correspond to a real physical effect, or they are due to some bias.

- **E1615.**

  This axial traverse is far from potentially perturbing influences such as the lead buffer and control rods. Thus, an axial symmetry is expected, and, indeed, a careful examination of the data shows that this is true in both the cases with PR down and at 600 mm. The same is observed by the calculation.

- **E1918.**

  Even if this traverse passes through the lead buffer that could introduce an axial perturbation, a pretty symmetric shape, as it is seen in the calculation, would be expected. However, with PR at 600 mm, there is a shift towards the top of the core, which is not expected. This traverse was made in two steps (negative first, then positive at a later time), so it is possible that this procedure introduced a bias even though new zero and reference values were obtained.

- **W2018.**

  This axial traverse, for both PR positions, shows an asymmetry not seen in the calculation. In both cases, the adjoint flux is higher below the core midplane. The only axial asymmetry that could cause this behavior is the fact that this traverse is adjacent to a control rod. Normally it would be assumed that when the control rod is fully inserted there would be a little perturbation, but this is not confirmed by the data. Another potential cause is the translation of the data due to uncertainty in the position of the device. If the data are translated 25 mm upwards, we see a much better agreement with the calculation. This translation has been introduced in **Figures 34, 40, 46, 52** and **58**.

- **W2211.**

  In this case a complete unperturbed symmetry as for E1615 is expected, and this is confirmed by both data and calculation.

- **EW.**

  In the EW traverse, a slightly higher adjoint flux on the negative (West) side is observed, while the calculation is completely symmetric. There is an east-west asymmetry because the west side contains slightly more fuel, and PR is on the East side. More refined calculations are required to investigate this effect.

- **NS.**

  In the North-South traverse, the data are showing a higher adjoint flux on the negative (north) side, while the calculation are showing the reverse. It would be expected that the additional lead on the south would cause an importance enhancement. Because of the anomalous data of W2018, if a 25 mm translation of the data is performed the agreement with the calculation is improved. This translation has been introduced in **Figures 37, 43, 49, 55** and **61**.

In conclusion, there are some traverses that show unexplained anomalies. E1918H is suspicious because of the fact that the negative traverse was done at a different time than the positive ones, and there is a suspicious 25 mm translation in both the W2018H and NSH traverses. On the contrary, when no perturbation is present from control rods or lead, as for E1615 and W2217, we see excellent agreement between data and calculations, and there are no unexplained anomalies.

III.B.1. Use of the ECCO code in conjunction with the JEF2.2 data.

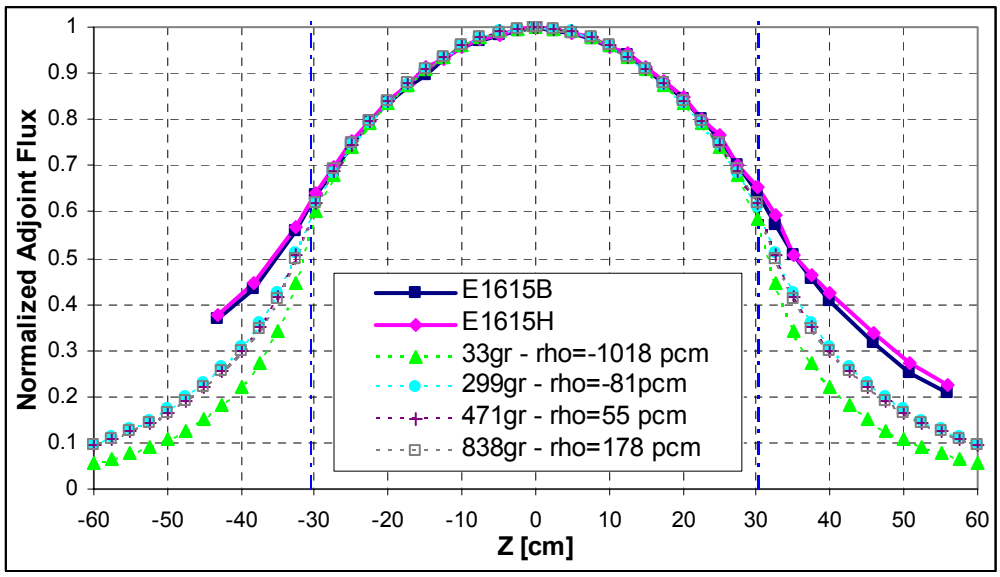

Figure 31: E1615 Effect due to the Energy Groups Number

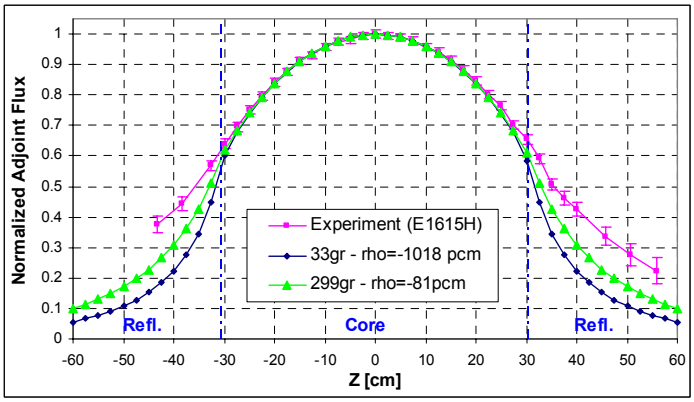

Figure 32: E1615H: JEF2-ECCO Calc./Exp. Comparison

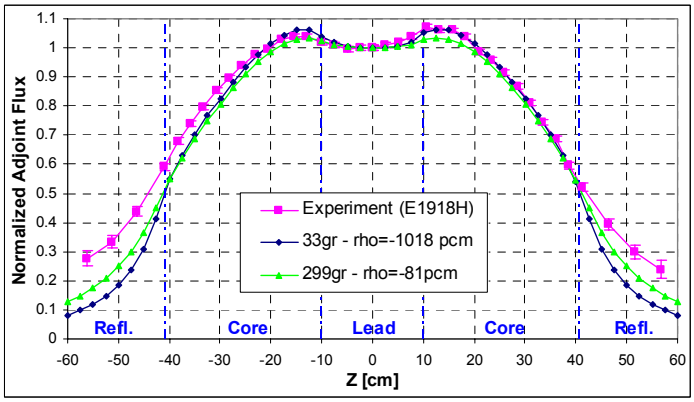

Figure 33: E1918H: JEF2-ECCO Calc./Exp. Comparison

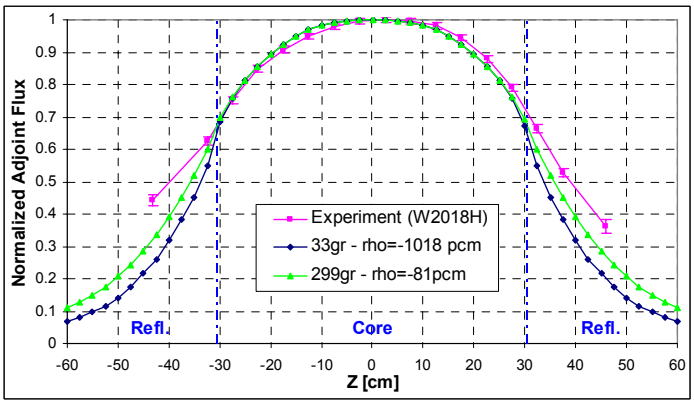

Figure 34: W2018H: JEF2-ECCO Calc./Exp. Comparison

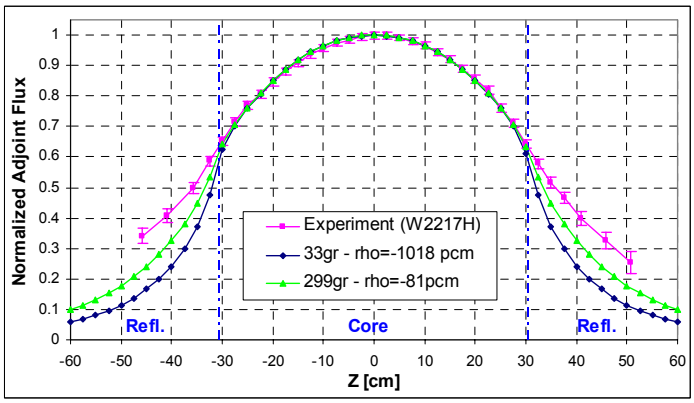

Figure 35: W2217H: JEF2-ECCO Calc./Exp. Comparison

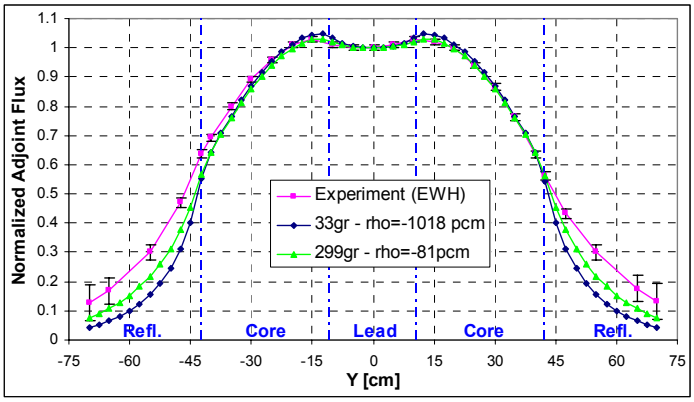

Figure 36: EWH: JEF2-ECCO Calc./Exp. Comparison

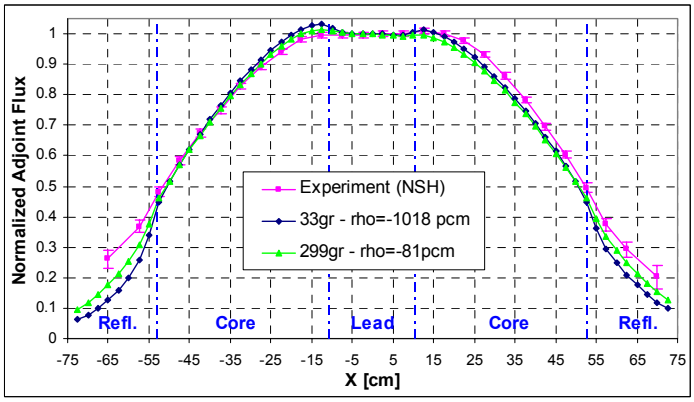

Figure 37: NSH: JEF2-ECCO Calc./Exp. Comparison

III.B.2. Use of the MC^2-2 code in conjunction with the ENDF/B-V data.

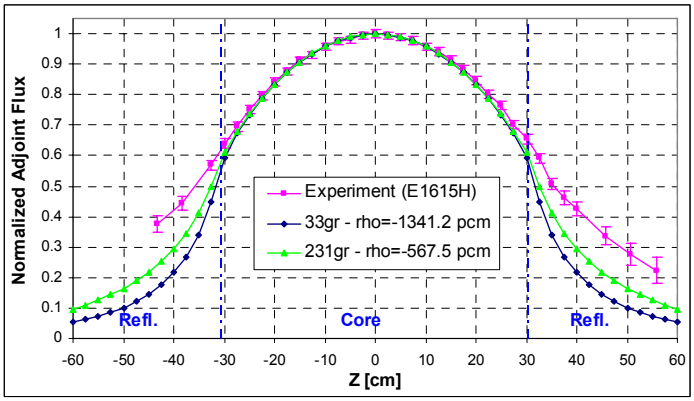

Figure 38: E1615H: ENDF/B-V-MC^2-2 Calc./Exp. Comparison

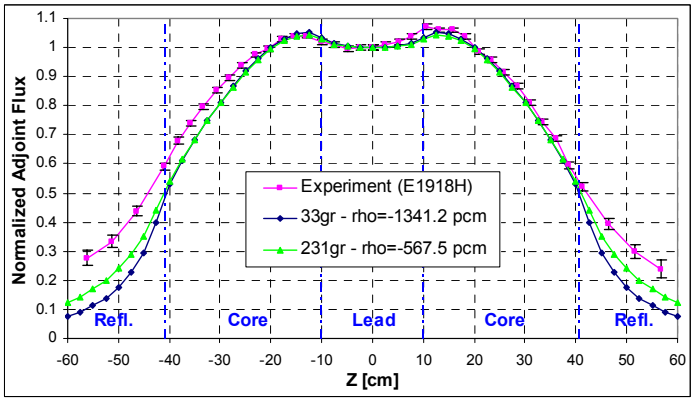

Figure 39: E1918H: ENDF/B-V-MC^2-2 Calc./Exp. Comparison

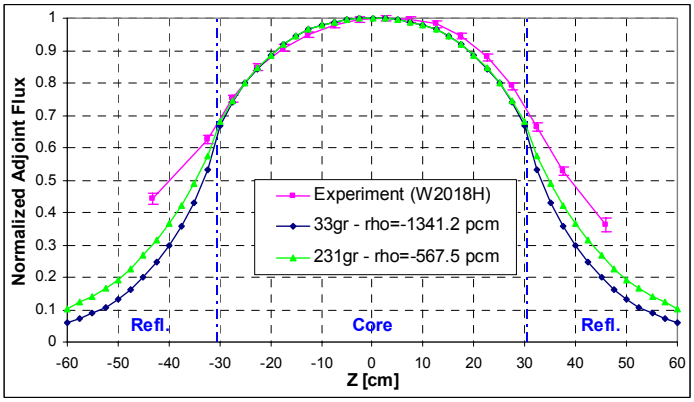

Figure 40: W2018H: ENDF/B-V-MC^2-2 Calc./Exp. Comparison

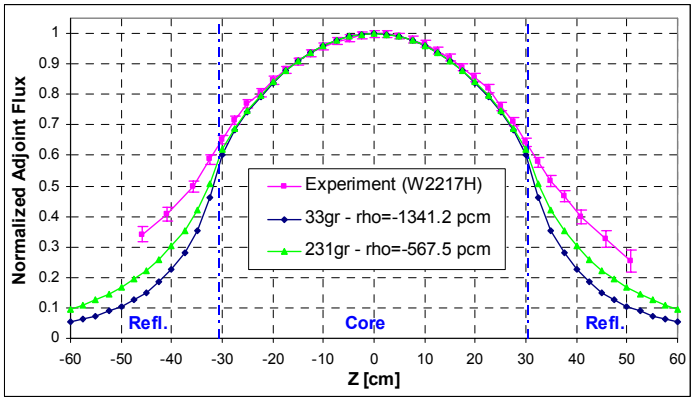

Figure 41: W2217H: ENDF/B-V-MC^2-2 Calc./Exp. Comparison

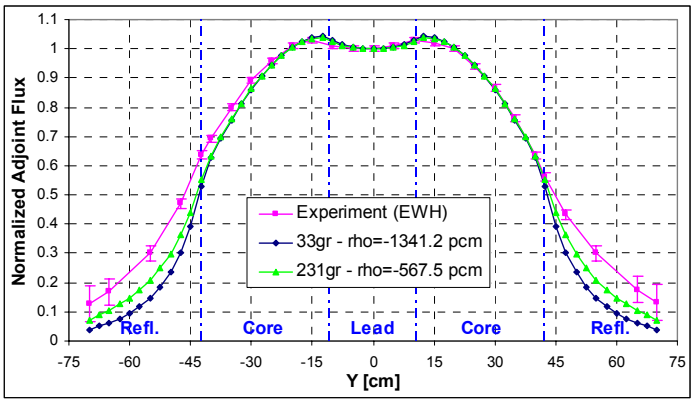

Figure 42: EWH: ENDF/B-V-MC^2-2 Calc./Exp. Comparison

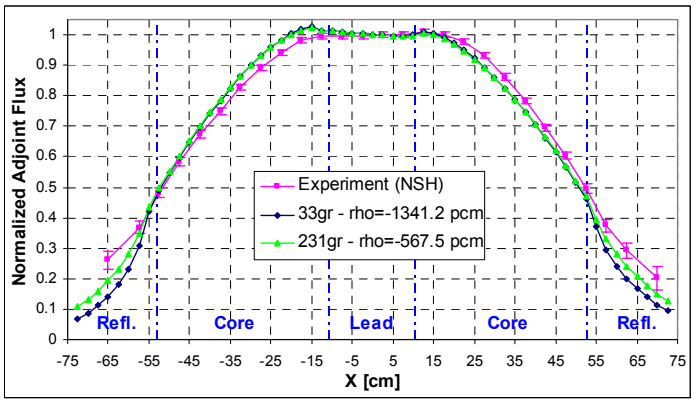

Figure 43: NSH: ENDF/B-V-MC^2-2 Calc./Exp. Comparison

III.B.3. Use of the MC^2-2 code in conjunction with the ENDF/B-VI data.

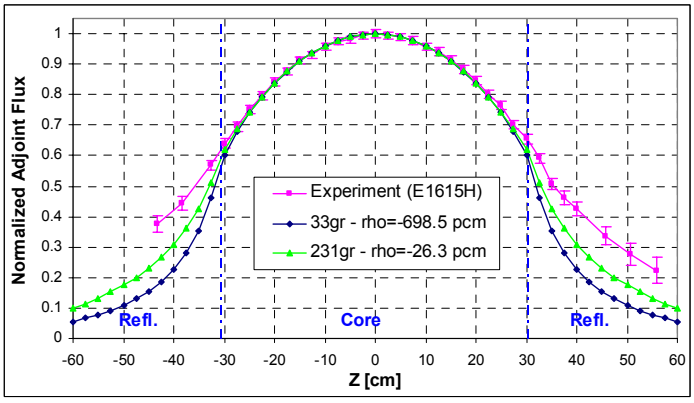

Figure 44: E1615H: ENDF/B-VI-MC^2-2 Calc./Exp. Comparison

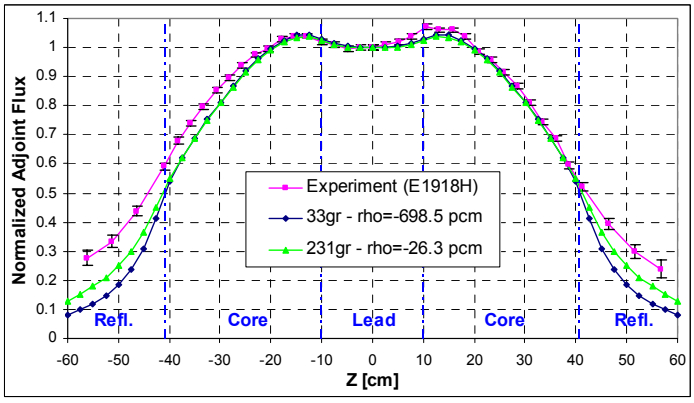

Figure 45: E1918H: ENDF/B-VI-MC^2-2 Calc./Exp. Comparison

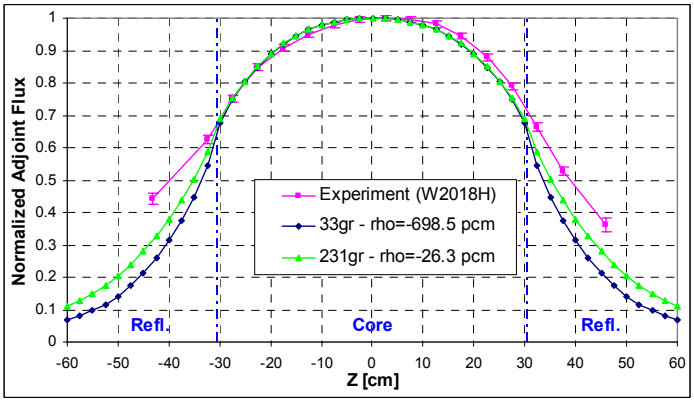

Figure 46: W2018H: ENDF/B-VI-MC^2-2 Calc./Exp. Comparison

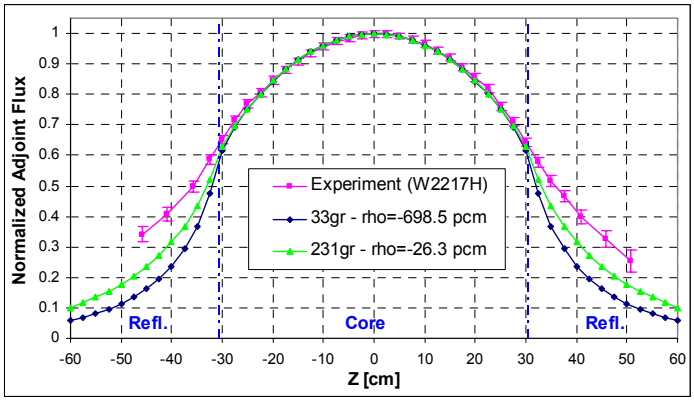

Figure 47: W2217H: ENDF/B-VI-MC^2-2 Calc./Exp. Comparison

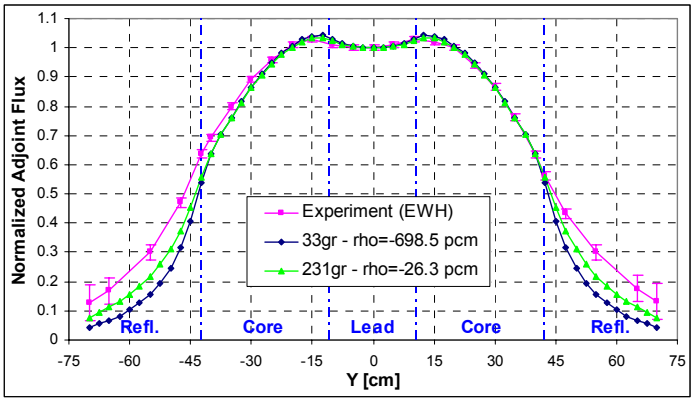

Figure 48: EWH: ENDF/B-VI-MC^2-2 Calc./Exp. Comparison

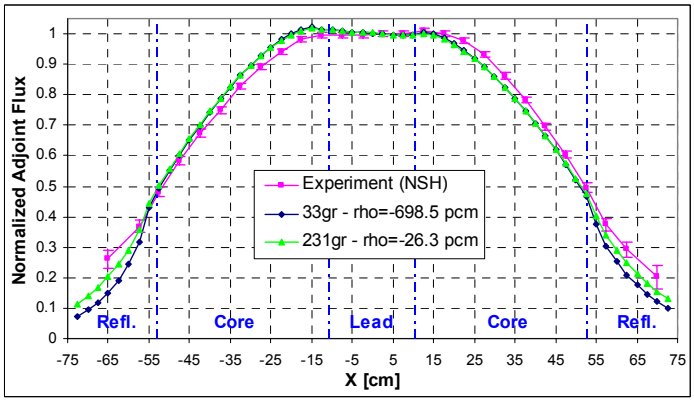

Figure 49: NSH: ENDF/B-VI-MC^2-2 Calc./Exp. Comparison

III.B.4. Use of the MC^2-2 code in conjunction with the JEF2.2 data.

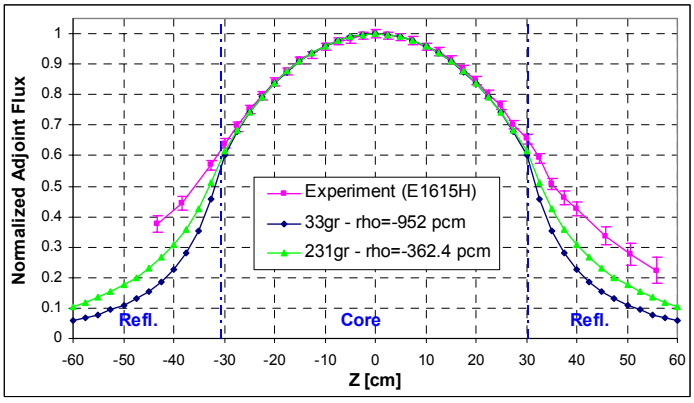

Figure 50: E1615H: JEF2.2-MC^2-2 Calc./Exp. Comparison

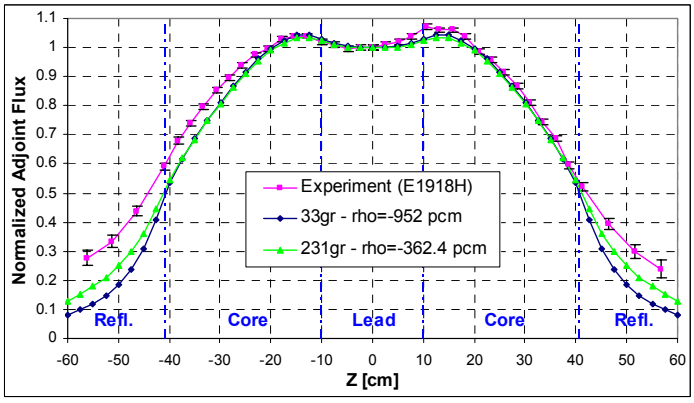

Figure 51: E1918H: JEF2.2-MC^2-2 Calc./Exp. Comparison

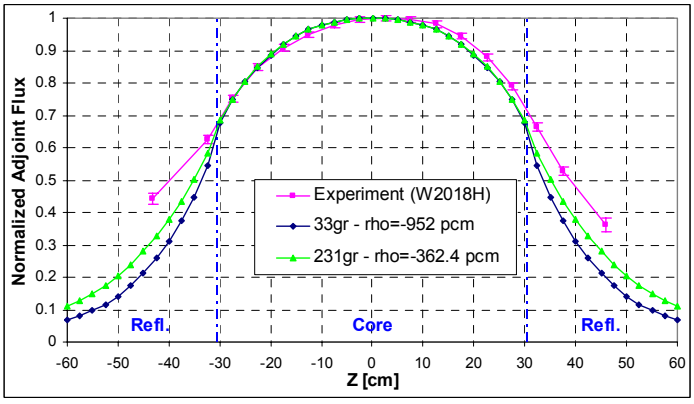

Figure 52: W2018H: JEF2.2-MC^2-2 Calc./Exp. Comparison

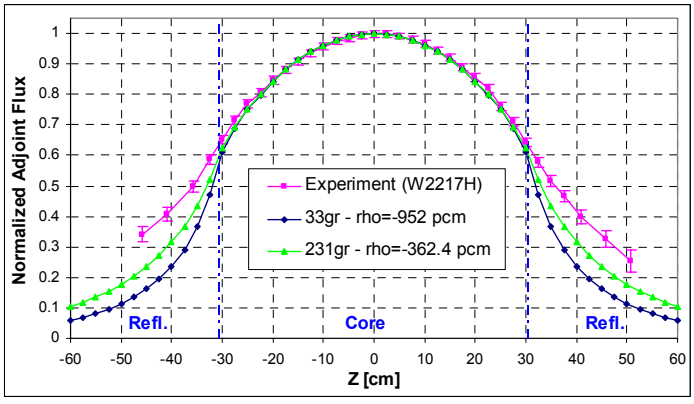

Figure 53: W2217H: JEF2.2-MC^2-2 Calc./Exp. Comparison

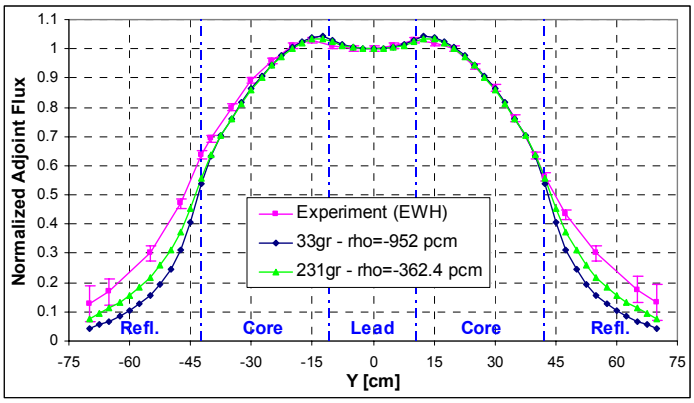

Figure 54: EWH: JEF2.2-MC^2-2 Calc./Exp. Comparison

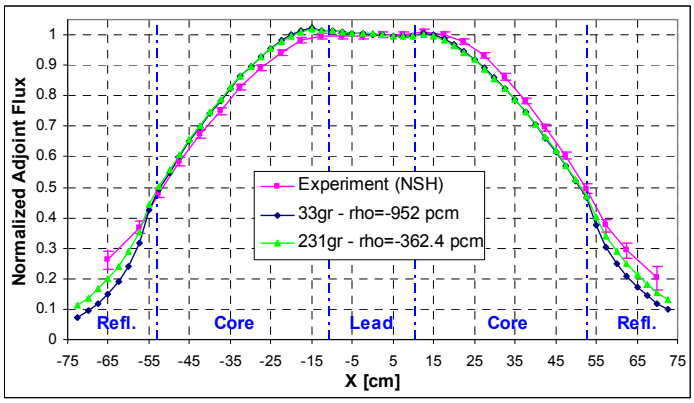

Figure 55: NSH: JEF2.2-MC^2-2 Calc./Exp. Comparison

III.B.5. Effect due to the nuclear data on the adjoint flux traverses.

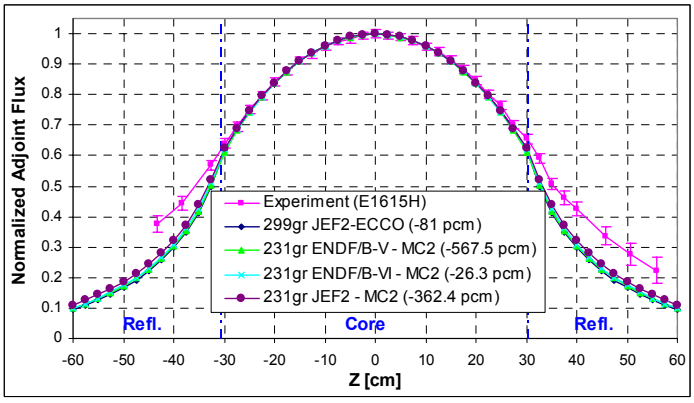

Figure 56: E1615H: Nuclear Data Impact on the Calculation

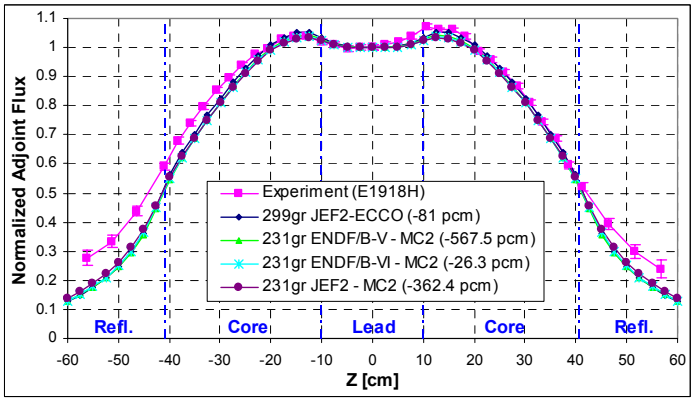

Figure 57: E1918H: Nuclear Data Impact on the Calculation

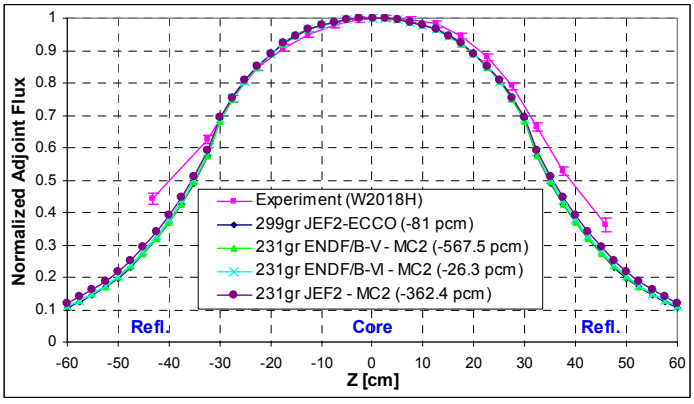

Figure 58: W2018H: Nuclear Data Impact on the Calculation

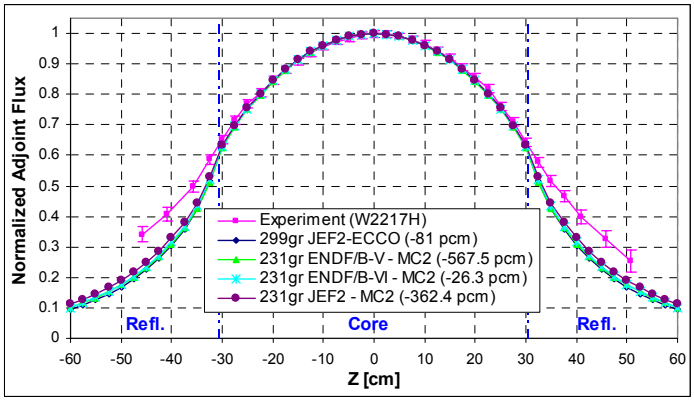

Figure 59: W2217H: Nuclear Data Impact on the Calculation

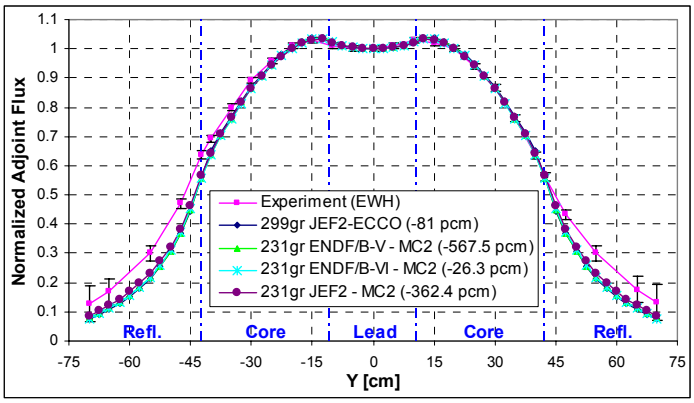

Figure 60: EWH: Nuclear Data Impact on the Calculation

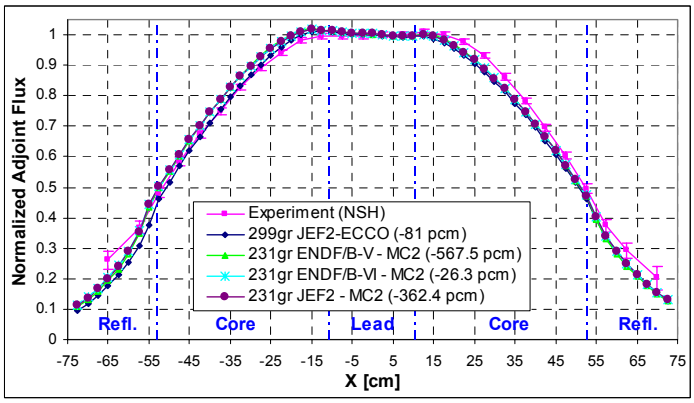

Figure 61: NSH: Nuclear Data Impact on the Calculation

III.C. Reaction rate traverses measurement and calculation.

U235 fission radial traverses EW and NS, and the Np237 EW radial traverse (see **Figures 29** and **30** for the channel locations) of the MUSE-4 critical configuration (1115 cells) have been calculated. In the following figures the comparison with the experiment is also performed and the behavior in proximity of the reflector region has been expanded.

The calculation results have been performed with the ERANOS code **[22]** suite in conjunction with the JEF2.2 **[23],** ENDF/B-V and ENDF/B-VI libraries. The multigroup cross sections have been condensed in different number of energy groups, in order to investigate the effects on the fission rate traverses. The processing of the cross-sections has been performed via the ECCO code **[24]** in conjunction with the JEF2.2 library only, and via the MC^2-2 code **[25]** using any nuclear data. The VARIANT code **[26]** was used with a three dimension geometry. All geometrical and material compositions are as shown for the model used to calculate the reactivity value. Transport theory was used in P_1 approximation. The core models assume that the Reference MUSE-4 configuration contains 1112 fuel cells. This corresponds to a total fuel mass of 1550.1 kg (using a mass of 0.697 kg as given in the MASURCA catalogue for MOX in one fuel rod). Note, however, that due to the Pu241 decay the number of fuel cells to achieve the criticality has increased to 1115 at the moment of the fission rate measurements. It is assumed that the subsequent effect on the calculated traverses is negligible.

In general, all the traverses show a good agreement between the calculation and the experiment in the margin of the uncertainty on the measurement if the number of energy group is sufficiently high (see **Figures 62** to **85**).

For the NS traverse a 2.5 cm translation has been applied.

For the U5 EW traverse an uncertainty too large on the experimental values has been provided, consequently a value of 2% has been used.

A good agreement between the calculation and the experiment is also found in proximity of the reflector. In the case of the NS traverse this agreement decreases because of the proximity of the void region too.

Concerning the impact of the nuclear data on the calculated traverses, **Figures 86** to **91** show that the MC^2-2 – ENDF/B-VI calculation overestimates the other simulations.

III.C.1. Use of the ECCO code in conjunction with the ECCO data.

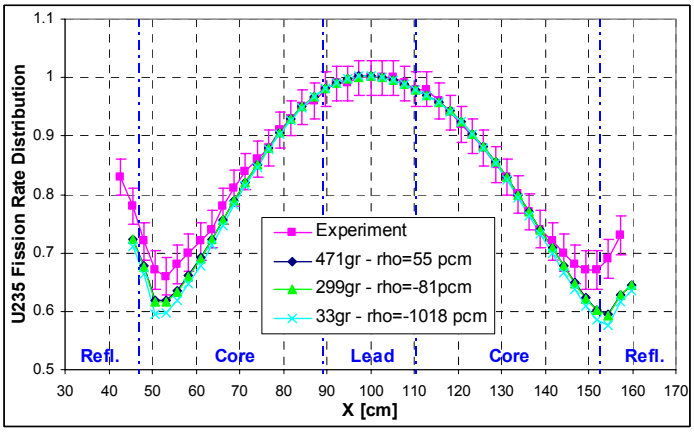

Figure 62: NS Traverse (JEF2-ECCO)

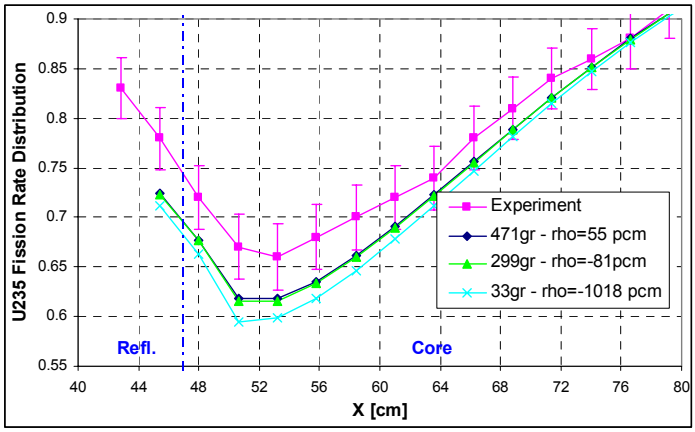

Figure 63: NS Traverse at the Interface (JEF2-ECCO)

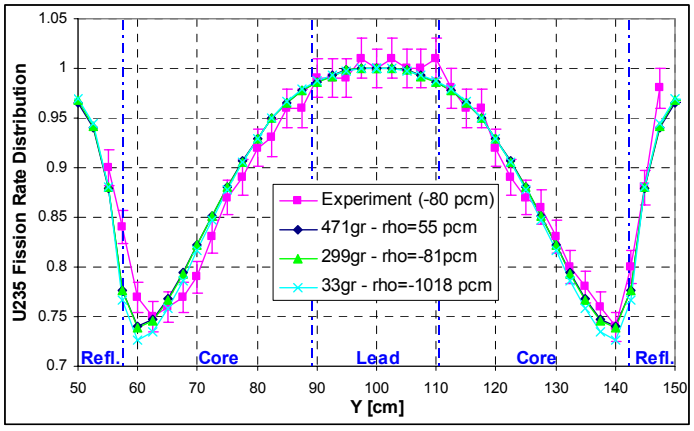

Figure 64: EW Traverse (JEF2-ECCO)

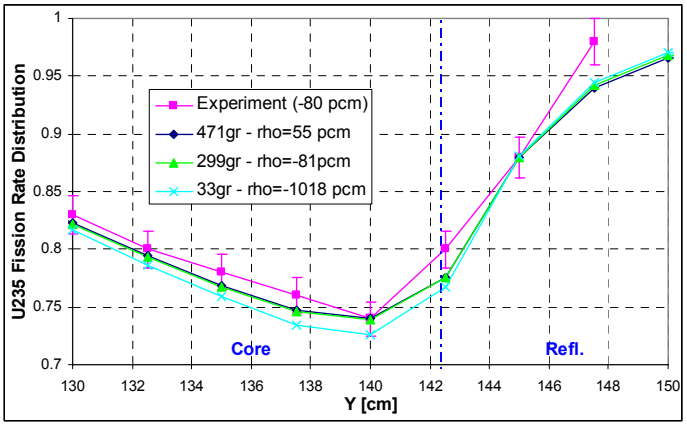

Figure 65: EW Traverse at the Interface (JEF2-ECCO)

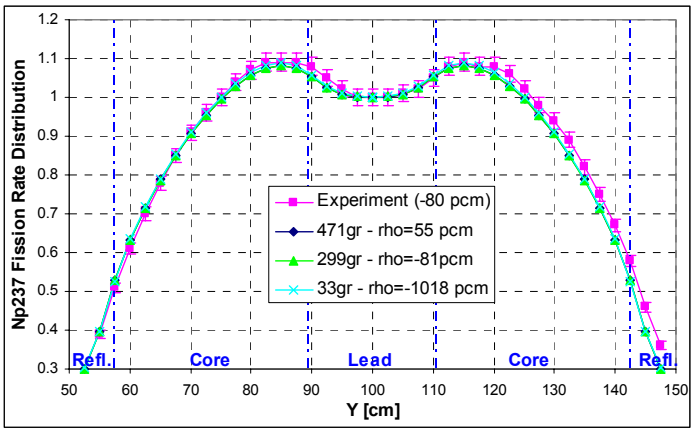

Figure 66: EW Traverse (JEF2-ECCO)

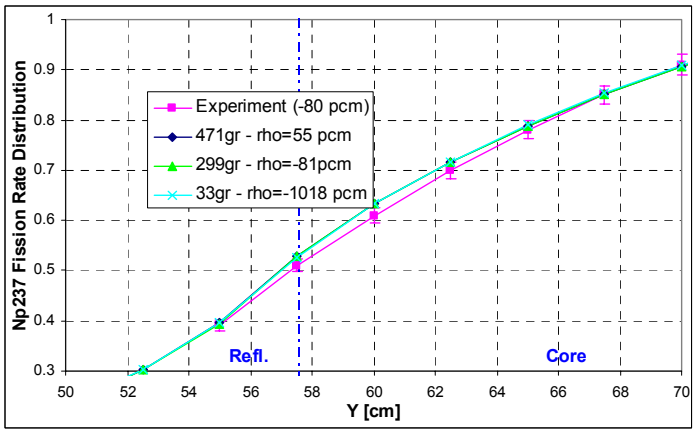

Figure 67: EW Traverse at the Interface (JEF2-ECCO)

III.C.2. Use of the MC^2-2 code in conjunction with the ENDF/B-V data.

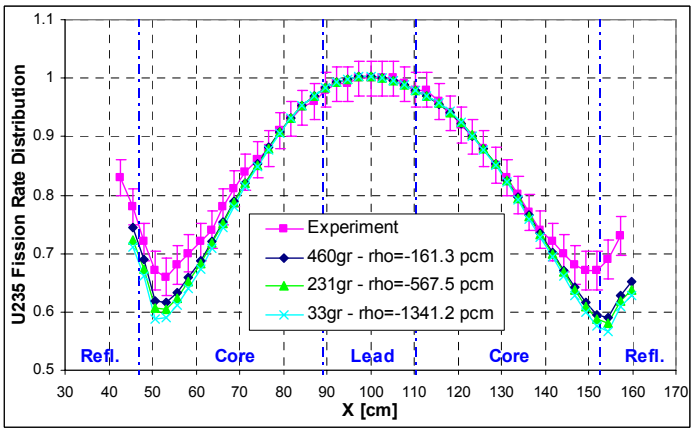

Figure 68: NS Traverse (ENDF/B-V-MC^2-2)

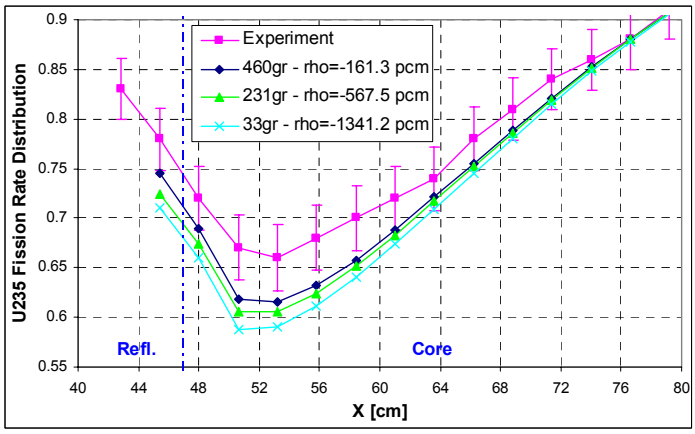

Figure 69: NS Traverse at the Interface (ENDF/B-V-MC^2-2)

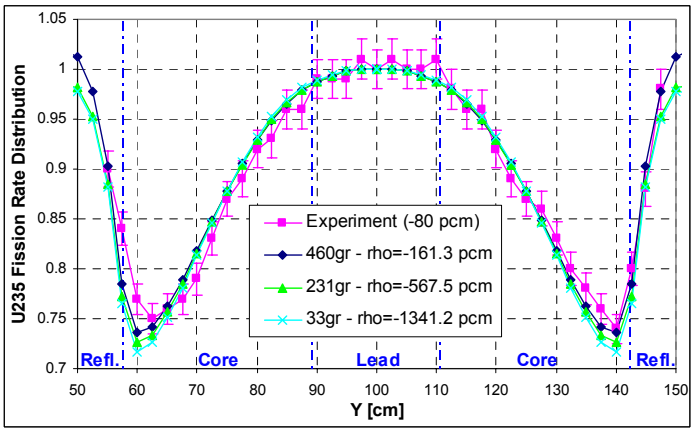

Figure 70: EW Traverse (ENDF/B-V-MC^2-2)

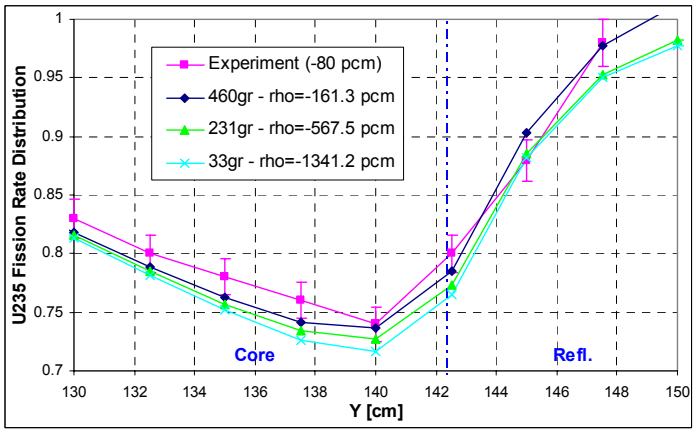

Figure 71: EW Traverse at the Interface (ENDF/B-V-MC^2-2)

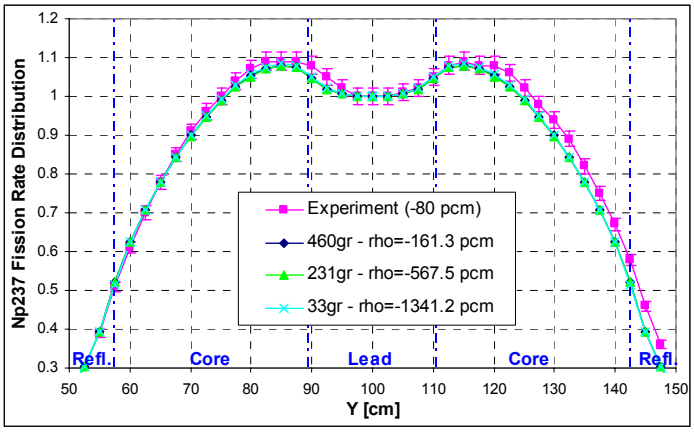

Figure 72: EW Traverse (ENDF/B-V-MC^2-2)

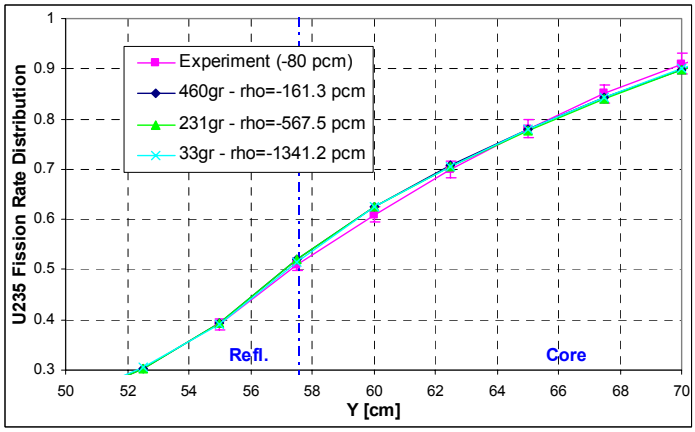

Figure 73: EW Traverse at the Interface (ENDF/B-V-MC^2-2)

III.C.3. Use of the MC^2-2 code in conjunction with the ENDF/B-VI data.

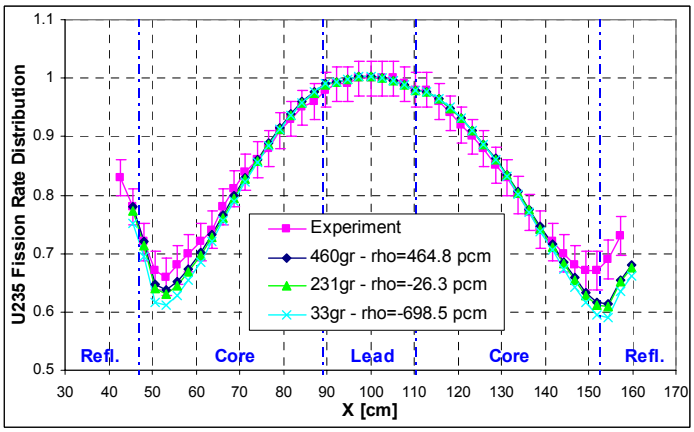

Figure 74: NS Traverse (ENDF/B-VI-MC^2-2)

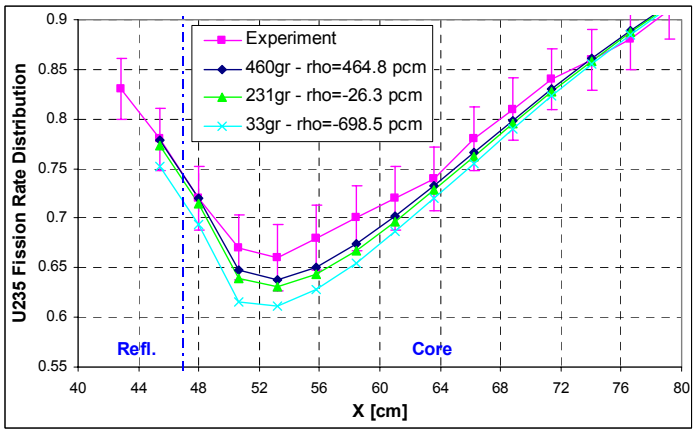

Figure 75: NS Traverse at the Interface (ENDF/B-VI-MC^2-2)

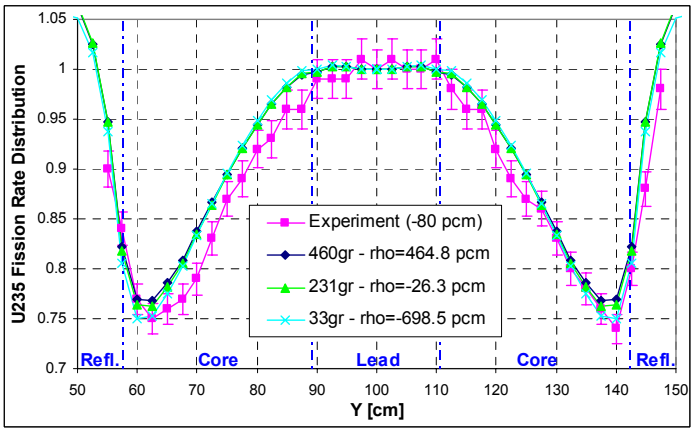

Figure 76: EW Traverse (ENDF/B-VI-MC^2-2)

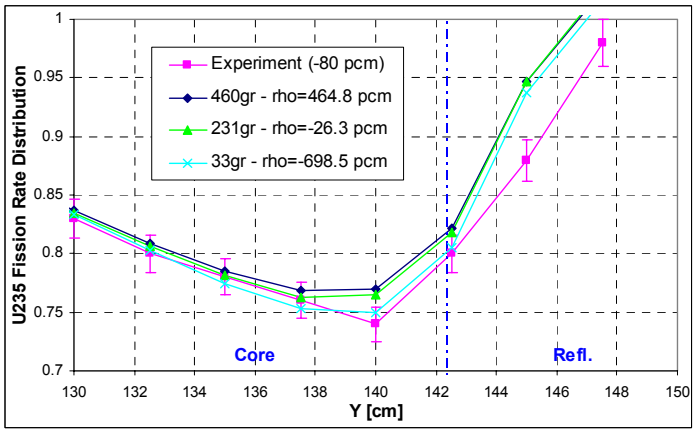

Figure 77: EW Traverse at the Interface (ENDF/B-VI-MC^2-2)

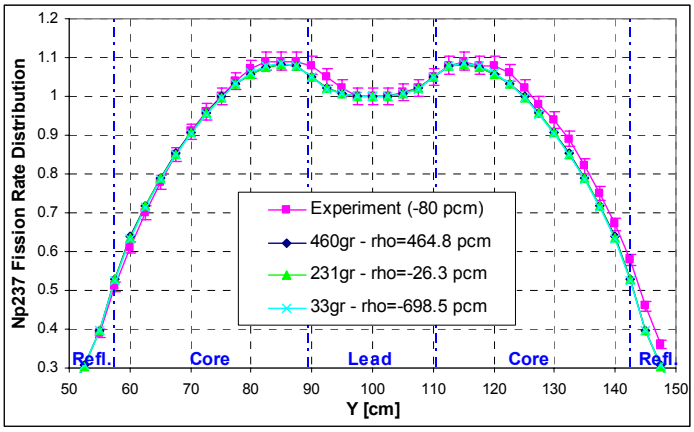

Figure 78: EW Traverse (ENDF/B-VI-MC^2-2)

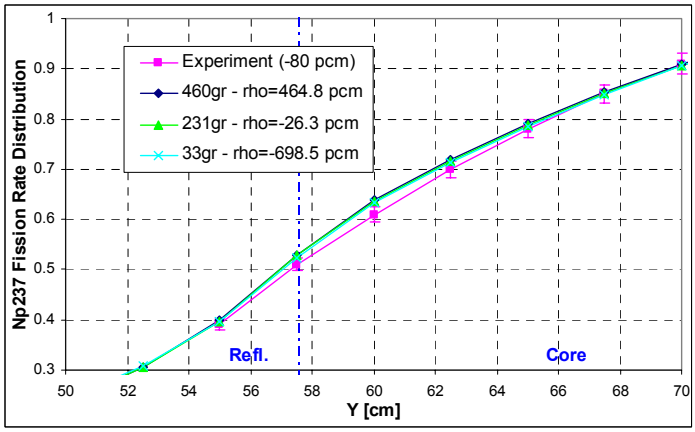

Figure 79: EW Traverse at the Interface (ENDF/B-VI-MC^2-2)

III.C.4. Use of the MC^2-2 code in conjunction with the JEF2.2 data.

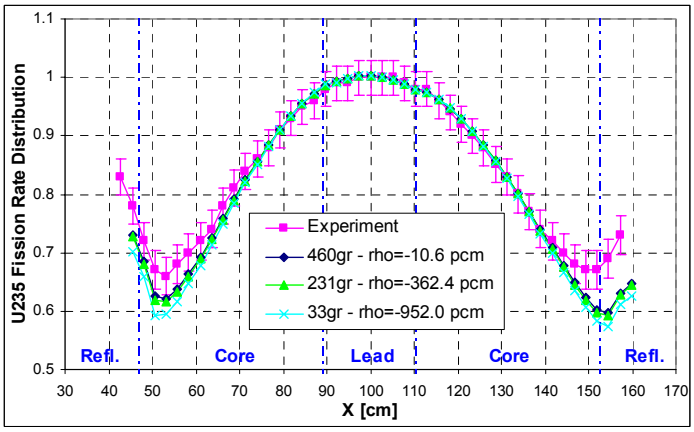

Figure 80: NS Traverse (JEf2.2-MC^2-2)

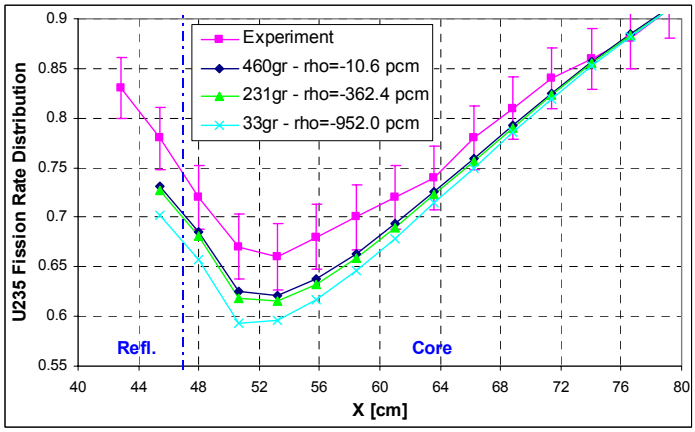

Figure 81: NS Traverse at the Interface (JEF2.2-MC^2-2)

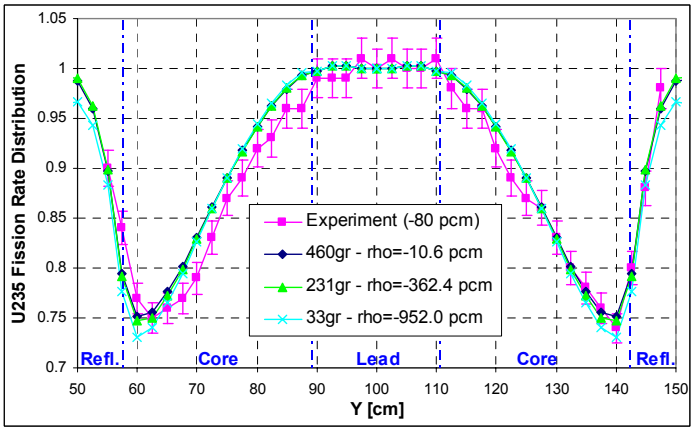

Figure 82: EW Traverse (JEF2.2-MC^2-2)

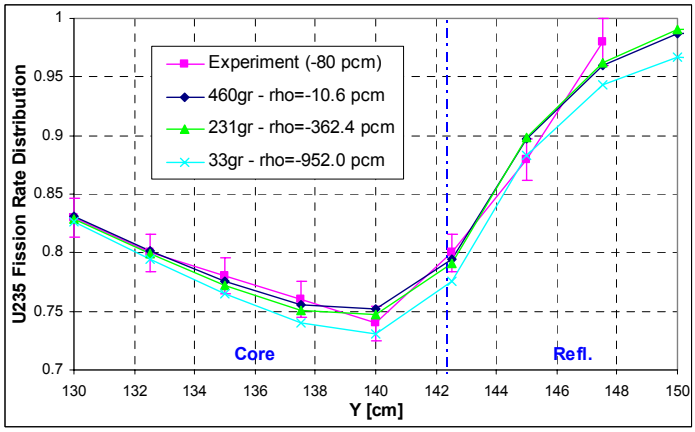

Figure 83: EW Traverse at the Interface (JEF2.2-MC^2-2)

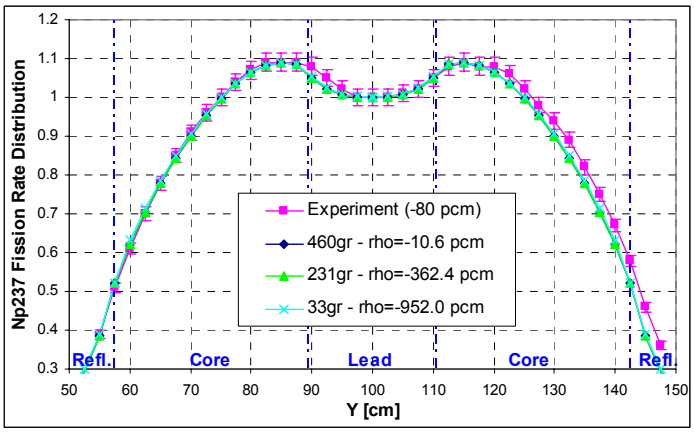

Figure 84: EW Traverse (JEF2.2-MC^2-2)

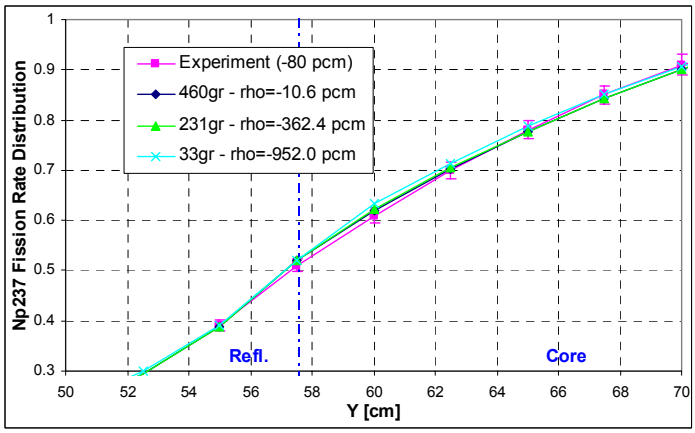

Figure 85: EW Traverse at the Interface (JEF2.2-MC^2-2)

III.C.5. Effect due to the nuclear data on the adjoint flux traverses.

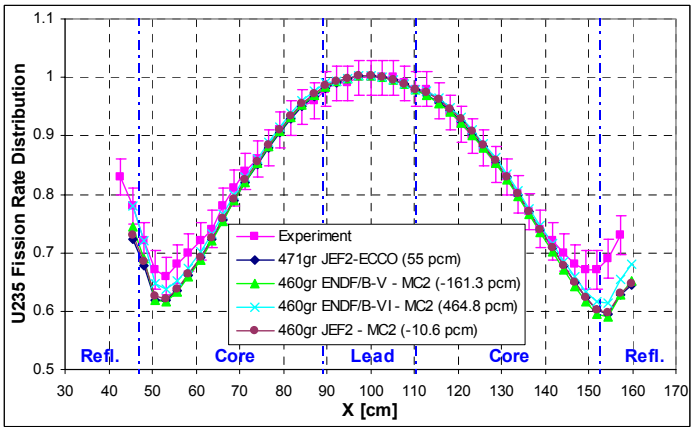

Figure 86: NS Traverse - Nuclear Data Impact

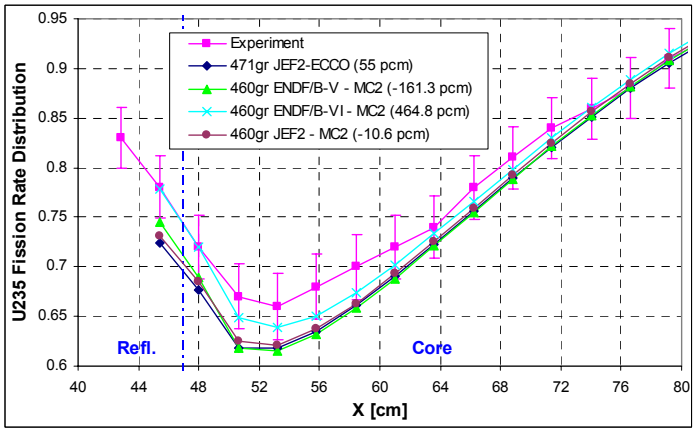

Figure 87: NS Traverse at the Interface - Nuclear Data Impact

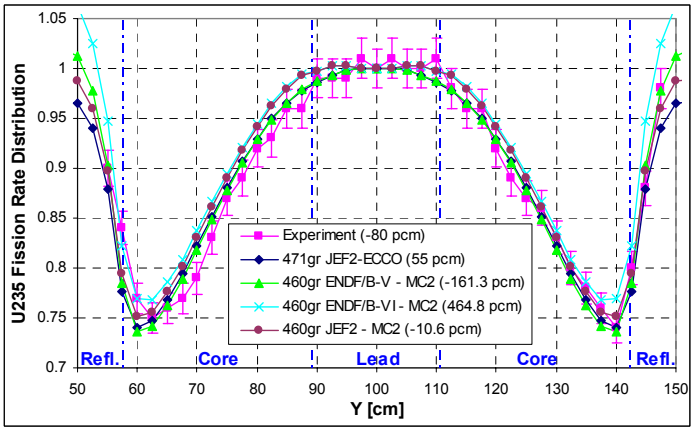

Figure 88: EW Traverse - Nuclear Data Impact

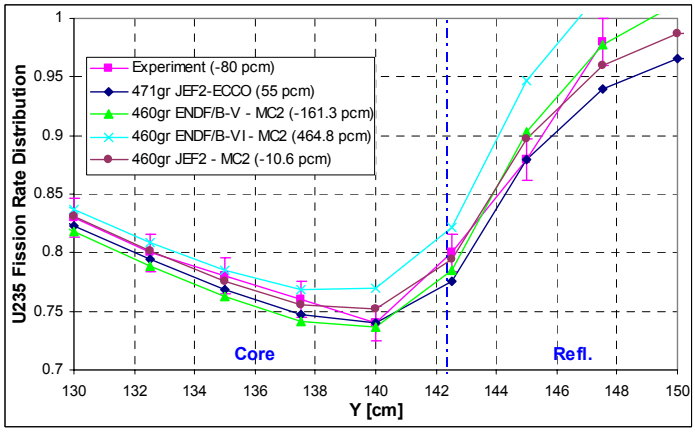

Figure 89: EW Traverse at the Interface - Nuclear Data Impact

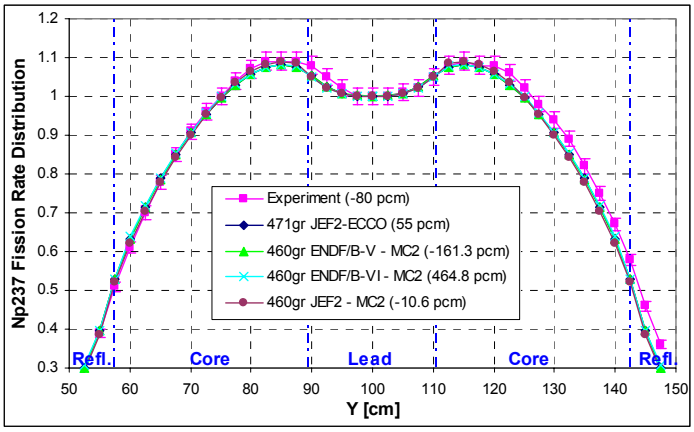

Figure 90: EW Traverse - Nuclear Data Impact

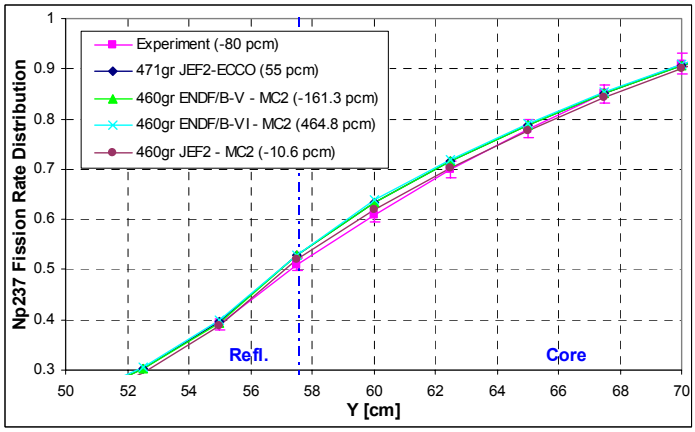

Figure 91: EW Traverse at the Interface - Nuclear Data Impact

III.D. Analysis of dynamic measurements

One of the main objectives of the MUSE-4 experimental program is to investigate the neutronic response to neutron pulses with frequencies of 1 to 4 kHz, and less than 1μs wide, generated at the reactor center by the (d,d) GENEPI accelerator. Detectors based on ^{235}U and ^{237}Np fission, located in the core, reflector and shielding regions are used for measuring the time dependent responses.

At present only measurements for the MUSE-4 SC0 configuration (see **Figure 9**) are available. The axial positioning of the control and pilot rods allowed variations in the reactivity, corresponding to different levels of subcriticality. The following configurations have been investigated:

- MUSE-4 SC0 with pilot rod out;
- MUSE-4 SC0 with pilot rod in;
- MUSE-4 SC0 with pilot rod and control rod "bc1" in.

III.D.1. MUSE-4 SC0 with pilot rod out.

In this section, the MUSE-4 SC0 configuration with both the control rod "bc1" and the pilot rod out has been studied (see **Figure 9**). The measured reactivity is -400 pcm.

In the point kinetic approximation the response *P(t)* to a neutron pulse is the sum of an exponential decay from the prompt multiplication plus a nearly constant offset due to the delayed neutrons. In particular, the prompt time dependence $P(t) \sim exp(-\alpha t)$, with $\alpha \cong \frac{\hat{\beta} - \rho}{\Lambda}$, $\hat{\beta}$ the effective fraction of delayed neutron and Λ the mean generation time characterizing the system under study, can be investigated for a method of reactivity measurement, the Pulsed Neutron Source (PNS) method.

As a preliminary analysis, a point kinetic model has been employed for the present study using the 3D kinetic module KIN3D **[29]** of the ERANOS code system **[22]**. The cross-sections have been processed via the ECCO code **[24]** with the JEF2.2 data **[23]**, while the MC^2-2 code **[25]** allows the processing of ENDF/B-V and -VI and JEF2.2 data libraries.

Due to the proximity to criticality, the best estimation for the reactivity provides positive values in some simulations, especially when using the ENDF/B-VI data library (see **Tables 4** to **7**). Since the study of a system driven by an external source requires a subcritical state, for the present analysis the calculation has been normalized to the experimental reactivity. This choice allows also investigation of the impact of nuclear data on the dynamic evolution of the system when the reactivity is the same in each simulation.

The results are shown in **Table 16** and **Figure 92**.
The main problem of the PNS method consists in the limitations of the technique. Indeed, the real configuration is often very different from a "point-reactor", and the experimental response depends in general on the position of the detectors.
As example, **Figures 93** to **95** show the measurements associated with some detectors, located in the core (detector F), in the reflector (detector C) and in the shielding (detector G). In order to reproduce the detector response by the calculation, a space-time solution of the transport equation, like the direct or the quasi-static methods (both available in KIN3D), has to be used.

In the same **Figures 93** to **95**, the experimental data are also compared with the calculated ones obtained with the direct method. The use of the quasi-static approximations gives similar results. In general, the agreement with the measurements can be considered satisfactory. Regarding the calculation, it can be observed that the effect of using different libraries during the transient is not significant if each calculation is normalized to the same reactivity.

Table 16: Comparison of Calculation and Experiment Results.

Experiment		
ρ [pcm]	β [pcm]	Λ [μs]
-400	335	0.56

Calculation				
	JEF2.2-ECCO	JEF2.2-MC^2-2	ENDF/B-V-MC^2-2	ENDF/B-VI-MC^2-2
ρ [pcm]	-400	-400	-400	-400
α [s^{-1}] from point-model	15154.8	14999.0	15905.3	14625.7
β (t=0) [pcm]	367	371	369	376
Λ (t=0) [μs]	0.51	0.52	0.49	0.53

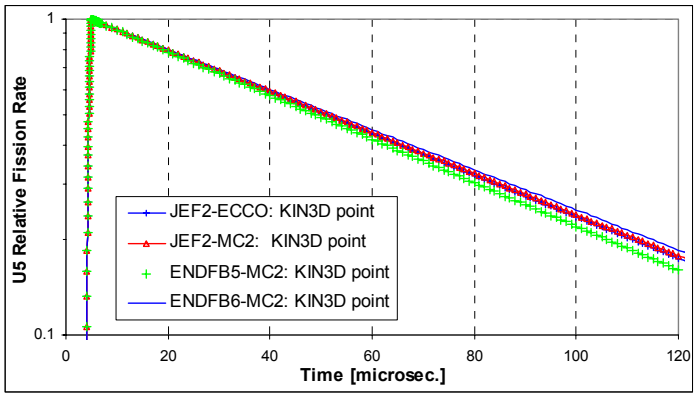

Figure 92: Point Model Comparison

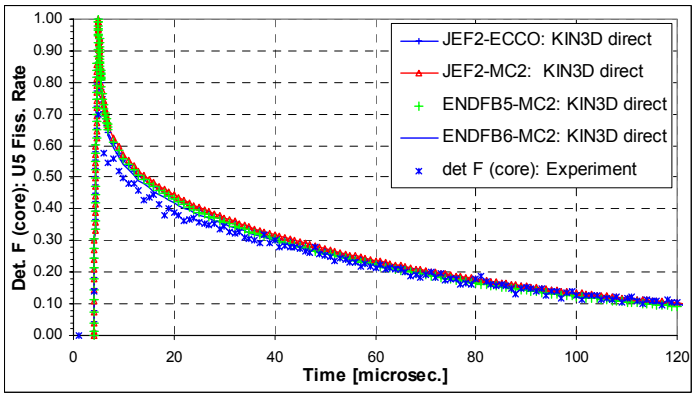

Figure 93: Detector F Comparison

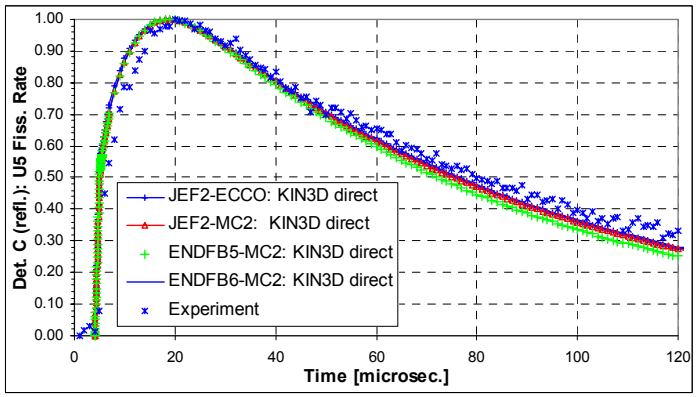

Figure 94: Detector C Comparison

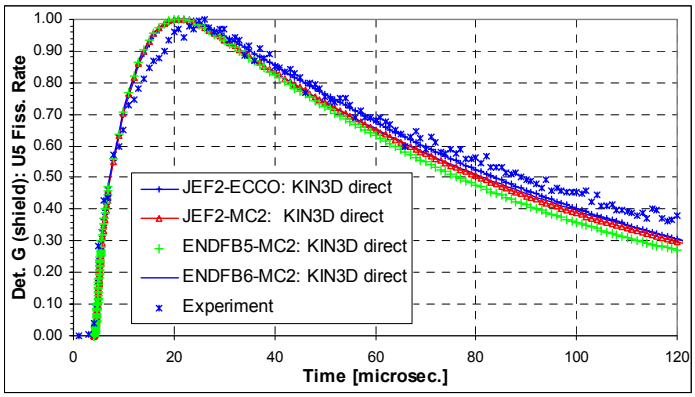

Figure 95: Detector G Comparison

III.D.2. MUSE-4 SC0 with pilot rod in.

In this section, the MUSE-4 SC0 configuration with the pilot rod down and the control rod "bc1" out has been studied (see **Figure 9**). The measured reactivity is -540 pcm.

As a preliminary analysis, a point kinetic model has been employed for the present study using the 3D kinetic module KIN3D **[29]** of the ERANOS code system **[22]**. The cross-sections have been processed via the ECCO code **[24]** with the JEF2.2 data **[23]**, while the MC^2-2 code **[25]** allows the processing of ENDF/B-V and -VI and JEF2.2 data libraries.

As in the case with pilot rod out, due to the close to criticality state, the best estimation for the reactivity provides positive values in some simulations, especially when using the ENDF/B-VI data library (see **Tables 4** to **7**). Consequently, for the present analysis the calculation has been normalized to the experimental reactivity.

The results are shown in **Table 17** and **Figure 96**.

Figures 97 to **99** show the measurements associated with some detectors, located in the core (detector F), in the reflector (detector C) and in the shielding (detector G). In order to reproduce the detector response by the calculation, a space-time solution of the transport equation, like the direct or the quasi-static methods (both available in KIN3D), has to be used.

In the same **Figures 97** to **99**, the experimental data are also compared with the calculated ones obtained with the direct method. The use of the quasi-static approximations gives similar results. In general, the agreement with the measurements can be considered satisfactory. Regarding the calculation, as in the case with pilot rod out, it can be observed that the effect of using different libraries during the transient is not significant if each calculation is normalized to the same reactivity.

Table 17: Comparison of Calculation and Experiment Results.

Experiment				
ρ [pcm]		β [pcm]		Λ [μs]
-540		335		0.56
Calculation				
	JEF2.2-ECCO	JEF2.2-MC^2-2	ENDF/B-V-MC^2-2	ENDF/B-VI-MC^2-2
ρ [pcm]	-540	-540	-540	-540
α [s^{-1}] from point-model	17886.9	17690.1	18763.1	17234.0
β (t=0) [pcm]	367	371	369	376
Λ (t=0) [μs]	0.51	0.52	0.49	0.53

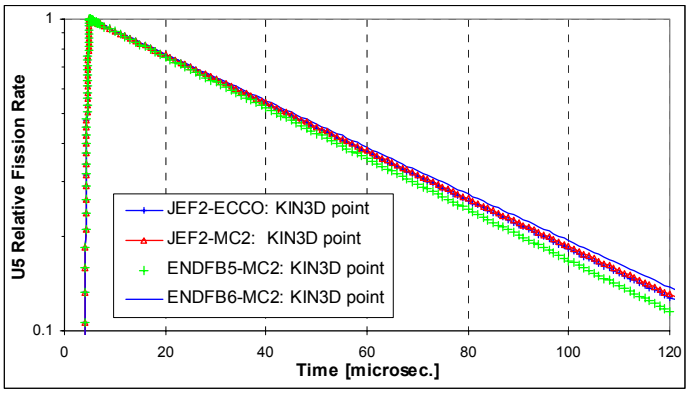

Figure 96: Point Model Comparison

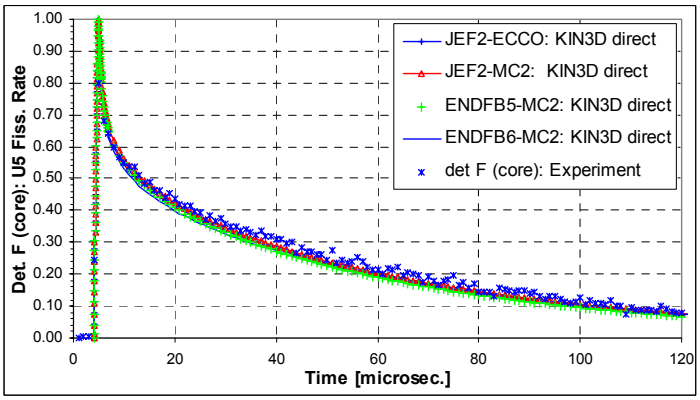

Figure 97: Detector F Comparison

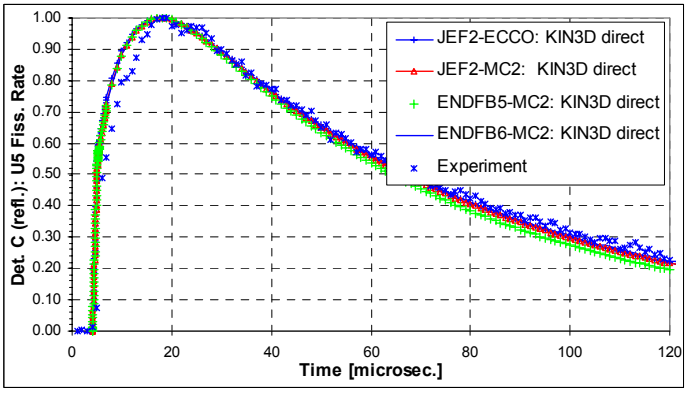

Figure 98: Detector C Comparison

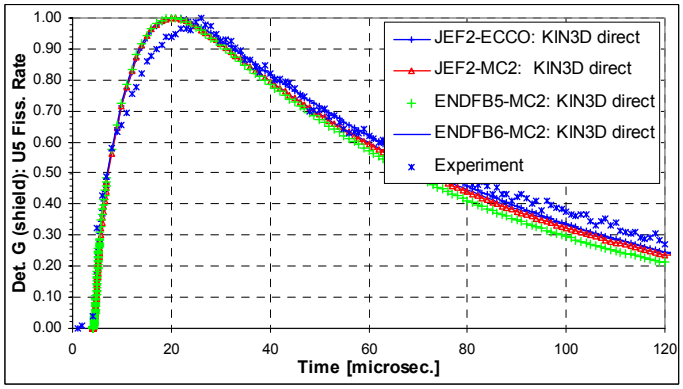

Figure 99: Detector G Comparison

III.D.3. MUSE-4 SC0 with pilot rod and control rod bc1 in.

In this section, the MUSE-4 SC0 configuration with both the pilot rod and the control rod "bc1" in has been studied (see **Figure 9**).

During the experimental phase, two values of reactivity were determined. The first is based on the Modified Source Multiplication (MSM) method that gives a reactivity value of about –4200 pcm. Using the Pulsed Neutrons Source (PNS) technique a reactivity value of –3200 pcm is obtained.

The MSM method determines subcritical reactivities by ratios of count rates corrected for changes in detector efficiencies and source importance between two subcritical states. In the PNS method, information on the subcritical level is deduced from the decay of the response P(t) arising from an external neutron pulse.

The wide discrepancy (-4200 vs. –3200 pcm) obtained using the two methods is being investigated by the experimentalists.

As a preliminary analysis, a point kinetic model has been employed for the present study using the 3D kinetic module KIN3D **[29]** of the ERANOS code system **[22]**. The cross-sections have been processed via the ECCO code **[24]** with the JEF2.2 data **[23]**, while the MC^2-2 code **[25]** allows the processing of ENDF/B-V and -VI and JEF2.2 data libraries. Because of the subcritical state, no normalization to the experimental reactivity has been performed. The results are shown in **Table 18** and **Figure 100**.

First, it can be seen in **Table 18** that the spread in the calculated reactivity value is of the order of the difference between the MSM and PNS inferred measurement values. It is also observed that the trend in the calculated α value is consistent with that in the calculated subcritical level, as expected (i.e., the highest α value is obtained for the approach with highest subcritical level).

Figures 101 to **103** show the measurements associated with some detectors, located in the core (detector F), in the reflector (detector C) and in the shielding (detector H).

In the same **Figures 101** to **103**, the experimental data are also compared with the calculated ones obtained with the direct method. The use of the quasi-static approximations gives similar results. In general, the agreement with the measurements can be considered satisfactory. Regarding the calculation, it the can be observed that the effect of using of different libraries during the transient becomes significant if each calculation is not normalized to the same reactivity. We will observe that this in contrast on what has been done in section **III.D. 1&2** where the calculations were normalized to the experimental reactivity.

Table 18: Comparison of Calculation and Experiment Results.

Experiment				
ρ [pcm]		β [pcm]	Λ [μs]	
-3200 (PNS)	-4200 (MSM)	335	0.56	
Calculation				
	JEF2.2-ECCO	JEF2.2-MC^2-2	ENDF/B-V-MC^2-2	ENDF/B-VI-MC^2-2
ρ [pcm]	-3800	-3512	-3845	-3061
α [s^{-1}] from point-model	82530.6	76049.2	86656.2	65555.3
β (t=0) [pcm]	371	375	372	380
Λ (t=0) [μs]	0.50	0.51	0.48	0.52

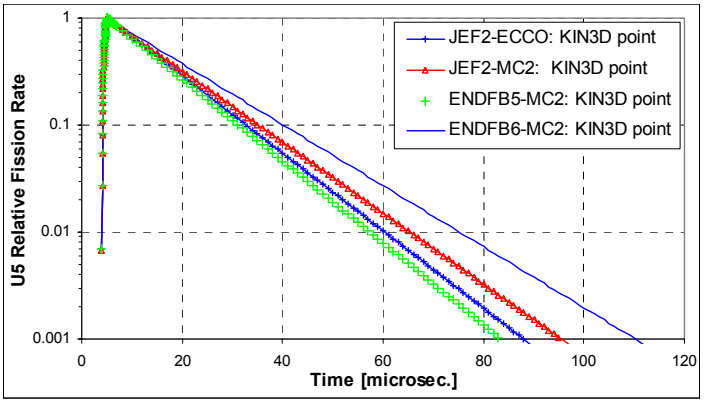

Figure 100: Point Model Comparison

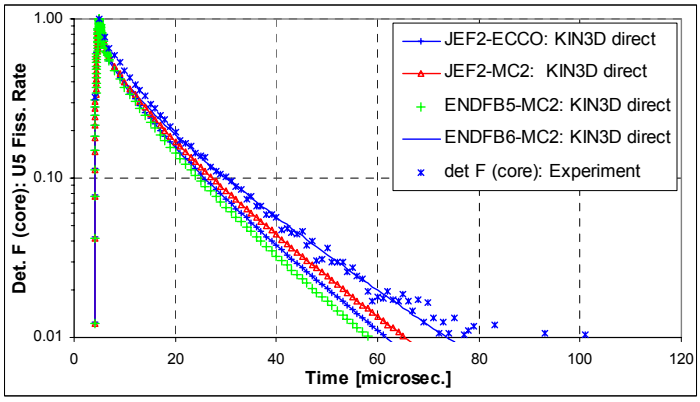

Figure 101: Detector F Comparison

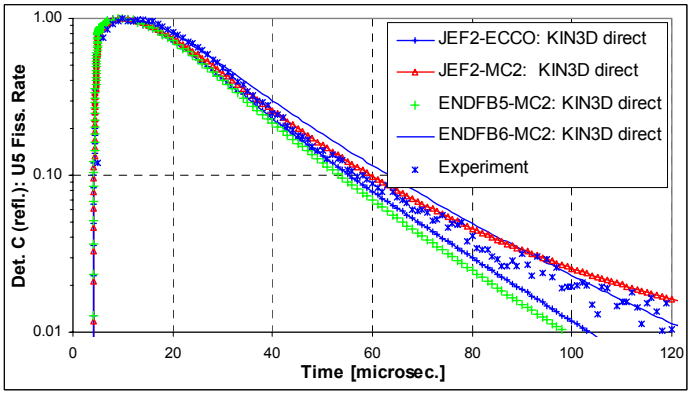

Figure 102: Detector C Comparison

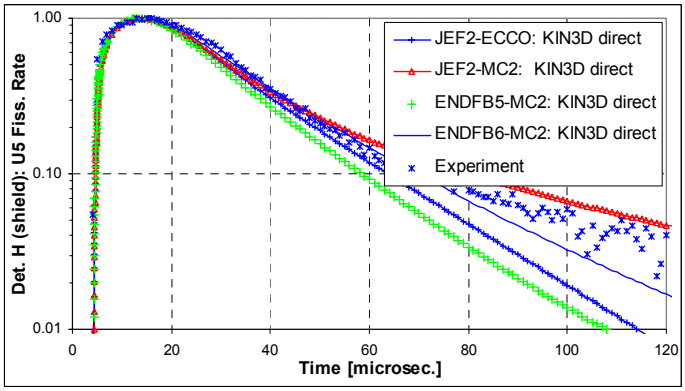

Figure 103: Detector H Comparison

III.D.4. The use of the PNS methods to infer the reactivity from the analysis of dynamic measurements.

Several analyses have been performed to extract information on the reactivity of the MUSE configurations **[11]**. In this section, preliminary studies have been devoted to the PNS method.

A first investigation has been performed in order to study any dependence of the flux response on the detector location. The calculation confirmed that the different detector responses (^{235}U fission rate) have approximately the same decay slope, but the prompt-area changes significantly especially in the shielding region. This behavior certainly raises some issues for other experimental techniques of reactivity measurement, such as the area-ratio method, which relates the prompt to delayed area ratio with ρ/β.

Additionally, it appears that after 20 μs from the injection of the neutron pulse, i.e. when the decay becomes less sensitive to the shape of the pulse, the detector positions indicate the same prompt time dependence (i.e. decay slope), even if it is different from the point kinetics behavior. As an example, **Figure 104** shows the case of the SC0 configuration with control and pilot rod down (calculations made via JEF2.2-ECCO).

The use of the average Λ in the prompt decay range (from 20 to 150 μs), estimated of 7.13709E-07 sec from the quasi-static calculation, has demonstrated that the PNS method could still apply. In fact, the technique leads to a reactivity determination of about –3550 pcm that is quite independent from the detector position (see **Table 19**) and in reasonable agreement with the absolute calculated value (-3800 pcm). Further investigations are needed on this aspect.

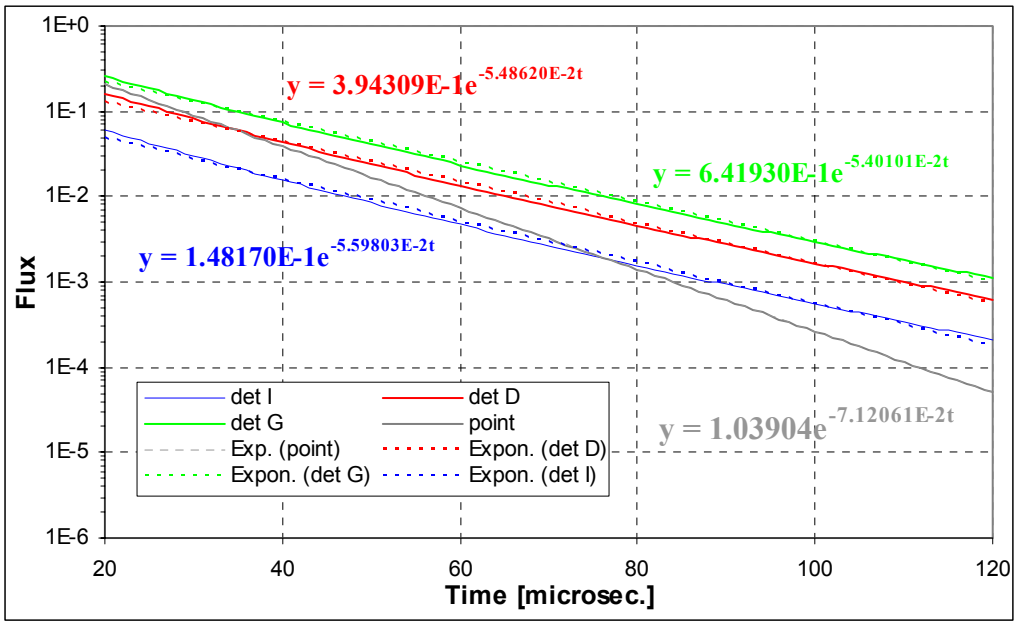

Figure 104: C-E Comparison.

Table 19: Estimated (JEF2.2-ECCO) Reactivity by the PNS Method at Different Detector Locations.

detector	α	β	Average Λ	Reactivity deduced with the PNS method
I (core)	5.59803E+4	370.59 pcm	7.13709E-07 sec	-3620 pcm
D (reflector)	5.48620E+4	370.59 pcm	7.13709E-07 sec	-3540 pcm
G (shielding)	5.40101E+4	370.59 pcm	7.13709E-07 sec	-3480 pcm

IV. MUSE-4 Benchmark

IV.A. Introduction

The study of the neutronics of ADS, in which an intense neutron source maintains a stationary power level, requires the extension of standard computational tools developed for critical reactors to solve steady-state and time–dependent problems. With this goal, the experiment MUSE-4 **[7,8]** (using the MASURCA reactor) became the object of the benchmark **[10]** proposed by OECD for the validation of the neutronic tools (codes and cross section data) to be used for the ADS design.

The benchmark model is oriented to compare simulation predictions based on available codes and nuclear data libraries with experimental data related to: TRU transmutation, criticality constants and time evolution of the neutronic flux following source variation, within "liquid" metal fast subcritical systems.

The benchmark has been divided in three steps. The first step will allow an understanding of the physics methods using different groups and tuning of the analysis programs with the experimental data of an already measured configuration (COSMO). In the second step, the MUSE-4 reference configuration (1112 cells) is proposed to simulate different reactor parameters (criticality constant, flux distribution...) in a nearly critical configuration. Finally, a third step is oriented to the simulation of reactor response to the external source in the subcritical reference configuration (976 cells).

Note that MASURCA can be operated in two modes. In the (nearly) critical configurations the intrinsic (Pu decay) neutron source plus an initial external source initiate a level of neutron flux that is afterwards maintained by reactivity control mechanisms. The neutron flux in MASURCA is in a very good approximation an eigenvector of the transport equation. In the two first steps of the requested calculations (COSMO and 1112 cells MUSE-4 reference configuration) the flux is assumed to be computed as the transport equation eigenvector. In the second mode of operation, with low values of the multiplication constant, the flux reaches rapidly the equilibrium value corresponding to the intrinsic source multiplied by the subcritical system. That equilibrium value is small (assumed negligible) and the main part of the neutron flux must be produced by the multiplication of an external deuterium-tritium neutron source placed near the MASURCA center.

IV.B. Geometry and material description.

The MASURCA facility is an arrangement of tubes of $10.6 \times 10.6 \times 164.16$ cm^3 each, building a parallel-piped assembly of 17×16 tubes, with a total dimension of $180.2 \times 169.6 \times 164.16$ cm^3 in the MUSE-4 configurations and 17×17 tubes in the COSMO configuration.

Figures 101 to **103** show the layout of MASURCA facility for the COSMO configuration. **Figures 104** to **106** show the critical reference and **Figure 107** the subcritical configuration for the MUSE-4 experiments. **Figures 108** and **109** show the axial view of the different types of MUSE-4 tubes, including the material labels. It should be noted that tubes 3* and 11* can be obtained rotating tubes 3 and 11 by 180° around its vertical (Z) axis. Tube 9* can be obtained rotating tube 9 to 90°, 180° or 270°, tube 12* can be obtained by rotating 270° tube 12, and tube 10** can be obtained as a mirror image of tube 10.

Detector positions are shown in **Figure 110**. All vertical channels are in the center of the tube. Note that horizontal and vertical channels are not included in the geometrical description in order to simplify the model.

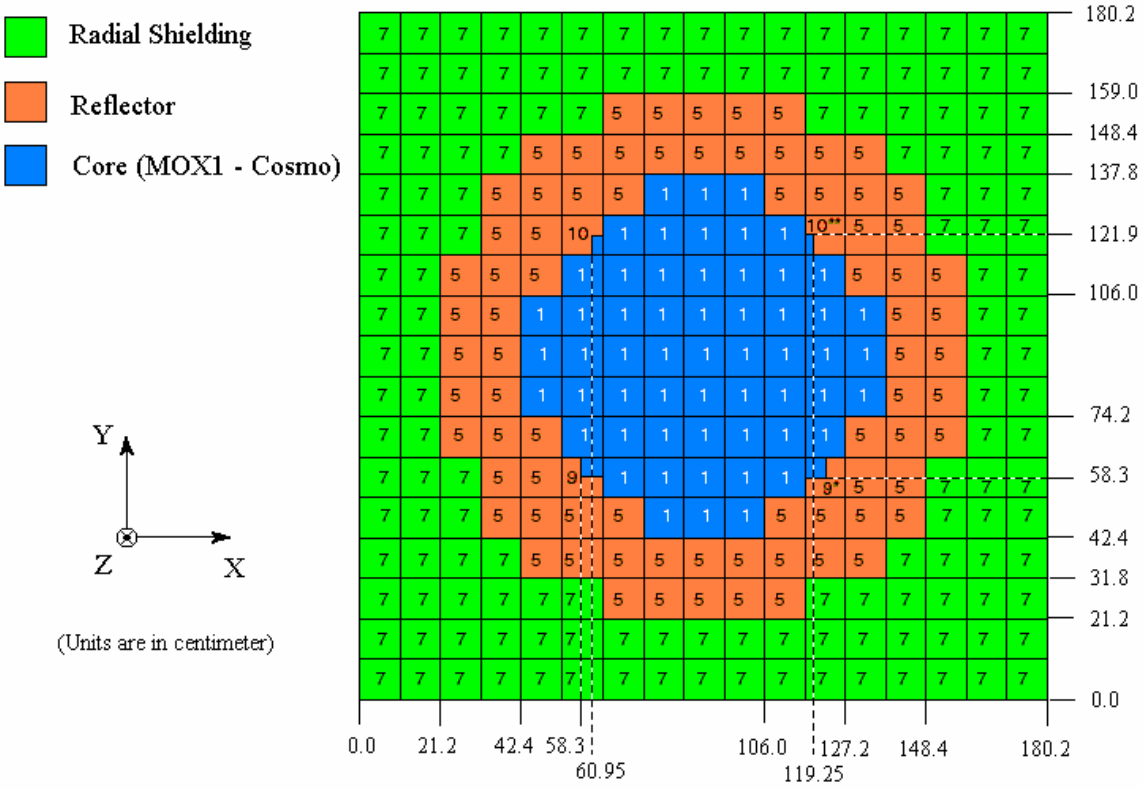

Figure 105: COSMO Configuration – Top View at Half Height

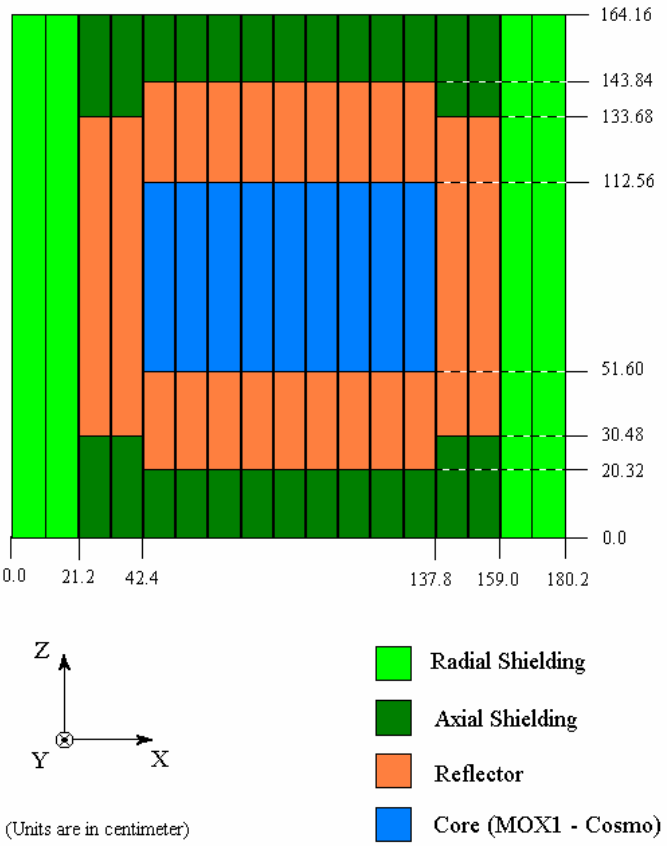

Figure 106: Cosmo Configuration - View X-Z at Y=84.8 cm

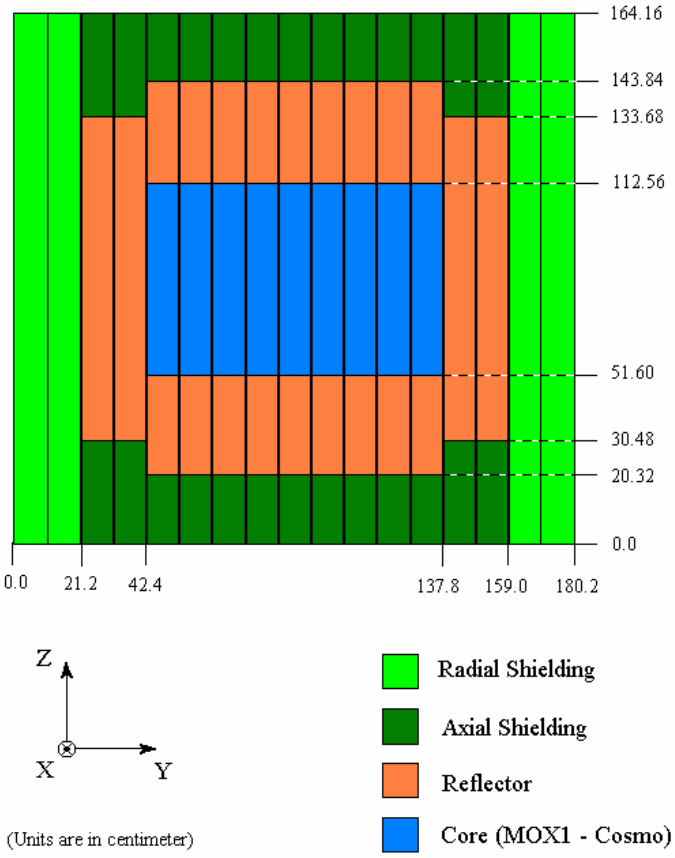

Figure 107: Cosmo Configuration - View Y-Z at X=90.1 cm

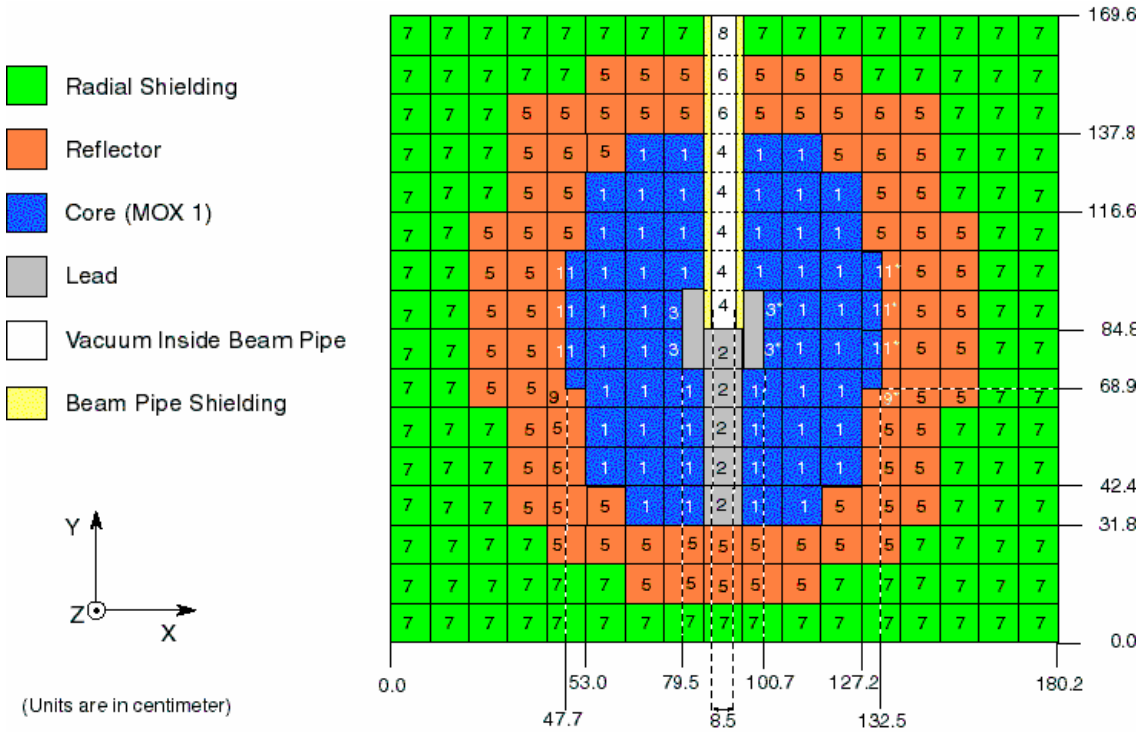

Figure 108: MUSE-4 Critical (1112 cells) Configuration – Top View at Half Height

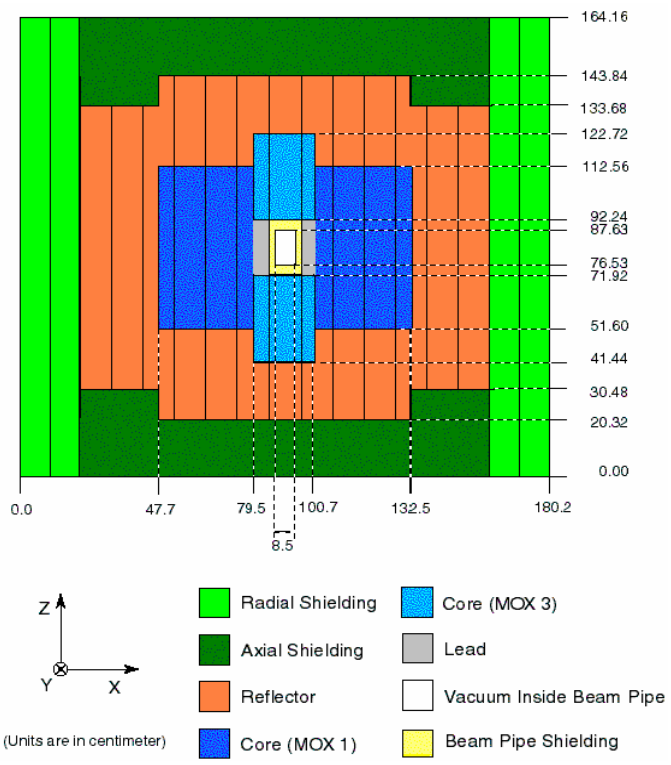

Figure 109: MUSE-4 Critical Config. – Side View #1 at Y=90.1 cm

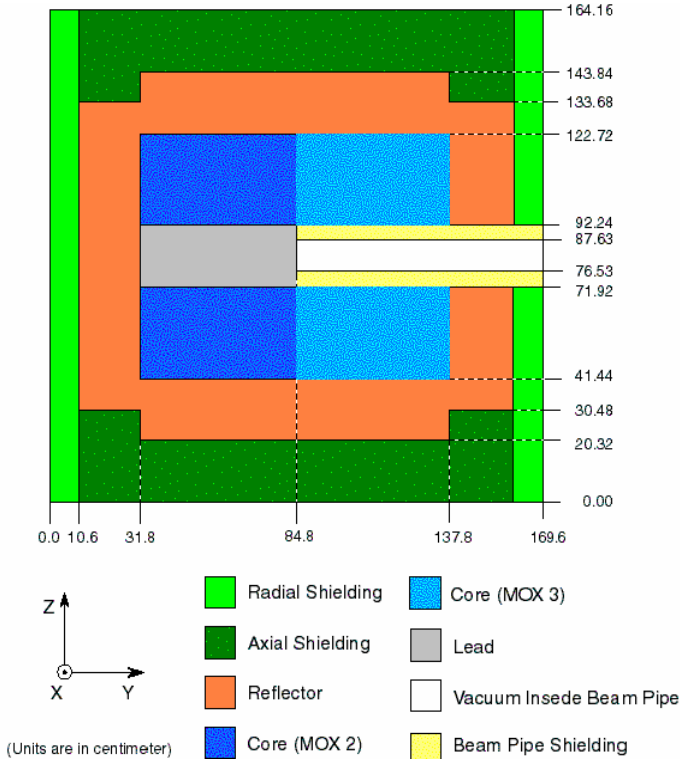

Figure 110: MUSE-4 Critical Config. – Side View #2 at X=90.1 cm

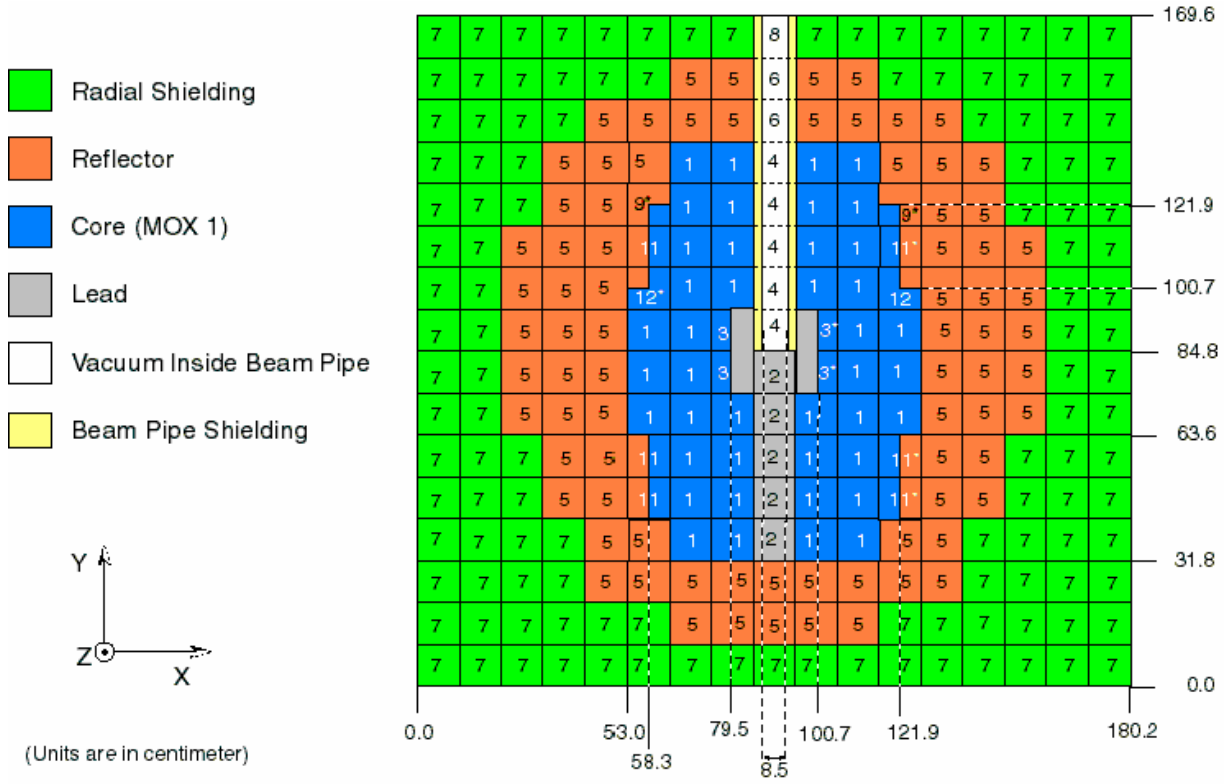

Figure 111: Configuration MUSE-4 976 Cells – Top View at Half Height

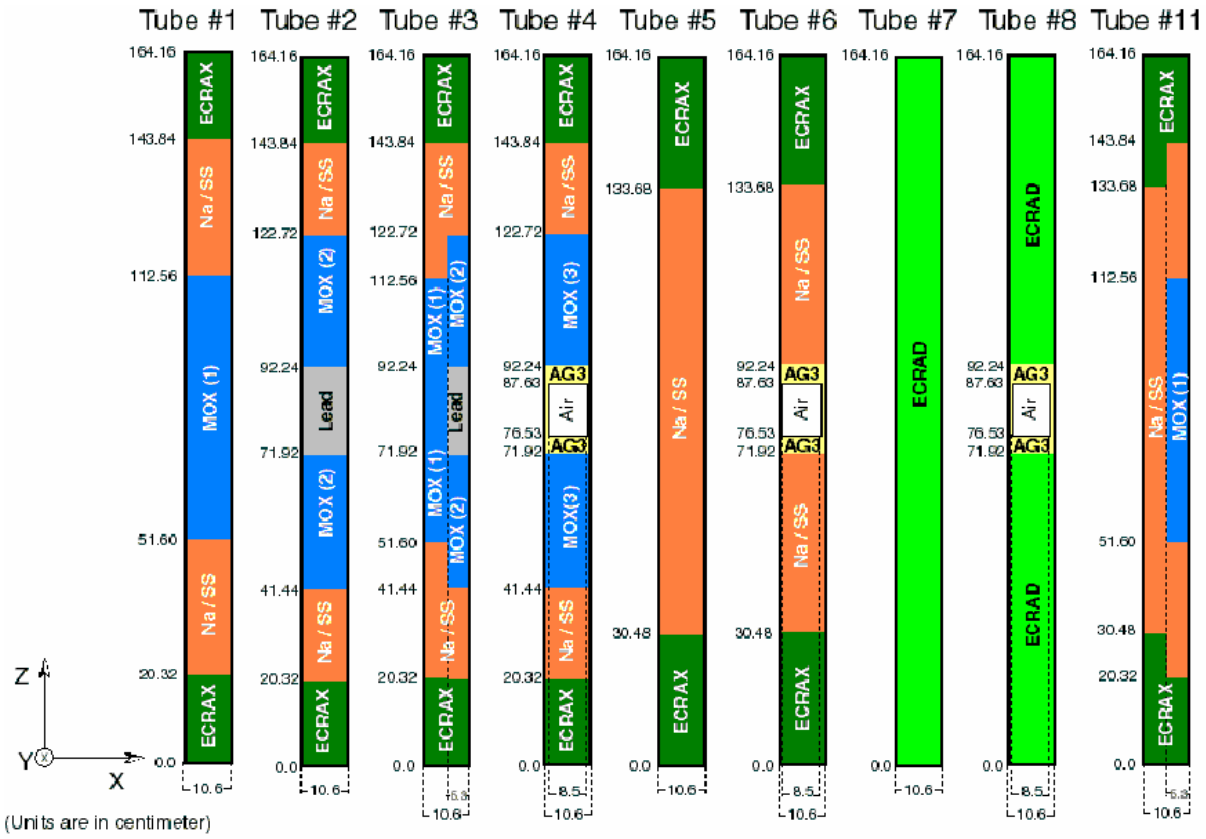

Figure 112: Axial View of the MUSE-4 Tubes 1 to 8 and 11

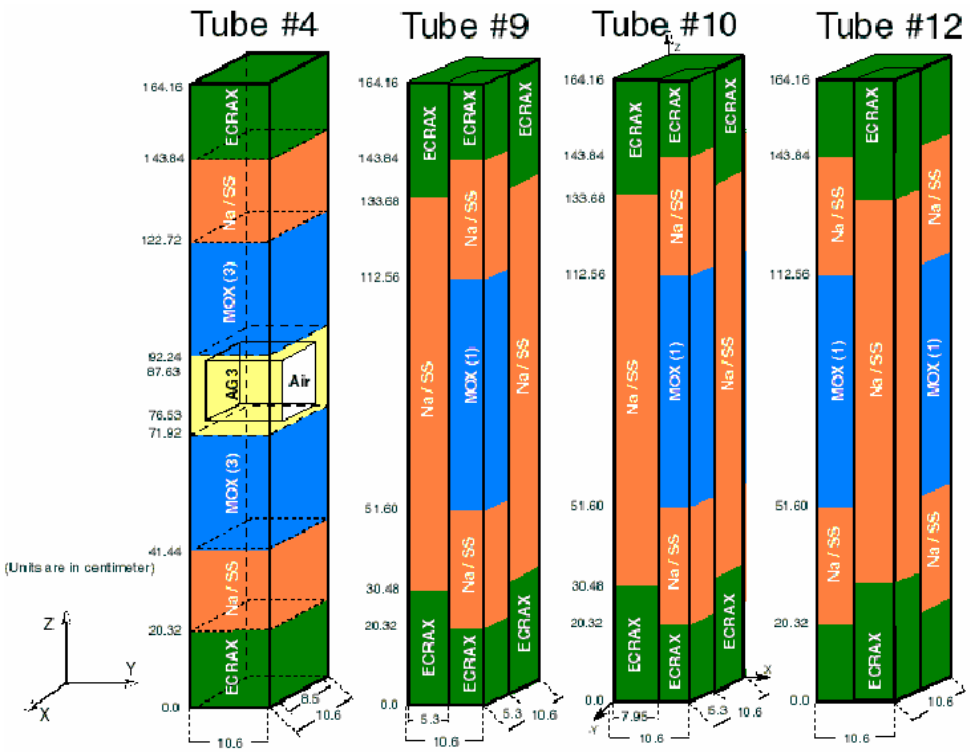

Figure 113: Axial View of the MUSE-4 Tubes 4 and 9

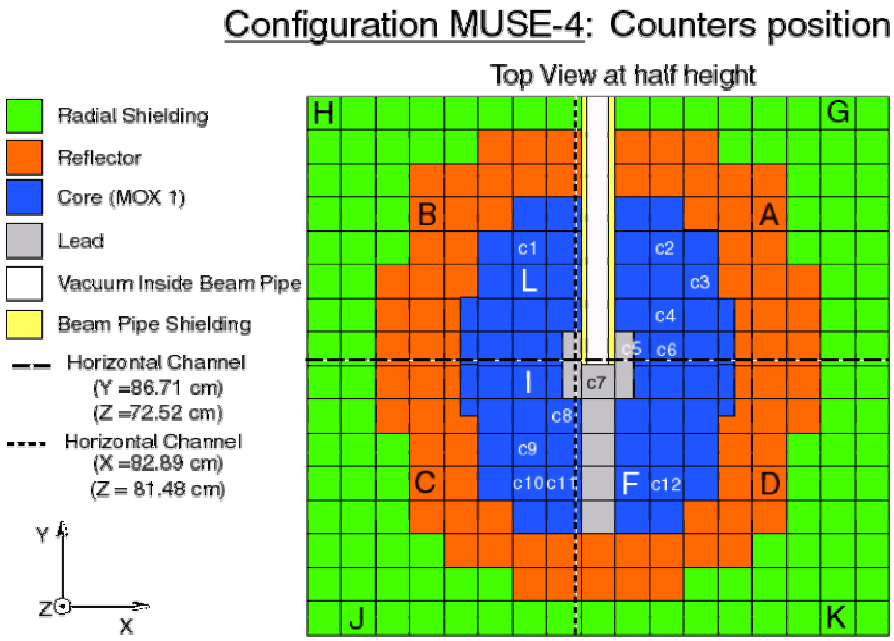

Figure 114: Detector Position

IV.C. Requested calculations

IV.C.1. COSMO calculations

1. Criticality constant, k_{eff}, for the COSMO configuration.

2. ^{235}U, ^{237}Np fission rate and ^{10}B (n,α) relative to Y = 90 cm ^{235}U fission in the following channels:
   - Horizontal channel at X = 82.89 cm and Z = 81.48 cm for: Y = 40, 50, 60, 70, 80, 90, 100, 110, 120, 130, 140 cm.
   - X =90.1 cm, Y = 90.1 cm and Z = 82.08 cm for all of them and Z = 42, 52, 62, 72, 92, 102, 112, 122 cm for ^{237}Np.

3. Fission reaction rates ratios of ^{238}U, ^{238}Pu, ^{239}Pu, ^{240}Pu, ^{241}Pu, ^{242}Pu, ^{241}Am, ^{243}Am, and capture in ^{55}Mn, ^{115}In, ^{197}Au always relative to ^{235}U fission at the following positions:
   - *Position 1*. X = 82.89 cm, Y = 90.1 cm and Z = 81.48 cm.
   - *Position 2*. X =90.1 cm, Y = 90.1 cm and Z = 82.08 cm.

4. Relative neutron spectrum in the same positions as point 3, normalized in such way that the integral will be 1. ERANOS 172 energy bins format and optionally an additional free energy binning are requested.

IV.C.2 Critical MUSE-4 reference configuration calculations

1. Criticality constant, k_{eff}, for the MUSE-4 1 112-cell reference configuration.

2. ^{235}U fission rate as a function of the position in the following channels:

- Horizontal channel E-W at Y = 86.71 cm and Z = 72.52 cm for: X = 5, 15, 25, 35, 45, 55, 65, 75, 85, 95, 90.1, 105, 115, 125, 135, 145, 155, 165, 175 cm.
- Horizontal channel N-S at X = 82.89 cm and Z = 81.48 cm for: Y = 40, 50, 60, 70, 80, 90, 100, 110, 120, 130, 140 cm.
- Vertical channels C7 (X = 90.1 cm, Y = 79.5 cm) and C9 (X = 68.9 cm, Y = 58.3 cm) at Z = 32, 42, 52, 62, 72, 82, 92, 102, 112, 122, 132 cm.

  All data normalized at the vertical channel C7 at position Z = 82 cm.

3. Reaction rates ratios of fission and capture in ^{238}U, ^{238}Pu, ^{239}Pu, ^{240}Pu, ^{241}Pu, ^{242}Pu, ^{241}Am, ^{243}Am, and capture in ^{55}Mn, ^{115}In, ^{197}Au at the center of the E-W, N-S and vertical channels c7 and c9, relative to ^{235}U fission, at c7 (X = 90.1 cm, Y = 79.5 cm) at position Z = 82 cm. Find co-ordinates on the attached tables for result reporting.

4. Relative neutron fluence spectrum in the same positions as point 3, normalized in such way that the integral will be 1. ERANOS 172 energy bins format and optionally an additional free energy binning are requested.

5. Mean neutron lifetime l and β_{eff}.

IV.C.3. Subcritical configuration calculations

1. Reactivity change between reference 1 112-cell configuration and 976-cell configuration of MUSE-4.

$$\Delta k_{eff} = k_{eff}(\text{conf. 976 cells}) - k_{eff}(\text{conf. ref. 1 112 cells})$$

2. ^{235}U fission rate as a function of the position in the following channels:

- Horizontal channel E-W at Y = 86.71 cm and Z = 72.52 cm for: X = 5, 15, 25, 35, 45, 55, 65, 75, 85, 90.1, 95, 105, 115, 125, 135, 145, 155, 165, 175 cm.
- Horizontal channel N-S at X = 82.89 cm and Z = 81.48 cm for: Y = 40, 50, 60, 70, 80, 90, 100, 110, 120, 130, 140 cm.
- Vertical channel C7 and C9 at Z = 32, 42, 52, 62, 72, 82, 92, 102, 112, 122, 132 cm.

  All data normalised at the vertical channel C7 at position Z = 82 cm.

3. Reaction rates ratios of fission and capture in ^{238}U, ^{238}Pu, ^{239}Pu, ^{240}Pu, ^{241}Pu, ^{242}Pu, ^{241}Am, ^{243}Am, and capture in ^{55}Mn, ^{115}In, ^{197}Au at the centre of the E-W, N-S and vertical channels, relative to ^{235}U fission. Find co-ordinates on the attached tables for result reporting.

4. Relative neutron spectrum in the same positions as point 3, normalized in such way that the integral will be 1. ERANOS 172 energy bins format and optionally an additional free energy binning are requested.

5. ^{235}U fission rate as a function of the time after the deuteron-tritium source pulse in the fixed detectors A, B, C, D, F, G, H, I and L, at Z = 95 cm, normalized in such a way to make maximum of each channel equal to 1. The deuteron beam is assumed to have a time structure of 1 μs pulses repeated at 1 kHz. The time step and range will be of 1 μs and 500 μs respectively. Calculation is requested for pulse #1 and for pulse after equilibrium ($n \to \infty$).

6. Mean neutron lifetime l and β_{eff}.

7. Difference between k_{eff} and k_{source} for the 976-cell MUSE-4 configuration. k_{source} is defined by:

$$\frac{Total\,number\,of\,neutrons\,transported}{Total\,number\,of\,source\,neutrons} = \frac{1}{1-k_{source}}$$

An equivalent definition is provided by the equation (⟨⟩ denotes integrated quantities):

$$k_{source} = \frac{\left\langle \nu_f \Sigma_f \Phi \right\rangle + \sum_x \left\langle x\Sigma_{(n,xn)} \Phi \right\rangle}{\left\langle S \right\rangle + \left\langle \nu_f \Sigma_f \Phi \right\rangle + \sum_x \left\langle x\Sigma_{(n,xn)} \Phi \right\rangle} = \frac{\left\langle \nu_f \Sigma_f \Phi \right\rangle + \sum_x \left\langle x\Sigma_{(n,xn)} \Phi \right\rangle}{\left\langle \Sigma_c \Phi \right\rangle + \left\langle \Sigma_f \Phi \right\rangle + \sum_x \left\langle x\Sigma_{(n,xn)} \Phi \right\rangle + \left\langle \vec{\Omega} \cdot \vec{\nabla} \Phi \right\rangle}$$

where S is the source strength.

8. Total time-averaged power produced in the MUSE subcritical core for an average pulse intensity of 10^7 neutrons per pulse and a repetition rate of 1 KHz.

IV.D. Calculations details.

The requested calculations have been performed using both the ERANOS **[22]** deterministic code system and VIM **[30]** probabilistic (Monte-Carlo) code. The VIM application has been limited to the Benchmark STEP 2 (MUSE-4 critical reference configuration).

- The basic data for the deterministic calculations have been taken from JEF2.2 **[23]**, ENDF/B-V and ENDF/B-VI libraries. The cross sections have been processed using both ECCO **[24]** (with JEF2.2) and MC^2-2 **[25]** (with ENDF-B/V, ENDF-B/VI and JEF2.2) codes. The eigenvalue calculations have been performed via VARIANT **[26]** (3D nodal transport code), implemented in the ERANOS code system. Finally, the dynamic calculations related to the STEP 3 have been carried out with the KIN3D code **[29]**.

  The Cell Calculation has been carried out as follows:

  a) *Resonance treatment:*

MC^2-2: Fast and accurate resonance integral methods are used in the narrow resonance resolved and unresolved resonance treatments.

ECCO: Subgroup method and probability tables.

b) A weighted fission spectrum from mix of all fissile nuclides with iterative procedure was used.

c) The (n,2n) is included in scattering matrix.

d) The weighting spectrum for scattering matrices is standard weighting using ultra-fine group spectrum.

e) *Method used for spectrum calculation, treatment of leakage in MC^2-2 and ECCO:*

The extended transport P_1, B_1, consistent P_1, and consistent B_1 fundamental mode ultra-fine-group equations are solved using continuous slowing-down theory and multigroup methods.

Leakage is calculated as a DB^2 term for core fundamental mode calculations. For non fissile compositions a leakage terms is derived from core and used as a source.

f) The number of energy groups used in the different calculation phases change as follows:

MC^2-2: 2082 groups. ECCO: 1968 groups. VARIANT: 2082 or 1968 groups for eigenvalue calculations and 460 groups for reaction rate distribution and spectrum calculations.

- The cross section data for Monte Carlo (VIM) calculations have been taken from ENDF/B-VI. The eigenvalue calculations were completed using ENDF/B-V and JEF-2.2 libraries.

No cell calculation for Monte Carlo code: the library is continuous energy.

For the eigenvalue calculations (JEF-2.2, ENDF/B-V) the following parameters have been used:
5000 histories per generation; 20 generations skipped before scoring, then 100 generations.

Monte Carlo parameters for the four traverse calculations:
5000 histories per generation; 20 generations skipped before scoring, then 1000 generations.
Geometric splitting using a factor of 3 across two nested rectangular surfaces 5 and 10 cm from the axes of the foil locations, respectively, to improve efficiency, one calculation for each traverse (E-W, N-S, C7, and C9). To reduce further the uncertainty in the reaction rates in the center foil in the C7 fuel element, geometric splitting across three nested cubic surfaces was applied, also with a factor of 3 across each surface.

Spectrum: The group fluxes are the integral over each group of the scalar flux (not flux per unit energy or lethargy), so integration over energy is merely the sum of the group fluxes.

Other observations: k_{eff} was not different when the AG3 was smeared in the vacuum it surrounds.

IV.E. MUSE-4 benchmark revised calculations

In this section the results of revised calculations are reported concerning the reactivity value of the three configurations when using the MC^2-2 code to process the cross sections and the dynamic study for the subcritical configuration. The details and the results of the other requested calculations have been already presented in the **Ref. 12.**

IV.E.1. Reactivity results

Criticality constant K_{eff} (final results):

ERANOS:

JEF2.2-ECCO-VARIANT: K_{eff} = 1.00071 (ρ = 71 pcm)

ENDF/B-V – MC^2-2 – VARIANT: K_{eff} = 1.00026 (ρ = +26 pcm)

ENDF/B-VI – MC^2-2 – VARIANT: K_{eff} = 1.00817 (ρ = +810 pcm)

JEF2.2 – MC^2-2 – VARIANT: K_{eff} = 1.00360 (ρ = +359 pcm)

VIM:

JEF2.2: K_{eff} = 1.00436 ± 0.0009 (ρ = 439 ± 90 pcm)

ENDF/B-V: K_{eff} = 1.0037 ± 0.0010 (ρ = 369 ± 100 pcm)

ENDF/B-VI: K_{eff} = 1.0052 ± 0.0009 (ρ = 517 ± 90 pcm)

The ERANOS results have been obtained in four steps. In the following we report the details for the case JEF2.2-ECCO, keeping in mind that a similar approach has been also used for the MC^2-2 calculations.

Step 1: investigation of the change on the reactivity results through the number of energy groups (NG) used. This dependence has been quoted for NG increasing from 33 up to 838.

Table 20: MUSE-4 Critical Configuration - K_{eff} ECCO - VARIANT

NG	JEF2.2 - ECCO	
	VARIANT[1] - ERANOS: K_{eff}	ρ [pcm]
33[2]	.98664	-1354
172[2]	.98933	-1079
231[2]	.99389	-615
471[2]	.99695	-306
838[2]	.99815	-185

[1] Flux and leakage expansion order 3 WITH SIMPLIFIED SPHERICAL HARMONIC (HS)

[2] With condensation from a fine step to NG

K_{eff} (reactivity) values with NG=838: K_{eff} = 0.99815 (ρ = -185 pcm)

This study shows a strong dependence of the calculated reactivity value on the number of energy group used. Besides the reactivity, a dependence has been also found for some reaction rate distributions. Indeed, in order to accurately account for the spectral effects at the interface core/reflector a detailed multigroup energy treatment is needed. By the way, significant difficulties occur when performing a deterministic calculation with an high number of energy groups: the computational resources, in term of time, disk space and memory, are very demanding. For this purpose, in **Appendix B** we propose different methods to process correctly the cross-sections over a board group energy structure (e.g. with the usual NG=33) able to reproduce the same results (reactivity and reaction rate distributions) of the fine spatial calculation.

Step 2: estimated correction introduced by a fine transport calculation (NG=1968).
In order to estimate the correction introduced by a fine transport calculation we propose the following figures, where the reactivity value is presented as a function of NG. We conclude that a fine transport calculation makes the following estimated correction: +105 pcm (see **Figure 111**)

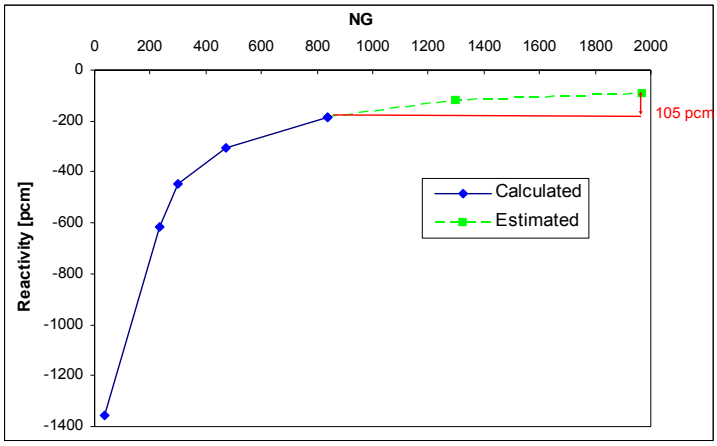

Figure 115: Reactivities JEF2.2 – ECCO – VARIANT

Final results at step 2:
K_{eff} =0.99920 (ρ = -80 pcm)

Step 3: application of the correction introduced by a P3 (full flux and leakage expansion order 3) transport calculation.
The order of this correction was calculated for NG=33:

Table 21: MUSE-4 Critical Config. - Transport P3 (Full Flux and Leakage Expansion Order 3) Correction

MUSE-4 Critical – NG=33	HS: ρ [pcm]	P3: ρ [pcm]	Δρ = P3 - HS
JEF2.2 – ECCO	-1354	-1283	+71

Final results at step 3 by application of the correction shown on column 4:

K_{eff} = 0.99991 (ρ = -9 pcm)

Step 4: application of the correction introduced by the P3 anisotropic scattering order 3 transport calculation. The order of this correction was calculated for NG=33:

Table 22: MUSE-4 Critical Configuration - Anisotropic Order 3 Transport Correction

MUSE-4 Critical – NG=33	P1: ρ [pcm]	P3: ρ [pcm]	Δρ = P3 – P1
JEF2.2 – ECCO	-1354	-1274	+80

Final results at step 4 by application of the correction shown on column 4:

K_{eff} = 1.00071 (ρ = 71 pcm)

Important. Originally the MC^2-2 results provided the following results:

Table 23: MUSE-4 Critical Configuration - K_{eff} MC^2-2 - VARIANT

NG	**ENDF/B-V – MC^2-2**		**ENDF/B-VI – MC^2-2**		**JEF2.2 – MC^2-2**	
	VARIANT[(1)] - ERANOS:		**VARIANT[(1)] - ERANOS**:		**VARIANT[(1)] - ERANOS**:	
	K_{eff}	ρ [pcm]	K_{eff}	ρ [pcm]	K_{eff}	ρ [pcm]
33[(2)]	1.01554	1530	1.02346	2292	1.02358	2304
231[(2)]	1.01105	1093	1.01757	1727	1.01605	1580
460[(2)]	1.00759	753	1.01440	1420	1.01185	1171
887[(2)]	1.00639	635	1.01278	1262	1.01032	1021

[(1)] Flux and leakage expansion order 3 WITH SIMPLIFIED SPHERICAL HARMONIC (HS)
[(2)] With condensation from a fine step to NG

the application of the same procedure as described above lead to the following best estimated results:

ENDF/B-V – MC^2-2 – VARIANT: K_{eff} = 1.00718 (ρ = +713 pcm)

ENDF/B-VI – MC^2-2 – VARIANT: K_{eff} = 1.01361 (ρ = +1343 pcm)

JEF2.2 – MC^2-2 – VARIANT: K_{eff} = 1.01066 (ρ = +1055 pcm)

The most evident issue is the huge discrepancy observed for the 33-group calculation between the ECCO and MC^2-2 results. An in-depth analysis has been carried out and we concluded that this discrepancy is due to an inconsistency in the MC^2-2 code when processing the total cross-section. Indeed, the solution of the Boltzmann equation with a deterministic multigroup P_N approximation can use the total cross-section weighted with the flux, the current or in a general case with an high order moment Φ_n (n >1) of the flux expansion in Legendre's Polynomials, but in order to proceed consistently with this choice an appropriate correction is to be introduced on the within-group scattering cross-section. The details are given in **Appendix A**.
After correction, the results given in **Table 22** change as follows:

Table 24: MUSE-4 Critical Configuration - K_{eff} MC^2-2 - VARIANT

NG	ENDF/B-V – MC^2-2		ENDF/B-VI – MC^2-2		JEF2.2 – MC^2-2	
	VARIANT(1) - ERANOS:		VARIANT(1) - ERANOS:		VARIANT(1) - ERANOS:	
	K_{eff}	ρ [pcm]	K_{eff}	.ρ [pcm]	K_{eff}	ρ [pcm]
33(2)	0.98075	-1963	0.98804	-1210	0.98514	-1508
231(2)	0.99141	-866	0.99819	-181	0.99522	-480
460(2)	0.99535	-467	1.00283	282	0.99874	-126
887(2)	0.99776	-225	1.00538	535	1.00131	131

(1) Flux and leakage expansion order 3 WITH SIMPLIFIED SPHERICAL HARMONIC (HS)
(2) With condensation from a fine step to NG

With the same approach, the reactivity results for the other configurations proposed in the benchmark have been revised as follows:

- COSMO configuration

ERANOS:

JEF2.2-ECCO-VARIANT: K_{eff} = 1.00190 (ρ = 190 pcm)
ENDF/B-V – MC^2-2 – VARIANT: K_{eff} = 1.00216 (ρ = 216 pcm)
ENDF/B-VI – MC^2-2 – VARIANT: K_{eff} = 1.00921 (ρ = 913 pcm)
JEF2.2 – MC^2-2 – VARIANT: K_{eff} = 1.00478 (ρ = 476 pcm)

- MUSE-4 Subcritical Configuration

ERANOS:

JEF2.2-ECCO-VARIANT: K_{eff} = 0.96863 (ρ = -3239 pcm)
ENDF/B-V – MC^2-2 – VARIANT: K_{eff} = 0.96796 (ρ = -3310 pcm)
ENDF/B-VI – MC^2-2 – VARIANT: K_{eff} = 0.97564 (ρ = -2497 pcm)
JEF2.2 – MC^2-2 – VARIANT: K_{eff} = 0.97188 (ρ = -2893 pcm)

IV.E.2. Dynamic results

The cooperation with Andrei Rineisky from FZK-Karlsruhe (Germany) led to the final dynamic results of the point 5 of the MUSE4 Benchmark - Step 3 (MUSE4 subcritical configuration). In particular the response of the detectors in the shielding and in the reflector has been improved. The **Figure 112** shows the new results obtained with KIN3D for each detector and the **Figures 117** and **128** show each detector response separately with the comparison with the other Monte-Carlo results when available. We can observe that the agreement with the other attendants to the Benchmark, using for the most part a Monte-Carlo code, is now very good.

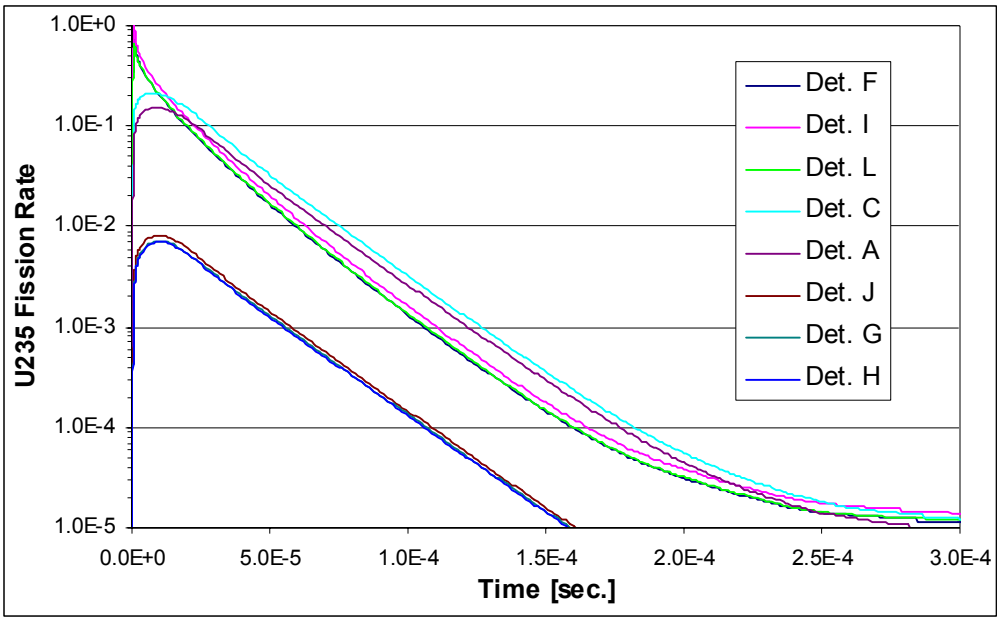

Figure 116: KIN3D Direct Method – All Detector Behaviors

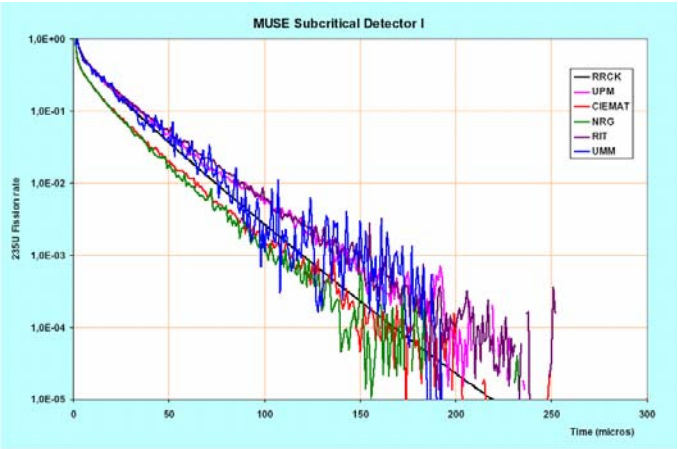

Figure 117: Detector I – Monte-Carlo Results

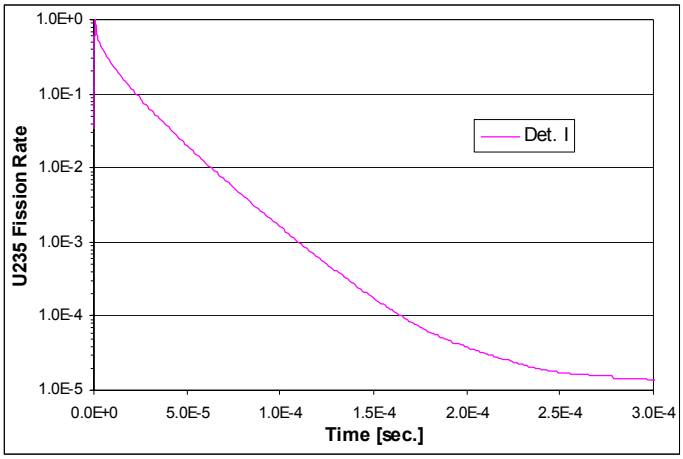

Figure 118: Detector I – KIN3D

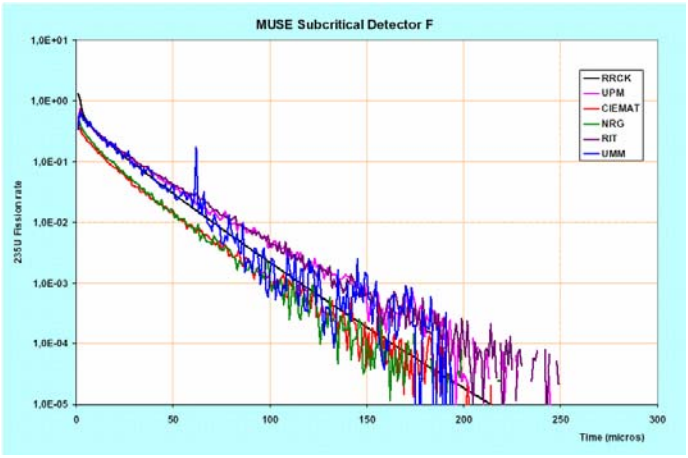

Figure 119: Detector F – Monte-Carlo Results

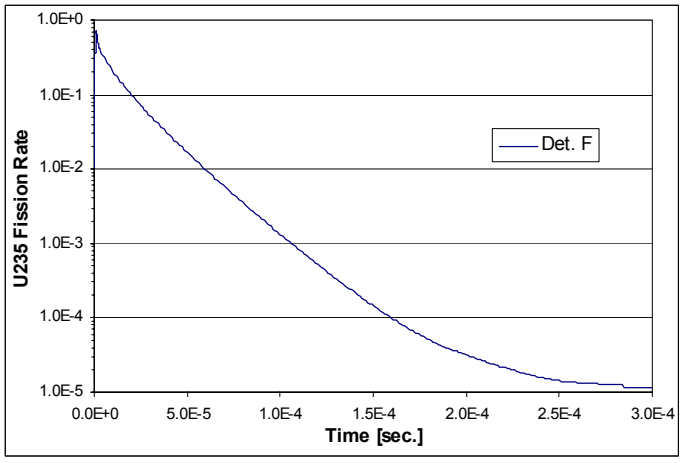

Figure 120: Detector F – KIN3D

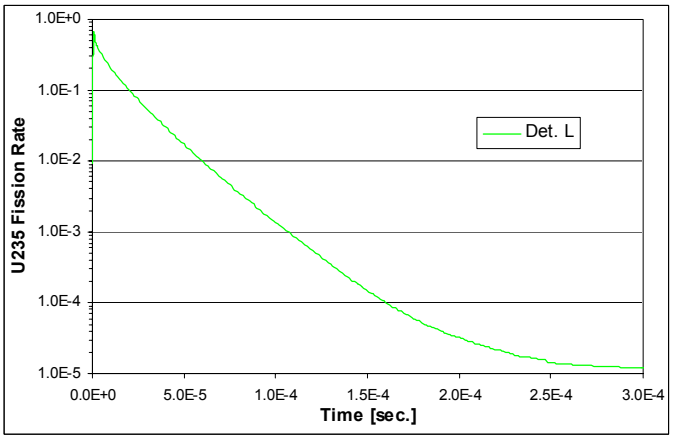

Figure 121: Detector L – KIN3D

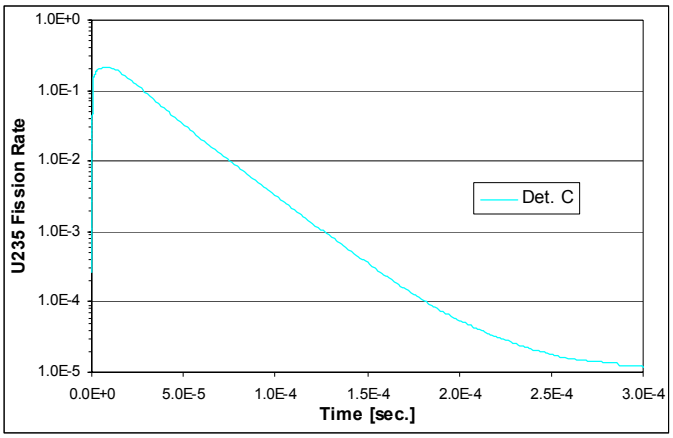

Figure 122: Detector C – KIN3D

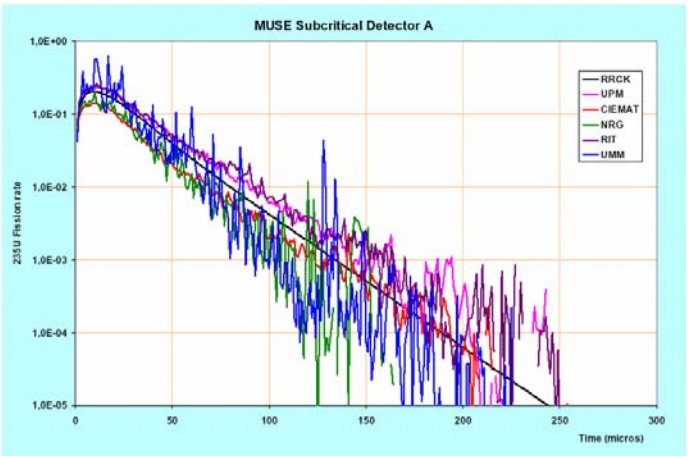

Figure 123: Detector A – Monte-Carlo Results

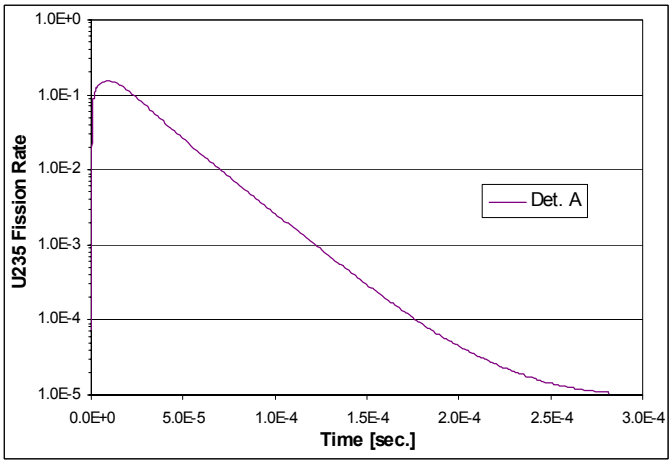

Figure 124: Detector A – KIN3D

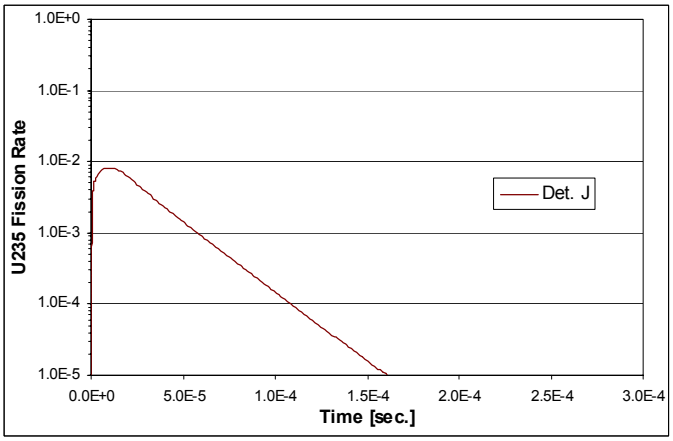

Figure 125: Detector J – KIN3D

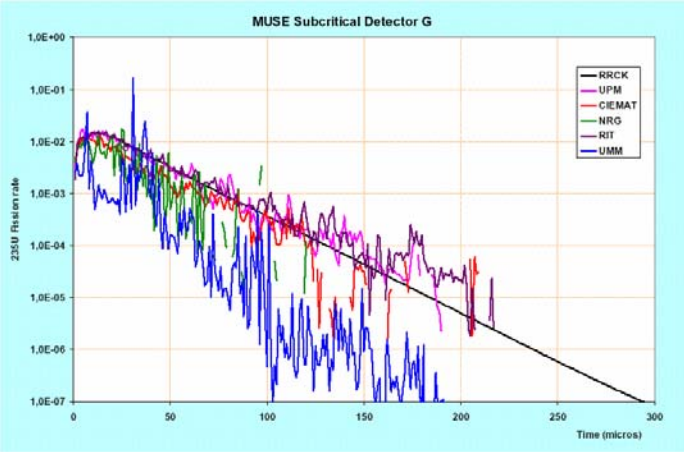

Figure 126: Detector G – Monte-Carlo Results

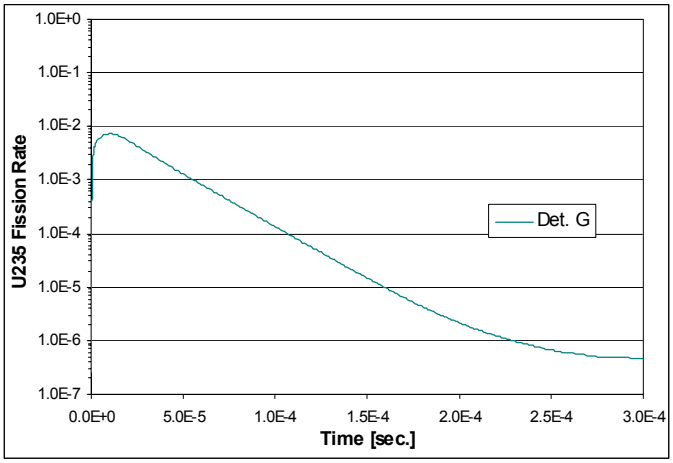

Figure 127: Detector G – KIN3D

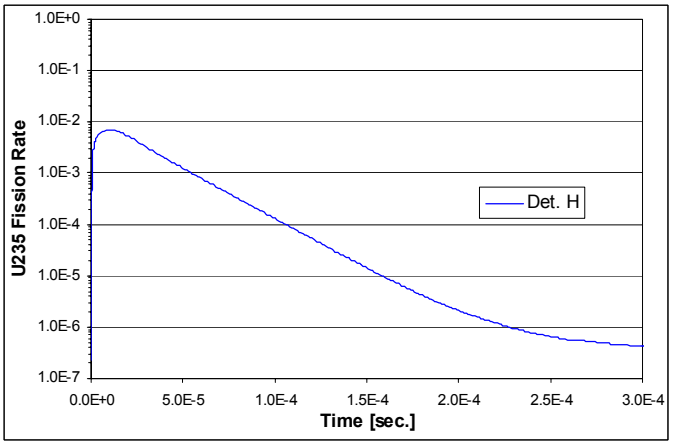

Figure 128: Detector H – KIN3D

V. Conclusions

This report has presented a review of the activities performed by the five teams involved in the MUSE-4 experimental program. More details about the contribution provided by ANL during the year 9/02 to 9/03 has been presented (see **Ref. 12** for an accurate description of the previous work). The ANL activity consisted both in direct participation in the experimental measurements in particular with the assistance given by G. Imel currently at CEA-CADARACHE and in the analysis by the calculation of the experimental data.

The analysis has been focused on the subcritical level determination, on adjoint flux and fission rate traverses, on the dynamic measurements.

The following observations have been made:

- **Reactivity calculation.**

  The study shows a strong dependence of the calculated reactivity value on the number of energy groups used. Indeed, in order to accurately account for the spectral effects at the interface core/reflector a detailed multigroup energy treatment is needed. Significant difficulties occur when performing a deterministic calculation with an high number of energy groups: the computational resources, in term of time, disk space and memory, are very demanding. For this purpose, different methods have been proposed in order to process correctly the cross-sections over a board group energy structure (e.g. with the usual NG=33), able to reproduce the same results (reactivity and reaction rate distributions) of the fine spatial calculation.

  The impact on the reactivity calculation due to the use of different nuclear data can be observed when the cross-sections are processed with the MC^2-2 code: moving from the ENDF/B-V to the ENDF/B-VI library causes a spread on the reactivity results of about 700 pcm. While the comparison between the JEF2.2-ECCO and JEF2.2- MC^2-2 results allows to estimate the effect due to the use of different codes (ECCO vs MC^2-2) when the nuclear data are the same: this effect is of about 150 pcm.

  The experiment-calculation discrepancy observed on the reactivity values fit well within the margin of the uncertainty in the cases JEF2.2-ECCO and ENDF/B-V - MC^2-2 ($\Delta \rho$ = 177 and 17 pcm respectively). Some difficulties appear when using the MC^2-2 code in conjunction with the JEF2.2 and ENDF/B-VI data. However, among the sources of uncertainties there is of course also the uncertainty associated to the nuclear data that has not been considered in the present analysis.

- **Adjoint flux distributions**

  The analysis of the experimental traverses with californium source for the MUSE-4 reference configuration has been performed. These traverses represent the adjoint flux distribution. The axial traverses have been performed at the positions E1615, E1818, W2018 and W2217. The positions E1615 and W2217 are relatively unperturbed, while the position E1918 is in the lead buffer zone and W2018 is near both to the lead buffer zone and to a control rod. The traverses were made at two reactivity levels: roughly –70 pcm with the pilot rod (PR) down and roughly –20 pcm with the PR at 600 mm. North-South (NS) and East-West (EW) radial traverses were also performed for the two reactivities.

  The calculation results show that the model does not accurately fit the adjoint flux outside the core when only 33 energy groups are used. The model consistently underestimates the adjoint flux in all the traverses. Indeed, a correct description of the slowing down of the neutrons and their reflection in the fuel at the interface core/reflector, needs the use of an higher number of energy groups NG.

  The discrepancies are sharply reduced when NG increases. In this case, the calculations performed for example via JEF2.2-ECCO with NG = 299, 471, 838 show approximately the same results, consequently a 299 energy group structure seems to be enough for the analysis of the experimental data. The same remark applies when the MC^2-2 code is used, but in this case 231 energy groups are employed instead of 299. Using 299 (or 231) energy groups the model still underestimates the adjoint flux, but the observed discrepancies seem to be within the margins if an uncertainty associated to the calculation would be taken in account together with the experimental one.

  All the measured traverses have been studied, but in the document just the adjoint flux distributions observed with pilot rod (PR) at 600 mm are discussed. Indeed, with PR inserted the measured and calculated results are about the same; slight differences appear just in the case of the E1918 traverse which is at the same time close to a control rod and it is also the closest traverse to the PR.

  The use of different nuclear data libraries doesn't seem to affect the calculated adjoint flux distributions if the same number of energy group is used.

  However, an asymmetry is observed in some data that is not seen in the model. This is especially true for the W2018H traverses, but it also appears for the E1918H traverse. At the present time, it is not clear whether the asymmetries seen in the data correspond to a real physical effect, or they are due to some bias.

- **Fission rate traverses.**

  U235 fission radial traverses EW and NS, and the Np237 EW radial traverse of the MUSE-4 critical configuration (1115 cells) have been calculated.

  In general, all the traverses show a good agreement between the calculation and the experiment in the margin of the uncertainty on the measurement if the number of energy group is sufficiently high. For the NS

traverse a 2.5 cm translation has been applied. For the U5 EW traverse an uncertainty too large on the experimental values has been provided, consequently a value of 2% has been used.

A good agreement between the calculation and the experiment is also found in proximity of the reflector. In the case of the NS traverse this agreement decreases because of the proximity of the void region too.

Concerning the impact of the nuclear data on the calculated traverses, the MC^2-2 – ENDF/B-VI calculation overestimates the other simulations.

- **Dynamic calculations**

During the MUSE-4 phase of the experimental program, one of the objectives is to investigate the neutronic response to neutron pulses with frequencies of 1 to 4 kHz, and less than 1μs wide, generated at the reactor center by the (d,d) GENEPI accelerator. Detectors based on ^{235}U and ^{237}Np fission, located in the core, reflector and shielding regions are used for measuring the time dependent responses.

Measurements are available for the MUSE-4 SC0 configuration. The axial positioning of the control and pilot rods allowed to produce different core configurations, corresponding to different levels of subcriticality. The following configurations have been investigated:

- MUSE-4 SC0 with pilot rod out;
- MUSE-4 SC0 with pilot rod in;
- MUSE-4 SC0 with pilot rod and control rod "bc1" in.

In the point kinetic approximation the response *P(t)* to a neutron pulse is the sum of an exponential decay from the prompt multiplication plus a nearly constant offset due to the delayed neutrons. In particular, the prompt time dependence $P(t) \sim exp(-\alpha t)$, with $\alpha \cong \frac{\hat{\beta} - \rho}{\Lambda}$, $\hat{\beta}$ the effective fraction of delayed neutron and Λ the mean generation time characterizing the system under study, can be investigated for a method of reactivity measurement, the Pulsed Neutron Source (PNS) method.

As a preliminary analysis, a point kinetic model has been employed for the present study.

Due to the proximity to critical state of the configurations with pilot rod in and out, since the best estimation for the reactivity provides positive values in some simulations, especially when using the ENDF/B-VI data library, the calculation has been normalized to the experimental reactivity (indeed, the study of a system driven by an external source requires a subcritical state). Instead, in the case of the configuration with control rod bc1 in, no normalization has been performed.

The main problem of the PNS method consists in the limitations of the technique. Indeed, the real configuration is often very different from a "point-reactor", and the experimental response depends in general on the position of the detectors. In order to reproduce the detector response by the calculation, a

space-time solution of the transport equation, like the direct or the quasi-static methods (both available in KIN3D), has to be used.

In general, the agreement with the measurements has been found satisfactory for each configuration analyzed. Regarding the calculation, it can be observed that the effect due to the use of different libraries during the transient is not significant if each calculation is normalized to the same reactivity. Instead, the effect is important if no normalization is performed.

Several analyses have been performed to extract information on the reactivity of the MUSE configurations, in particular using the PNS method.

A first investigation has been performed to study any dependence of the flux response on the detector location. The calculation confirmed that the different detector responses (^{235}U fission rate) have approximately the same decay slope, but the prompt-area changes significantly especially in the shielding region. This behavior certainly raises some issues for other experimental techniques of reactivity measurement, such as the area-ratio method, which relates the prompt to delayed area ratio with ρ/β.

Additionally, it appears that after 20 μs from the injection of the neutron pulse, i.e. when the decay becomes less sensitive to the shape of the pulse, the detector positions indicate the same prompt time dependence (i.e. decay slope), even if it is different from the point kinetics behavior. It has been demonstrated that using an average Λ in the prompt decay range (from 20 to 150 μs), the PNS method could still apply. Further investigations are needed on this aspect.

Besides the analysis of the experimental data, the MUSE-4 benchmark proposed by the OECD has been completed.

The benchmark has been divided in three steps. The first step allows an understanding of the analysis methods of the different groups and tuning of the simulation programs with the experimental data of an already measured configuration (COSMO). In the second step, the MUSE-4 reference configuration (1112 cells) is proposed to simulate different reactor parameters (criticality constant, flux distribution...) in a nearly critical configuration. Finally, a third step is oriented to the simulation of reactor response to the external source in the subcritical reference configuration (976 cells).

In particular, the reactivity values calculated via the MC^2-2 code have been revised: an in-depth analysis lead to the detection of an inconsistency in the code when processing the total cross-section. Indeed, the solution of the Boltzmann equation with a deterministic multigroup P_N approximation can use the total cross-section weighted with the flux, the current or in a general case with an high order moment Φ_n (n >1) of the flux expansion in Legendre's Polynomials, but in order to proceed consistently with this choice an appropriate correction is to be introduced on the within-group scattering cross-section. The details are given in this document.

Finally, also the dynamic calculations requested by the benchmark have been revised after a correction of a bug in the KIN3D code. It has been show that the new results are in an excellent agreement with the Monte-Carlo simulations performed by the other teams attending to this benchmark.

Appendix A: MC^2-2 inconsistency in P_N approximation and its impact on reflector effects

I. Introduction

The existence of space and energy neutron flux distribution transients is a well known phenomena which affects the calculation of fast reactors where the core is surrounded by fertile blankets and/or reflectors. The present interest for fast neutron reactors as TRU burners of relatively low power and small core size (high leakage) underlines the need for an accurate treatment of neutron reflection. In fact, the treatment of reflector effects can introduce significant uncertainties on K_{eff} and power distribution calculated values **[27,31]**. Moreover, the solution of the Boltzmann equation with a deterministic multigroup P_N approximation can use the total cross-section weighted with the flux, the current or in a general case with a high order moment Φ_n (n >1) of the flux expansion in Legendre's Polynomials. In this Section we demonstrate that in order to proceed consistently with this choice an appropriate correction is to be introduced on the within-group scattering cross-section.

II. Reflector effects study

In order to simplify this study, we investigated a 1D model. Fuel and reflector compositions are provided in **Table 25.**

Table 25: Fuel and reflector compositions

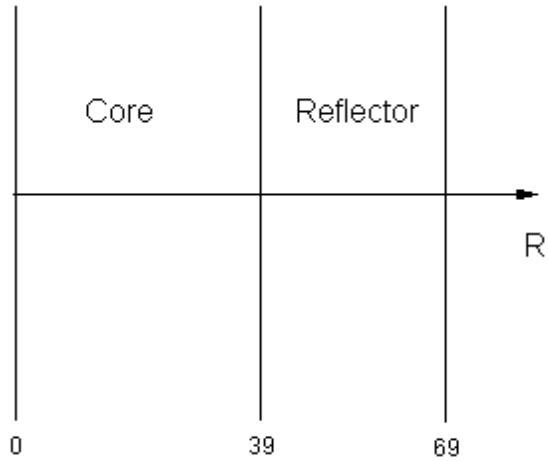

Region	Isotope	Density × 10^{+24} at/cm^3
Zone1- Fuel	Pu239	1.5×10^{-3}
	U238	5.0×10^{-3}
	Fe56	7.0×10^{-3}
	Cr52	1.5×10^{-3}
	Na23	1.0×10^{-2}
	O16	1.5×10^{-2}
Zone2 - Reflector	Fe56	5.0×10^{-2}
	Cr52	1.5×10^{-2}
	Na23	5.0×10^{-3}

For the simplified model under study different calculations have been performed using the ERANOS deterministic code system **[22]** coupled with the JEF2.2 cross-section library **[23]**, to solve the Boltzmann multigroup transport equations with different approximations: P_0* (use of the transport cross-section), P_1 with current-weighted total cross-section and P_1 with flux-weighted total cross-section. The cross-sections have been

processed in 33 energy broad group structure via ECCO **[24]** and MC^2-2 **[25]** for the purpose of comparison between the two codes. The following reactivity results have been obtained.

Table 26: ECCO- MC^2-2 Reactivity Results [pcm]

ρ [pcm]	P_0* (use of Σ_{tr})	P_1 consistent (current-weighted total)	P_1 consistent (flux-weighted total)
MC^2-2 – ERANOS	-5018	-5114	+4001
ECCO – ERANOS	-5114	-5340	-5581

Inspection of **Table 26** shows that MC^2-2 gives huge discrepancies on the reactivity values in P_1 approximation when using the total cross-section weighted with the current or with the flux. This discrepancy of about 9500 pcm for the simplified problem under study remains large in the case of a realistic fast reactor configuration: for example, in the case of the MUSE-4 configuration, set up in France by the CEA-Cadarache in the frame of the experimental program on the ADS, more than 3000 pcm discrepancy has been observed.
In particular, the results obtained with MC^2-2 using the current-weighted total cross-section are in a good agreement with those ones provided by ECCO-ERANOS in the corresponding case. Further, in this case the results are also comparable to those ones obtained with the P_0* approximation.

The discrepancies mentioned above do not exist, anyway, when the cross-sections are processed with the ECCO code: in this case the choice of a current or flux-weighted cross-section has a not significant impact on the reactivity in P_1 approximation.

Additional investigations lead us to the conclusion that the inconsistency shown by MC^2-2 is due to an incorrect formulation. Indeed, the use of the flux-weighted total cross-section requires a correction to be applied to the within-group scattering order 1 cross-section, $\Sigma^1_{g\to g}$. On the contrary, the use of the current-weighted total cross-section requires a correction to be applied to the within-group scattering order 0 cross-section, $\Sigma^0_{g\to g}$. Just in this last case, the correction is made automatically by ERANOS. Consequently, the results provided by MC^2-2 with current-weighted total cross-section are correct. Instead, in the case of the flux-weighted total cross-section they are wrong.

In order to support these conclusions a new MC^2-2 calculation has been made with flux-weighted total cross-section, where the $\Sigma^1_{g\to g}$ cross-section has been replaced with the corresponding one provided by the ECCO code in the same case. The calculated reactivity values are shown in the following table:

Table 27: MC^2-2 Reactivity Results with Flux-Weighted Total Cross-Section

ρ [pcm]	MC^2-2 – ERANOS standard	MC^2-2 – ERANOS with $\Sigma^1_{g\to g}$ from Ecco just for the fuel region	MC^2-2 – ERANOS with $\Sigma^1_{g\to g}$ from Ecco for the fuel and reflector regions
P_1 consistent	+4001	+3732	-5203

Inspection of **Table 27** allows to stress at same time two important aspects. First, as expected, the result in column 4 demonstrates that MC^2-2, like ECCO, provides comparable values of reactivity in the two situations of current or flux-weighted total cross-section provided that the within-group scattering cross-section is adjusted consistently with this choice. On the other hand, the result shown in column 3 point out that this kind of problem is relevant especially in presence of reflector zone at the core boundary. Indeed the correction of the $\Sigma^1_{g\to g}$ cross-section just in the fuel region has a small impact: less than 300 pcm in this specific case, to be compared with a reactivity effect of about 9000 pcm coming from the reflector.

The corrections to be applied to the $\Sigma^n_{g\to g}$ (n=0,1) cross-section can be motivated by looking at the P_1 equations in the multigroup approximation and requiring the use of the same total (current or flux-weighted) in both of them. For this purpose, a detailed demonstration is provided in the following paragraph where the analysis has been also extended to a general case of total cross-section weighted with any order moment Φ_n (n=0 flux, n =1 current, and n >1) of the flux expansion in Legendre's Polynomials.

III. Theoretical approach

The starting point is the time-independent transport equation:

$$\vec{\Omega}\cdot\vec{\nabla}\Phi(\vec{r},E,\vec{\Omega})+\Sigma_t(E)\Phi(\vec{r},E,\vec{\Omega})= \\ =\iint\Phi(\vec{r},E',\vec{\Omega}')\Sigma_s(\vec{r},E'\to E,\vec{\Omega}'\to\vec{\Omega})dE'\,d\vec{\Omega}'+S(\vec{r},E,\vec{\Omega}) \qquad \text{Eq.1}$$

with the source term defined by:

$$S(\vec{r},E,\vec{\Omega})=\frac{1}{K}\chi(E)\iint\nu\Sigma_f(\vec{r},E',\vec{\Omega}')\Phi(\vec{r},E',\vec{\Omega}')dE'\,d\vec{\Omega}'+S_{ext}(\vec{r},E,\vec{\Omega}) \qquad \text{Eq.2}$$

Using the hypothesis of fundamental mode:

$$\Phi(\vec{r},E,\vec{\Omega})=\Phi(E,\vec{\Omega})e^{i\vec{B}\cdot\vec{r}} \qquad \text{Eq.3}$$

$$S(\vec{r},E,\vec{\Omega})=S(E,\vec{\Omega})e^{i\vec{B}\cdot\vec{r}} \qquad \text{Eq.4}$$

the P_N approximation, which makes use of the flux, the source and the cross-sections expansion in Legendre's Polynomials, is obtained by solving the following sequence of equations with the condition $\Phi_{N+1} = 0$:

$$iB(n+1)\Phi_{n+1}(E) + iBn\Phi_{n-1}(E) + (2n+1)\Sigma_t\Phi_n(E) = \\ = (2n+1)S_n(E) + (2n+1)\int \Sigma_s^n(E' \to E)\Phi_n(E')dE', \qquad n = 0,1,2,..,\infty \quad \text{Eq.5}$$

In particular, in the case of the P_1 approximation, we derive two equations:

$$iB\Phi_1 + \Sigma_t\Phi_0 = S_0 + \int \Sigma_s^0(E' \to E)\Phi_0(E')dE' \quad \text{Eq.6}$$

$$\frac{iB}{3}\Phi_0 + \Sigma_t\Phi_1 = S_1 + \int \Sigma_s^1(E' \to E)\Phi_1(E')dE' \quad \text{Eq.7}$$

One can verify that the moments Φ_0 and Φ_1 have the meaning of flux and current respectively.

Eqs.6 and 7 are usually expressed in a multigroup form by introducing the quantities:

$$\Phi_g^n = \int_{\Delta E_g} \Phi_n(E)dE \quad \text{Eq.8}$$

$$\Sigma_{t,g}^n = \frac{1}{\Phi_n}\int_{\Delta E_g} \Sigma_t\Phi_n(E)dE \quad \text{Eq.9}$$

$$\Sigma_{g' \to g}^n = \frac{1}{\Phi_n}\int_{\Delta E_g} dE \int_{\Delta E_{g'}} \Sigma_s^n(E' \to E)\Phi_n dE' \quad \text{Eq.10}$$

(Note that the total cross-section is flux-weighted when n=0, on the contrary it is current-weighted if n=1).

Finally, the multigroup form of the P_1 equation is the following one:

$$\left(\Sigma_{t,g}^0 - \Sigma_{g \to g}^0 - \Sigma_{g' \to g}^0\right)\Phi_0^g = -iB\Phi_1 + S_0 \quad \text{Eq.11}$$

$$\left(\Sigma_{t,g}^1 - \Sigma_{g \to g}^1 - \Sigma_{g' \to g}^1\right)\Phi_1^g = -\frac{iB}{3}\Phi_0 + S_1 \quad \text{Eq.12}$$

where, the contribution of the within-group scattering has been isolated for the scattering term.
One can observe that in the equations presented above there is an inconsistency: the total cross-section is weighted with the flux in **Eq.11**, with the current in **Eq.12**.

The following choices are possible:

1) Use of the flux-weighted total cross-section.

In this case, we leave unchanged **Eq. 11** and we add and subtract $\Sigma_{t,g}^{0}$ in **Eq.12**:

$$\left(\Sigma_{t,g}^{0} - \Sigma_{t,g}^{0} + \Sigma_{t,g}^{1} - \Sigma_{g\to g}^{1} - \Sigma_{g'\to g}^{1}\right)\Phi_{1}^{g} = -\frac{iB}{3}\Phi_{0} + S_{1} \qquad \text{Eq.13}$$

Consequently, the following correction has to be applied:

$$\Sigma_{g\to g}^{1,cor} = \Sigma_{t,g}^{0} - \Sigma_{t,g}^{1} + \Sigma_{g\to g}^{1} \qquad \text{Eq.14}$$

2) Use of the current-weighted total cross-section.

In this case, we live unchanged **Eq. 12** and we add and subtract $\Sigma_{t,g}^{1}$ in **Eq.11**:

$$\left(\Sigma_{t,g}^{1} - \Sigma_{t,g}^{1} + \Sigma_{t,g}^{0} - \Sigma_{g\to g}^{0} - \Sigma_{g'\to g}^{0}\right)\Phi_{0}^{g} = -iB\Phi_{1} + S_{0} \qquad \text{Eq.15}$$

The following correction has to be applied:

$$\Sigma_{g\to g}^{0,cor} = \Sigma_{t,g}^{1} - \Sigma_{t,g}^{0} + \Sigma_{g\to g}^{0} \qquad \text{Eq.16}$$

What stated above can also be generalized to the case of a P_N approximation with N>1.

An easy exercise allows to show that the use of the total cross-section weighted with the m^{th} moment Φ_m of the flux requires the following correction on the n^{th} moment ($n \neq m$) of the within-group scattering cross-section:

$$\Sigma_{g\to g}^{n,cor} = \Sigma_{g\to g}^{n} + \Sigma_{t,g}^{m} - \Sigma_{t,g}^{n}, \qquad n = 0,1,\ldots,m-1,m+1,\ldots N \qquad \text{Eq.17}$$

where N is the order of the P_N approximation.

IV. Conclusions

Spectral transient effects at the interface core/reflector can influence strongly the calculated parameters of small-medium size TRU burner fast reactors. These effects can be investigated using a multigroup P_N transport approximation but one has to be very careful in the choice of the weight-function (flux, current or in a general case with an high order moment Φ_n (n >1) of the flux expansion in Legendre's Polynomials) for the cross-sections processing. In this memo we have shown that in order to proceed consistently with this choice an appropriate correction is to be introduced on the within-group scattering cross-section. In particular, in the case of P_1 approximation the choice of the flux-weighted total cross-section requires a correction to be applied to the within-group scattering order 1 cross-section, $\Sigma_{g\to g}^{1}$. On the contrary, the use of the current-weighted total cross-section requires a correction to be applied to the within-group scattering order 0 cross-section, $\Sigma_{g\to g}^{0}$. Our work lead to the detection of an incorrect formulation in the MC^2-2 code, where the required correction on the within-group scattering cross-section is not performed.

The inconsistencies observed so far when using MC^2-2 to process the cross-sections, are significant especially in presence of reflector zone at the core boundary, since a direct calculation shows that the effects coming from the fuel region have only a small impact.

Appendix B: Methods for interface core/reflector effects treatment

I. Iterative method

In view of the significant energy spectrum effects, the reference calculations, e.g. to analyze experiments, should be performed at a very large energy group level, or using a continuous energy Monte Carlo calculation. This approach is obviously impractical for routine pre-conceptual and design calculations. A simple procedure can be implemented to obtain effective, broad group cross-sections for the reflectors, which will reproduce most of the effects. In fact, the broad group cross sections are defined in order to conserve reaction rates, i.e.:

$$\sigma_I \Phi_I = \sum_{i \in I} \sigma_i \varphi_i \qquad \text{Eq.18}$$

where I and i are the broad and fine group structure index respectively. The φ_i are calculated in the fundamental mode approximation. The Φ_I are unknown, and one can use the following (classical) iterative procedure to improve the broad group cross-sections:

$$\sigma_I^{(0)} = \frac{\sum_{i \in I} \sigma_i \varphi_i}{\Phi_I^{(0)} \left(= \sum_{i \in I} \varphi_i \right)} \qquad \text{Eq.19}$$

$$\sigma_I^{(1)} = \frac{\sum_{i \in I} \sigma_i \varphi_i}{\Phi_I^{(1)}} \qquad \text{Eq.20}$$

$$\sigma_I^{(K)} = \frac{\sum_{i \in I} \sigma_i \varphi_i}{\Phi_I^{(K)}} \qquad \text{Eq.21}$$

where the $\Phi_I^{(K)}$ are calculated with the $\sigma_I^{(K-1)}$ and K is the iteration index.

The procedure converges rather rapidly, as it is shown in **Figure 129**, where the K_{eff} value (obtained at each iteration K with the $\sigma_I^{(K)}$), is shown as a function of the iteration number. This procedure is a powerful tool, since only one fine group macrocell calculation is needed, the iterative $\Phi_I^{(K)}$ calculation being performed at the broad group level. For the present work we have used the Sn code BISTRO **[32]** to calculate the macrocell fluxes, but this procedure can be eventually easily implemented in a cell code like ECCO **[24]**, where fluxes will be calculated using the collision probability method.

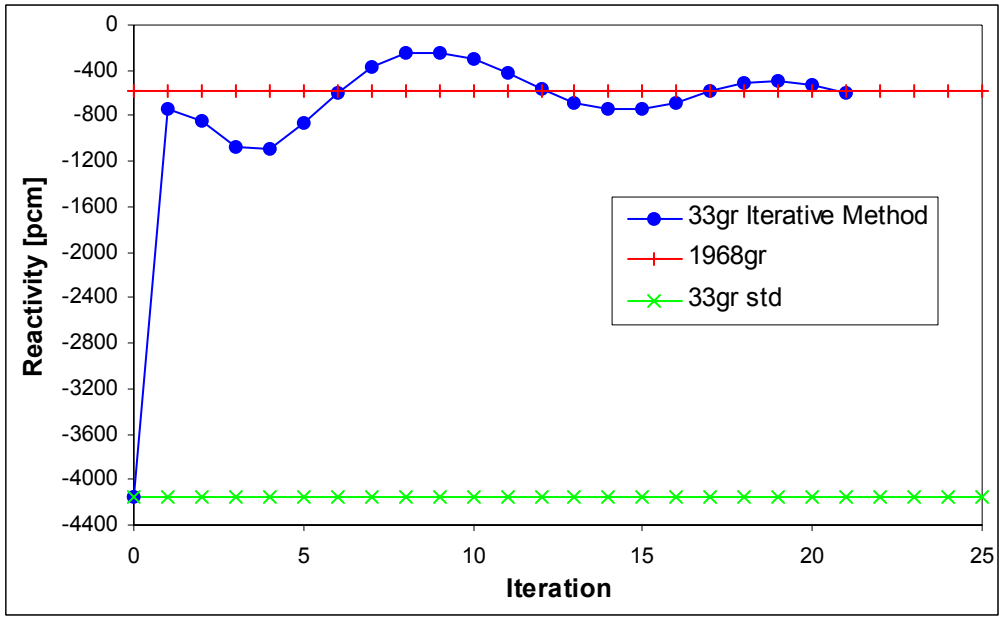

Figure 129: Iterative behavior of proposed method

II. Macrocell method

In order to define a standard procedure to take in account the effects at reflector/core interface in a fast reactor, the same simplified 1D model as presented in **Table 25** has been investigated.

For the present investigation the ERANOS code system has been used. In particular the reactivity and flux (or reaction rates) traverses have been calculated via the BISTRO code **[32]** in S_4P_1 approximation. The cross-section have been processed with the ECCO **[24]** code and its associated multigroup library JEF2.2 **[23]**.

In a first attempt, in order to stress and to quantify the spectral effects at the interface core/reflector, the spectrum indices $\frac{\Sigma_{f,U238}\Phi}{\Sigma_{f,U235}\Phi}$, $\frac{\Sigma_{C,U238}\Phi}{\Sigma_{f,U235}\Phi}$ and $\frac{\Sigma_{f,Np237}\Phi}{\Sigma_{f,U235}\Phi}$ have been drawn from a fine (1968 energy group) 1D calculation and traced in the following figures.

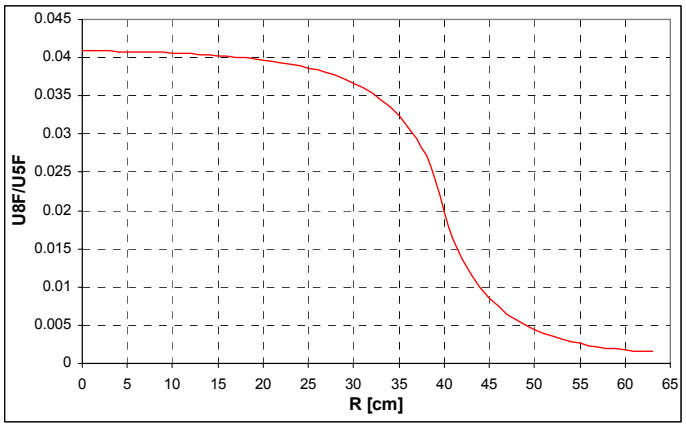

Figure 130: $\Sigma_{f,U238}/\Sigma_{f,U235}$ Traverse

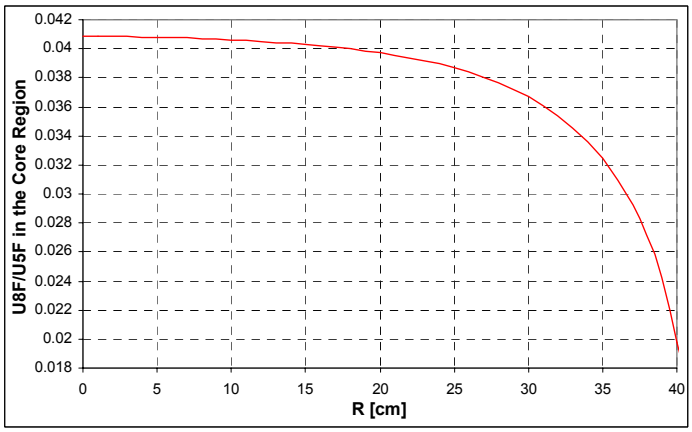

Figure 131: $\Sigma_{f,U238}/\Sigma_{f,U235}$ Traverse in the Core

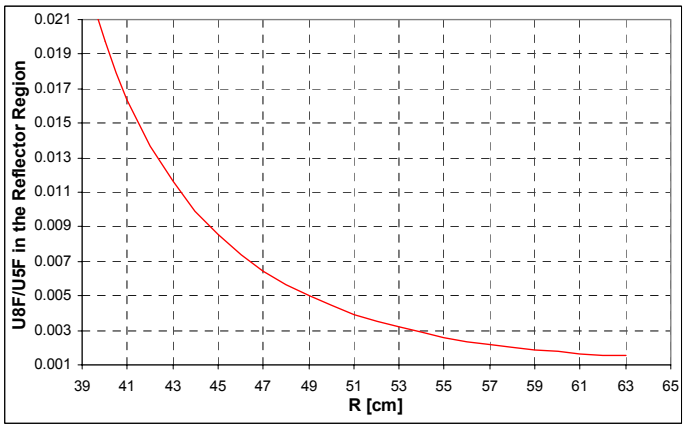

Figure 132: $\Sigma_{f,U238}/\Sigma_{f,U235}$ Traverse in the Reflector

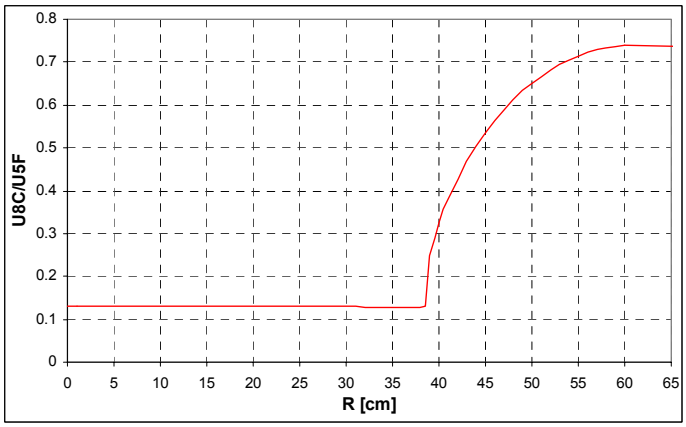

Figure 133: Figure 4: $\Sigma_{C,U238}/\Sigma_{f,U235}$ Traverse

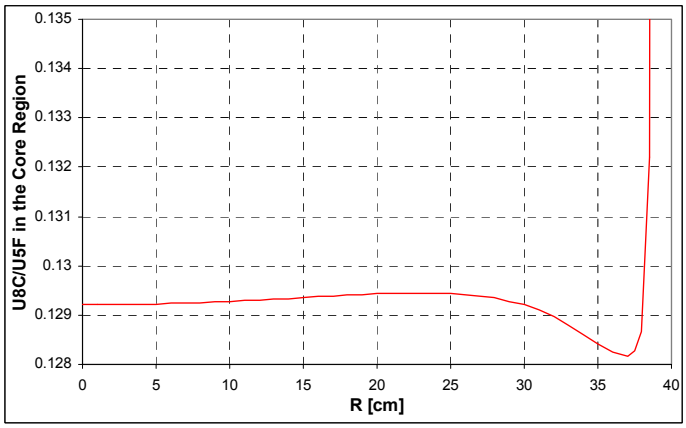

Figure 134: $\Sigma_{C,U238}/\Sigma_{f,U235}$ Traverse in the Core

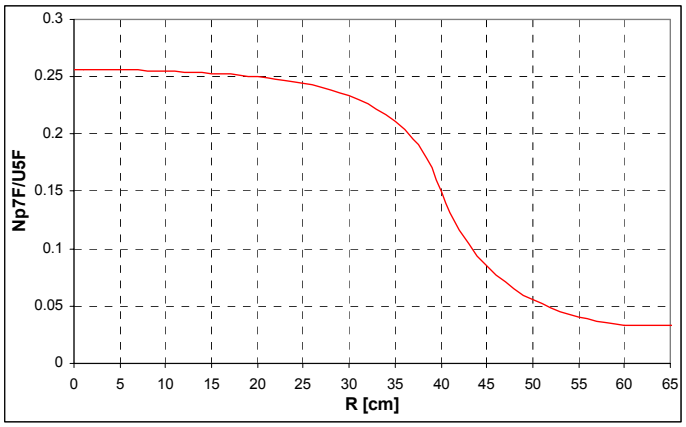

Figure 135: $\Sigma_{f,Np237}/\Sigma_{f,U235}$ Traverse

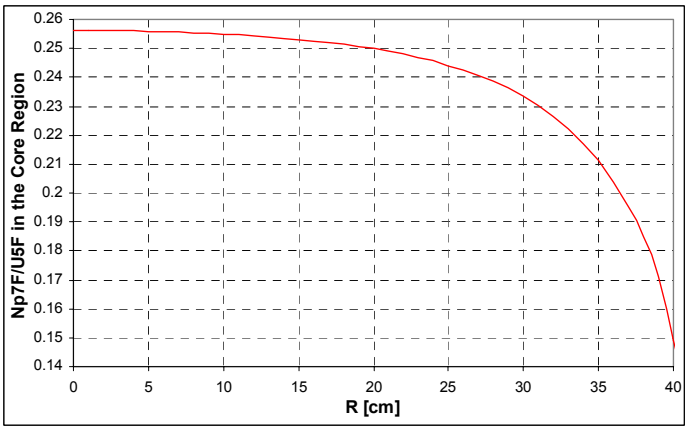

Figure 136: $\Sigma_{f,Np237}/\Sigma_{f,U235}$ Traverse in the Core

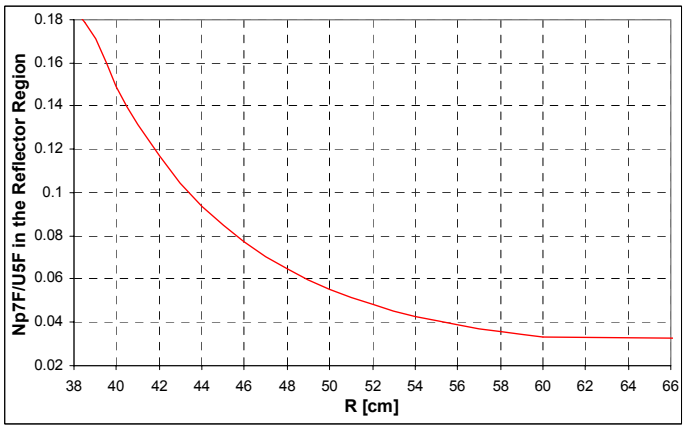

Figure 137: $\Sigma_{f,Np237}/\Sigma_{f,U235}$ Traverse in the Reflector

The figures presented above show that the spectrum effects are significant not just in the reflector but in the core too. In particular, for the high energy **Figures 130** to **132** show that there is a transitional zone at the interface that extends from 10 cm inside the core to 10 cm in the reflector. At low energy (**Figures 133** and **134**), the regions involved seem to increase on both the sides of the core-reflector interface. Finally the $\frac{\Sigma_{f,Np237}\Phi}{\Sigma_{f,U235}\Phi}$ traverses (**Figures 135** to **137**) quantify the spectrum effects over all the energy range.

The information provided by the spectral index is also observed in different points of the core and reflector regions. The spectral distribution provided in the following figures has been obtained via a condensation of fluxes and currents from the fine 1D calculation to 200 macrogroups. In particular, the case labeled “avg” corresponds to the average flux or current spectrum obtained from the spatial calculation, while ECCO refers to the spectra calculated in the standard way with the cell code ECCO. The ECCO standard procedure will be detailed in the next paragraph.

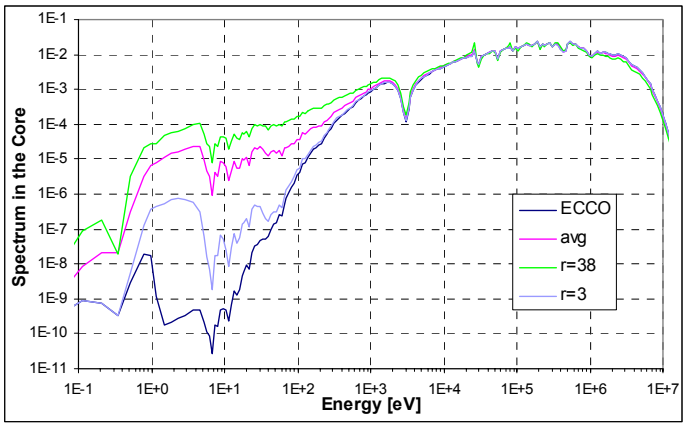

Figure 138: Spectral Flux Distribution in the Core

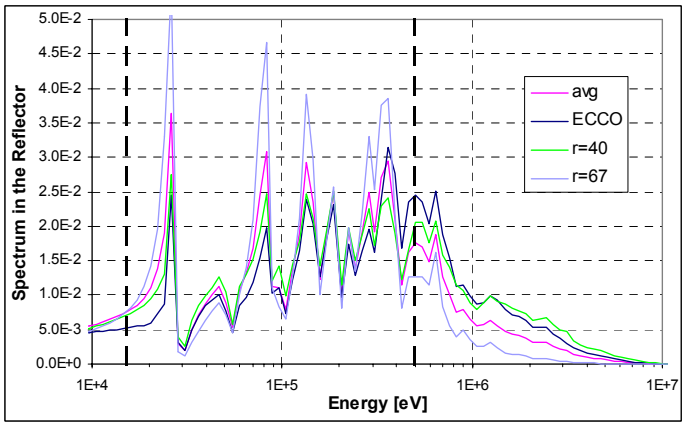

Figure 139: Spectral Flux Distribution in the Reflector

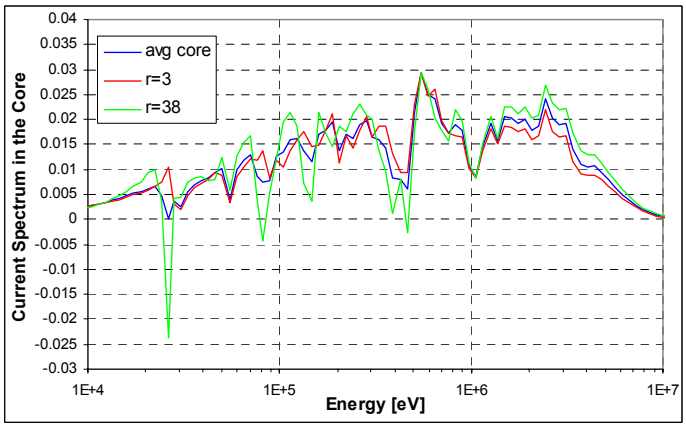

Figure 140: Spectral Current Distribution in the Core

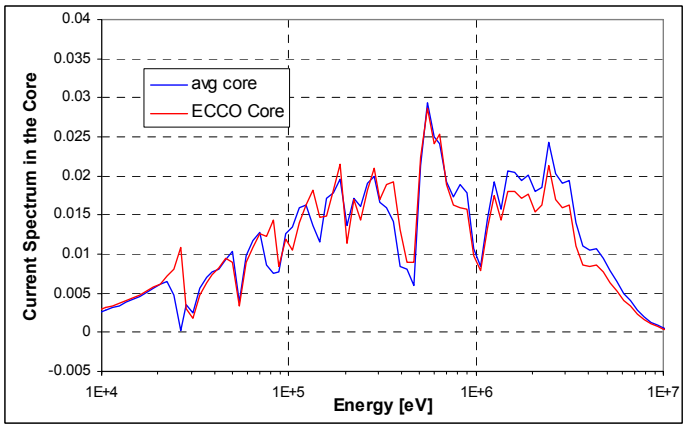

Figure 141: Spectral Current Distribution in the Core

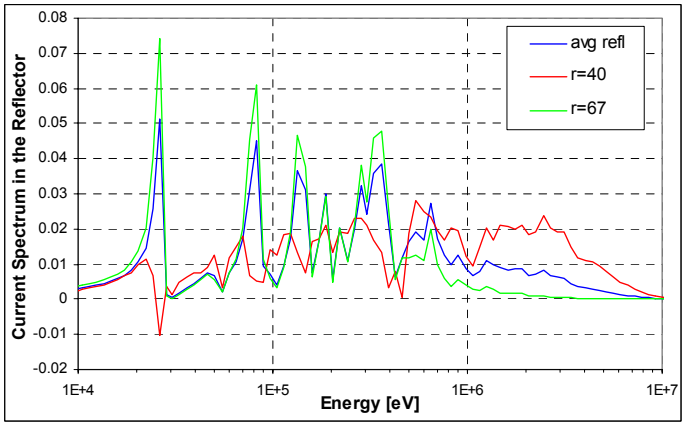

Figure 142: Spectral Current Distribution in the Reflector

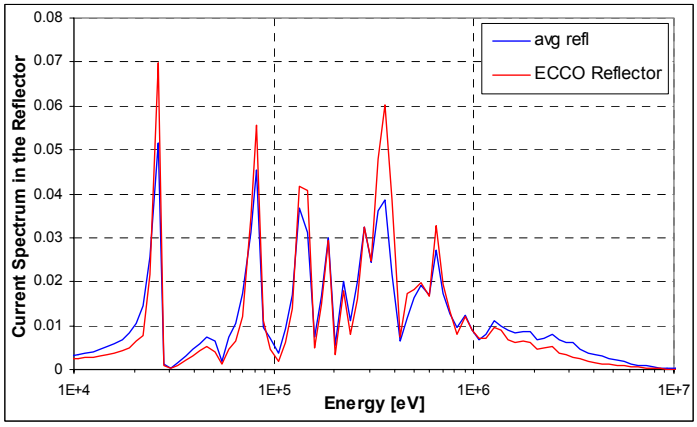

Figure 143: Spectral Current Distribution in the Reflector

Figure 138 shows that the flux spectrum at the interface (r = 38) is shifted to lower energy compared with the average one. At the core center (r = 3) the spectrum is obviously harder.

Similarly, **Figure 139** shows some significant changes in the spectral distribution of the flux when moving from the interface to the other reflector boundary.

Finally, in **Figures 140** to **143** different plots of the spectral current distributions in the core and in the reflector are also presented.

The effects observed will certainly have an impact on the reactivity values, besides flux and reaction rates distributions. In particular, we focused our analysis on the dependence of this impact on the energy group number (NG) used in the spatial calculation. The traverses of adjoint flux, U235 fission rate, U238 fission and capture rate, Np237 fission rate and Pu239 fission rate have been the object of the present analysis, but in the following we selected the most interesting.
For this purpose the cross-section have been processed with ECCO in three different way.

II.1. Standard ECCO calculation

With standard ECCO we refer to a calculation providing separately the cross sections for the core and the reflector regions which are assumed to be infinite. In this case the calculation related to the reflector region are performed with a user-specified value for the buckling. This value is assumed to be constant in each energy group and it is given by a semi-empirical formula in the conventional ECCO calculation route:

$$B^2 = \frac{5}{8}\left(\frac{\pi}{h}\right)^2$$

where h is the thickness of reflector zone. This formula has been historically developed for the treatment of fertile blankets but is inappropriate in the case of a reflector. Indeed, conventional fast reactor analysis code systems such as ERANOS are clearly optimised for highly absorbing media like blankets, but not for reflector cell calculations.
The source term appearing in reflector cell calculations can either be provided by introducing traces of fissile material (emitting fission neutrons), or by computing neutron leakage from the core (with a softer spectrum) by the separate fuel cell calculation. The last option has been used here.
For the calculation related to the core region an iterative procedure is used to provide a buckling giving K_{eff} =1 in the cell calculation.

In the following figures each traverse has been normalized to 1 at the core center and the case with NG=1968 is always considered as the reference calculation. The effects on the distribution and the reactivity through NG are stressed. Finally, an expanded of the interface zone is shown.
We can notice that the effects on the reactivity are very huge: about 2500 pcm moving from NG=33 to NG=1968. With NG=471 we still have 250 pcm of discrepancy compared with the reference.
Referring to the reaction rate distributions, the case with NG=299 can be already considered as representative of the reference calculation in this case.

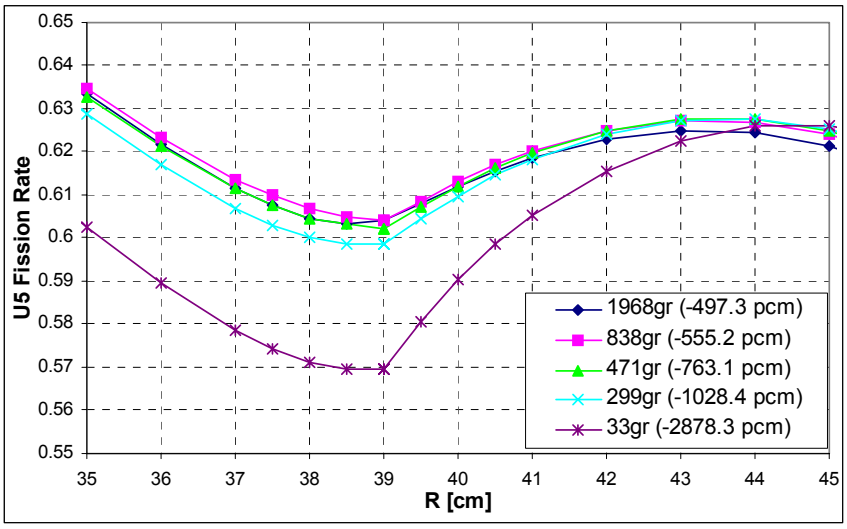

Figure 144: U5 Fission Rate Distribution at the Interface

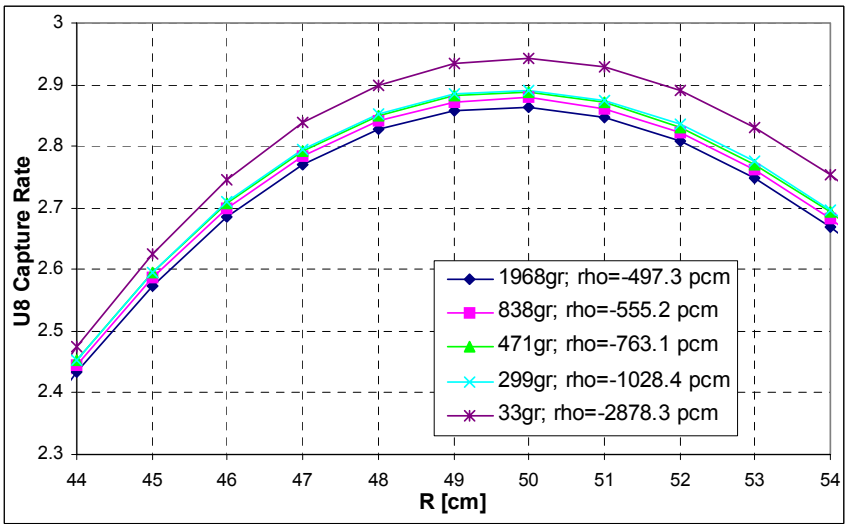

Figure 145: U8 Capture Rate Distribution in the Reflector

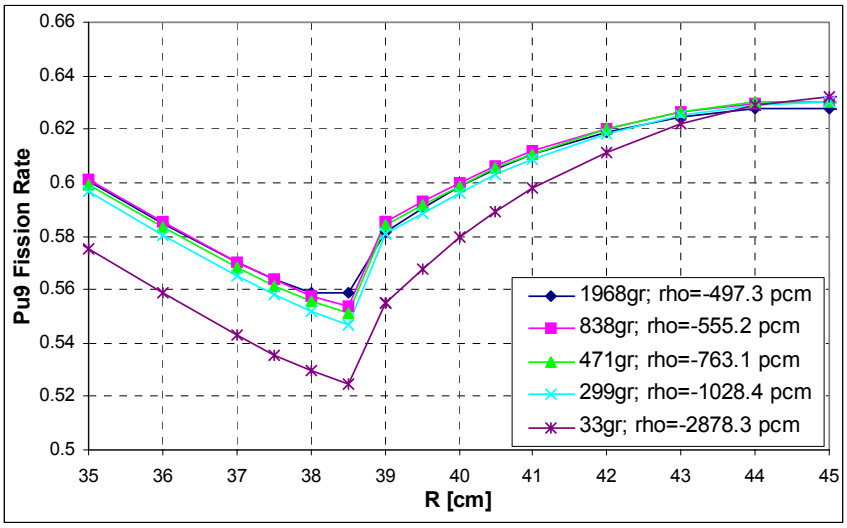

Figure 146: Pu9 Fission Rate Distribution at the Interface

In this procedure, that we called standard ECCO, a dependence has been also noticed on the buckling provided in the cell calculation for the core and the reflector cross-sections. First, the following figure shows that the reference calculation (NG=1968) is not affected by a different choice of the buckling: the impact both on the reactivity and on the reaction rate distribution (in the following figure represented just by the U5 fission rate) is negligible. Indeed, a different buckling changes the flux solution of the cell code which is used as weighting function for cross-section condensation. In the case of the fine reference calculation (NG=1968), no cross-section condensation is performed, consequently the results are not affected by a different values of buckling.

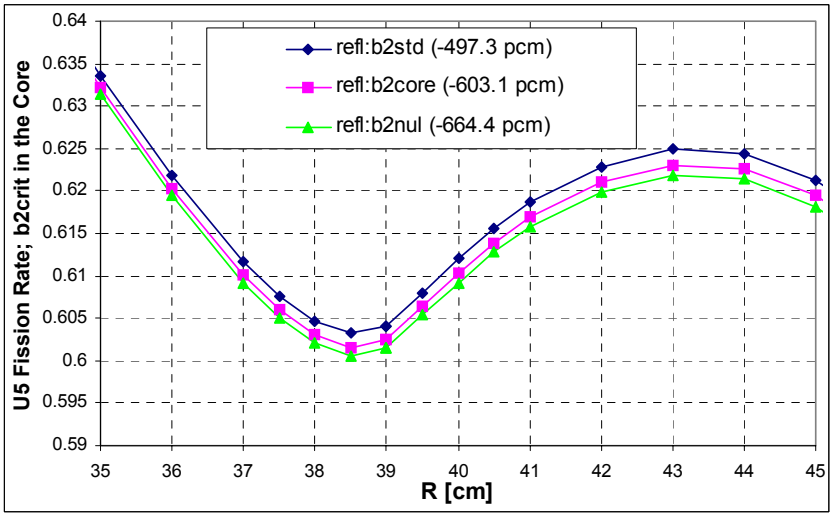

Figure 147: Impact of the Buckling Value Provided in the Reflector on the Fine Reference Calculation

On the contrary, with NG=33 the buckling produces a significant change of the weighting function. **Figure 148** shows the effects due to a change of the buckling value in the reflector.

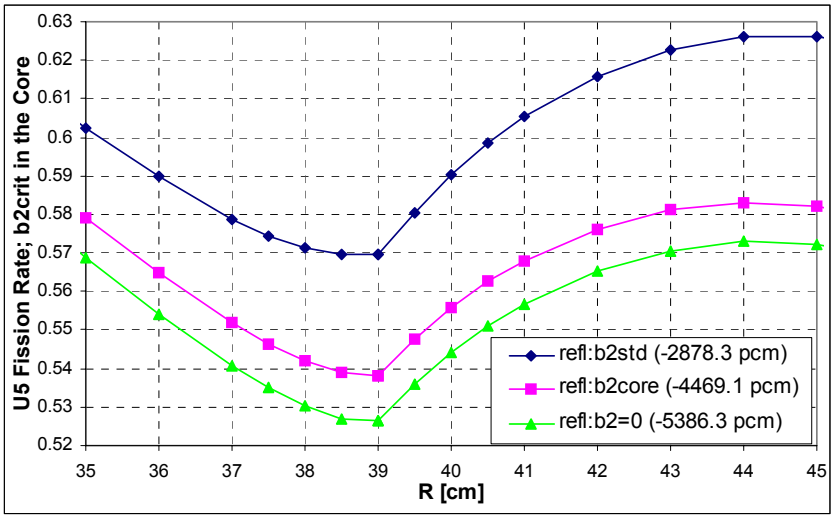

Figure 148: Impact of the Buckling Value Provided in the Reflector on the Calculation with NG=33

II.2. Standard macrocell calculation

A macrocell ECCO calculation allows to take into account the core coupled with the reflector: the cross sections are processed for both the regions weighted with the corresponding flux calculated in each one. In this way, the processing of the cross sections takes better account of the spatial effects at the core/reflector interface. At the present time this option in the ECCO code is available just for mono-dimensional geometries and P_1 order cross sections. Given a single buckling value, giving the value in the axial direction, will be applied to each region and, as in the previous case, it is assumed to be constant in each energy group. To better reproduce the problem, in the present analysis the macrocell has been performed in cylindrical geometry, using the ERANOS module for the spatial condensation from the fine to a boarder energy group structure.

The results of reactivity, adjoint flux and reaction rate traverses obtained with the standard macrocell procedure are presented in the following figures.

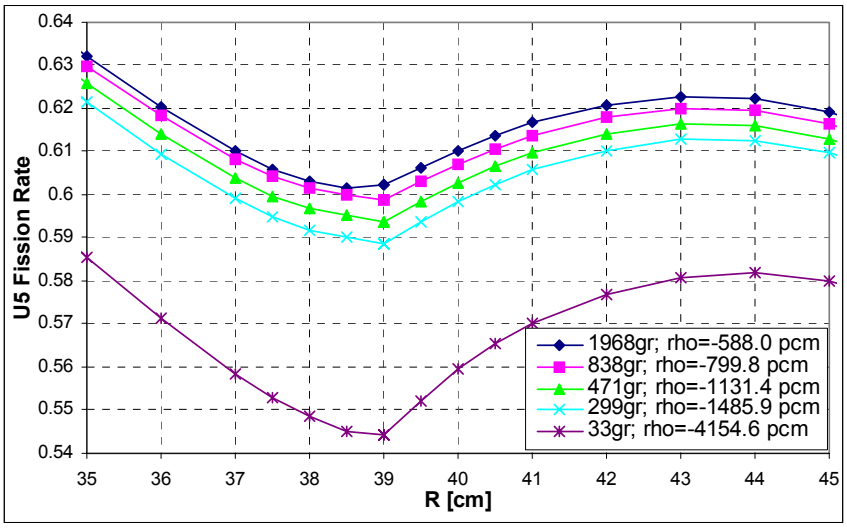

Figure 149: U235 Fission Rate Distribution at the Interface

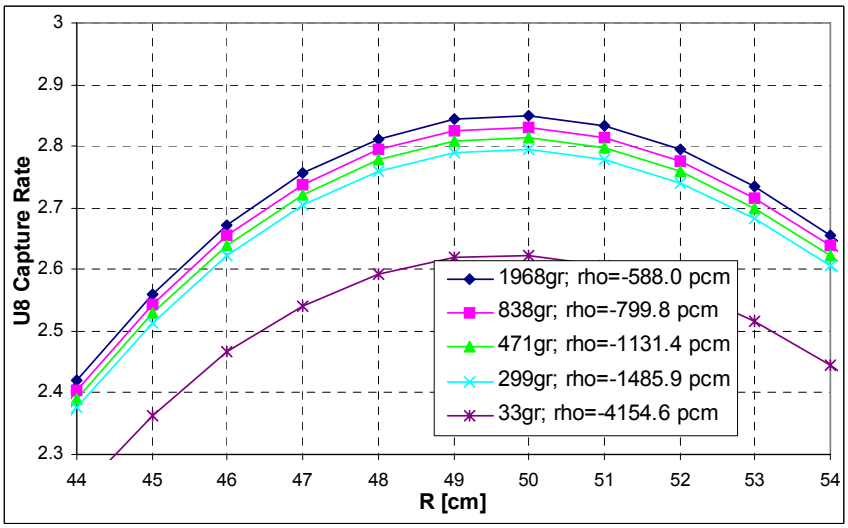

Figure 150: U238 Capture Rate Distribution in the Reflector

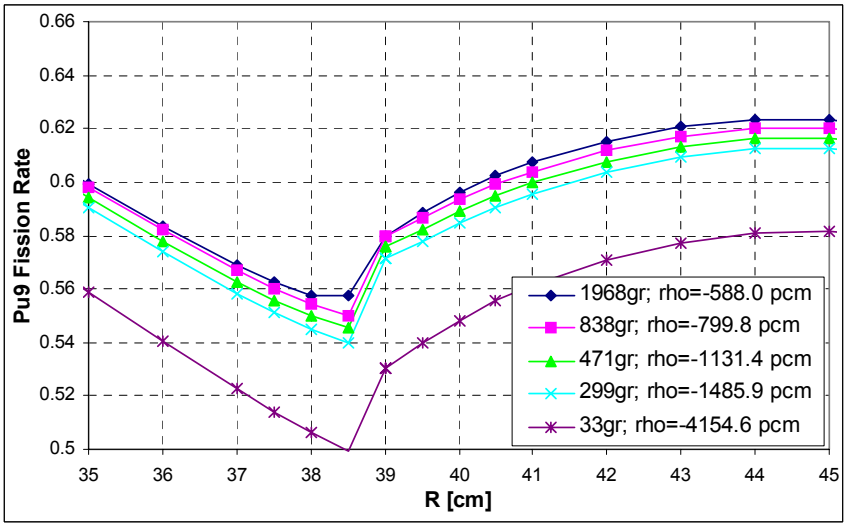

Figure 151: Pu239 Fission Rate Distribution at the Interface

Also in the case of the standard macrocell a dependence of the results on the value chosen for the buckling has been observed. In conclusion, this method doesn't seem satisfactory because the 33-group calculation shows huge discrepancies compared with the reference one. During this analysis, an inconsistency in the condensation module of ERANOS was found: all the cross-sections to be weighted with the current (e.g. P1-total, transport and all the cross-sections of order 1) are condensed with D*Φ, where D is the diffusion coefficient.

II.3. Improved macrocell calculation

Our investigation motivated the conception of a new macrocell, which makes properly use of the currents when needed. The results are shown in the following figures and we can observe that the case with NG=33 reproduces the reference calculation in a satisfactory manner both for the reactivity value and spatial distribution. The results could be still improved if the reflector is divided into two regions (see **Figures 152** to **154**)

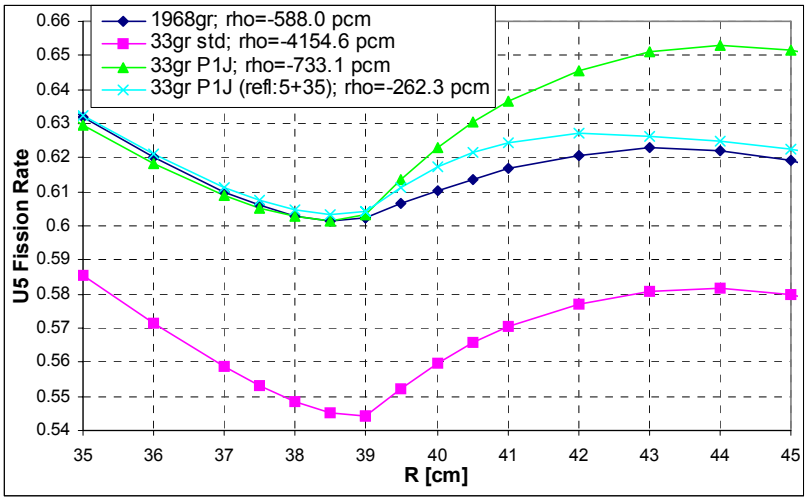

Figure 152: U235 Fission Rate Distribution at the Interface

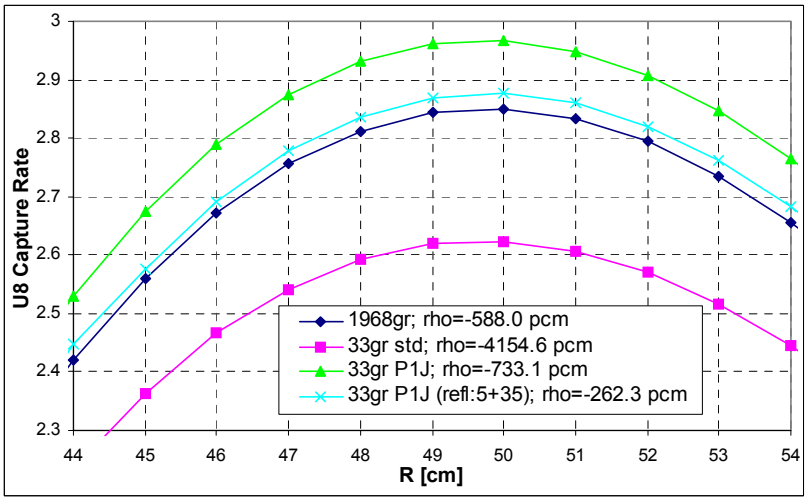

Figure 153: U238 Capture Rate Distribution in the Reflector

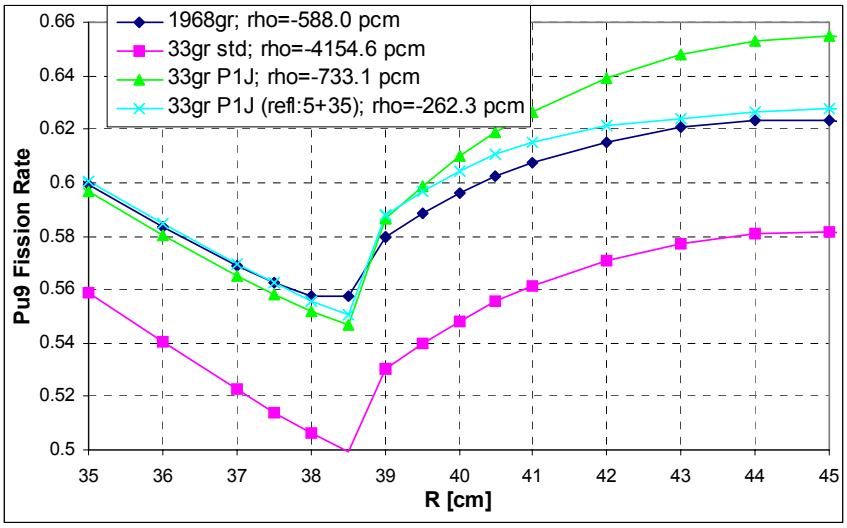

Figure 154: Pu239 Fission Rate Distribution at the Interface

II.4. Perturbation calculation.

In view of the results obtained with the improved macrocell method, we are interested in performing a perturbation calculation between the standard ECCO calculation, where the cross-section are processed separately for the core and the reflector with a 0D cell flux and the "improved macrocell" option. The aim of this study is to see which effects have been neglected in the ECCO standard option, which has been commonly used so far.

The perturbation calculation performed in this analysis are related to the multiplication factor and the ratio $\frac{\langle \Sigma_{f,U5} \Phi \rangle_{r=0}}{\langle \Sigma_{f,U5} \Phi \rangle_{r=38}}$, indicative of the slope on the fission rate distribution moving from the core center up to the interface with the reflector.

- Perturbation calculation for K_{eff}.

We recall that the multiplication factor is –733.1 pcm in the case of the improved macrocell using just 2 regions (core + reflector) and –2878.3 pcm in the case of the ECCO standard option, for a discrepancy of 2145.2 pcm.

Table 28 shows the perturbation components for each isotope. We can notice that the main contributors are Fe56 and in a smaller part Cr52 (see **Tables 29** and **30** for the the breakdown of the perturbation components by energy group), with the transport cross-section mainly in the energy range 30KeV - 1 MeV, which corresponds to the zone of the unsolved resonances (see **Figures 155** and **156**)

Table 28: Perturbation Calculation for Keff between Improved Macrocell and ECCO Standard

%	Capture	Fission	Transport	Elastic	Inelastic	N,XN	SUM
U238	-4.97	0.73	3.50	0.75	0.52	-0.01	0.52
Pu239	-4.84	6.24	4.23	-0.03	0.26	0.00	5.86
Fe56	-170.7	0.0	-1389.1	0.1	-3.9	0.1	-1563.7
Cr52	-16.5	0.0	-326.9	2.3	-0.6	0.0	-341.7
Na	-3.4	0.0	2.4	-0.6	0.0	0.0	-1.6
O	-1.1	0.0	1.9	1.8	0.0	0.0	2.6
Total	-201.5	7.0	-1704.0	4.3	-3.7	0.1	-1898.0

Table 29: Fe56 Contribution in pcm

Gr.	Energy [MeV]	Capture	Fission	Transport	Elastic	Inelastic	N,XN	SUM
1	1.964E+1	0.0	0.0	0.0	0.0	0.0	0.1	0.1
2	1.000E+1	-0.2	0.0	-0.3	0.0	0.1	0.0	-0.4
3	6.065E+0	-0.2	0.0	-0.5	0.0	-0.1	0.0	-0.7
4	3.679E+0	0.0	0.0	-1.8	-0.9	-0.1	0.0	-2.8
5	2.231E+0	0.0	0.0	-5.7	0.5	0.1	0.0	-5.1
6	1.353E+0	0.0	0.0	-12.4	0.8	-4.0	0.0	-15.6
7	8.209E-1	-0.6	0.0	-79.5	1.0	0.0	0.0	-79.0
8	4.979E-1	-3.1	0.0	-166.9	-0.1	0.0	0.0	-170.0
9	3.020E-1	-2.2	0.0	-213.6	-8.2	0.0	0.0	-223.9
10	1.832E-1	-2.7	0.0	-192.8	-0.2	0.0	0.0	-195.7
11	1.111E-1	-8.8	0.0	-313.4	-3.5	0.0	0.0	-325.7
12	6.738E-2	0.3	0.0	8.1	-16.5	0.0	0.0	-8.1
13	4.087E-2	-5.2	0.0	-286.5	0.5	0.0	0.0	-291.2
14	2.479E-2	0.0	0.0	-127.1	36.1	0.0	0.0	-91.0
15	1.503E-2	0.0	0.0	1.8	-0.9	0.0	0.0	0.9
16	9.119E-3	0.0	0.0	0.4	-1.9	0.0	0.0	-1.6
17	5.531E-3	0.0	0.0	0.0	-0.4	0.0	0.0	-0.4
18	3.355E-3	0.0	0.0	0.0	0.0	0.0	0.0	0.0
19	2.035E-3	0.0	0.0	0.0	-0.2	0.0	0.0	-0.3
20	1.234E-3	-2.1	0.0	0.2	1.1	0.0	0.0	-0.9
21	7.485E-4	0.0	0.0	0.2	-1.6	0.0	0.0	-1.4
22	4.540E-4	0.0	0.0	0.0	-1.4	0.0	0.0	-1.3
23	3.043E-4	0.0	0.0	0.0	-2.3	0.0	0.0	-2.2
24	1.486E-4	0.0	0.0	0.0	-1.7	0.0	0.0	-1.7
25	9.166E-5	0.0	0.0	0.0	0.6	0.0	0.0	0.6
26	6.790E-5	0.0	0.0	0.0	1.1	0.0	0.0	1.1
27	4.017E-5	0.0	0.0	0.0	-1.0	0.0	0.0	-1.0
28	2.260E-5	0.0	0.0	0.0	-0.3	0.0	0.0	-0.3
29	1.371E-5	0.0	0.0	0.0	0.4	0.0	0.0	0.4
30	8.315E-6	0.0	0.0	0.0	-0.4	0.0	0.0	-0.4
31	4.000E-6	-135.0	0.0	0.5	-0.5	0.0	0.0	-135.0
32	5.400E-7	-10.9	0.0	0.0	0.0	0.0	0.0	-10.9
33	1.000E-7	-0.1	0.0	0.0	0.0	0.0	0.0	-0.1
SUM		-170.7	0.0	-1389.1	0.1	-3.9	0.1	-1563.7

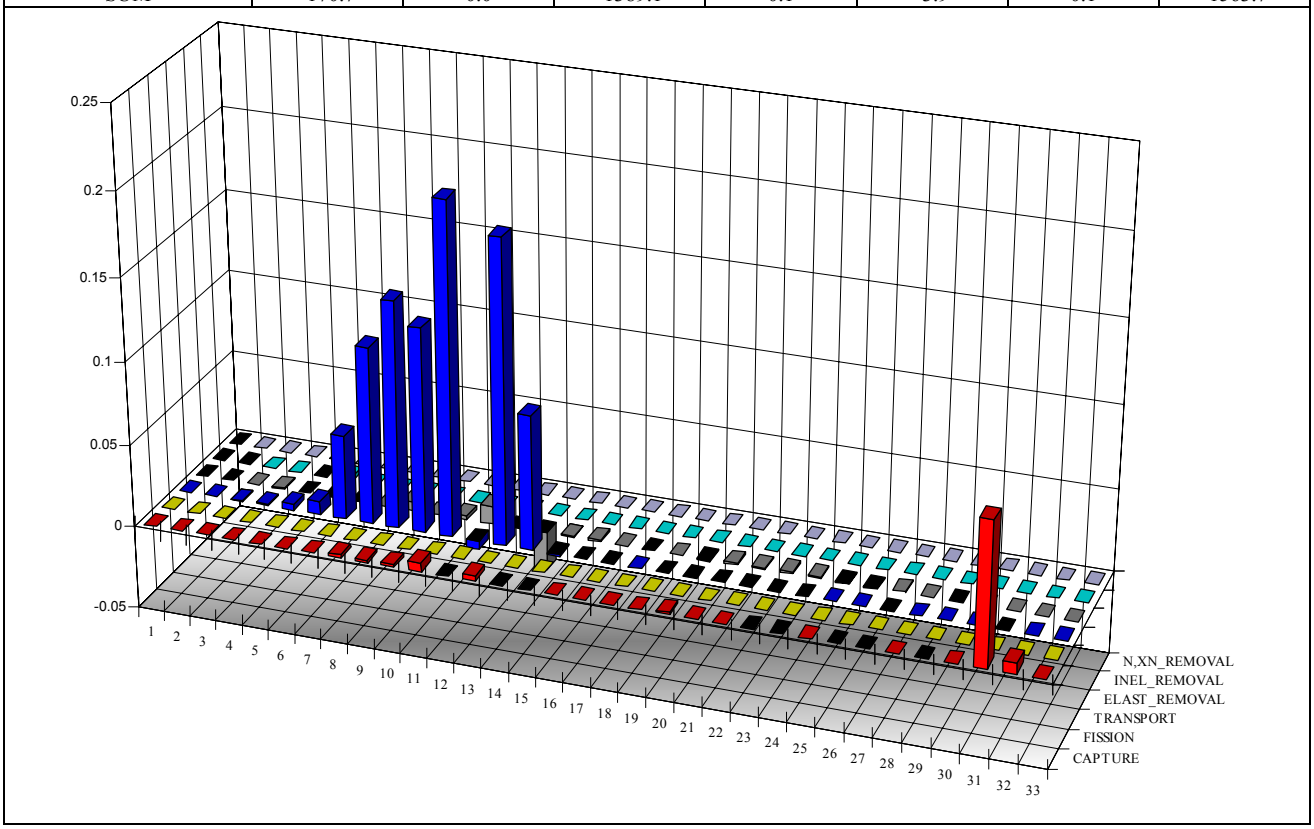

Table 30: Cr52 Contribution in pcm

Gr.	Energy [MeV]	Capture	Fission	Transport	Elastic	Inelastic	N,XN	SUM
1	1.964E+1	0.0	0.0	0.0	0.0	0.0	0.0	0.0
2	1.000E+1	-0.1	0.0	-0.1	0.0	0.0	0.0	-0.1
3	6.065E+0	0.0	0.0	0.0	0.0	0.1	0.0	0.0
4	3.679E+0	0.0	0.0	1.0	-0.3	-0.3	0.0	0.3
5	2.231E+0	0.0	0.0	0.4	0.4	-0.4	0.0	0.3
6	1.353E+0	0.0	0.0	0.4	0.5	0.0	0.0	0.9
7	8.209E-1	-0.1	0.0	-11.1	1.1	0.0	0.0	-10.1
8	4.979E-1	0.2	0.0	-38.6	0.0	0.0	0.0	-38.4
9	3.020E-1	-0.6	0.0	-13.1	-1.9	0.0	0.0	-15.5
10	1.832E-1	-0.8	0.0	-103.3	-0.2	0.0	0.0	-104.3
11	1.111E-1	-3.3	0.0	-149.6	-0.6	0.0	0.0	-153.5
12	6.738E-2	-0.3	0.0	-13.0	-0.2	0.0	0.0	-13.5
13	4.087E-2	-0.7	0.0	4.2	-1.3	0.0	0.0	2.2
14	2.479E-2	-0.4	0.0	-4.2	5.4	0.0	0.0	0.9
15	1.503E-2	0.0	0.0	0.1	-0.1	0.0	0.0	0.0
16	9.119E-3	0.0	0.0	0.0	-0.2	0.0	0.0	-0.2
17	5.531E-3	0.0	0.0	0.0	0.0	0.0	0.0	0.0
18	3.355E-3	0.0	0.0	0.0	0.0	0.0	0.0	0.0
19	2.035E-3	-0.1	0.0	0.0	0.0	0.0	0.0	-0.1
20	1.234E-3	0.0	0.0	0.0	0.1	0.0	0.0	0.1
21	7.485E-4	0.0	0.0	0.0	-0.1	0.0	0.0	-0.1
22	4.540E-4	0.0	0.0	0.0	-0.1	0.0	0.0	-0.1
23	3.043E-4	0.0	0.0	0.0	-0.2	0.0	0.0	-0.2
24	1.486E-4	0.0	0.0	0.0	-0.1	0.0	0.0	-0.1
25	9.166E-5	0.0	0.0	0.0	0.0	0.0	0.0	0.0
26	6.790E-5	0.0	0.0	0.0	0.1	0.0	0.0	0.1
27	4.017E-5	0.0	0.0	0.0	-0.1	0.0	0.0	-0.1
28	2.260E-5	0.0	0.0	0.0	0.0	0.0	0.0	0.0
29	1.371E-5	0.0	0.0	0.0	0.0	0.0	0.0	0.0
30	8.315E-6	0.0	0.0	0.0	0.0	0.0	0.0	0.0
31	4.000E-6	-9.5	0.0	0.0	0.0	0.0	0.0	-9.5
32	5.400E-7	-0.8	0.0	0.0	0.0	0.0	0.0	-0.8
33	1.000E-7	0.0	0.0	0.0	0.0	0.0	0.0	0.0
SUM		-16.5	0.0	-326.9	2.3	-0.6	0.0	-341.7

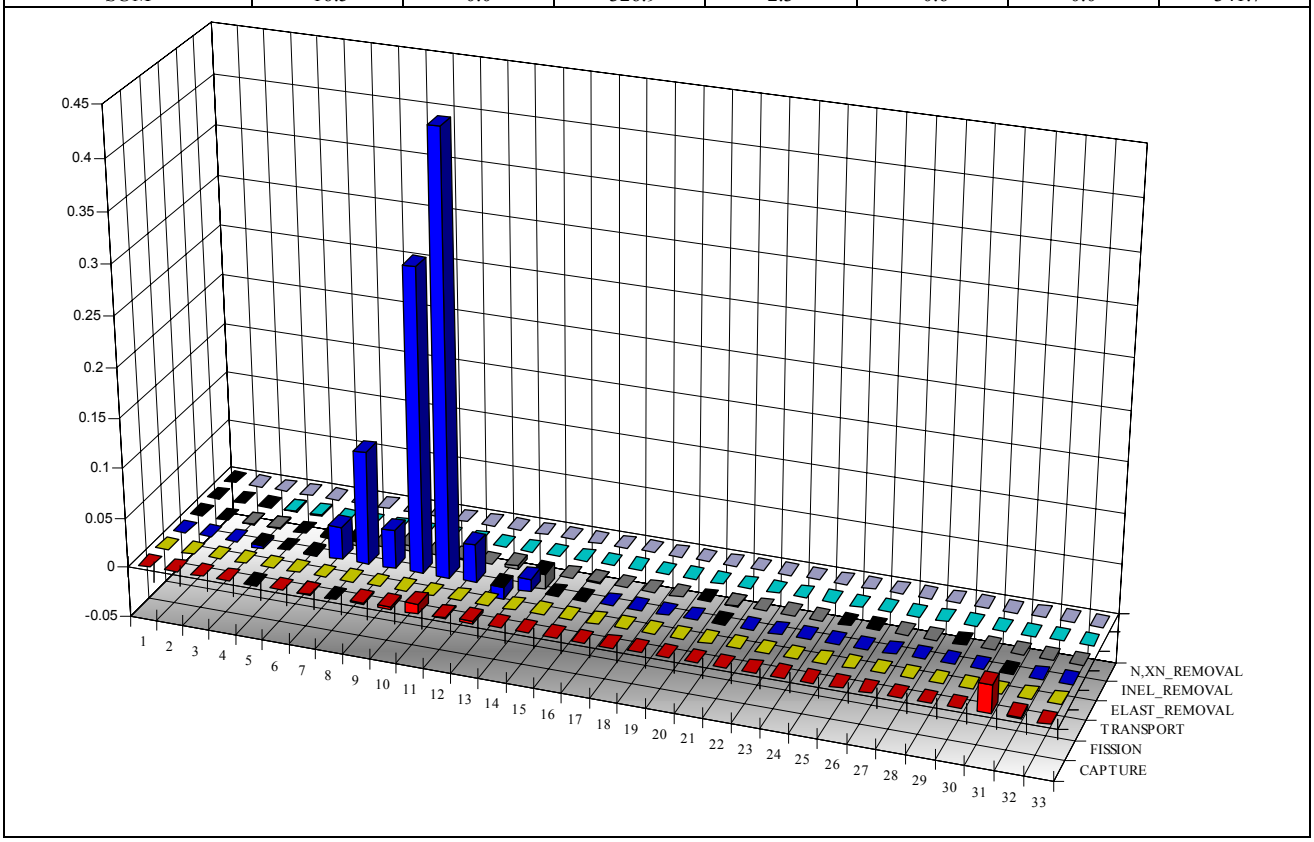

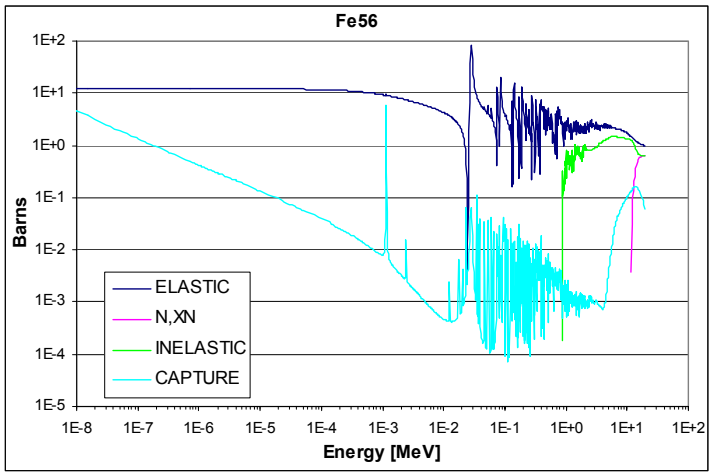

Figure 155: Fe56 Cross-Sections

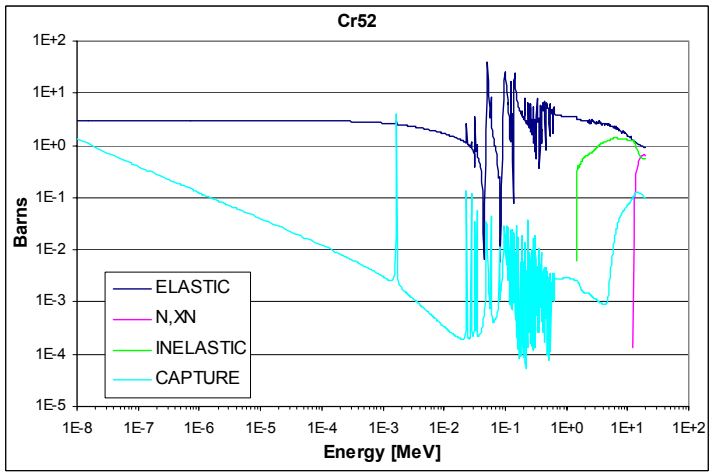

Figure 156: Cr52 Cross-Sections

- Perturbation calculation for $\frac{\langle \Sigma_{f,U5} \Phi \rangle_{r=0}}{\langle \Sigma_{f,U5} \Phi \rangle_{r=38}}$

As far as the ratio $\frac{\langle \Sigma_{f,U5} \Phi \rangle_{r=0}}{\langle \Sigma_{f,U5} \Phi \rangle_{r=38}}$, the value is 4.42E-2 in the case of the improved macrocell and 4.66E-2 for the ECCO standard option. The discrepancy is then: (ECCO standard – Improved macrocell)/Improved macrocell = 5%. **Table 31** shows the perturbation components for each isotope. We can notice that the main contributors are again Fe56 and in a smaller part Cr52 (see **Tables 32** and **33** for the the breakdown of the perturbation components by energy group), with the transport and elastic cross-section once again mainly in the energy range 30KeV - 1 MeV.

Table 31: Perturbation Calculation for $\frac{\langle \Sigma_{f,U5} \Phi \rangle_{r=0}}{\langle \Sigma_{f,U5} \Phi \rangle_{r=38}}$ between Improved Macrocell and ECCO Standard.

%	Capture	Fission	Transport	Elastic	Inelastic	N,XN	SUM
U238	0.38	0.00	-0.06	0.01	0.00	0.00	0.33
Pu239	0.04	0.21	0.10	0.00	0.00	0.00	0.35
Fe56	0.81	0.00	3.20	-0.78	0.00	0.00	3.23
Cr52	0.06	0.00	0.60	0.02	0.00	0.00	0.68
Na	0.02	0.00	-0.38	0.05	0.00	0.00	-0.31
O	0.00	0.00	-0.01	0.03	0.00	0.00	0.02
Total	1.31	0.21	3.45	-0.67	0.00	0.00	4.3

Table 32: Fe56 Contribution in %

Gr.	Energy [MeV]	Capture	Fission	Transport	Elastic	Inelastic	N,XN	SUM
1	1.964E+1	0.00	0.00	0.00	0.00	0.00	0.00	0.00
2	1.000E+1	0.00	0.00	0.00	0.00	0.00	0.00	0.00
3	6.065E+0	0.00	0.00	0.00	0.00	0.00	0.00	0.00
4	3.679E+0	0.00	0.00	0.00	0.00	0.00	0.00	0.00
5	2.231E+0	0.00	0.00	-0.01	0.00	0.00	0.00	-0.01
6	1.353E+0	0.00	0.00	0.00	-0.01	0.00	0.00	-0.01
7	8.209E-1	0.00	0.00	0.01	0.00	0.00	0.00	0.01
8	4.979E-1	0.00	0.00	0.19	0.12	0.00	0.00	0.31
9	3.020E-1	0.00	0.00	0.23	-0.12	0.00	0.00	0.11
10	1.832E-1	0.00	0.00	0.37	0.00	0.00	0.00	0.36
11	1.111E-1	0.01	0.00	0.71	0.10	0.00	0.00	0.82
12	6.738E-2	0.00	0.00	-0.02	-0.13	0.00	0.00	-0.16
13	4.087E-2	0.01	0.00	1.30	-0.02	0.00	0.00	1.29
14	2.479E-2	0.00	0.00	0.44	-0.49	0.00	0.00	-0.06
15	1.503E-2	0.00	0.00	-0.01	-0.14	0.00	0.00	-0.15
16	9.119E-3	0.00	0.00	-0.01	-0.05	0.00	0.00	-0.05
17	5.531E-3	0.00	0.00	0.00	0.00	0.00	0.00	-0.01
18	3.355E-3	0.00	0.00	0.00	0.00	0.00	0.00	0.00
19	2.035E-3	0.00	0.00	0.00	-0.02	0.00	0.00	-0.02
20	1.234E-3	-0.04	0.00	0.01	-0.04	0.00	0.00	-0.07
21	7.485E-4	0.00	0.00	0.01	0.00	0.00	0.00	0.01
22	4.540E-4	0.00	0.00	0.00	0.00	0.00	0.00	0.00
23	3.043E-4	0.00	0.00	0.00	0.00	0.00	0.00	0.00
24	1.486E-4	0.00	0.00	0.00	0.00	0.00	0.00	0.00
25	9.166E-5	0.00	0.00	0.00	0.01	0.00	0.00	0.01
26	6.790E-5	0.00	0.00	0.00	0.02	0.00	0.00	0.02
27	4.017E-5	0.00	0.00	0.00	-0.01	0.00	0.00	-0.01
28	2.260E-5	0.00	0.00	0.00	0.01	0.00	0.00	0.01
29	1.371E-5	0.00	0.00	0.00	-0.02	0.00	0.00	-0.02
30	8.315E-6	0.00	0.00	0.00	0.00	0.00	0.00	0.00
31	4.000E-6	0.81	0.00	0.00	0.01	0.00	0.00	0.82
32	5.400E-7	0.01	0.00	0.00	0.00	0.00	0.00	0.01
33	1.000E-7	0.00	0.00	0.00	0.00	0.00	0.00	0.00
SUM		0.81	0.00	3.20	-0.78	0.00	0.00	3.23

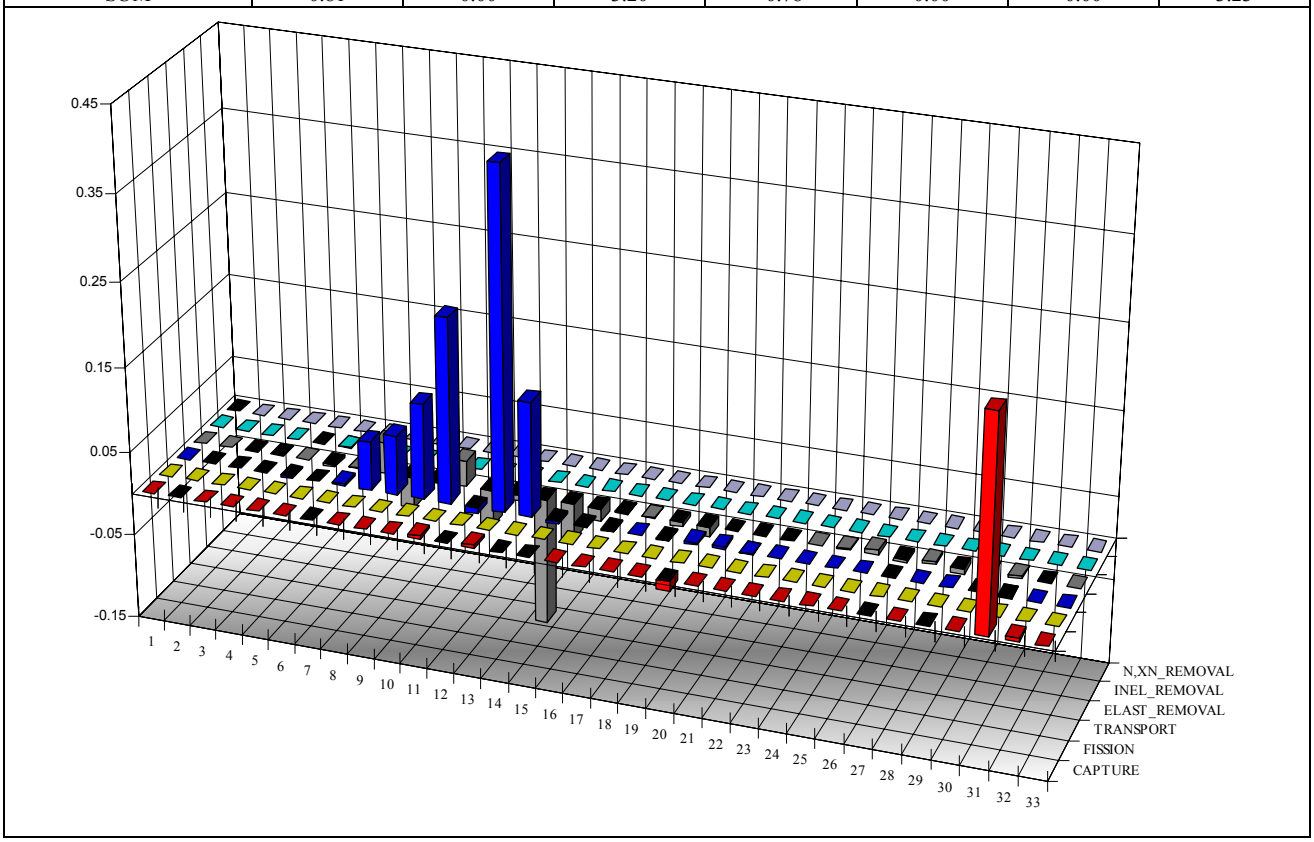

Table 33: Cr52 Contribution in %

Gr.	Energy [MeV]	Capture	Fission	Transport	Elastic	Inelastic	N,XN	SUM
1	1.964E+1	0.00	0.00	0.00	0.00	0.00	0.00	0.00
2	1.000E+1	0.00	0.00	0.00	0.00	0.00	0.00	0.00
3	6.065E+0	0.00	0.00	0.00	0.00	0.00	0.00	0.00
4	3.679E+0	0.00	0.00	0.00	0.00	0.00	0.00	0.00
5	2.231E+0	0.00	0.00	0.00	0.00	0.00	0.00	0.00
6	1.353E+0	0.00	0.00	0.00	-0.01	0.00	0.00	-0.01
7	8.209E-1	0.00	0.00	0.00	0.00	0.00	0.00	0.00
8	4.979E-1	0.00	0.00	0.03	0.08	0.00	0.00	0.11
9	3.020E-1	0.00	0.00	0.01	-0.03	0.00	0.00	-0.02
10	1.832E-1	0.00	0.00	0.16	0.00	0.00	0.00	0.16
11	1.111E-1	0.00	0.00	0.34	0.02	0.00	0.00	0.36
12	6.738E-2	0.00	0.00	0.06	0.00	0.00	0.00	0.06
13	4.087E-2	0.00	0.00	-0.01	0.06	0.00	0.00	0.05
14	2.479E-2	0.00	0.00	0.01	-0.07	0.00	0.00	-0.06
15	1.503E-2	0.00	0.00	0.00	-0.02	0.00	0.00	-0.02
16	9.119E-3	0.00	0.00	0.00	-0.01	0.00	0.00	-0.01
17	5.531E-3	0.00	0.00	0.00	0.00	0.00	0.00	0.00
18	3.355E-3	0.00	0.00	0.00	0.00	0.00	0.00	0.00
19	2.035E-3	0.00	0.00	0.00	0.00	0.00	0.00	0.00
20	1.234E-3	0.00	0.00	0.00	0.00	0.00	0.00	0.00
21	7.485E-4	0.00	0.00	0.00	0.00	0.00	0.00	0.00
22	4.540E-4	0.00	0.00	0.00	0.00	0.00	0.00	0.00
23	3.043E-4	0.00	0.00	0.00	0.00	0.00	0.00	0.00
24	1.486E-4	0.00	0.00	0.00	0.00	0.00	0.00	0.00
25	9.166E-5	0.00	0.00	0.00	0.00	0.00	0.00	0.00
26	6.790E-5	0.00	0.00	0.00	0.00	0.00	0.00	0.00
27	4.017E-5	0.00	0.00	0.00	0.00	0.00	0.00	0.00
28	2.260E-5	0.00	0.00	0.00	0.00	0.00	0.00	0.00
29	1.371E-5	0.00	0.00	0.00	0.00	0.00	0.00	0.00
30	8.315E-6	0.00	0.00	0.00	0.00	0.00	0.00	0.00
31	4.000E-6	0.06	0.00	0.00	0.00	0.00	0.00	0.06
32	5.400E-7	0.00	0.00	0.00	0.00	0.00	0.00	0.00
33	1.000E-7	0.00	0.00	0.00	0.00	0.00	0.00	0.00
SUM		0.06	0.00	0.60	0.02	0.00	0.00	0.68

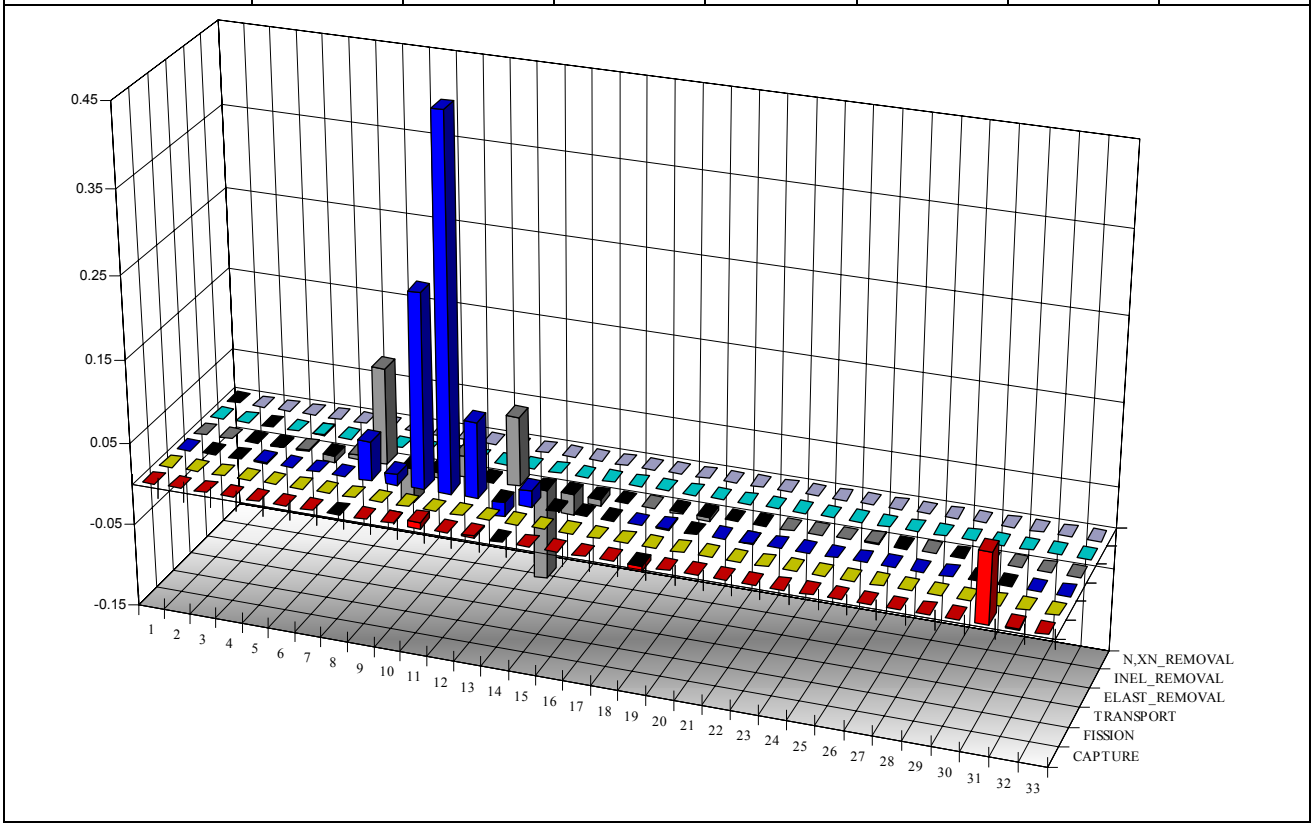

II.5. Application of the improved macrocell option to a 2D model.

After an extensive study of the effects located at the interface core/reflector for a simple 1D model, we want to complete our analysis by an application to a more realistic model in RZ geometry. The effort performed at this point will also represents the base for the development of a standard procedure for the treatment of the core/reflector interface effects in a general 3D geometry.

Two RZ models have been object of our study. **Table 34** shows geometry and composition of the first system. A second model, which will be investigate later in this document, has been obtained by reducing the height of the core zone in order to strengthen the fraction of neutrons escaping from the core in the reflector and produce situation with high effects at the interface.

Table 34: Geometry and Isotopic Compositions for a 2D Model

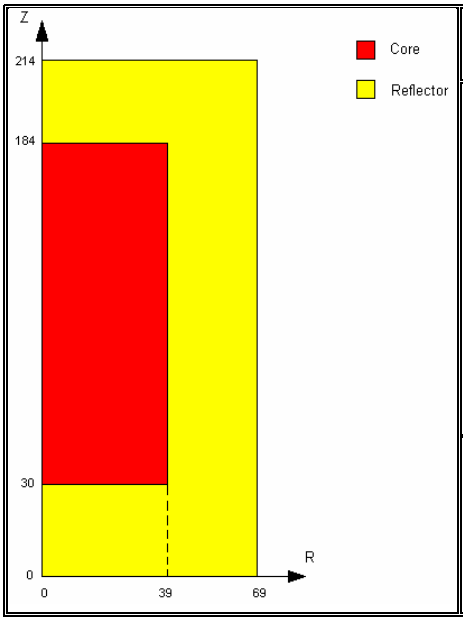

Region	Isotope	Density × 10^{+24} at/cm^3
Zone1- Core	Pu239	1.5×10^{-3}
	U238	5.0×10^{-3}
	Fe56	7.0×10^{-3}
	Cr52	1.5×10^{-3}
	Na23	1.0×10^{-2}
	O16	1.5×10^{-2}
Zone2 - Reflector	Fe56	5.0×10^{-2}
	Cr52	1.5×10^{-2}
	Na23	5.0×10^{-3}

Figures 157 to **159** show the radial traverses, calculated at Z=103 cm and normalized to 1 at the core center (R=0);

Figures 160 to **162** show the axial traverses, calculated along the radial position R=10 cm and normalized to 1 at Z=97 cm.

These traverses have been obtained using cross-sections obtained in the standard way (ECCO standard option) and the case with NG=1968 is always considered as the reference case. An expanded viewat the interface is performed in order to stress the effects on the distribution and the reactivity through NG.

We can notice that the effects on the reactivity are very huge: about 4000 pcm moving from NG=33 to NG=1968. With NG=471 we still have 600 pcm of discrepancy compared with the reference.

The reactivity value calculated with JEF2.2/MCNP4C is –109 ± 13 pcm, which is in good agreement with the fine calculation.

Referring to the reaction rate distributions, both axial and radial traverses exhibit a similar behavior: the case with NG=299 can be already considered as representative of the reference calculation in this case.

Note that, because of the high computational resources (memory and disk space) required by the fine calculation (NG=1968) just in this case a spatial grid a little bit boarder has been used. Within a distance of 5 cm from the interface both in the core and in the reflector side the same grid as in the other calculations with lower NG has been kept. The grid effects both on reactivity and on spatial distributions have been investigated and they were found to be negligible.

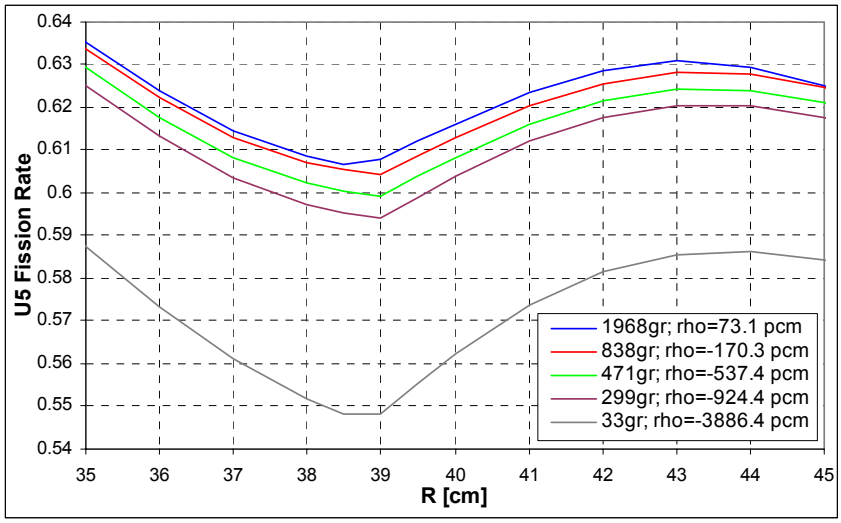

Figure 157: U235 Fission Rate Radial (Z=103 cm) Traverse at the Interface

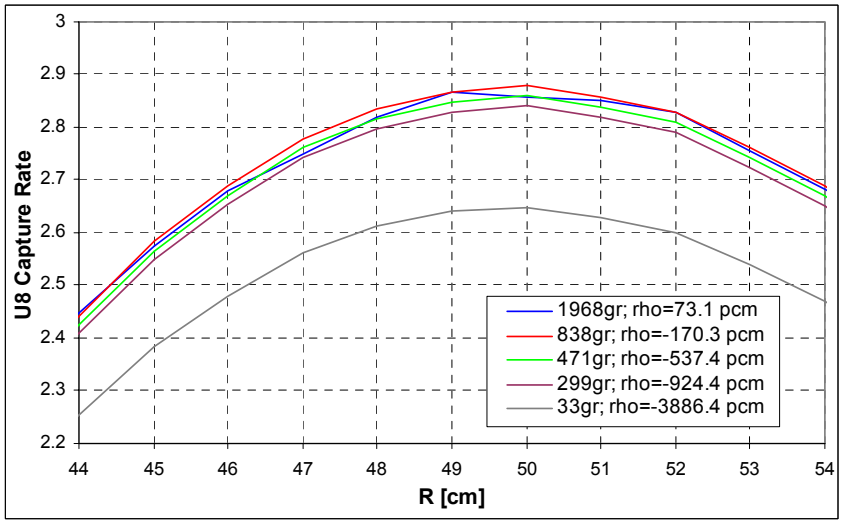

Figure 158: U238 Capture Rate Radial (Z=103 cm) Traverse in the Reflector

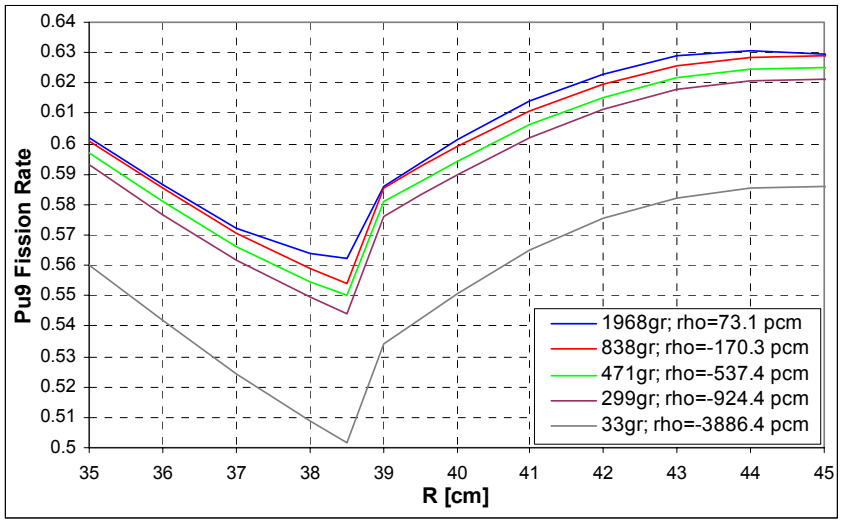

Figure 159: Pu239 Fission Rate Radial (Z=103 cm) Traverse at the Interface

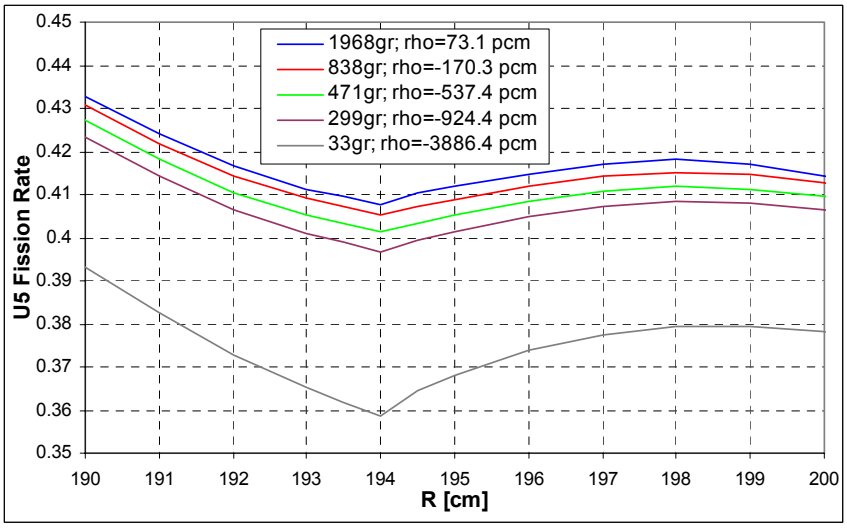

Figure 160: U235 Fission Rate Axial (R=10 cm) Traverse at the Interface

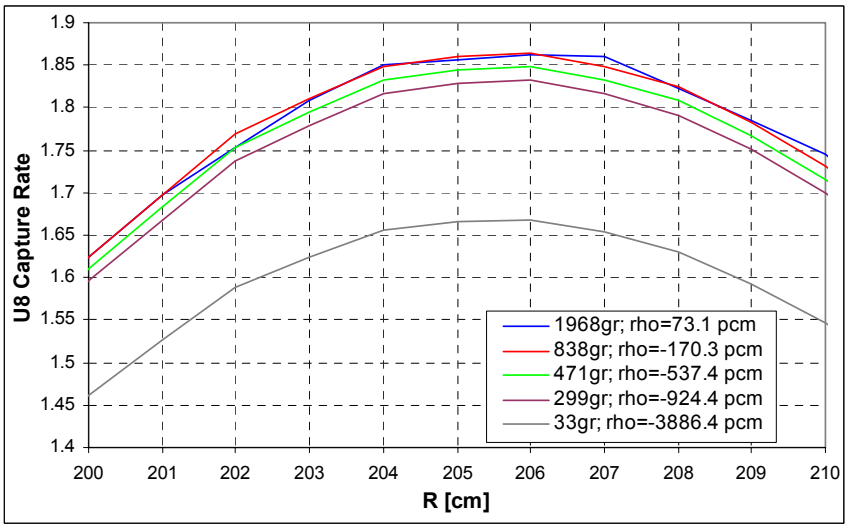

Figure 161: U238 Capture Rate Axial (R=10 cm) Traverse in the Reflector

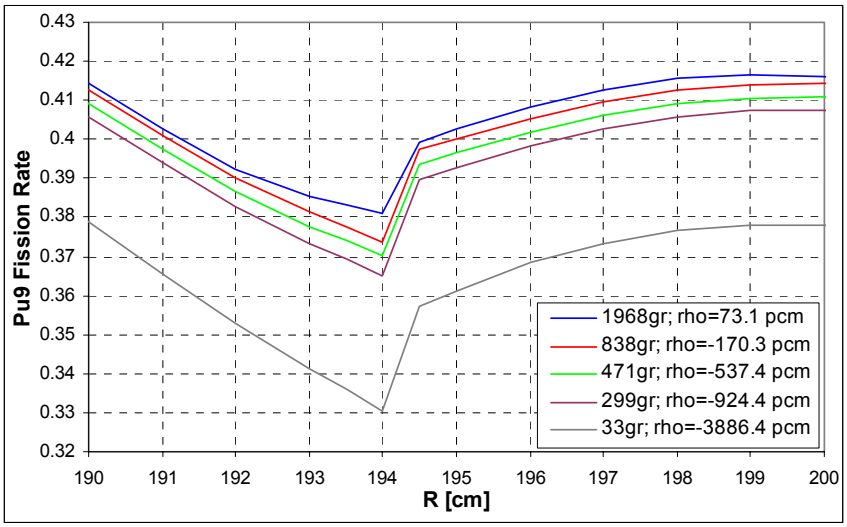

Figure 162: Pu239 Fission Rate Axial (R=10 cm) Traverse at the Interface

So far we investigated the impact through NG in term of reactivity and reaction rate traverses of the system under study. Our goal at this point is to find a method to process the cross-sections with low NG (in particular with NG=33 to be consistent with the energy group structure usually adopted) able to reproduce approximately the same results provided by the fine calculation (NG=1968). In this attempt, we consider our objective reached if the new cross-sections recover 90% of discrepancy observed on the reactivity and reduce the discrepancies on the traverses to about 2%.

For this purpose, the following procedure has been used. A 1D model has been drawn from the radial direction of the 2D problem as shown in **Figure 163**. In the flux calculation we provided an axial buckling, determined in order to give with NG=1968 the same multiplication factor of the corresponding 2D calculation. In order to satisfy this requirement, the buckling has been calculated to be of a value of 2.6E-4. In fact, using the formula for cylindrical coordinates: $B^2_{ax}=(\pi/H)^2$ we derive H=194.8 cm with an extrapolated distance of 20.41 cm. **Table 35** shows that the reactivity change through NG for the 1D model so defined reproduce approximately the same variation of the original 2D system.

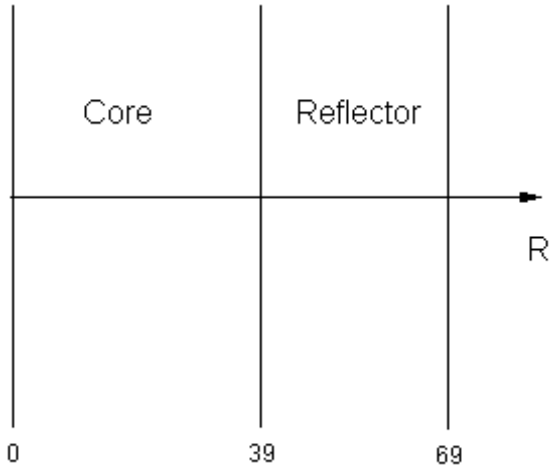

Figure 163: 1D Geometry for Cross-Sections Condensation

Table 35: Reactivity Value for 1D and 2D Models

NG	1D model with B^2_{ax}=2.6E-4	2D Model
33	-3741.3 pcm	-3886.4 pcm
299	-1070.2 pcm	-924.4 pcm
471	-714.3 pcm	-537.4 pcm
838	-383.3 pcm	-170.3 pcm
1968	-171.2 pcm	73.1 pcm

Once fixed the 1D model, according to the improved macrocell scheme we chose to collapse the cross-sections from NG=1968 to NG=33 using as weighting function the flux and the currents solution of this 1D model. The cross-sections so obtained are then used in the original 2D system and the results are reported in the following figures. In particular the case with the reflector divided into two regions appears to be very satisfactory: in the comparison NG=1968 vs NG=33 the discrepancy on the reactivity is reduced from 4000 to 150 pcm and the traverses both radial and axial agree within a margin less than 1%.

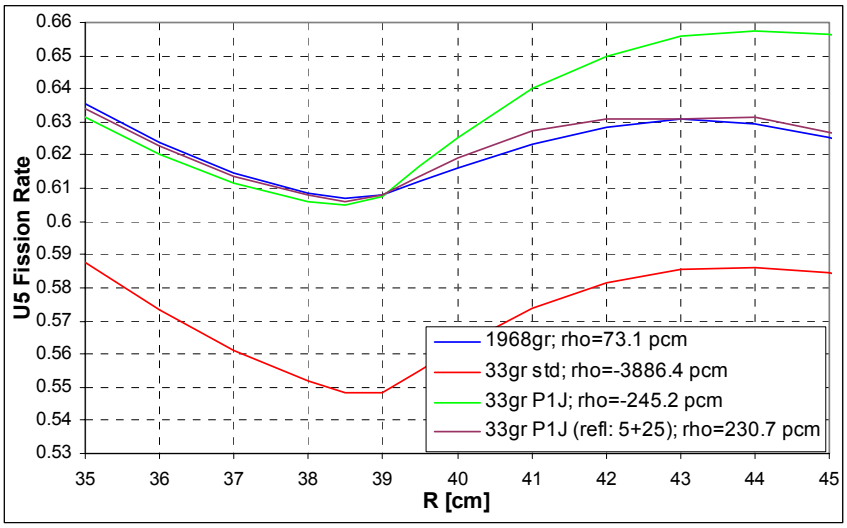

Figure 164: U235 Fission Rate Radial (Z=103 cm) Traverse at the Interface Using the Improved Macrocell Scheme

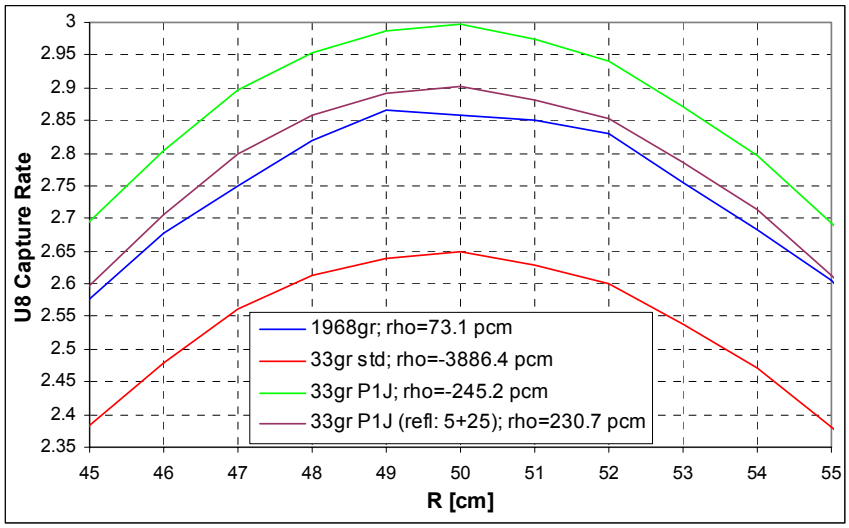

Figure 165: U238 Capture Rate Radial (Z=103 cm) Traverse in the Reflector Using the Improved Macrocell Scheme

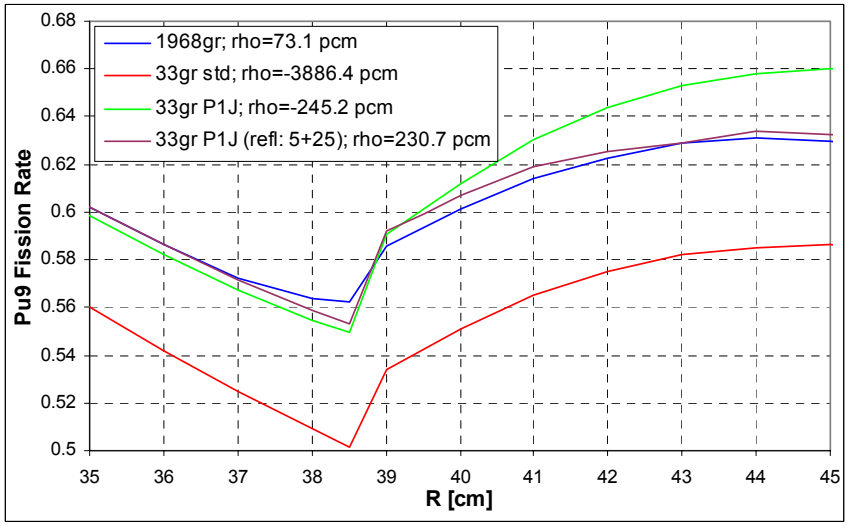

Figure 166: Pu239 Fission Rate Radial (Z=103 cm) Traverse at the Interface Using the Improved Macrocell Scheme

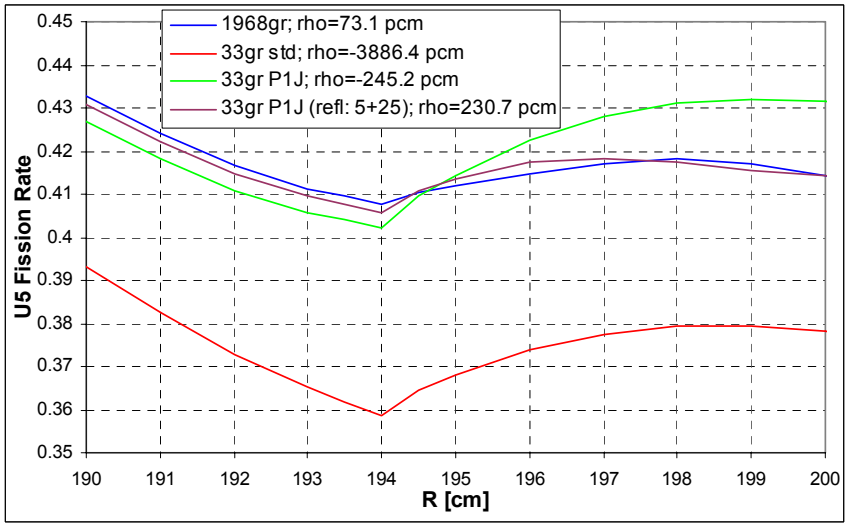

Figure 167: U235 Fission Rate Axial (R=10 cm) Traverse at the Interface Using the Improved Macrocell Scheme

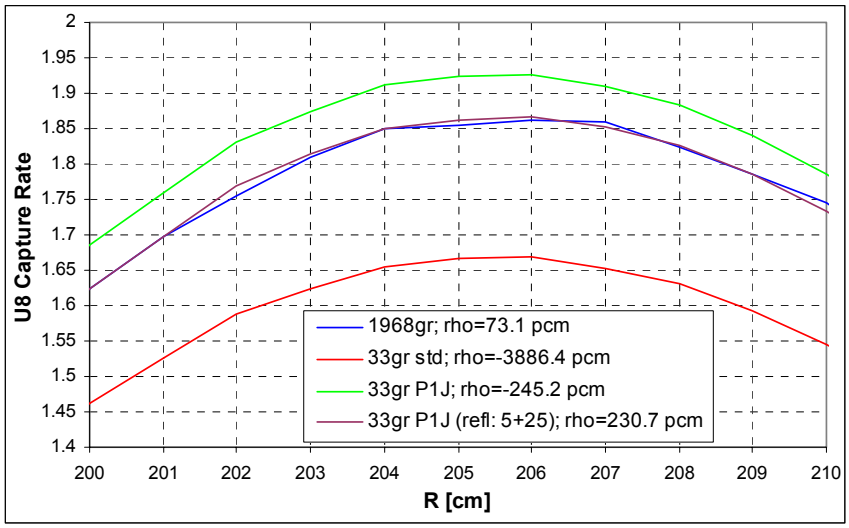

Figure 168: U238 Capture Rate Axial (R=10 cm) Traverse in the Reflector Using the Improved Macrocell Scheme

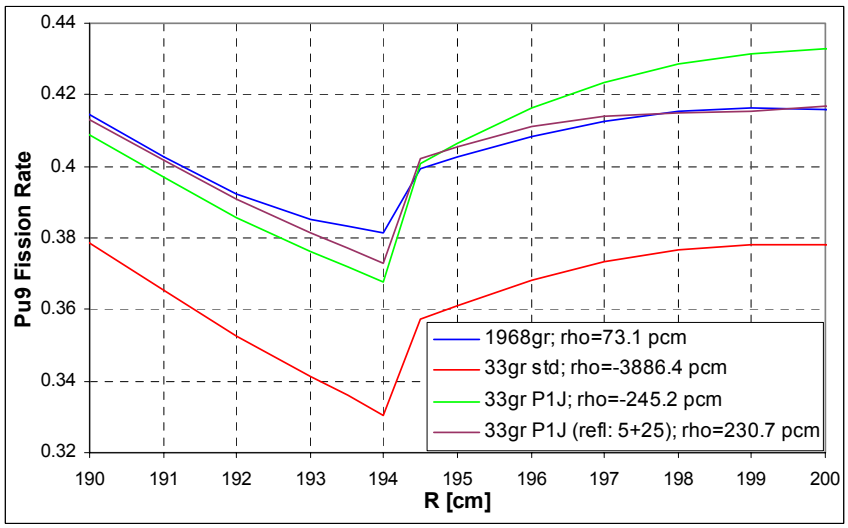

Figure 169: Pu239 Fission Rate Axial (R=10 cm) Traverse at the Interface Using the Improved Macrocell Scheme

As anticipated, we want to investigate also a second model with smaller height of the core zone, in order to strengthen the fraction of neutrons escaping from the core in the reflector and produce situation with high effects at the interface.

Table 36 shows geometry and composition of the new 2D model.

Table 36: Geometry and Isotopic Compositions for a 2D Model

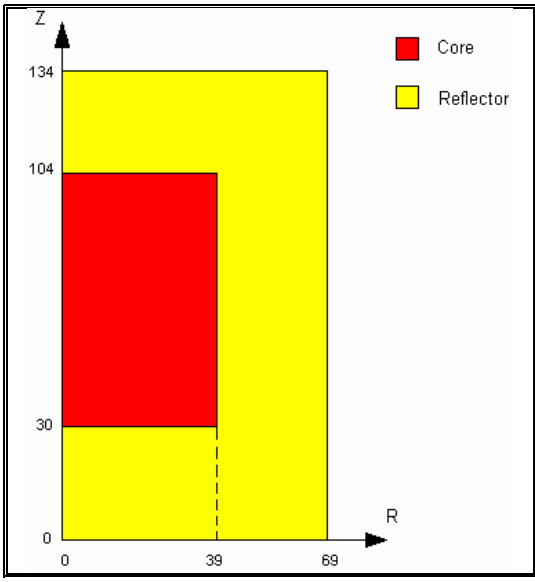

Region	Isotope	Density × 10^{+24} at/cm^3
Zone1- Core	Pu239	1.88×10^{-3}
	U238	6.25×10^{-3}
	Fe56	7.0×10^{-3}
	Cr52	1.5×10^{-3}
	Na23	1.0×10^{-2}
	O16	1.5×10^{-2}
Zone2 - Reflector	Fe56	5.0×10^{-2}
	Cr52	1.5×10^{-2}
	Na23	5.0×10^{-3}

As in the previous example, the following figures report reactivity and traverses calculated in the standard way. The reactivity value calculated with JEF2.2/MCNP4C is –31 ± 13 pcm, which is in good agreement with the fine calculation.

Again, the radial traverses (see **Figures 170** to **172**) are normalized to 1 at the core center (R=0) and the axial ones (see **Figures 173** to **175**) at Z=59 cm.

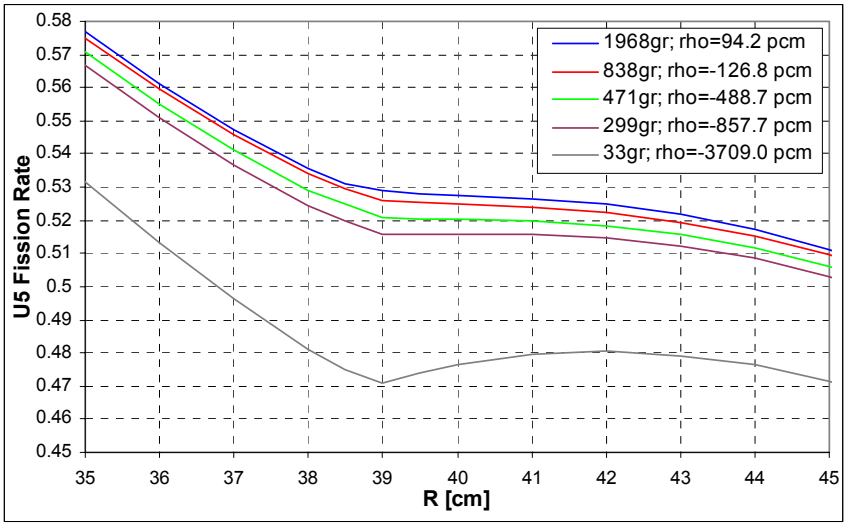

Figure 170: U235 Fission Rate Radial (Z=65 cm) Traverse at the Interface

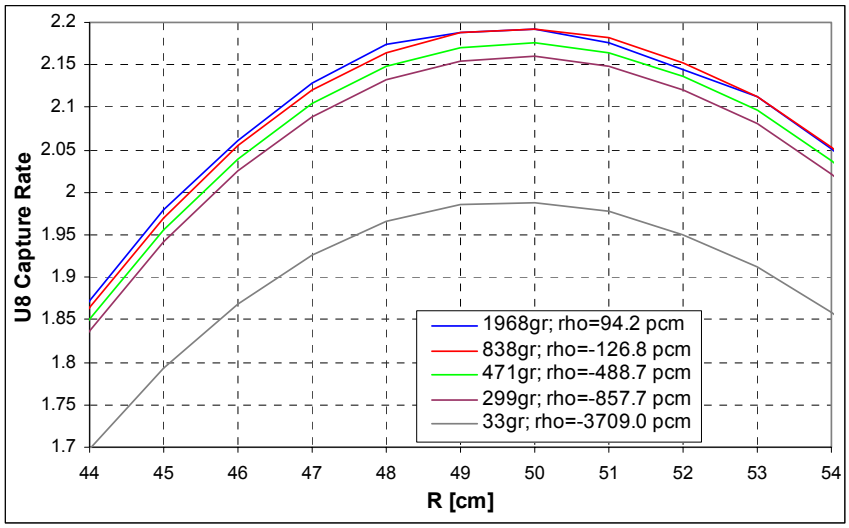

Figure 171: U238 Capture Rate Radial (Z=65 cm) Traverse in the Reflector

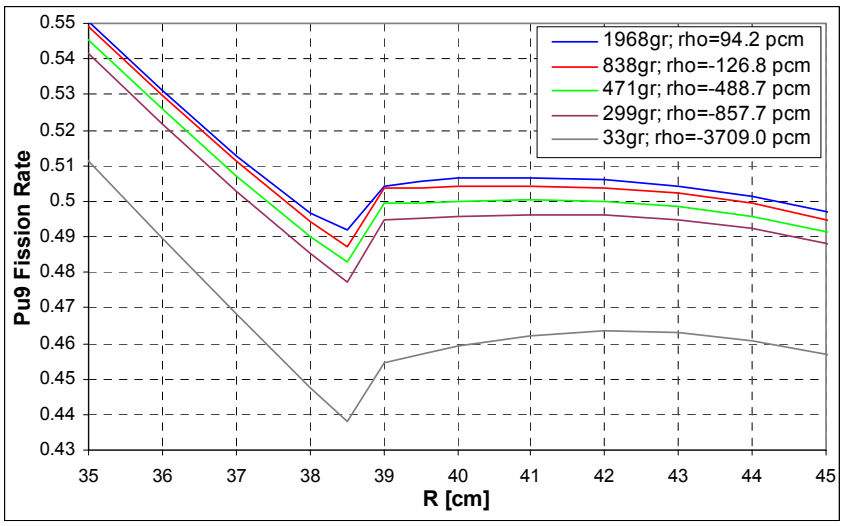

Figure 172: Pu239 Fission Rate Radial (Z=65 cm) Traverse at the Interface

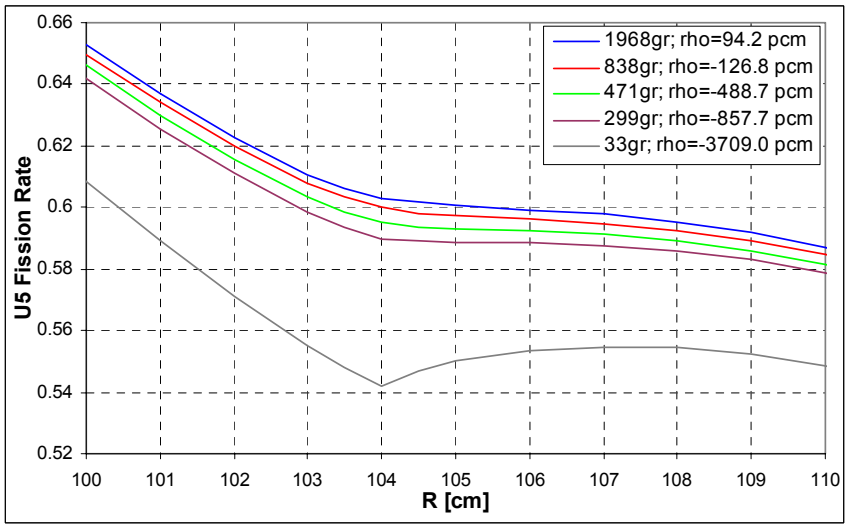

Figure 173: U235 Fission Rate Axial (R=10 cm) Traverse at the Interface

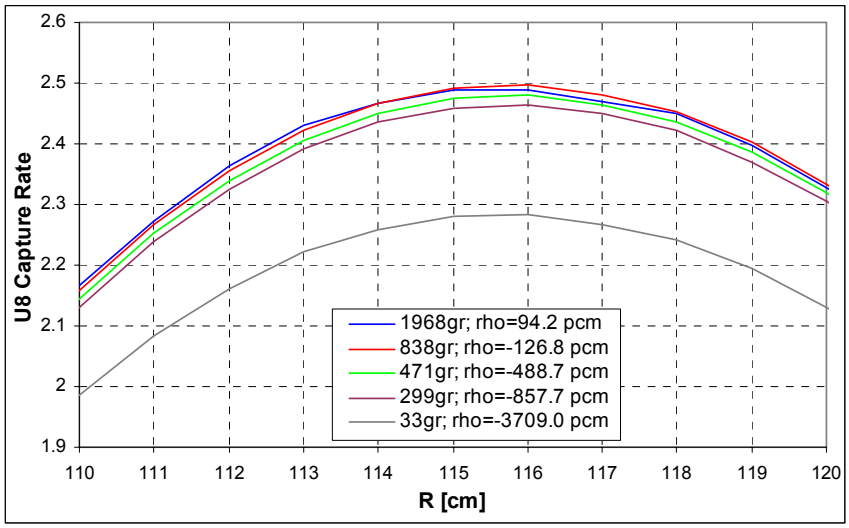

Figure 174: U238 Capture Rate Axial (R=10 cm) Traverse in the Reflector

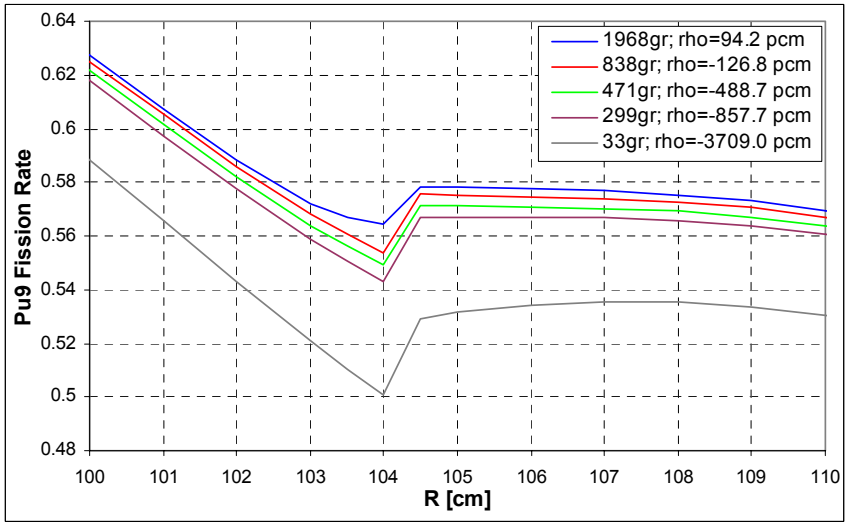

Figure 175: Pu239 Fission Rate Axial (R=10 cm) Traverse at the Interface

In order to process the 33-group cross-sections able to reproduce approximately the same results provided by the fine calculation (NG=1968) the same procedure as in the previous case has been used. The 1D model has been drawn from the radial direction of the 2D problem is again as shown in **Figure 163** and the axial buckling has been evaluated to be of a value of 7.8E-4, corresponding to H=112.5 cm with an extrapolated distance of 19.3 cm. **Table 37** shows the reactivity values for the 1D and the original 2D model.

Table 37: Reactivity Value for 1D and 2D Models

NG	1D model with B^2_{ax} =7.8E-4	2D Model
33	-2443.4 pcm	-3709.0 pcm
299	-517.1 pcm	-857.7 pcm
471	-257.8 pcm	-488.7 pcm
838	-11.1 pcm	-126.8 pcm
1968	138.9 pcm	94.2 pcm

Because of the high interface core/reflector effects, this time the improved macrocell gives good results if both the core and the reflector are splitted into two regions.

In the following figures, we observe that the calculation labelled “33gr P1J”, corresponding to the case of a macrocell with a single region for reflector and core, recovers just 200 pcm of the 3800 pcm of reactivity discrepancy observed between the 33-group standard and the reference calculation. Splitting the reflector into two regions (case “33gr P1J (refl:8+22)”) about 1100 pcm of this discrepancy is recovered. Just by splitting the core into two regions (case “33gr P1J (core:9+31)”) an important gain is obtained. If the reflector is splitted into two regions also the discrepancy on the rate distributions is dramatically reduced. The results so obtained are satisfactory for us, because the 33-group calculation reproduce the reference one within the margin of discrepancy requested both on reactivity value and fission rate (or flux) distribution.

Anyway, the final results we obtained could be still improved if a different size for the sub-regions in the core and in the reflector is chosen. A similar choice has not yet been possible because in the current procedure the total cross-section is current-weighted. Consequently, it happens that the condensation with the current given by small sub-regions (5 cm e.g.), introduce negative values in few groups of the total cross-sections with consequent error found by the code. A better solution could be represented by using a flux-weighted cross-section, but at the moment this application is of a smaller interest.

Finally, for better results we could also split the core and the reflector into more than two regions. We want to avoid this option, because is less practicable in the case of a general geometry in 3 dimensions. Indeed, our study demonstrated that the procedure adopted for this 2D model will be certainly successful also in the case of more complicated geometry, provided that the radial and axial reflector are made of the same material.

At this stage, any information cannot be provided for cases where radial and axial reflectors are made of different materials. It could be possible that the more appropriate solution for this kind of problem is a 2D macrocell.

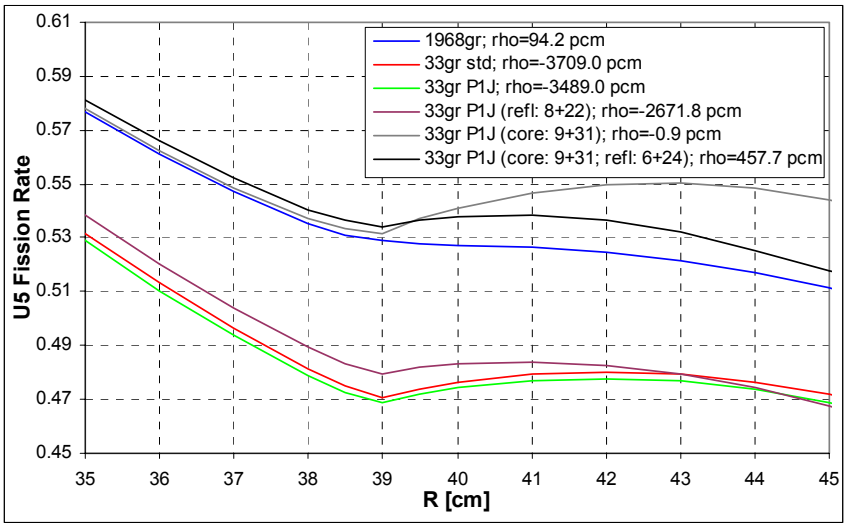

Figure 176: U235 Fission Rate Radial (Z=65 cm) Traverse at the Interface Using the Improved Macrocell Scheme

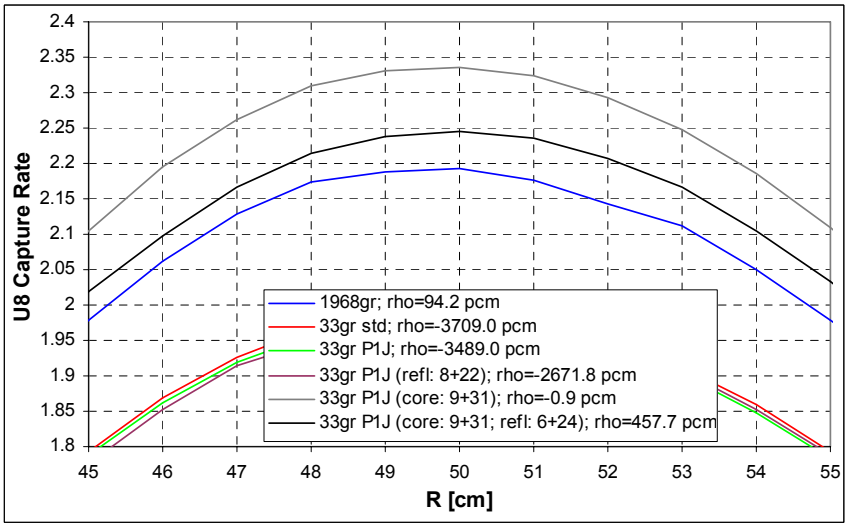

Figure 177: U238 Capture Rate Radial (Z=65 cm) Traverse in the Reflector Using the Improved Macrocell Scheme

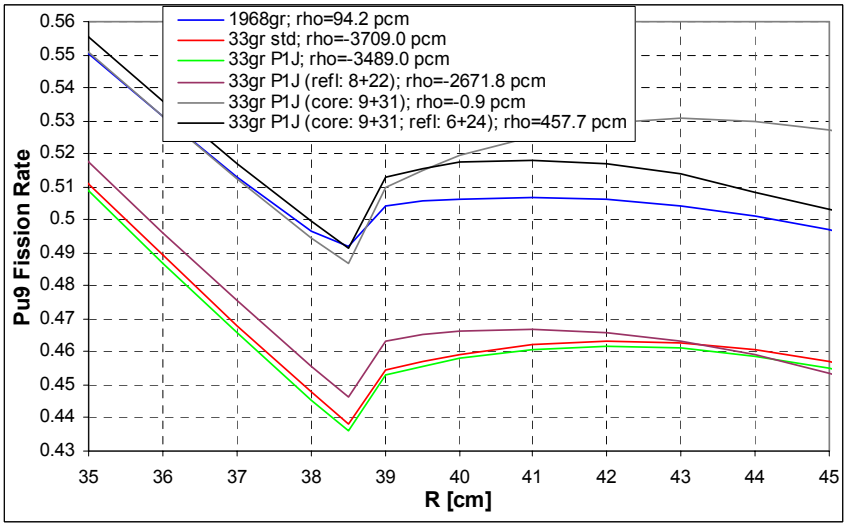

Figure 178: Pu239 Fission Rate Radial (Z=65 cm) Traverse at the Interface Using the Improved Macrocell Scheme

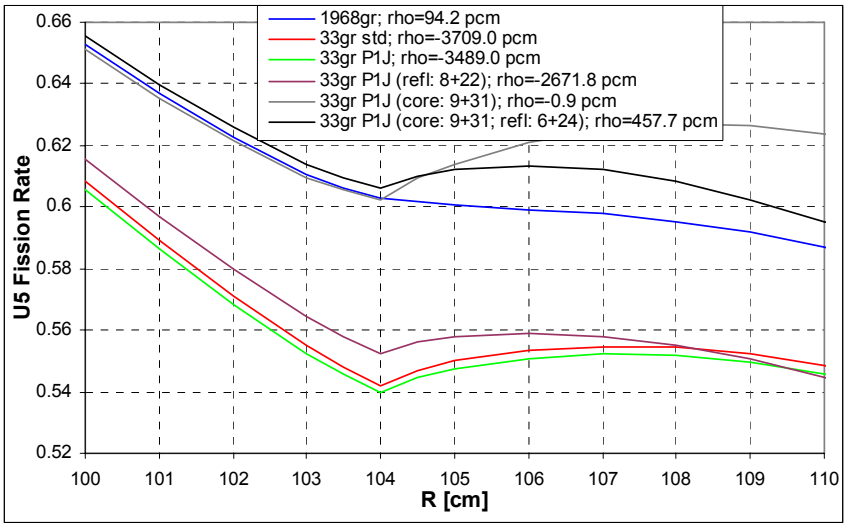

Figure 179: U235 Fission Rate Axial (R=10 cm) Traverse at the Interface Using the Improved Macrocell Scheme

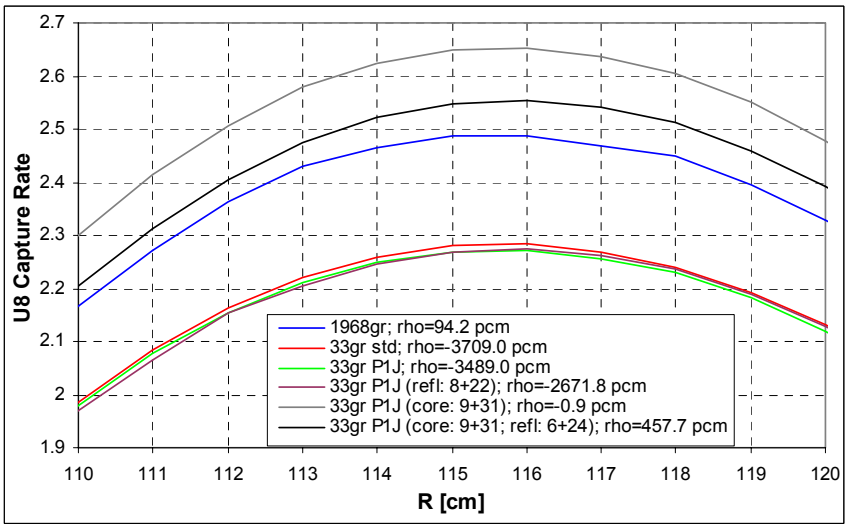

Figure 180: U238 Capture Rate Axial (R=10 cm) Traverse in the Reflector Using the Improved Macrocell Scheme

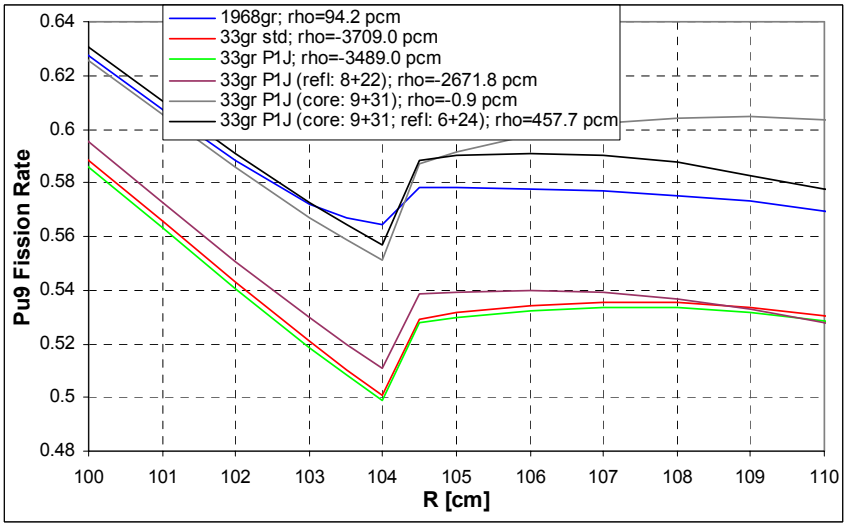

Figure 181: Pu239 Fission Rate Axial (R=10 cm) Traverse at the Interface Using the Improved Macrocell Scheme

References

[1] M. SALVATORES,
"Accelerator Driven System (ADS), Physics Principles and Specifities",
J. Phys. IV France 9, pp. 7-17; 7-33, 1999

[2] M. DELPECH et al.,
"The Am and Cm Transmutation",
Int. Conf. Global99 on Physics and Feasibility, Jackson, Wyoming – USA, August 29 – September 3, 1999

[3] M. SALVATORES, M. MARTINI, I. SLESSAREV,
"MUSE1: a First Experiment at MASURCA to Validate the Physics of Subcritical Multiplying Systems Relevant to ADS",
International Conference, Kalmar, Sweden, June 3-7, 1996

[4] R. SOULE, M. SALVATORES, R. JACQMIN,
"Validation of Neutronic Methods Applied to the Analysis of Fast Subcritical Systems: the MUSE2 Experiment",
International Conference Global'97, Yokohama, Japan, October 5-10, 1997

[5] J.F. LEBRAT, R. SOULE, M. MARTINI, C.A. BOMPAS, P. BERTRAND, P. CHAUSSONNET, J.P. CHAUVIN, M. SALVATORES , G. ALIBERTI, G. RIMPAULT,
"Experimental Investigation of Multiplying Subcritical Media in Presence of an External Source Operating in Pulsed or Continuos Mode: the MUSE3 Experiment",
International Conference, Prague, Czech Rep., 1999

[6] G. ALIBERTI, G. RIMPAULT, R. JACQMIN, J.F. LEBRAT, R. SOULE, J.P. CHAUVIN , G. GRANGET, M. SALVATORES,
"Analysis of the MUSE-3 Subcritical Experiment",
Int. Conf. Global2001, France, Paris, September 2001

[7] J.F. LEBRAT, R. SOULE, M. MARTINI, G. ALIBERTI, G. RIMPAULT, C.A. BOMPAS, P. BERTRAND, P. CHAUSSONNET, J.P. CHAUVIN, M. SALVATORES,
"Experimental Investigation of Multiplying Subcritical Media Coupled with an Accelerator: the MUSE Experiment",

International Conference, Icenes, Portugal, October 5-10, 1997

[8] R. SOULE, W. ASSAL. D. VILLAMARIN
"Geometrical and Physical Data Associated to the MUSE4 ReferenceCconfiguration",
CEA – Cadarache internal report

[9] J.VOLLAIRE, A. BILLEBAUD, R. BRISSOT. C. LE BRUN, E, LIATARD,
"Calibration and Monitoring of the GENEPI Neutron Source for the MUSE IV Experiment",
LPSC, IN2P3-CNRS/UJF/INPG, 6 June 2003

[10] D. VILLAMARIN, R. SOULE, E. GONZALEZ,
"Benchmark on Computer Simulation of MASURCA Critical and Subcritical Experiments (MUSE-4 Benchmark)",
NEA/SEN/NSC/WPPT(2001)5

[11] C. JAMMES, G. PERRET, G. IMEL,
"First MUSE-4 Experimental Results Based on Time Series Analysis",
PHYSOR 2002, International Conference on the New Frontiers of Nuclear Technology : Reactor Physics, Safety and High-performance Computing, Seoul, Korea, October 7-10, 2002

[12] G. ALIBERTI, G. PALMIOTTI, G. IMEL, C.G. STENBERG., R. BLOMQUIST, J. LIAW, P.J. FINCK,
"Analysis of the Experimental Measurements on the MUSE-4 Critical Configuration, Experimental Results Based on Time Series Analysis and MUSE-4 Benchmark on Computer Simulation of MASURCA",
ANL-DOE Annual Report, September 2002.

[13] M. PLASCHY, C.A. BOMPAS, G. RIMPAULT,
"Paramètres de sûreté de l'expérience MUSE-4",
CEA-Cadarache internal report (NT /DEN/SPRC/LEPH/99/231).

[14] "The Muse experiment for subcritical Neutronics Validation",
CEA-Cadarache internal report.

[15] J.VOLLAIRE, A. BILLEBAUD, R. BRISSOT. C. LE BRUN, E, LIATARD,
"Calibration and Monitoring of the GENEPI Neutron Source for the MUSE IV Experiment ",
Internal report (LPSC, IN2P3-CNRS/UJF/INPG, 6 June 2003).

[16] W ASSAL,
"Geometrical and Physical Description of the MASURCA Instrumental Assemblies Used for the β_{eff} Measurements During the MUSE-4 Experiments",
CEA-Cadarache internal report (NT SPEx/LPE/03/046).

[17] R. SOULE, W ASSAL, D. VILLAMARIN,
"Geometrical and Physical Data Associated to the MUSE-4 Reference Configuration",
CEA-Cadarache internal report (NT SPEx/LPE/01/015 December 21, 2001).

[18] R. SOULE, W ASSAL,
"Geometrical and Physical Description of the MASURCA Pilot Rod during the MUSE-4 Experiment",
CEA-Cadarache internal report (NT SPEx/LPE/02/053 July 9, 2002).

[19] R. SOULE, W ASSAL,
"Geometrical and Physical Description of the Instrumental Assemblies Used by the CNRS/ISN during the MUSE-4 Experiments",
CEA-Cadarache internal report (NT SPEx/LPE/02/067 November 11, 2002).

[20] W ASSAL,
"Geometrical and Physical Description of the MASURCA Safety Rods during the MUSE-4 Experiments",
CEA-Cadarache internal report (NT SPEx/LPE/02/063 March 7, 2003).

[21] M. THOMAS, C. JAMMES,
"Preliminary Numerical Estimation of Physical Quantities for Reference Core MUSE-4 Experiments",
CEA-Cadarache internal report (NT SPEx/LPE/02/024 January 21, 2003).

[22] G. PALIMIOTTI, R.F. BURSTALL, E. KIEFHABER, W. GEBHARDT, J.M. RIEUNIER,
"New Methods Developments and Rationalization of Tools for LMFBR Design in the Frame of the European Collaboration",
FR'91 International Conference on Fast Reactors and Related Fuel Cycles, Kyoto, Japan, October 28 – November 1,1991

[23] OECD/NEA Report 17,
"The JEF-2.2 Nuclear Data Library", April 2000

[24] G. RIMPAULT,
"Algorithmic Features of the ECCO Cell Code for Treating Heterogeneous Fast Reactor Subassemblies",
Intl. Conf. On Mathematics and Computations, Reactor Physics, and Environmental Analyses, Portland, OR, April 30- May 4, 1995

[25] H. HENRYSON, II, B.J. TOPPEL, C.G. STENBERG,
"MC^2-2: A Code to Calculate Fast Neutron Spectra and Multigroup Cross-Sections",
ANL-8144, June 1976.

[26] G. PALMIOTTI, C.B. CARRICO and E.E. LEWIS,
"Variatonal Nodal Transport Methods with Anisotropic Scattering",
Nucl. Sc. Eng., 115, p.233 (1993)

[27] J. F. LEBRAT, R. JACQMIN, F. GABRIELLI, M. CARTA, V. PELUSO, G. BUZZI, G. BIANCHINI, A. D'ANGELO, G. ALIBERTI, G. PALMIOTTI,
"Fast Reactor Core-Reflector Interface Effects Revisited",
Proc. PHYSOR 2002 Conference, Seoul (Korea), October 2002

[28] C. DESTOUCHES, G. IMEL, M. THOMAS, G. PERRET, R. SOULE, J.M. LAURENS, P. CHAUSSONNET,
"MUSE4 Reference configuration californium source traverses",
CEA – Cadarache internal report

[29] A. RINEISKI, W. MASCHEK, G. RIMPAULT,
"Performance of Neutron Kinetics Models for ADS Transient Analyses",
AccAPP/ADTTA'01, ANS 2001 Winter Meeting November 11-15, 2001, Reno, Nevada,U.S.A.

[30] R. N. BLOMQUIST
"VIM Continuous Energy Monte Carlo Transport Code",
Proceedings of the International Conference on Mathematics and Computations, Reactor Physics, and Environmental Analyses, April 30 – May 4, 1995, Portland, OR.

[31] R. N. HILL, T. H. FANNING, P. J. FINCK,
"An Evaluation of Multigroup Flux Predictions in the EBR-II Core",
Proc. ANS Topical on Advances in Reactor Physics", Charleston, March 1992

[32] G. PALMIOTTI, J.M. RIEUNIER, C. GHO, M. SALVATORES, "BISTRO Optimized Two Dimensional Sn Transport Code", Nuclear Science and Engineering, 104, 26 (1990)